

Contents

1	Introduction to time-dependent density functional theory	1
1.1	Introduction	1
1.2	Electronic structure methods	1
1.3	Ground-state density functional theory	2
1.4	Historical overview of time-dependent density functional theory	4
1.5	The time-dependent Kohn–Sham equations	4
1.6	Linear and nonlinear response of the density	7
1.7	Description of the accessible response properties	8
1.7.1	Dipole polarizabilities, excitation energies, oscillator strengths	8
1.7.2	General multipole-multipole polarizabilities	9
1.7.3	Hyperpolarizabilities	9
1.7.4	Van der Waals dispersion coefficients	10
1.7.5	Geometrical derivatives	10
1.8	Overview of the thesis	11
2	Implementation of time-dependent density functional response equations	13
	<i>S.J.A. van Gisbergen, J.G. Snijders, and E.J. Baerends, to be submitted as feature article to Comp. Phys. Commun.</i>	
2.1	Abstract	13
2.2	General introduction	13
2.3	Description of desired properties	15
2.4	The time-dependent Kohn–Sham equations	17
2.5	Perturbative solution to time-dependent Kohn–Sham equations	19
2.6	Efficient implementation of matrix-vector multiplication	24
2.6.1	Use of auxiliary basis functions	24
2.6.2	Use of full molecular symmetry	26
2.6.3	Parallelization	28
2.6.4	Distance effects and linear scaling techniques	29
2.7	Selected molecular applications	30
2.7.1	Influence of asymptotic behavior of v_{xc}	30
2.7.2	Excitation energies of small molecules	31
2.7.3	Frequency-dependent hyperpolarizabilities	33
2.7.4	Van der Waals dispersion coefficients	33

2.8	Conclusions	34
2.9	Acknowledgements	35
3	A density functional theory study of frequency-dependent polarizabilities and Van der Waals dispersion coefficients for polyatomic molecules	41
	<i>S.J.A. van Gisbergen, J.G. Snijders, and E.J. Baerends, J.Chem.Phys. 103, 9347-9354 (1995)</i>	
3.1	Abstract	41
3.2	Introduction	41
3.3	The model	42
3.4	Implementation	44
3.5	Description of basis sets and parameters in the calculations	45
3.6	Comparison with other theoretical methods	46
3.6.1	Static and frequency-dependent polarizabilities	46
3.6.2	Isotropic dispersion coefficients	48
3.6.3	Anisotropic dispersion coefficients	49
3.7	Evaluation of two semiempirical methods	50
3.8	Conclusions	51
3.9	Acknowledgements	52
4	Improved density functional theory results for frequency-dependent polarizabilities, by the use of an exchange-correlation potential with correct asymptotic behavior	59
	<i>S.J.A. van Gisbergen, V.P. Osinga, O.V. Gritsenko, R. van Leeuwen, J.G. Snijders, and E.J. Baerends, J.Chem.Phys. 105, 3142-3151 (1996)</i>	
4.1	Abstract	59
4.2	Introduction	59
4.3	Theoretical introduction	61
4.3.1	Frequency-dependent linear response in DFT	61
4.3.2	A model potential with correct asymptotic behavior	62
4.4	Details of calculation and atomic results	63
4.4.1	Description of the program and details of the calculations	63
4.4.2	Atomic results	65
4.5	Molecular results	68
4.5.1	Average polarizabilities	68
4.5.2	Anisotropy in the polarizability	70
4.5.3	Frequency dependence of molecular polarizabilities	72
4.6	Concluding remarks	74
4.7	Acknowledgements	75
5	Application of time-dependent density functional response theory to Raman scattering	77
	<i>S.J.A. van Gisbergen, J.G. Snijders, and E.J. Baerends, Chem.Phys.Lett. 259, 599-604 (1996)</i>	
5.1	Abstract	77

5.2	Introduction	77
5.3	Description of the calculation method	78
5.4	Details of the calculation	79
5.5	Results and discussion	80
5.6	Conclusions	83
5.7	Acknowledgements	84
6	Density functional results for isotropic and anisotropic multipole polarizabilities and C_6, C_7, and C_8 Van der Waals dispersion coefficients for molecules	85
	<i>V.P. Osinga, S.J.A. van Gisbergen, J.G. Snijders, and E.J. Baerends, J.Chem.Phys.</i>	
106 ,	5091-5101 (1996)	
6.1	Abstract	85
6.2	Introduction	86
6.3	Theoretical introduction	87
	6.3.1 Frequency-dependent linear response in DFT	87
	6.3.2 Van der Waals dispersion coefficients	89
6.4	Computational details	90
6.5	Polarizability results	91
	6.5.1 Results for Van der Waals coefficients	93
6.6	Concluding remarks	98
6.7	Acknowledgments	99
7	Time-dependent density functional results for the dynamic hyperpolarizability of C_{60}	107
	<i>S.J.A. van Gisbergen, J.G. Snijders, and E.J. Baerends, Phys.Rev.Lett.</i>	
	78 , 3097:3100	
	<i>(1997)</i>	
7.1	Abstract	107
7.2	Introduction	107
7.3	Outline of theoretical approach	108
7.4	Frequency-dependent hyperpolarizability of C_{60}	109
7.5	Comparison with experimental and theoretical results	112
8	Density functional theory response property calculations with accurate exchange-correlation potentials	115
	<i>S.J.A. van Gisbergen, F. Kootstra, P.R.T. Schipper, O.V. Gritsenko, J.G. Snijders, and</i>	
	<i>E.J. Baerends, Phys.Rev.A</i>	
	57 , 2556:2571 (1998)	
8.1	Abstract	115
8.2	Introduction	115
8.3	Outline of the theory	118
8.4	Computational details	121
	8.4.1 Atomic calculations	121
	8.4.2 Molecular calculations	122
8.5	Results and discussion	124
	8.5.1 Atomic results, polarizabilities	124

8.5.2	Atomic results, excitation energies of Helium	129
8.5.3	Atomic results, excitation energies of Beryllium	133
8.5.4	Molecular polarizability results	137
8.6	Conclusions and future directions	138
8.7	Acknowledgements	139
9	Calculating frequency-dependent hyperpolarizabilities using time-dependent density functional theory	141
	<i>S.J.A. van Gisbergen, J.G.Snijders, and E.J.Baerends, submitted to J.Chem.Phys.</i>	
9.1	Abstract	141
9.2	Introduction	141
9.3	The basic equations	143
9.4	Expansion of basic equations	146
9.5	Expansion of xc potential	149
9.6	Expressions for the higher-order Kohn–Sham matrices in DFT	151
9.7	Solving the nonlinear response equations using the $(2n + 1)$ -theorem	151
9.8	Approximations used in DFT response calculations	154
9.9	Implementation	156
9.10	Tests on the implementation and discussion of effects of a finite auxiliary basis set	158
9.11	Summary and outlook	161
9.12	Acknowledgements	161
	Summary and outlook	163
	Samenvatting en vooruitblik	167
	Dankwoord	171
	List of publications	173
	Bibliography	175

Chapter 1

Introduction to time-dependent density functional theory

1.1 Introduction

This introductory chapter contains a short historical overview of ground-state density functional theory, and of early applications of time-dependent density functional theory. A review is given of the Runge–Gross derivation of the time-dependent Kohn–Sham equations, which are the basic equations of time-dependent density functional theory. A description of the response properties which are relevant to this thesis, is also included.

1.2 Electronic structure methods

The starting point for a (nonrelativistic) quantummechanical calculation on an N -particle system is the Schrödinger equation:

$$H\Psi(\mathbf{r}_1, \mathbf{r}_2, \dots, \mathbf{r}_N) = E\Psi(\mathbf{r}_1, \mathbf{r}_2, \dots, \mathbf{r}_N). \quad (1.1)$$

Here, the total wavefunction Ψ is very complicated, as it depends upon the coordinates of all particles (nuclei and electrons) in the system. The problem is reduced if the electronic motion is separated from the much slower nuclear motion, the so-called Born–Oppenheimer approximation. In that case, the problem reduces to the determination of the electronic wavefunction at fixed nuclear positions. Although easier than the original problem, this problem is still unsolvable. Additional approximations are needed in order to obtain a solution. Although not adopted in this thesis, a very common starting point is formed by Hartree–Fock (HF) theory, in which the approximation is made that the total electronic wavefunction can be written in the form of a single Slater-determinant of N_{el} spin orbitals, where N_{el} is the number of electrons in the system. The orbitals are then optimized, such that the Hartree–Fock energy

$$E^{\text{HF}} = \langle \Psi^{\text{HF}} | H | \Psi^{\text{HF}} \rangle / \langle \Psi^{\text{HF}} | \Psi^{\text{HF}} \rangle \quad (1.2)$$

is minimal, under the constraint that the orbitals remain orthonormal. The resulting orbitals are called the Hartree–Fock orbitals.

The Hartree–Fock approach, often called SCF approach, after the self-consistent field equations which have to be solved, provides a cheap and relatively simple *ab initio* approach for the calculation of electronic structures. By approximating the total electronic wavefunction as a Slater determinant, the Fermi correlation between the electrons, originating from the Pauli exclusion principle, is automatically taken into account. However, in Hartree–Fock (HF) theory, effects of *electron correlation* are neglected, the correlation energy being defined as the difference between the HF energy and the exact energy. There are many *ab initio* approaches to the electron correlation problem. One approach is to take more than one Slater determinant into account, as in the multiconfiguration SCF (MCSCF) approach. In this way, the description of the dissociation of H_2 , which is inadequately described in simple Hartree–Fock theory, can be considerably improved. It is said that MCSCF describes the *static* correlation effects. A different approach is the Møller–Plesset (MP) perturbation theory approach. This approach, commonly abbreviated as MP2, MP3, MP4, etc., depending upon the order of the perturbation theory, includes the other type of correlation effects, the *dynamic* correlation effects, which are responsible for the difference between the exact and Hartree–Fock answers for Helium. Both types of correlation are taken into account in a configuration interaction (CI) calculation, where instead of just the simple HF Slater determinant, also many excited configurations are taken into account. This increases the freedom of the trial wavefunction and leads to a decrease of the total energy with respect to the HF energy. All approaches to the electron correlation problem mentioned here have one disadvantage in common: although possibly very accurate, they are very time consuming, forbidding the treatment of large molecules. On the other hand, in many cases HF theory is of insufficient accuracy. This explains why there has been such a wide-spread interest in density functional theory (DFT) in the last decades. DFT provides a first principles approach in which correlation effects are approximately taken into account, while the computational efficiency is at least as good as for HF theory. This makes DFT a valuable tool for problems of a size which cannot be treated anymore with the expensive conventional *ab initio* techniques. The essentials of DFT are described in the following section.

1.3 Ground-state density functional theory

The key point of density functional theory is that it is not necessary to calculate the very complicated complete electronic wavefunction $\Psi_{\text{el}}(\mathbf{r}_1, \mathbf{r}_2, \dots, \mathbf{r}_N)$, which depends upon the coordinates of all electrons, for a full description of the system. Instead, the knowledge of the electron density, $\rho(\mathbf{r})$, a simple function of three spatial coordinates, is sufficient, a fact which was first proven by Hohenberg and Kohn[1].

The first part of the Hohenberg–Kohn (HK) theorem, originally formulated for a system in a nondegenerate ground-state, states that, up to a trivial constant in the external potential, a one-to-one mapping exists between external potentials and electron densities. In other words, once the electron density is known, the external potential, and consequently the Hamiltonian of the system are in principle uniquely determined. The knowledge of the Hamiltonian in its turn determines the total electronic wavefunction. Consequently, every quantummechanical observable is a functional of the ground-state density.

For a system without external perturbations, this can be intuitively understood, as was

first pointed out by Bright Wilson[2]. He argued that the cusps in the electron density determined the positions of the nuclei, the gradients of the density at the nuclei determined their nuclear charges, while the integrated density determines the total number of electrons in the system. Therefore it has been determined what system we are dealing with and the Hamiltonian for this system can be written down. This seems to suggest that the Hohenberg–Kohn theorem is in fact rather empty. However, the Bright Wilson argument is in fact oversimplified, as it is not obvious how the argument should be generalized to a system in an external potential.

The second part of the HK theorem states that the exact electron density can be obtained from a variational principle which involves only the density. The exact density is that density which minimizes the energy as a functional of the density.

Although people were at first somewhat skeptical about the practical usefulness of DFT, this rapidly changed when Kohn and Sham[3] introduced what would later be called the Kohn–Sham equations. Kohn and Sham considered a system of noninteracting particles (to which they attributed no physical meaning), moving in an effective local potential, the Kohn–Sham potential, of which the density would be identical to the associated interacting particle system. No proof is available that such an effective potential should exist. If it exists, however, it is unique. The Kohn–Sham potential can be subdivided in three parts: the external potential, the Hartree potential from the Coulomb interaction with the electron cloud and an unknown part, the exchange-correlation potential. This exchange-correlation (xc) potential is an unknown functional of the density. It contains all the many-body exchange and correlation effects. The accuracy of DFT calculations largely depends on the appropriateness of the approximations made for the xc potential, and related xc functionals, such as the xc energy functional.

The first approximation for the xc potential which was used was the local density approximation (LDA), either in exchange-only (x-only) form or with inclusion of correlation effects. The once popular $X\alpha$ approach falls into this category of local density schemes. The LDA is based upon the theory of the homogeneous electron gas. For this simple system, the exchange energy and potential are known exactly, and accurate approximations for the correlation parts are known from analytical parametrizations, such as the one by Vosko–Wilk–Nusair[4], obtained from fits to accurate Monte Carlo simulations by Ceperley and Alder[5]. The approximation is that a system can locally be described as an electron gas with a density equal to the local density of the system. This assumption seems reliable in systems with slowly varying densities (such as certain metals), but not in molecules, where the density changes rapidly. In spite of this, LDA works satisfactorily even in molecules, which is well-understood by now[6, 7], although it can be drastically improved upon by using generalized gradient approximations (GGAs). The GGAs are based upon the theory of the (weakly) inhomogeneous electron gas, and take the gradient of the density into account, in addition to the density itself. Very good accuracy is reached for many systems and properties with the GGAs, although cases are known in which also these GGAs give qualitatively incorrect results, because the description of some effects requires an ultra-nonlocal density dependence in the functionals, for which a gradient expansion is insufficient. Several textbooks[6, 7] on (ground-state) DFT are available for the interested reader in which more detailed information about ground-state DFT can be found.

1.4 Historical overview of time-dependent density functional theory

The first steps towards a time-dependent DFT were taken by Peuckert[8] and Zangwill and Soven[9]. Although there was no formal justification at the time, Zangwill and Soven were the first to apply the adiabatic local density approximation (ALDA), to be introduced later on, for the calculation of the dynamic photoresponse of a finite system, their initial application being to the photoabsorption of the rare gases[9]. Both Deb and Ghosh[10, 11, 12, 13] and Bartolotti[14, 15, 16, 17] formulated a time-dependent DFT for a restricted set of external perturbations. Bartolotti considered adiabatic processes, while Ghosh and Deb treated the important case of potentials periodic in time. A theoretical breakthrough came with the work of Runge and Gross in which a set of single-particle equations for basically all time-dependent external potentials was derived, usually called time-dependent Kohn–Sham equations. This provided the solid theoretical framework for the approach suggested by Zangwill and Soven.

In the early applications of time-dependent DFT[18, 19, 20, 21, 22, 23, 9, 24, 25, 26, 27, 28, 29] atomic and solid-state systems were treated almost exclusively. In the atomic applications of TDDFT, extensive use was made of the spherical symmetry of the system. This simplified the equations enormously, but at the same time prevented the treatment of molecules, for which the applied techniques were not sufficiently general. A single early attempt to treat small molecules was made by Levine and Soven[19], but their single-center expansion is only applicable to the smallest of molecules. Apart from the atomic systems, the treatment of infinite systems also started early. In this respect, the work of Gies and Gerhardt[28, 29] should be mentioned. These early atomic and solid-state applications are described in the book by Mahan and Subbaswamy[30] and in review papers on time-dependent DFT[31, 32, 33], in which further references, description of techniques, and early results can be found. The first molecular calculations based on generally applicable implementations[34, 35], to which the underlying work belongs, have come about only recently.

1.5 The time-dependent Kohn–Sham equations

The presentation in this section was taken from available reviews on time-dependent density functional theory[31, 36, 32, 33, 37], particularly from the most recent review by Gross and coworkers[33]. The starting point is formed by the time-dependent Schrödinger equation [atomic units (a.u.) used throughout the thesis, unless otherwise stated]:

$$i\frac{\partial}{\partial t}\Psi(t) = \hat{H}(t)\Psi(t), \quad (1.3)$$

where the Hamiltonian \hat{H} consists of the kinetic energy \hat{T} , the Coulomb interaction \hat{W} , and the time-dependent external potential $\hat{V}(t)$:

$$\hat{H} = \hat{T} + \hat{W} + \hat{V}(t). \quad (1.4)$$

In the Runge–Gross paper[38], systems evolving from a fixed initial state $\Psi(t_0) = \Psi_0$ are considered. The external potential $\hat{V}(t)$ may consist of several external time-dependent

potentials, each of which is required to be expandable in a Taylor series around the finite time t_0 . The proof by Runge and Gross[38] now shows that *the densities $\rho(\mathbf{r}, t)$ and $\rho'(\mathbf{r}, t)$ of two systems evolving from the same initial state $\Psi(t_0)$ under the influence of, respectively, the scalar potentials $v(\mathbf{r}, t)$ and $v'(\mathbf{r}, t)$, both Taylor expandable about t_0 and differing by more than a purely time-dependent function $c(t)$, will always differ*. This is the time-dependent analogue of the first part of the HK theorem.

As a consequence, the time-dependent external potential, belonging to a certain time-dependent density $\rho(\mathbf{r}, t)$, is unique up to a purely time-dependent function $c(t)$. It determines the total time-dependent wavefunction, which in turn is unique up to a time-dependent phase factor $\alpha(t)$:

$$\Psi(t) = e^{-i\alpha(t)} \tilde{\Psi}[\rho](t). \quad (1.5)$$

From this it is clear that the expectation value of a time-dependent quantummechanical operator $\hat{O}(t)$ [which does not contain derivative or integral operators on t] is a completely *unique* functional of the density:

$$O[\rho](t) = \langle \tilde{\Psi}[\rho](t) | \hat{O}(t) | \tilde{\Psi}[\rho](t) \rangle. \quad (1.6)$$

In this treatment, only scalar potentials are considered, thus excluding vector potentials $\mathbf{A}(\mathbf{r}, t)$. This implies that an extension of the present scheme is needed for a complete treatment of magnetic effects. This extension is called time-dependent current-density functional theory (TDCDFT), because the time-dependent density $\rho(\mathbf{r}, t)$ is not sufficient for the complete description of magnetic systems, for which the current-density $\mathbf{j}(\mathbf{r}, t)$ is needed as well. Such an extension is described in Ref.[33]. An approximate current-density functional for the static case was proposed by Vignale and Rasolt[39, 40, 41], which is based on the density and the paramagnetic current-density. An application to magnetizabilities of the Vignale–Rasolt approximation was given by Colwell, Lee, and Handy[42, 43]. Interesting new proposals were recently given by Capelle and Gross[44], who made a connection between spin-density functional theory and current-density functional theory, and based new approximations on this connection. In the present thesis, however, only electric fields will be considered.

In the ground-state case, one uses the Rayleigh–Ritz minimum principle for the total energy, in the second part of the HK theorem, in order to arrive at a formal method for obtaining the electron density. Such an approach is not possible in the time-dependent case, as no minimum energy principle is available. Instead a stationary action principle is invoked.

Solving the time-dependent Schrödinger equation with the above-mentioned boundary condition at t_0 is equivalent to finding the stationary point of the action integral \mathcal{A} :

$$\mathcal{A} = \int_{t_0}^{t_1} dt \langle \Psi(t) | i \frac{\partial}{\partial t} - \hat{H}(t) | \Psi(t) \rangle, \quad (1.7)$$

which, in view of the correspondence between the time-dependent densities and wavefunctions, can be regarded as a density functional $\mathcal{A}[\rho]$:

$$\mathcal{A}[\rho(\mathbf{r}, t)] = \int_{t_0}^{t_1} dt \langle \Psi[\rho](t) | i \frac{\partial}{\partial t} - \hat{H}(t) | \Psi[\rho](t) \rangle, \quad (1.8)$$

which must have a stationary point at the exact time-dependent density. This exact density can be found from the Euler–Lagrange equation:

$$\frac{\delta \mathcal{A}[\rho]}{\delta \rho(\mathbf{r}, t)} = 0 \quad (1.9)$$

The density functional $\mathcal{A}[\rho]$ can be rewritten as:

$$\mathcal{A}[\rho] = \mathcal{B}[\rho] - \int_{t_0}^{t_1} dt \int d\mathbf{r} \rho(\mathbf{r}, t) v(\mathbf{r}, t), \quad (1.10)$$

where the universal functional \mathcal{B} (universal for a particular choice for the Coulomb interaction \hat{W}), given by

$$\mathcal{B}[\rho] = \int_{t_0}^{t_1} dt \langle \Psi[\rho](t) | i \frac{\partial}{\partial t} - \hat{T} - \hat{W} | \Psi[\rho](t) \rangle, \quad (1.11)$$

plays the role of the universal functional $F[\rho]$ in the time-independent theory[6, 7].

The above provides a formal way to obtain the time-dependent electron density $\rho(\mathbf{r}, t)$, but not a practical algorithm. In order to apply the above theory, a set of time-dependent KS equations has to be introduced. In order to do so, one assumes that a noninteracting particle system exists, of particles moving in a local time-dependent potential $v_s(\mathbf{r}, t)$, of which the density is identical to the density of the interacting system. As in the ground-state case, the existence of such a potential $v_s(\mathbf{r}, t)$ is an assumption, which has never been proven. However, if it exists, it must be unique, because of the Runge–Gross theorem (the time-dependent version of the HK theorem), and then the exact time-dependent density can be obtained from the time-dependent Kohn–Sham (KS) equations:

$$i \frac{\partial}{\partial t} \phi_j(\mathbf{r}, t) = \left(-\frac{\nabla^2}{2} + v_s[\rho](\mathbf{r}, t) \right) \phi_j(\mathbf{r}, t), \quad (1.12)$$

with the density obtained from the noninteracting orbitals:

$$\rho(\mathbf{r}, t) = \sum_{j=1}^N | \phi_j(\mathbf{r}, t) |^2. \quad (1.13)$$

The potential $v_s[\rho, t]$ is usually called the time-dependent KS potential and written as:

$$v_s[\rho](\mathbf{r}, t) = v(\mathbf{r}, t) + \int d\mathbf{r}' \frac{\rho(\mathbf{r}', t)}{|\mathbf{r} - \mathbf{r}'|} + v_{xc}(\mathbf{r}, t). \quad (1.14)$$

Here, $v(\mathbf{r}, t)$ is the external field and $v_{xc}(\mathbf{r}, t)$ is the time-dependent exchange-correlation potential, the unknown part of $v_s(\mathbf{r}, t)$, which has to be approximated for practical applications. It is related to the xc part \mathcal{A}_{xc} of the action functional \mathcal{A} by the relation

$$v_{xc}[\rho](\mathbf{r}, t) = \frac{\delta \mathcal{A}_{xc}[\rho]}{\delta \rho(\mathbf{r}, t)}, \quad (1.15)$$

where the xc part of the action functional is defined by

$$\mathcal{A}_{xc}[\rho] = \mathcal{B}_s[\rho] - \mathcal{B}[\rho] - \frac{1}{2} \int_{t_0}^{t_1} dt \int d\mathbf{r} \int d\mathbf{r}' \frac{\rho(\mathbf{r}, t) \rho(\mathbf{r}', t)}{|\mathbf{r} - \mathbf{r}'|}, \quad (1.16)$$

where \mathcal{B}_s is the noninteracting counterpart of \mathcal{B} .

1.6 Linear and nonlinear response of the density

For the determination of properties like polarizabilities and excitation energies only the knowledge of the linear density response of the system is required, implying that only a perturbative solution to the time-dependent KS equations is required, which considerably simplifies the problem.

Following Gross *et al.*[33] once more, we consider an external potential v_{ext} of the form:

$$v_{\text{ext}}(\mathbf{r}, t) = \begin{cases} v_0(\mathbf{r}) & ; t \leq t_0 \\ v_0(\mathbf{r}) + v_1(\mathbf{r}, t) & ; t > t_0 \end{cases} \quad (1.17)$$

Expanding the density $\rho(\mathbf{r}, t)$ as a functional of the external potential v_{ext} in a functional Taylor series, which is allowed for our case of small perturbations, we get:

$$\rho(\mathbf{r}, t) = \rho_0(\mathbf{r}) + \rho_1(\mathbf{r}, t) + \rho_2(\mathbf{r}, t) + \dots, \quad (1.18)$$

where $\rho_0(\mathbf{r})$ is the unperturbed density of $t < t_0$, which can be obtained from the ground-state Kohn–Sham equations in the potential $v_0(\mathbf{r})$.

In general, the first-order time-dependent density can be calculated from the *exact* linear response function χ :

$$\rho_1(\mathbf{r}, t) = \int d\mathbf{r}' \int dt' \chi(\mathbf{r}, t; \mathbf{r}', t') v_1(\mathbf{r}', t'), \quad (1.19)$$

where the density-density response function is given by the functional derivative

$$\chi(\mathbf{r}, t; \mathbf{r}', t') = \left. \frac{\delta \rho[v_{\text{ext}}](\mathbf{r}, t)}{\delta v_{\text{ext}}(\mathbf{r}', t')} \right|_{v_0}, \quad (1.20)$$

which has to be evaluated at the initial (ground-state) potential v_0 . Similarly, for the KS system of noninteracting electrons, one finds the first-order change in the density from[33]:

$$\rho_1(\mathbf{r}, t) = \int d\mathbf{r}' \int dt' \chi_s(\mathbf{r}, t; \mathbf{r}', t') v_s^1(\mathbf{r}', t'), \quad (1.21)$$

where χ_s is the noninteracting linear density-density response function, and $v_{s,1}(\mathbf{r}, t)$ is the KS potential in first-order of the external field, given by:

$$v_{s,1}(\mathbf{r}, t) = v_1(\mathbf{r}, t) + \int d\mathbf{r}' \frac{\rho_1(\mathbf{r}', t)}{|\mathbf{r} - \mathbf{r}'|} + \int d\mathbf{r}' \int dt' f_{\text{xc}}[\rho_0](\mathbf{r}, t; \mathbf{r}', t') \rho_1(\mathbf{r}', t'). \quad (1.22)$$

Here the xc kernel f_{xc} has been introduced. It is the functional derivative of the time-dependent xc potential $v_{\text{xc}}(\mathbf{r}, t)$ with respect to the time-dependent density $\rho(\mathbf{r}, t)$:

$$f_{\text{xc}}(\mathbf{r}, t; \mathbf{r}', t') = \frac{\delta v_{\text{xc}}(\mathbf{r}, t)}{\rho(\mathbf{r}', t')}. \quad (1.23)$$

After a Fourier transformation the equation for the first-order density change reads:

$$\begin{aligned} \rho_1(\mathbf{r}, \omega) &= \int d\mathbf{r}' \chi_s(\mathbf{r}, \mathbf{r}', \omega) v_1(\mathbf{r}', \omega) \\ &+ \int d\mathbf{r}' \int d\mathbf{r}'' \chi_s(\mathbf{r}, \mathbf{r}'; \omega) \left(\frac{1}{|\mathbf{r}' - \mathbf{r}''|} + f_{\text{xc}}[\rho_0](\mathbf{r}', \mathbf{r}''; \omega) \right) \rho_1(\mathbf{r}'', \omega). \end{aligned} \quad (1.24)$$

The KS response function is known in terms of the unperturbed KS orbitals $\phi_j(\mathbf{r})$, their occupation numbers f_j (in this thesis these are assumed to be equal to 0 or 1, while Casida[37] explicitly allows for fractional occupation numbers), and their orbital energies ε_j :

$$\chi_s(\mathbf{r}, \mathbf{r}'; \omega) = \sum_{j,k} (f_k - f_j) \frac{\phi_j(\mathbf{r}) \phi_k^*(\mathbf{r}) \phi_j^*(\mathbf{r}') \phi_k(\mathbf{r}')}{\omega - (\varepsilon_j - \varepsilon_k) + i\eta}, \quad (1.25)$$

where η is a positive infinitesimal. If we consider the real density response of a molecule in an applied electric field, one is allowed to choose real KS orbitals ϕ_j , which is the usual choice in quantumchemical programs, and the infinitesimal η can be set to zero. If we furthermore make use of the fact that there is no contribution from jk if j , and k are both occupied or both virtual, we can simply write for the response function:

$$\chi_s(\mathbf{r}, \mathbf{r}'; \omega) = \sum_i^{\text{occ}} \sum_a^{\text{virt}} \phi_a(\mathbf{r}) \phi_i(\mathbf{r}) \phi_a(\mathbf{r}') \phi_i(\mathbf{r}') \times \left(\frac{2(\varepsilon_i - \varepsilon_a)}{(\varepsilon_i - \varepsilon_a)^2 + \omega^2} \right), \quad (1.26)$$

which is the form which has actually been implemented in our work[34]. As an aside, we note that from the infinitesimal η one can obtain the imaginary part of the response function which is needed if one is interested in photoabsorption, governed by the imaginary part of the polarizability. The calculation of polarizabilities at imaginary frequencies, which are required for the determination of Van der Waals dispersion coefficients, is as trivial as changing $+\omega^2$ to $-\omega^2$ in the simplified expression for the response function.

Similar equations may be written down for the nonlinear density response. This has been done in detail in Ref.[33] for the second- and third-order densities. From these nonlinear density changes, the nonlinear optical response of a system, determined by its hyperpolarizability tensors, can be calculated. How this is done in the most efficient manner, using the $(2n + 1)$ -theorem of perturbation theory, is described in Chapter 9.

It should be emphasized that, although for the most general case the time-dependent xc functionals depend upon the initial state Ψ_0 , this is not true for the perturbative regime considered here, because in this case, Ψ_0 is a single Slater determinant of a time-independent ground-state. It has been explained in, for example, Ref.[33] that in that case there is no Ψ_0 dependence in the different orders of the time-dependent xc potential needed in the perturbative approach.

1.7 Description of the accessible response properties

1.7.1 Dipole polarizabilities, excitation energies, oscillator strengths

The linear response of a molecule to a frequency-dependent electric perturbation is given by the linear polarizability tensor $\alpha_{ij}(\omega)$:

$$\mu_i = \mu_i^{(0)} + \sum_j \alpha_{ij}(\omega) E_j(\omega), \quad (1.27)$$

where $\mu_i - \mu_i^{(0)}$ is the change in the dipole moment of the molecule in direction i . The linear dipole polarizability tensor $\alpha(\omega)$ has poles at the vertical excitation energies ω_i . The

strengths of the poles are given by the oscillator strengths f_i , or, equivalently, by the transition dipole moments μ_i [45]:

$$\alpha_{\text{av}}(\omega) = \sum_i \frac{f_i}{\omega_i^2 - \omega^2} = \frac{2}{3} \sum_i \frac{\omega_i \mu_i^2}{\omega_i^2 - \omega^2} \quad (1.28)$$

If the frequency of the external perturbation is sufficiently large, absorption of light can occur. This photabsorption $\sigma(\omega)$ is described by the imaginary part of the polarizability tensor, and can also be calculated, using the identity

$$\frac{1}{x + i\eta} = \mathcal{P} \frac{1}{x} + i\pi\delta(x), \quad (1.29)$$

from the transition dipole moments and excitation energies (see for example [30, 46, 47]):

$$\sigma(\omega) = \frac{4\pi\omega}{c} \text{Im}[\alpha(\omega)] = \frac{4\pi^2}{3c} \omega \sum_{i,j} n_i(1 - n_j) |\langle i | v_{s,1} | j \rangle|^2 \delta(\omega - \varepsilon_i - \varepsilon_j) \quad (1.30)$$

Although the excitation energies ω_i and the oscillator strengths f_i can be obtained from our implementation, no photoabsorption calculations have been performed.

1.7.2 General multipole-multipole polarizabilities

If, instead of the dipole case considered above, one considers the reaction of a general molecular multipole moment q^{lm} , specified by the quantum numbers l , and m , to a general multipole electric field $E^{l'm'}$ the general multipole-multipole polarizability $\alpha_{mm'}^{ll'}$ is required:

$$q^{lm} = q_0^{lm} + \sum_{l'm'} \alpha_{mm'}^{ll'} E^{l'm'}. \quad (1.31)$$

In order to study such polarizabilities, we consider external fields of general multipole form [although in practice limited to the octupole ($l = 3$) case]:

$$\delta v_{\text{ext}}^{lm}(\mathbf{r}, \omega) = \sqrt{\frac{4\pi}{2l+1}} E r^l Z_{lm}(\hat{r}) \cos(\omega t), \quad (1.32)$$

where the function Z_{lm} stands for a real combination of spherical harmonics Y_{lm} .

1.7.3 Hyperpolarizabilities

The nonlinear response of a dipole moment to external electric fields is also considered in this thesis. This response is governed by the hyperpolarizability tensors. For the static case, the expansion of the dipole moment in different orders of the applied fields can be written as

$$\mu_i = \mu_i^{(0)} + \alpha_{ij} E_0^j + \frac{1}{2!} \beta_{ijk} E_0^j E_0^k + \frac{1}{3!} \gamma_{ijkl} E_0^j E_0^k E_0^l + \dots, \quad (1.33)$$

where summation over repeated indices is implied. In addition to the static linear polarizability tensor α , the nonlinear polarizability tensors (hyperpolarizability tensors) β , and γ

have been introduced, while $\mu_i^{(0)}$ is once more the i -th component of the permanent dipole moment. Frequency-dependent hyperpolarizability tensors β are calculated analytically in this thesis. The second and higher hyperpolarizabilities can be obtained from finite field differentiation of β . In principle, the determination of hyperpolarizabilities, in which general multipole moments and electric fields are involved, is no more difficult than the dipole case considered here. However, because of the limited, although growing, interest in such properties, the calculation of such multipole hyperpolarizabilities has not yet been implemented.

1.7.4 Van der Waals dispersion coefficients

The long-range interaction between two neutral spherically symmetric systems is dominated by an induced dipole-induced dipole interaction, governed by the isotropic Van der Waals dispersion coefficient C_6 :

$$E_{\text{disp}}(A, B) = \frac{C_6(A, B)}{R_{AB}^6}, \quad (1.34)$$

where R_{AB} is the distance between the systems A and B , and E_{disp} is called the dispersion energy. It can be shown[48, 45] that the dispersion coefficient C_6 can be calculated from the polarizabilities of the two monomers at *imaginary* frequencies $i\omega$:

$$C_6(A, B) = \frac{3}{\pi} \int_0^\infty \alpha_A(i\omega)\alpha_B(i\omega)d\omega. \quad (1.35)$$

At smaller separations R_{AB} , other dispersion effects also become important, originating from more general induced multipole-induced multipole interactions, and varying with distance as C_7/R^7 , C_8/R^8 , and so on. For the determination of these higher dispersion coefficients, one needs higher multipole-multipole polarizabilities than the simple dipole-dipole polarizabilities.

For systems which are not spherically symmetric, the dispersion energy depends not only on the distance between the two systems, but also their relative orientation, which can be described by a set of Euler angles for each molecule. The complicated equations for the most general case, where both the anisotropy of the dispersion interaction and the higher multipole coefficients are accounted for, can be found in Chapter 6, as well as in the original Refs.[49, 50].

Recently, proposals have been made to obtain the entire dispersion energy in a TDDFT framework and not only the long-range dispersion energy[33, 51]. This is an important topic in DFT, as the ground-state GGA functionals have great difficulties in calculating Van der Waals energies accurately. For example, the position and depth of the Van der Waals wells for weakly interacting systems are often poorly predicted. Such a TDDFT approach involves the determination of the full interacting response function at imaginary frequencies. Although expensive, this is in principle possible using our implementation. So far, this intriguing option has not been put to practice, however.

1.7.5 Geometrical derivatives

If one is not exclusively interested in a spectroscopic property at the equilibrium geometry, but also in the effect of nuclear vibrations on such a property, an expansion in terms of

normal vibration modes q_α of the molecule is useful. Taking the polarizability tensor as an example, we can write:

$$\alpha_{ij}(\omega) = \alpha_{ij}(\omega) |_0 + \sum_{\alpha} \left(\frac{\partial \alpha_{ij}(\omega)}{\partial q_{\alpha}} \right) |_0 q_{\alpha} + \frac{1}{2} \sum_{\alpha, \beta} \left(\frac{\partial^2 \alpha_{ij}(\omega)}{\partial q_{\alpha} \partial q_{\beta}} \right) |_0 q_{\alpha} q_{\beta} + \dots \quad (1.36)$$

Here, all derivatives have to be evaluated at the point 0 which is the equilibrium geometry, where all q_α are zero. In this Taylor expansion, the effect of small distortions from the equilibrium geometry are considered.

Similar to this expression for the linear polarizability, one can consider geometrical derivatives of the dipole moment μ , the hyperpolarizability tensors β , and γ , the excitation energies ε_i , the oscillator strengths f_i , and so on. The derivatives of the dipole moment $\partial\mu/\partial q_\alpha$ determine the infrared (IR) intensities[52], the polarizability derivatives determine the intensity and depolarization ratios of Raman scattering[53]. The derivatives of the hyperpolarizability tensors govern the hyper-Raman effect[53], and geometrical derivatives of excitation energies can be used in order to estimate the intensity of the resonance Raman effect, an example of which is given in [54, 55]. The oscillator strength derivatives are needed in the calculation of excitation spectra in which vibronic effects are important, such as in the C₆₀ and C₇₀ molecules[56].

Apart from these applications of the geometrical derivatives, they are also needed if the vibrational average of a quantity is required. Such a vibrationally averaged value corresponds more directly to the experimentally measured quantity than the value at the nuclear equilibrium geometry. Vibrational effects are usually of limited importance in linear polarizability studies, but can be very significant for hyperpolarizabilities [57, 58, 59, 60, 61]. Of all the possible applications mentioned here, only the case of Raman scattering is explicitly studied in this thesis, in Chapter 5.

The evaluation of geometrical derivatives, such as $\delta\alpha_{ij}/\delta q_\alpha$ can be performed analytically or by finite differentiation. Although the analytic approach is certainly possible[62], the finite difference technique has been used in our work, in keeping with the ADF implementation for the IR intensities. In this approach, one first evaluates the derivatives with respect to Cartesian nuclear displacements of the symmetry-unique atoms, which are afterwards transformed to normal coordinate derivatives. The disadvantage of this approach is that the number of derivatives which has to be evaluated increases linearly with system size.

1.8 Overview of the thesis

In order to present a general overview of our work in the beginning of the thesis, the chapters are not strictly given in the chronological order of publishing. In Chapter 2, a broad outline of our implementation is given, which does not enter the details of the equations, but considers general efficiency aspects.

In Chapter 3, published in *J. Chem. Phys.* **103**, 9347-9354 (1995) our first application of time-dependent DFT is presented. In this paper frequency-dependent dipole polarizabilities and C₆ Van der Waals dispersion coefficients were calculated in the adiabatic LDA. Both the isotropic and the anisotropic part of the polarizabilities and dispersion coefficients were

compared to literature values, and two semiempirical models were evaluated on the basis of our results. For the anisotropic polarizabilities and dispersion coefficients, the adiabatic LDA performed quite satisfactorily, but systematic overestimations were found for the isotropic parts.

In Chapter 4, this systematic overestimation was considered in more detail, and a solution was presented in the form of a model xc potential (the Van Leeuwen–Baerends potential, abbreviated as LB94) with correct Coulombic asymptotic behavior. In this paper, *J. Chem. Phys.* **105**, 3142-3151 (1996), it was shown that this simple correction to the LDA xc potential yields substantial improvements in average polarizabilities as well as in their frequency dependence, in comparison to the LDA results.

An application of TDDFT to Raman scattering, *Chem. Phys. Lett.* **259**, 599-604 (1996), is presented in Chapter 5. It is shown that LDA, GGA, and LB94 potentials all yield good results (comparing favorably to TDHF and SOPPA results) for Raman intensities and depolarization ratios for five diatomics.

In Chapter 6, *J. Chem. Phys.* **106**, 5091-5101 (1997), the generalization of Chapter 3 to general multipole-multipole polarizabilities and related dispersion coefficients is considered. Both isotropic and anisotropic quadrupole-quadrupole polarizabilities and C_6 , C_7 , and C_8 dispersion coefficients were calculated. For the higher multipole polarizabilities, the importance of a correct description of the outer region of the molecule increases. For this reason, the overestimation given by the LDA and GGA potentials grows and it becomes more important to use a potential with correct asymptotic behavior, such as the LB94 potential. The results obtained with the LB94 potential are again satisfactory.

In Chapter 7, published in *Phys. Rev. Lett.* **78**, 3097-3100 (1997), the first TDDFT calculation of a frequency-dependent molecular hyperpolarizability is presented. The hyperpolarizability of C_{60} was chosen for this study, because of the large discrepancies between the various available experimental and semiempirical results. Our results strongly support the most recent experimental findings and are in qualitative agreement with Hartree–Fock calculations which appeared a few months later.

In Chapter 8, *Phys. Rev. A* **57**, 2556-2571 (1998), the relative importance of the approximations for the xc potential and the xc kernel, which both enter the linear response equations, is evaluated. To this end, we use accurate xc potentials, obtained from reliable *ab initio* densities, in order to remove one of the two approximations. From our results for atomic excitation energies and atomic as well as molecular polarizabilities, we conclude that usually improvements to the xc potential are more important than improvements to the xc kernel.

The theory underlying the efficient calculation of hyperpolarizabilities could only be presented very briefly in Chapter 7. A more technical and complete account is given in Chapter 9, *submitted for publication*, dealing with the theoretical and technical aspects of frequency-dependent hyperpolarizability calculations in the DFT framework.

Finally, summaries in English and Dutch, acknowledgements, a list of publications, and the bibliography are given.

Chapter 2

Implementation of time-dependent density functional response equations

2.1 Abstract

Time-dependent density functional theory provides a first principles method for the calculation of frequency-dependent polarizabilities, hyperpolarizabilities, excitation energies and many related response properties. In recent years, the molecular results obtained by several groups have shown that this approach is in general more accurate than the time-dependent Hartree–Fock approach, and is often competitive in accuracy with computationally more demanding conventional *ab initio* approaches. In this paper, our implementation of the relevant equations in the Amsterdam Density Functional program is described. We will focus on certain aspects of the implementation which are necessary for an efficient evaluation of the desired properties, enabling the treatment of large molecules. Such an efficient implementation is obtained by: using the full symmetry of the molecule, using a set of auxiliary functions for fitting the (zeroth- and first-order) electron density, using a highly vectorized and parallelized code, using linear scaling techniques, and, most importantly, by solving the response equations iteratively.

2.2 General introduction

In Density Functional Theory (DFT), based on the seminal papers by Hohenberg and Kohn[1] and Kohn and Sham[3], the electron density is obtained exactly from a single-particle equation for an electron moving in an effective field of the other electrons. This effective field can be subdivided into the Coulomb field of the nuclei, the Coulomb or Hartree term which comes from the Coulomb interaction of the electron with the electron density and finally, the unknown exchange-correlation (xc) potential. This xc potential contains all the many-body effects, and has to be approximated for practical applications. Important approximations are the Local Density Approximation (LDA), in which it is assumed that, locally, the quantum system under study can be approximated by a homogeneous electron gas. Although this might not seem appropriate for atoms and molecules, the LDA has been remarkably success-

ful. More recently, the generalized gradient approximations (GGAs), have been developed. Instead of taking only the electron density into account, as in the LDA, the gradient of the density is also considered. This has led to important improvements in accuracy with respect to the LDA. With these functionals, accurate results for such properties as binding energies, molecular geometries, and vibrational frequencies can be obtained.

However, ordinary DFT is restricted to ground-state problems. Excitation energy calculations within ground-state DFT are possible, through so-called Δ SCF techniques[63, 64, 65, 66], but the theoretical basis is less solid than for ordinary ground-state properties, and several nontrivial theoretical complications make this approach less appealing than the time-dependent DFT approach to excitation energies described here. Important properties such as frequency-dependent polarizabilities and hyperpolarizabilities, their derivatives with respect to vibrational modes of the molecule, as well as Van der Waals dispersion coefficients, are either not at all accessible or not easily accessible through ground-state DFT. For this reason, the development of time-dependent DFT in the beginning of the previous decade[9, 26, 27, 67, 23, 11, 12, 19, 68, 69, 70, 71, 72, 30, 16, 73], represented an important extension of DFT, for which the rigorous theoretical basis was given by Runge and Gross[38]. Until recently, however, calculations on frequency-dependent optical response were performed for atomic and solid state systems only.

This situation has changed by now, partly because of the growing interest of quantum chemists in DFT, partly because of the increasing know-how on molecular response calculations. At the moment, both by ourselves[34, 74, 75, 76, 77, 78, 79] and in other groups[37, 80, 81, 35, 82, 83, 84, 85, 86, 87] implementations of the linear (and nonlinear) DFT response equations for molecules have been accomplished. In this work, our own implementation will be described. Because the applied techniques are not restricted to our own implementation, which we have named ADF-RESPONSE[88], but have also been used or can also be used in other codes, this work may also prove useful for improved understanding of other implementations.

The calculations can be split into two types in a natural way. The calculation of excitation energies and oscillator strengths is equivalent to the solution of an eigenvalue problem. The calculation of a frequency-dependent polarizability α or first hyperpolarizability β is equivalent to the solution of one or several sets of linear equations. Furthermore, the geometrical derivatives of these properties can be determined, by evaluating the derivatives through finite difference techniques, in which the response calculations are performed in a loop over different molecular geometries. The derivatives give access to such properties as Raman scattering[75], resonance Raman scattering, and hyper-Raman scattering. However, because the outer loop over molecular geometries poses no separate problems, our description will be limited to the two basic types of calculation mentioned above. For each of these, one has the choice between an iterative and a direct solution. As the iterative solution is less demanding both in memory and in CPU requirements, we will focus on the iterative approach. The direct solution of the eigenvalue or linear equations is feasible for small systems only.

In the quantum chemical programs in which the molecular time-dependent DFT calculations have been performed, one uses either Gaussian or Slater-type orbitals (GTOs or STOs), centered on the atoms. The GTOs have useful properties, which allow for an efficient, ana-

lytical, evaluation of Coulomb type integrals. The STOs resemble the atomic orbitals more closely, because of their cusp at the nucleus and their slower decay in the outer region of the atom. For this reason, the number of STOs required for a calculation of a certain accuracy is usually considerably smaller than the number of GTOs. The Amsterdam Density Functional program (ADF) [89, 90, 91], in which our implementation of the response equations has been performed, uses STOs, in contrast to most other molecular DFT codes.

The one-particle eigenfunctions which appear in ground-state DFT, are called the Kohn–Sham (KS) orbitals, being solutions to the KS equations. One can choose to evaluate the matrix elements which appear in the response equations between these KS orbitals (eigenfunctions) or between the primitive, atom-centered, GTO or STO basis orbitals, the Atomic Orbitals (AOs) which form the basis into which the KS orbitals are expanded. The first option has the advantage that the molecular symmetry can be fully exploited, with dramatic savings in memory and in CPU time for highly symmetric systems. The AO approach, on the other hand, provides the opportunity to make use of distance effects. This is due to the fact that integrals which depend on the overlap of two AOs centered on nuclei which are far apart are negligible and need not be calculated. This approach is therefore better suited for large systems of low symmetry. The advantages and disadvantages of both approaches will be discussed below, together with additional efficiency aspects of the implementation that have not yet been mentioned.

The outline of the rest of this paper is as follows. First, the properties under consideration are briefly introduced, after which the theoretical basis of our approach, formed by the time-dependent Kohn–Sham(TDKS) equations in the density functional framework, is presented. We continue by introducing the linear response equations which can be obtained from a perturbative expansion of the TDKS equations, and which give access to the frequency-dependent polarizabilities and excitation energies. Finally we turn to a discussion of how these response equations can be solved efficiently, focusing on the matrix-vector multiplication which is the most time consuming part of both the excitation energy and polarizability calculations.

2.3 Description of desired properties

In this section, the properties we are trying to calculate are introduced. The molecular dipole moment μ_i in Cartesian direction i can be expanded in different orders of applied static external electric fields E_0^j, E_0^k, E_0^l , in directions j, k, l :

$$\mu_i = \mu_i^{(0)} + \alpha_{ij} E_0^j + \frac{1}{2!} \beta_{ijk} E_0^j E_0^k + \frac{1}{3!} \gamma_{ijkl} E_0^j E_0^k E_0^l + \dots, \quad (2.1)$$

where here, and in the following, summation over repeated indices is implied. The static linear polarizability tensor α , and the nonlinear polarizability tensors (hyperpolarizability tensors) β , and γ have been introduced here, while $\mu_i^{(0)}$ is the i -th component of the permanent dipole moment.

In the present paper we will be dealing mainly with the simplest and most important case, in which only the change in the *dipole* moment is considered due to perturbations of

electric *dipole* fields. In a more complete formulation, one considers the effect of general multipolar electric fields, which act not only on the dipole moment, but also on the quadrupole, octupole, and higher multipole moments of the molecule. This leads to the definition of general multipole-multipole polarizabilities and hyperpolarizabilities. We have discussed the case of multipole-multipole polarizabilities in more detail in a previous paper[77], in which calculations of the more general multipole-multipole polarizabilities and the Van der Waals dispersion coefficients which are related to them have been presented. Here, we will restrict ourselves to the dipole case for the sake of readability.

If the applied electric fields are small, the magnitude of the change in the dipole moment depends linearly on the electric field strength, and the behavior of the system is consequently determined by the linear polarizability tensor α . For larger fields (for example strong laser fields), the first hyperpolarizability tensor β , the second hyperpolarizability tensor γ , and even higher-order tensors may become important. If the applied field becomes much larger still, the Taylor expansion does not converge anymore, and a nonperturbative approach is called for. A similar expansion could be given for the total energy, which is an equivalent formulation in case the so-called Hellmann–Feynman theorem[92, 93] holds, which is the case in DFT.

The equation above is valid for static electric fields. In order to describe the usual experimental situation in which the external electric fields are frequency-dependent, the equation has to be extended. Expanding the dipole moment, which becomes time-dependent now, in orders of electric fields with a static and a frequency-dependent component $E = E_0 + E_\omega \cos(\omega t)$ in directions i, j, k, \dots , we get a more general form of the static equation above[94]:

$$\begin{aligned} \mu_i(t) &= \mu_i^{(0)} + \alpha_{ij}(0;0)E_0^j + \alpha_{ij}(-\omega;\omega)E_\omega^j \cos(\omega t) + \frac{1}{2}\beta_{ijk}(0;0,0)E_0^j E_0^k \\ &+ \frac{1}{4}\beta_{ijk}(0;\omega,-\omega)E_\omega^j E_\omega^k + \beta_{ijk}(-\omega;0,\omega)E_0^j E_\omega^k \cos(\omega t) \\ &+ \frac{1}{4}\beta_{ijk}(-2\omega;\omega,\omega)E_\omega^j E_\omega^k \cos(2\omega t) + \dots, \end{aligned} \quad (2.2)$$

where a widely used notation has been used for α , and β . The frequencies after the semi-colon refer to the frequencies of the applied electric fields, while the sum of these frequencies is placed in front of the semi-colon, with a minus sign. The sum frequencies determine the time dependence of the dipole moment.

We note in passing that this expression is valid for molecular systems at small ω values, where no absorption occurs. In case absorption needs to be included in the treatment, for example in periodic systems, a generalization is needed in which also terms behaving as $\sin(\omega t)$ occur, describing a time dependence of the dipole moment which is out of phase with the time dependence of the perturbation.

In first order, the dipole moment acquires a time dependence of the same frequency as the applied field. In higher order, more interesting effects become visible, such as Second Harmonic Generation (SHG), which is governed by the tensor $\beta(-2\omega;\omega,\omega)$, the final term in Equation (2.2). In that case, the dipole moment oscillates with a frequency twice as high as the frequency of the external electric field.

The frequency-dependent polarizability is directly related to (vertical) excitation energies ω_i , oscillator strengths f_i , and transition dipole moments μ_i [45]:

$$\alpha_{\text{av}}(-\omega; \omega) = \sum_i \frac{f_i}{\omega_i^2 - \omega^2} = \frac{2}{3} \sum_i \frac{\omega_i \mu_i^2}{\omega_i^2 - \omega^2} \quad (2.3)$$

where α_{av} is the average polarizability, equal to the average of the α_{xx} , α_{yy} , and α_{zz} components. From this equation it is clear that the poles of the polarizability tensor are directly related to the exact excitation energies. Although only the dipole-allowed and spin-allowed transitions have a nonzero contribution in this summation, the TDDFT approach allows the determination of triplet excitation energies, as well as excitation energies with zero oscillator strength. In the next section, the theoretical basis, upon which our determination of these properties rests, will be described.

2.4 The time-dependent Kohn–Sham equations

Ground-state DFT is based on the papers by Hohenberg and Kohn[1] and by Kohn and Sham[3]. The main result is that the density of a system is identical to the density of an associated noninteracting particle system moving in a *local* potential $v_s(\mathbf{r})$, defined by the Kohn–Sham equations (atomic units are used throughout):

$$\left[-\frac{\nabla^2}{2} + v_s[\rho](\mathbf{r}) \right] \phi_i(\mathbf{r}) = \varepsilon_i \phi_i(\mathbf{r}). \quad (2.4)$$

Here the local potential $v_s[\rho](\mathbf{r})$ is the so-called Kohn–Sham potential, consisting of the external potential v_{ext} (the Coulomb field of the nuclei and external fields if present), the Hartree potential v_H , which is trivially calculated from the density, and the xc potential v_{xc} , which is the only unknown part:

$$v_s(\mathbf{r}) = v_{\text{ext}}(\mathbf{r}) + v_H(\mathbf{r}) + v_{\text{xc}}(\mathbf{r}). \quad (2.5)$$

The Kohn–Sham orbitals ϕ_i move in the effective field v_s , which depends upon the electron density $\rho(\mathbf{r})$. This density is exactly obtained by summing the squares of the Kohn–Sham orbitals and multiplying by their occupation numbers n_i :

$$\rho(\mathbf{r}) = \sum_i^{\text{occ}} n_i |\phi_i(\mathbf{r})|^2. \quad (2.6)$$

As the KS potential $v_s(\mathbf{r})$ and the density $\rho(\mathbf{r})$ are interdependent, the equations have to be solved in a Self-Consistent Field (SCF) scheme, which means that one iteratively adapts the effective potential v_s and the density ρ until the difference in, for example, the energy between two subsequent cycles is sufficiently small. In the most straightforward fashion, this can be performed by mixing the density of the previous cycle with a (small) part of the density in the present cycle. This "simple damping" approach usually converges very slowly, and in practice the Direct Inversion in the Iterative Subspace (DIIS) procedure by Pulay

and co-workers[95, 96] is much to be preferred. In the DIIS approach, not only the result of the previous cycle, but the results of all, or many, previous cycles are taken into account, in order to obtain the optimal guess for the next cycle. If one is close to self-consistency, this procedure converges quadratically. Using DIIS, it typically takes about five to fifteen cycles to converge the SCF equations above.

In order to solve the KS equations an approximation for the xc potential $v_{xc}(\mathbf{r})$ is required, the simplest one being the LDA, based upon the local density of the system. The GGAs go beyond this and take the local gradient of the density into account as well, allowing for a much improved accuracy in the results for energies and geometries. Many other approximations, for example those based directly on the KS orbitals, are available.

The usual ground-state DFT scheme enables one to determine the density, and consequently the dipole moment, of a molecule with or without external electric fields. This affords the determination of the *static* polarizability and hyperpolarizability tensors α , β , and γ , by performing calculations in small electric fields of varying magnitudes and directions. In this so-called finite-field (FF) approach, the tensors are then determined from finite difference techniques. The main advantage of this approach is that no programming work is needed. Any standard DFT code will allow the determination of static properties in this manner. However, for the determination of higher-order tensors, such as γ , one needs very well-converged solutions to the KS equations in order to make reliable predictions, which may be technically hard to achieve and which will certainly lead to considerable increases in CPU time. A further disadvantage of this approach is the fact that results for many different electric fields have to be combined in case all components of a certain tensor are required, which, if not automated, costs additional human time.

The most fundamental disadvantage of the FF approach, however, is that one has access to static properties only. The *frequency-dependent* polarizability and hyperpolarizability tensors are not accessible. Excitation energies and oscillator strengths can also not be obtained from FF calculations. This is an important drawback of the FF approach, as it makes a direct comparison with experimental results impossible. Especially for hyperpolarizabilities it is known that there are substantial differences between the frequency-dependent and zero frequency results.

If one is interested in the time-dependent properties mentioned above, a time-dependent theory is required. In the DFT framework, this means that one has to start from the time-dependent KS (TDKS) equations as derived by Runge and Gross[38]:

$$i\frac{\partial}{\partial t}\phi_i(\mathbf{r}, t) = \left[-\frac{\nabla^2}{2} + v_s(\mathbf{r}, t)\right]\phi_i(\mathbf{r}, t) \equiv F_s\phi_i(\mathbf{r}, t). \quad (2.7)$$

The time-dependent KS potential $v_s(\mathbf{r}, t)$ is subdivided in the same manner as its static counterpart:

$$v_s(\mathbf{r}, t) = v_{\text{ext}}(\mathbf{r}, t) + v_H(\mathbf{r}, t) + v_{xc}(\mathbf{r}, t), \quad (2.8)$$

the Hartree potential being explicitly given by:

$$v_H(\mathbf{r}, t) = \int d\mathbf{r}' \frac{\rho(\mathbf{r}', t)}{|\mathbf{r} - \mathbf{r}'|}, \quad (2.9)$$

and the time-dependent xc potential $v_{xc}[\rho](\mathbf{r}, t)$ being an unknown functional of the time-dependent density $\rho(\mathbf{r}, t)$, now given by:

$$\rho(\mathbf{r}, t) = \sum_i^{\text{occ}} n_i |\phi_i(\mathbf{r}, t)|^2 . \quad (2.10)$$

If a certain approximation for the time-dependent xc potential $v_{xc}(\mathbf{r}, t)$ has been chosen, the TDKS equations can be solved iteratively, to yield the time-dependent density of a system, which may be exposed to an external time-dependent electric field. If one is interested in effects due to extremely large laser fields, the perturbative expansion of the dipole moment becomes meaningless, and the TDKS equations have to be solved nonperturbatively. This has until now been performed for atoms, by Ullrich and Gross[97, 98, 33], and more recently also by others[99], and gives access to such effects as higher harmonic generation (HHG), which are not accessible in a perturbative approach. The drawback of this is that the calculations are very time consuming, forbidding the treatment of medium-sized molecules. If one restricts oneself to properties which are accessible through perturbative methods, as we will do here, a much more efficient approach is possible, allowing the treatment of large molecules (> 100 atoms). This approach will be the subject of the next section. For more information on time-dependent DFT in general, the reader is referred to the excellent reviews by Gross and coworkers[31, 32, 33]. A review paper which is more focussed on quantum chemistry is given by Casida[37].

2.5 Perturbative solution to time-dependent Kohn–Sham equations

The linear response equations which have to be solved can be presented in several equivalent ways[31, 34, 37, 79]. Here, we adopt a notation close to that of our original paper[34] on the calculation of frequency-dependent polarizabilities and to that of Casida[37]. As we will focus mainly on efficiency matters in this work, only the first-order perturbed equations will be discussed. In another paper[79], we have indicated in detail how the first hyperpolarizability tensors $\beta_{ijk}(-\omega_\sigma; \omega_j, \omega_k)$ can immediately be obtained from the solutions to these first-order equations. The techniques which are needed for the determination of the hyperpolarizabilities are the same as those for the polarizabilities discussed here.

As our working equations have been derived from first principles several times[31, 32, 33, 34, 37], these equations will be presented without derivation, after which the most time consuming parts of the calculations will be discussed in detail. In the following, real orbitals will be used and the complex conjugate signs will be discarded. Although the spin index σ will be kept at the start, the discussion will later be narrowed down to the spin-restricted case where $\phi_{i\uparrow}(\mathbf{r}) = \phi_{i\downarrow}(\mathbf{r})$. In this manner, it will be easier to focus on those aspects of the theory which are relevant to the present discussion.

For a linear polarizability calculation, the first-order change in the time-dependent density ρ_σ , of the spin σ electrons, which will depend on the frequency ω of the external electric field, has to be determined. In terms of products of occupied KS orbitals $\phi_{i\sigma}(\mathbf{r})$ with virtual

KS orbitals $\phi_{a\sigma}(\mathbf{r})$, the first-order density can be written as:

$$\rho_{\sigma}^{(1)}(\mathbf{r}, \omega) = \sum_{i,a} [P_{ia}^{\sigma}(\omega)\phi_{a\sigma}(\mathbf{r})\phi_{i\sigma}(\mathbf{r}) + P_{ai}^{\sigma}(\omega)\phi_{a\sigma}(\mathbf{r})\phi_{i\sigma}(\mathbf{r})], \quad (2.11)$$

P being the first-order density matrix on eigenfunction basis. As the zeroth-order density of Equation (2.6) (the converged SCF density which comes out of an ordinary ground-state DFT calculation) only contains products of occupied orbitals, the first-order density can be written exclusively in terms of products of occupied and virtual orbitals. For this reason, only components P_{ai} or P_{ia} are nonzero and have been included in the summation (where, at variance with our earlier work[34], we have adopted the usual convention that a denotes a virtual orbital, while i stands for an occupied orbital). Using the expansion of the KS orbitals in the AO basis [$\phi_{i\sigma}(\mathbf{r}) = \sum_{\mu} C_{\mu i}^{\sigma}\chi_{\mu}(\mathbf{r})$], the first-order density can also be transformed to AO basis:

$$\rho_{\sigma}^{(1)}(\mathbf{r}, \omega) = \sum_{\mu\nu} P_{\mu\nu}^{\sigma}(\omega)\chi_{\mu}(\mathbf{r})\chi_{\nu}(\mathbf{r}). \quad (2.12)$$

Later, we shall show that the scaling of the calculations can be improved from N^4 to N^3 by making use of an additional set of functions $\{f_i\}$, called the auxiliary basis set or fit set, in terms of which $\rho_{\sigma}^{(1)}$ can be expressed as:

$$\rho_{\sigma}^{(1)}(\mathbf{r}, \omega) \approx \sum_i a_i^{\sigma}(\omega)f_i(\mathbf{r}). \quad (2.13)$$

All three expressions for the first-order density will be used. It should be emphasized that Equations (2.11) and (2.12) are equivalent, while an additional approximation is introduced in Equation (2.13). The severity of this approximation depends upon the quality of the fit set (which, like the AO basis, is an atom-centered set of STOs in our case).

By expanding the KS equations to first order in the applied field, it can be shown that the first-order density, as determined by the density matrix elements in KS orbital basis, can be obtained from the solution of the following set of linear equations for the density matrix elements P_{jb}^{σ} and P_{bj}^{σ} [37, 86, 100]:

$$\begin{aligned} \sum_{jb\tau} [\delta_{\sigma\tau}\delta_{ij}\delta_{ab}(\varepsilon_{a\sigma} - \varepsilon_{i\sigma} + \omega) + K_{ia\sigma,jb\tau}] P_{jb}^{\tau} + \sum_{jb\tau} K_{ia\sigma,bj\tau} P_{bj}^{\tau} &= -[\delta v_{\text{ext}}]_{ia\sigma} \\ \sum_{jb\tau} [\delta_{\sigma\tau}\delta_{ij}\delta_{ab}(\varepsilon_{a\sigma} - \varepsilon_{i\sigma} - \omega) + K_{ai\sigma,bj\tau}] P_{bj}^{\tau} + \sum_{jb\tau} K_{ai\sigma,jb\tau} P_{jb}^{\tau} &= -[\delta v_{\text{ext}}]_{ai\sigma} \end{aligned} \quad (2.14)$$

where δ_{ij} is the Kronecker delta, ω is the frequency of the applied field, $\varepsilon_{a\sigma}$ and $\varepsilon_{i\sigma}$ are KS spin orbital energies, and where the matrix elements of the external electric fields are given by

$$[\delta v_{\text{ext}}]_{ia\sigma} = [\delta v_{\text{ext}}]_{ai\sigma} = \int d\mathbf{r} \phi_{i\sigma}(\mathbf{r}) \delta v_{\text{ext}}(\mathbf{r}) \phi_{a\sigma}(\mathbf{r}). \quad (2.15)$$

The external potential can be of general multipole form, labeled with the quantum numbers l and m [77]:

$$\delta v_{\text{ext}}^{lm}(\mathbf{r}, \omega) = \sqrt{\frac{4\pi}{2l+1}} E r^l Z_{lm}(\hat{r}) \cos(\omega t), \quad (2.16)$$

where the function Z_{lm} stands for a real combination of spherical harmonics Y_{lm} . In the present paper, we will restrict ourselves to the dipole case ($l = 1$), for which the functions Z_{lm} simply reduce to x , y , and z .

The four-index matrix K , the so-called coupling matrix, consists of a Coulomb (or Hartree) part and an xc part

$$K_{ij\sigma,kl\tau} = K_{ij\sigma,kl\tau}^{\text{Coul}} + K_{ij\sigma,kl\tau}^{\text{xc}}, \quad (2.17)$$

given by:

$$K_{ij\sigma,kl\tau}^{\text{Coul}} = \int d\mathbf{r} \int d\mathbf{r}' \phi_{i\sigma}(\mathbf{r}) \phi_{j\sigma}(\mathbf{r}) \frac{1}{|\mathbf{r} - \mathbf{r}'|} \phi_{k\tau}(\mathbf{r}') \phi_{l\tau}(\mathbf{r}'), \quad (2.18)$$

and

$$K_{ij\sigma,kl\tau}^{\text{xc}}(\omega) = \int d\mathbf{r} \int d\mathbf{r}' \phi_{i\sigma}(\mathbf{r}) \phi_{j\sigma}(\mathbf{r}) f_{\text{xc}}^{\sigma\tau}(\mathbf{r}, \mathbf{r}', \omega) \phi_{k\tau}(\mathbf{r}') \phi_{l\tau}(\mathbf{r}'). \quad (2.19)$$

Here, we have introduced the Fourier-transform of the so-called xc kernel f_{xc} , which is the functional derivative of the time-dependent xc potential for the spin- σ electrons $v_{\text{xc}}^{\sigma}(\mathbf{r}, t)$ with respect to the time-dependent density of the spin- τ electrons $\rho_{\tau}(\mathbf{r}', t')$:

$$f_{\text{xc}}^{\sigma\tau}(\mathbf{r}, \mathbf{r}', t - t') = \frac{\delta v_{\text{xc}}^{\sigma}(\mathbf{r}, t)}{\delta \rho_{\tau}(\mathbf{r}', t')}. \quad (2.20)$$

This kernel determines the first-order change in the time-dependent xc potential due to the applied electric perturbation. In this work, we will restrict ourselves to the so-called Adiabatic LDA (ALDA) to this kernel, in which this complicated functional is reduced to a spatially local, frequency-independent, real function, evaluated at the local SCF density $\rho_0(\mathbf{r})$:

$$f_{\text{xc}}^{\text{ALDA},\sigma\tau}(\mathbf{r}, \mathbf{r}', \omega) = \delta(\mathbf{r} - \mathbf{r}') \frac{dv_{\text{xc}}^{\text{LDA},\sigma}}{d\rho_{\tau}} \Big|_{\rho_{\tau}=\rho_{0,\tau}(\mathbf{r})}. \quad (2.21)$$

In the adiabatic approximation it is assumed that the functional derivative in Equation (2.20) is nonzero only for $t = t'$, which can only be expected to be true for slow time-dependent processes. Practice shows however[78] that the adiabatic approximation is probably much less severe than other approximations, such as the approximation for the ground-state xc potential, which determines the KS orbitals ϕ_i and one-electron energies ε_i , and the other approximation in Equation (2.21), namely the approximation of spatial locality, which is not present in more elaborate approximations for the xc kernel[101].

We consider the response due to a real spin-independent external perturbation δv_{ext} . If we restrict ourselves to the real density response (which is sufficient for (hyper)polarizabilities, excitation energies, and oscillator strengths) it is possible to simplify Equations (2.14) considerably by making use of the symmetry properties of the coupling matrix K . In case the ALDA is used one has that, because of the choice for real KS orbitals, $K_{ia\sigma,jb\tau} = K_{ia\sigma,bj\tau}$. When this is substituted in Equation (2.14), one obtains for the real parts $\text{Re}\delta P_{jb}^{\tau} = 1/2(P_{jb}^{\tau} + P_{bj}^{\tau})$

of the density matrix elements, after some algebra¹:

$$\sum_{bj\tau} \left[\delta_{\sigma\tau} \delta_{ab} \delta_{ij} (\varepsilon_i - \varepsilon_a) - 2K_{ia\sigma, jb\tau} - \omega^2 \frac{\delta_{\sigma\tau} \delta_{ab} \delta_{ij}}{(\varepsilon_i - \varepsilon_a)} \right] (\text{Re} \delta P_{jb}^\tau)(\omega) = [\delta v_{\text{ext}}(\omega)]_{ia\sigma}, \quad (2.22)$$

which can be written in vector notation as:

$$[\Delta - 2K](\text{Re} \delta P) = \delta v_{\text{ext}}, \quad (2.23)$$

where the matrix Δ is a trivial diagonal matrix: $\Delta_{ia\sigma, jb\tau} = \delta_{\sigma\tau} \delta_{ij} \delta_{ab} [(\varepsilon_i - \varepsilon_a) - \omega^2 / (\varepsilon_i - \varepsilon_a)]$. It is important to stress that this matrix equation is now half the size of the previous ones in Equation (2.14), with vectors of length $N_{\text{occ}} \times N_{\text{virt}}$ instead of $2N_{\text{occ}} \times N_{\text{virt}}$ (N_{occ} and N_{virt} being equal to the number of occupied and virtual orbitals, respectively). This makes the TDDFT response equations simpler than the related TDHF equations for which the equality $K_{ia\sigma, jb\tau} = K_{ia\sigma, bj\tau}$ does not hold[37].

The real part of the first-order density matrix P , obtained from the solution of the linear Equations (2.23), gives access to the frequency-dependent polarizability[31, 34, 104]. At an excitation energy, a finite external perturbation δv_{ext} leads to an infinite change in the density matrix P in Equation (2.23). This implies that the matrix $\Delta - 2K$ will possess a zero eigenvalue at the excitation energy. This leads, after a unitary transformation, to the following eigenvalue equation from which the excitation energies and oscillator strengths can be obtained[37, 35, 100]:

$$\Omega \mathbf{F}_i = \omega_i^2 \mathbf{F}_i, \quad (2.24)$$

where the components of the four-index matrix Ω are given by:

$$\Omega_{ia\sigma, jb\tau} = \delta_{\sigma\tau} \delta_{ij} \delta_{ab} (\varepsilon_a - \varepsilon_i)^2 + 2\sqrt{(\varepsilon_a - \varepsilon_i)} K_{ia\sigma, jb\tau} \sqrt{(\varepsilon_b - \varepsilon_j)}. \quad (2.25)$$

The desired excitation energies are equal to ω_i , and the oscillator strengths are obtained from the eigenvectors \mathbf{F}_i [37]. For a spin-restricted calculation, the Ω -matrix can be split in two separate singlet and triplet parts Ω^{S} and Ω^{T} , by performing a unitary transformation on the density matrix elements P_{ia}^σ [86, 105, 100]:

$$\begin{aligned} u_{ia} &= \frac{1}{\sqrt{2}} (P_{ia}^\uparrow + P_{ia}^\downarrow) \\ v_{ia} &= \frac{1}{\sqrt{2}} (P_{ia}^\uparrow - P_{ia}^\downarrow), \end{aligned} \quad (2.26)$$

in which spin-flip processes (for the triplet excitation energies) are separated from the processes which keep the total spin unchanged (singlet excitation energies). This leads to the following forms for the singlet and triplet Ω -matrices [105, 86, 100]:

$$\begin{aligned} \Omega_{ia, jb}^{\text{S}} &= \delta_{ij} \delta_{ab} (\varepsilon_a - \varepsilon_i)^2 + 2\sqrt{(\varepsilon_a - \varepsilon_i)} \times 2 \left[K_{ij, kl}^{\text{Coul}} + \frac{1}{4} (f_{\text{xc}}^{\uparrow\uparrow} + f_{\text{xc}}^{\downarrow\downarrow} + f_{\text{xc}}^{\uparrow\downarrow} + f_{\text{xc}}^{\downarrow\uparrow}) \right] \sqrt{(\varepsilon_b - \varepsilon_j)}. \\ \Omega_{ia, jb}^{\text{T}} &= \delta_{ij} \delta_{ab} (\varepsilon_a - \varepsilon_i)^2 + 2\sqrt{(\varepsilon_a - \varepsilon_i)} \times 2 \left[\frac{1}{4} (f_{\text{xc}}^{\uparrow\uparrow} + f_{\text{xc}}^{\downarrow\downarrow} - f_{\text{xc}}^{\uparrow\downarrow} - f_{\text{xc}}^{\downarrow\uparrow}) \right] \sqrt{(\varepsilon_b - \varepsilon_j)}, \end{aligned} \quad (2.27)$$

¹The set of equations (2.14) can be transformed in a set of equations for $P_{jb}^\tau + P_{bj}^\tau$ and $P_{jb}^\tau - P_{bj}^\tau$ by respectively adding and subtracting the two equations. By combining the new coupled equations, the equation for the real density response is obtained. All this proceeds in a manner quite similar to time-dependent Hartree-Fock theory[102, 103] and can be written down in the familiar time-dependent Hartree-Fock language[37, 86].

where $f_{xc}^{\sigma\tau}$ stands for the functional derivative $\delta v_{xc}^\sigma / \delta \rho_\tau$, and where $\frac{1}{4} (f_{xc}^{\uparrow\uparrow} + f_{xc}^{\downarrow\downarrow} + f_{xc}^{\downarrow\uparrow} + f_{xc}^{\uparrow\downarrow})$ is equal to the spin-restricted kernel $f_{xc} = \delta v_{xc} / \delta \rho$.

The triplet equivalent $\frac{1}{4} (f_{xc}^{\uparrow\uparrow} + f_{xc}^{\downarrow\downarrow} - f_{xc}^{\downarrow\uparrow} - f_{xc}^{\uparrow\downarrow})$ is usually named G_{xc} [105] and can be obtained from the derivative of the xc energy density of the homogeneous electron gas with respect to the spin-polarization parameter ζ [105, 106, 107]. These singlet and triplet matrices can be diagonalized separately. For a spin-unrestricted calculation, a similar procedure would give rise to more general spin states, but that case is not considered here.

Let us consider the equations for the excitation energies and for the polarizability in more detail. In both cases, a direct solution is possible in principle. This requires calculating and storing all matrix elements of the coupling matrix K , however. For this four-index matrix, this implies storing $N_{occ}^2 \times N_{virt}^2$ matrix elements, which becomes unfeasible for a typical calculation with more than 1000 basis functions. Apart from the memory requirements, the CPU time also gets out of hand with this approach. Both the solution of the set of linear equations and the solution of the eigenvalue problem would require a number of floating point operations which would scale as $N_{occ}^3 \times N_{virt}^3$. Again, this is very forbidding for large molecules or basis sets.

An alternative and preferable approach is to solve the equations iteratively, as was already stressed by Olsen and coworkers[108] for the similar (multiconfiguration) Hartree–Fock case. For the solution of the linear equations, one typically uses conjugate gradient techniques. We have previously explained the details of our approach[34], which is based upon the DIIS procedure[95, 96] mentioned above, also used in the iterative solution for the ground-state KS equations[91]. For the iterative solution of the eigenvalue equation, one has to make a restriction to a few selected eigenvalues, usually the lowest excitation energies. We employ the Davidson algorithm[109, 110, 111], which has been shown to be very efficient[108]. One particular implementation of this algorithm has earlier been described in this journal[112].

In the iterative solution for the polarizability, one tries to find accurate trial vectors for the density matrix P , which solve the set of linear Equations (2.14) to within a certain threshold. For the eigenvalue equation in Equation (2.24), the aim is to find accurate approximations to the eigenvectors \mathbf{F}_i . In both cases an initial guess for P or \mathbf{F}_i is needed. One can use the approximation $K = 0$ as a reliable starting point. For the polarizability calculation this initial guess for the density matrix yields the so-called "uncoupled" polarizability, which is usually a fair estimate of the converged result, the "coupled" polarizability. In the excitation energy calculation, the excitation energies in the first cycle are equal to the differences between eigenvalues of occupied and unoccupied KS orbitals. This is known[113] to be a good approximation in many cases, and is explicitly used as a "zeroth-order" approximation for the excitation energy in the approach by Petersilka and Gross[101, 105].

Both iterative procedures require the results of repeated matrix-vector multiplications (in our case the matrix is K , the diagonal Δ -matrix being trivial), without the need for storing or even knowing the individual matrix elements. The key problem has thus been reduced to the construction of an efficient routine for performing the matrix-vector multiplication $K \cdot p$. The efficient implementation of such a matrix-vector multiplier is the subject of the following section.

2.6 Efficient implementation of matrix-vector multiplication

As mentioned, almost all of the CPU time in the response calculations resides in the matrix-vector multiplication $K \cdot p$, where K is the square coupling matrix, with Coulomb and xc parts, and p is a vector of length $N_{\text{occ}} \times N_{\text{virt}}$. This matrix-vector product occurs both in the equations for the excitation energies and oscillator strengths and in the equations for the polarizability. The efficient evaluation of this product is discussed in the following subsections, each dealing with a separate aspect of improving the efficiency. The use of auxiliary basis functions, the use of molecular symmetry, use of parallelization techniques, as well as prescreening, cutoff, and linear scaling techniques, are discussed in this order.

2.6.1 Use of auxiliary basis functions

The matrix-vector product $\mathbf{p}_{\text{out}} = K \cdot \mathbf{p}_{\text{in}}$ under consideration, has the following form:

$$\begin{aligned}
 [p_{\text{out}}]_{ia} &= \sum_{jb} K_{ia,jb} [p_{\text{in}}]_{jb} = \sum_{jb} \int d\mathbf{r} \int d\mathbf{r}' \phi_i(\mathbf{r}) \phi_a(\mathbf{r}) \\
 &\quad \times \left[\frac{1}{|\mathbf{r} - \mathbf{r}'|} + f_{\text{xc}}^{\text{ALDA}}(\mathbf{r}) \delta(\mathbf{r} - \mathbf{r}') \right] \phi_j(\mathbf{r}') \phi_b(\mathbf{r}') [p_{\text{in}}]_{jb} \quad (2.28)
 \end{aligned}$$

The first step is to define the density $\rho_{\text{in}}(\mathbf{r}) = \sum_{jb} [p_{\text{in}}]_{jb} \phi_j(\mathbf{r}) \phi_b(\mathbf{r})$ and transform it to AO basis, by using the expansion of the KS orbitals ϕ_j and ϕ_b in this basis:

$$\phi_j(\mathbf{r}) = \sum_{\mu} C_{\mu j} \chi_{\mu}(\mathbf{r}). \quad (2.29)$$

In this way, the density ρ_{in} can be written in terms of an AO density matrix P^{in} :

$$\rho_{\text{in}}(\mathbf{r}) = \sum_{\mu\nu} [P^{\text{in}}]_{\mu\nu} \chi_{\mu}(\mathbf{r}) \chi_{\nu}(\mathbf{r}), \quad (2.30)$$

where the AO density matrix coefficients $[P^{\text{in}}]_{\mu\nu}$ are known in terms of the AO coefficients $C_{\mu j}$. The transformation from the KS basis to the AO basis is not very time consuming, provided that it is performed in two separate steps, where the first step consists of a transformation to a mixed basis representation of AOs and occupied orbitals.

At this point, nothing has been gained, as one still needs to go through four loops: those over i , a , μ , and ν , resulting in an N^4 algorithm. However, by fitting the density, the loops over μ and ν can be replaced by a single loop over the fit functions f_i , improving the scaling to N^3 :

$$\rho_{\text{in}}(\mathbf{r}) \approx \tilde{\rho}_{\text{in}}(\mathbf{r}) = \sum_i a_i f_i(\mathbf{r}). \quad (2.31)$$

In the RESPONSE part of the ADF program, the density fit is performed in the same manner as for the zeroth-order density. First, the density is split in atom pair densities, for which the AO representation is needed. Then this atom pair density is fitted with fit functions which are centered on the two atoms in the pair. This fit per atom pair ensures

that the fitting procedure scales as N^2 with increasing system size. The fit coefficients a_i are determined from the requirement that the integrated squared difference between the true atom pair densities $\rho_{\text{at.p.}}$ and the fitted densities $\tilde{\rho}_{\text{at.p.}}$

$$\int d\mathbf{r} [\rho_{\text{at.p.}}(\mathbf{r}) - \tilde{\rho}_{\text{at.p.}}(\mathbf{r})]^2 \quad (2.32)$$

should be minimal, under the constraint that the total atom pair charge remains unchanged. The quality of the fit can be controlled by adding suitable functions to the fit set, and checked by calculating the difference integral of Equation (2.32). More details about the fitting procedure in ADF can be found in References [89, 114]. Using this fitted density, the expression for the matrix-vector product becomes:

$$\sum_{jb} K_{ia,jb} [p_{\text{in}}]_{jb} = \int d\mathbf{r} \phi_i(\mathbf{r}) \phi_a(\mathbf{r}) \int d\mathbf{r}' \left[\frac{1}{|\mathbf{r} - \mathbf{r}'|} + f_{\text{xc}}^{\text{ALDA}}(\mathbf{r}) \delta(\mathbf{r} - \mathbf{r}') \right] \sum_i a_i f_i(\mathbf{r}') \quad (2.33)$$

This equation is of the form

$$[p_{\text{out}}]_{ia} = \int d\mathbf{r} \phi_i(\mathbf{r}) v_{\text{ind}}(\mathbf{r}) \phi_a(\mathbf{r}), \quad (2.34)$$

where the induced potential $[v_{\text{ind}}]$ has been introduced. We use this description because the induced potential depends upon the density change ρ_{in} which is induced by the external perturbation. The induced potential is, in terms of the fitted density, given by:

$$v_{\text{ind}}(\mathbf{r}) = \int d\mathbf{r}' \left[\frac{1}{|\mathbf{r} - \mathbf{r}'|} + f_{\text{xc}}^{\text{ALDA}}(\mathbf{r}) \delta(\mathbf{r} - \mathbf{r}') \right] \sum_i a_i f_i(\mathbf{r}'). \quad (2.35)$$

The matrix elements of the induced potential v_{ind} in Equation (2.34) are calculated by numerical integration. A separate section of the ADF program[90, 115] determines the coordinates \mathbf{r}_k and the weights w_k of the quadrature points, from the geometry of the molecule and the desired accuracy in the integrals, typically leading to a few thousand integration points per atom. The numerical integral evaluation for a general integrand $g(\mathbf{r})$ can be written as:

$$\int g(\mathbf{r}) d\mathbf{r} = \sum_k w_k g(\mathbf{r}_k), \quad (2.36)$$

which, for the induced potential matrix elements results in:

$$[p_{\text{out}}]_{ia} = \sum_k w_k \phi_i(\mathbf{r}_k) v_{\text{ind}}(\mathbf{r}_k) \phi_a(\mathbf{r}_k) \quad (2.37)$$

The two most expensive steps in the evaluation of the matrix-vector product are the evaluation of the potential v_{ind} in all the integration points \mathbf{r}_k and the evaluation of the $N_{\text{occ}} \times N_{\text{virt}}$ numerical integrals occurring in Equation (2.34). Each of these integrals requires an operation count which scales linearly with the total number of integration points for the molecule, N_{point} . The total CPU time involved in the evaluation of the integrals, once v_{ind} is known in the integration points, is proportional to $N_{\text{occ}} \times N_{\text{virt}} \times N_{\text{point}}$, where typically $N_{\text{point}} \gg N_{\text{virt}} > N_{\text{occ}}$.

For the integral calculation to be the time-determining step, one needs an efficient evaluation of the induced potential in the integration points. This proceeds as follows. As we use STOs for the fit functions, the Coulomb potential belonging to the fitted density can be obtained analytically[116]:

$$v^{\text{Coul}}(\mathbf{r}) = \int d\mathbf{r}' \left[\frac{\sum_i a_i f_i(\mathbf{r}')}{|\mathbf{r} - \mathbf{r}'|} \right] = \sum_i a_i g_i(\mathbf{r}), \quad (2.38)$$

where the functions g_i are known. The part of the induced potential involving the ALDA xc kernel is trivial, because of the delta function. In short, the induced potential is obtained as:

$$v_{\text{ind}}(\mathbf{r}) = \int d\mathbf{r}' \left[\frac{1}{|\mathbf{r} - \mathbf{r}'|} + f_{\text{xc}}^{\text{ALDA}}(\mathbf{r})\delta(\mathbf{r} - \mathbf{r}') \right] \sum_i a_i f_i(\mathbf{r}') = \sum_i a_i \left[g_i(\mathbf{r}) + f_{\text{xc}}^{\text{ALDA}}(\mathbf{r}) \times f_i(\mathbf{r}) \right], \quad (2.39)$$

which leads to a favorable N^3 scaling.

2.6.2 Use of full molecular symmetry

Once the induced potential has been calculated in the integration points, one needs to calculate $N_{\text{occ}} \times N_{\text{virt}}$ integrals as in Equation (2.34). As pointed out, the calculation time for this will be proportional to $N_{\text{occ}} \times N_{\text{virt}} \times N_{\text{point}}$. However, as one knows the transformation properties of all occupied and virtual orbitals [the irreducible representations (irreps) Γ to which they belong, as well as the columns α of these irreps are known], as well as the transformation properties of the external potential, and consequently the induced potential, group theory can be used to reduce the number of required operations considerably.

The savings are three-fold. In the first place, one does not need all the integration points of the molecule, but only those which belong to the symmetry-unique wedge, substantially reducing the cost *per integral*. This implies that N_{point} is reduced by a factor which is equal to the number of group operators (which, for example, is no less than 48 for the O_h symmetry). This is usually the most important gain in time, as the CPU time needed for the expensive calculation of the induced potential in the integration points is automatically reduced by the same factor.

In the second place, one can use the symmetry properties to minimize the *number* of integrals which need to be calculated. Already on the basis of the irreps to which the orbitals and the operator belong, one can predict many integrals to be zero. Entire blocks of integrals do not need to be calculated for this reason. The third saving is the most trivial one. Equivalent symmetry blocks (for the excitation energy calculations) or equivalent external fields (for the polarizability calculations) can (and should) be treated at the same time. This implies that, for example, the x and y direction of a molecule with cylinder symmetry around the z -axis can be treated simultaneously.

All this will be made more explicit below. In the following group theoretical approach, we follow Cornwell[117], although adopting a different notation. We consider the set of $N_{\text{occ}} \times N_{\text{virt}}$ integrals

$$\int d\mathbf{r} \phi_i(\mathbf{r}) v(\mathbf{r}) \phi_a(\mathbf{r}), \quad (2.40)$$

where ϕ_i and ϕ_a are KS orbitals, and the operator $v(\mathbf{r})$ is typically the induced potential. The KS orbitals occurring in this equation can be labeled by the irrep and column of the irrep to which they belong. In order to make full use of group theory, one has to ensure that the operators (or potentials) $v(\mathbf{r})$ can be labeled similarly. This can be done by choosing proper external perturbations δv_{ext} in Equation (2.16), or proper symmetry-adapted trial vectors for \mathbf{F}_i in an excitation energy calculation. For the external perturbations, this means that one treats linear combinations of the regular spherical harmonics (such as x , y , and z in the dipole polarizability case), instead of the spherical harmonics themselves, which does not affect the final results in any way. One furthermore has to make sure that the operators belonging to different columns of a multidimensional irrep q will transform as a set of *irreducible tensor operators* for that irrep, as defined in, for example, Cornwell[117].

The matrix element for the specific KS orbitals i and a is nonzero only if it contains a part which transforms according to the A1 irrep, or, in other words, if it contains a part which is completely symmetrical. Furthermore, the value of the integral is identical to the contribution of its completely symmetrical part. One can easily establish whether or not an integral vanishes from the knowledge of the Clebsch–Gordan series, which specifies how the direct product of two irreps can be expressed in a direct sum of all irreps Γ^r of the symmetry group[117]:

$$\Gamma^p \otimes \Gamma^q \approx \sum_r \oplus n_{pq}^r \Gamma^r. \quad (2.41)$$

In case the orbitals i and a transform according to the irreps Γ^p and Γ^q respectively, the corresponding matrix element will vanish, unless the integer n_{pq}^r is nonzero, where Γ^r is the irrep the operator belongs to. Many point groups which describe the symmetry of molecules are *simply reducible*, meaning that n_{pq}^r is equal to 0 or 1 for all p, q, r . In such a case, the equations given below will simplify considerably.

If one considers products of basis functions $\{\phi_j^p\}$ belonging to irrep Γ^p [j denotes the column, in the range $l = 1 \dots \dim(\Gamma^p)$] with basis functions $\{\psi_k^q\}$ of the irrep Γ^q , one obtains a set of $\dim(\Gamma^p) \times \dim(\Gamma^q)$ product functions, which, with the use of the Clebsch–Gordan coefficients $\langle \Gamma^p j, \Gamma^q k | \Gamma^r l \alpha \rangle$, can be symmetry-combined to $\alpha = 1 \dots n_{pq}^r$ sets of functions $\theta_{l,\alpha}^r$ transforming according to column l of irrep Γ^r :

$$\theta_{l,\alpha}^r(\mathbf{r}) = \sum_{j=1}^{d_p} \sum_{k=1}^{d_q} \langle \Gamma^p j, \Gamma^q k | \Gamma^r l \alpha \rangle \phi_j^p(\mathbf{r}) \psi_k^q(\mathbf{r}), \quad (2.42)$$

where d_p stands for the dimension of irrep Γ^p , and $\alpha = 1 \dots n_{pq}^r$. For the most common case of simply reducible groups, this simplifies, as n_{pq}^r is always equal to zero or one. With the notation for the Clebsch–Gordan coefficients established, the Wigner–Eckart theorem can now be formulated. For a set of irreducible tensor operators Q_k^q , with irrep label q and column label k , the following relation holds for the matrix elements between orbitals ϕ_i^r and ψ_j^p [117]:

$$\left(\phi_i^r, Q_k^q \psi_j^p \right) = \sum_{\alpha=1}^{n_{pq}^r} \langle \Gamma^p j, \Gamma^q k | \Gamma^r l \alpha \rangle^* (r || Q^q || p)_\alpha \quad (2.43)$$

In words, the theorem states that the values of the set of integrals $\left(\phi_i^r, Q_k^q \psi_j^p \right)$ can, in combination with the knowledge of the Clebsch–Gordan coefficients, be obtained for all values

of j , k , and l from the possibly much smaller set of $\alpha = 1 \dots n_{pq}^r$ "reduced matrix elements" $(r \parallel Q^q \parallel p)_\alpha$, which are independent of l , k , and j . The strategy is therefore to evaluate the reduced matrix elements in the cheapest possible manner and to obtain all desired nonzero matrix elements by multiplication with the correct Clebsch–Gordan coefficients, the determination of which is cheap. The reduced matrix elements are obtained from the basic integrals:

$$(r \parallel Q^q \parallel p)_\alpha = \frac{1}{d_r} \sum_{j,k,l} (\phi_l^r, Q_k^q \phi_j^p) \times \langle \Gamma^q k, \Gamma^p j \mid \Gamma^r l \alpha \rangle \quad (2.44)$$

It can be explicitly shown that the total integrand of the right-hand side of this equation is invariant under the $A1$ -projector, which projects out the totally symmetric component. This implies that only the points in the irreducible wedge are needed for the evaluation of the reduced matrix elements. It is important to realize that this is not true for the individual basic integrals on the right-hand side, which are not necessarily totally symmetric. However, when multiplied by the Clebsch–Gordan coefficients and combined with the other contributions, the total (the reduced matrix element) will be totally symmetric. If one uses only points from the symmetry-unique wedge, the contribution of the individual basic integrals will consequently be calculated incorrectly, but the reduced matrix element will be correct. Afterwards, the basic integrals are obtained from the reduced matrix elements, as in Equation (2.43). Needless to say, only the basic integrals will be calculated of which the associated Clebsch–Gordan coefficient is nonzero.

Summarizing this section, we can say that the use of symmetry permits a significant speed-up of the response calculations, mainly due to the fact that the number of integration points can be strongly reduced, but also due to the significantly smaller number of integrals which have to be evaluated. More details on the use of the full molecular symmetry in the ADF-RESPONSE code are available in the form of an internal report[118].

2.6.3 Parallelization

The major part of the CPU time depends linearly on the number of integration points N_{point} . Even if only the work which has to be performed in all integration points can be divided between different processors, a reasonably well parallelized code results already. In the ADF program, this is done as follows[91]. The total number of integration points is subdivided into N_{block} blocks, each with the same length L_{block} . This machine-dependent block length is chosen such that vectorization proceeds effectively.

The blocks are divided equally between the different processors (nodes). After this, each processor calculates the induced potential (the response operator) in its own blocks of integration points and determines the contribution from those blocks of integration points to the matrix elements. After all nodes are finished with their parts of the numerical integration, there will be communication between the nodes, in order to calculate the total value of the integrals. The transformations from AO to KS orbital basis and vice versa have also been parallelized in the ADF-RESPONSE code. This results in an overall parallelization of typically 99% of the ADF-RESPONSE code, which gives good speed-ups up to a considerable number of processors.

In ADF, a high-level portable parallelization library, the PP library, has been set up[91], which is based on the low-level routines of either the public-domain Parallel Virtual Machine (PVM) [119] or the Message Passing Interface (MPI) protocols. The high-level routines have been used for the parallelization of the ADF-RESPONSE code[88], implying that for the parallelization of this part of ADF, the same techniques have been used as for the rest of the ADF program. A detailed description of the parallelization of ADF, including timing results, can be found in Ref. [91].

2.6.4 Distance effects and linear scaling techniques

Instead of calculating matrix elements between occupied and virtual KS orbitals, such as

$$\int d\mathbf{r} \phi_i(\mathbf{r}) [v_{\text{ind}}(\mathbf{r})] \phi_a(\mathbf{r}), \quad (2.45)$$

it is also possible to calculate the AO matrix elements

$$\int d\mathbf{r} \chi_\mu(\mathbf{r}) [v_{\text{ind}}(\mathbf{r})] \chi_\nu(\mathbf{r}), \quad (2.46)$$

and transform to eigenfunction basis afterwards. The disadvantage of this, so-called direct, approach is obvious. Even if no symmetry is present, the number of integrals which has to be evaluated is far bigger in the second case. If the number of primitive basis functions is N_{bas} , one needs to evaluate $N_{\text{bas}} \times (N_{\text{bas}} + 1)/2$ integrals, instead of $N_{\text{occ}} \times N_{\text{virt}}$, the latter number possibly being substantially smaller. If the symmetry is high and the basis set is large, the difference in the number of integrals becomes huge.

For large molecules, which are usually nonsymmetric, the AO approach will become preferable however, because distance effects can be employed. Two AOs, centered on nuclei which are far apart, will have very small overlap, resulting in a negligible value for the integral of Equation (2.46). In general, an AO will have nonvanishing overlaps with only a fixed number of AOs situated on close-lying atoms, inside a certain radius R . Because only integrals involving AOs on these neighbors need to be calculated, the number of integrals will, for large systems, scale linearly with the number of atoms. This is the desirable linear scaling which is aimed at in ground-state DFT calculations as well. Such linear scaling is not reached for the eigenfunction approach, as the KS orbitals are hardly ever localized on a few atoms, but are usually spread out over the entire molecule.

The use of distance effects can be applied at three levels[114]. In the outermost loop for the calculation of the KS matrix, which is the loop over atom pairs in ADF, those pairs of atoms can be skipped, for which all AOs centered on the two atoms of the pair have negligible overlap. The number of integrals which has to be evaluated scales linearly if this first step is implemented, but an efficient linear scaling of the entire calculation is only realized if two more steps are implemented.

For a certain atom pair, it is not necessary to evaluate matrix elements between all AOs on atom 1 and atom 2. Only those AO pairs for which the overlap matrix element $S_{\mu\nu} = \int d\mathbf{r} \chi_\mu(\mathbf{r}) \chi_\nu(\mathbf{r})$ is larger than some threshold value need to be taken into account. This overlap matrix element is estimated from an approximation to the tails of the AOs. The third and final step is at the level of an individual integral. Each of the N_{block} blocks

of integration points (each with L_{block} points), has a contribution to the total integral, but for some blocks this contribution will be negligible. A simple criterion[87] for judging if a certain integration block needs to be taken into account, is to calculate the maximum value of the products of the AOs in the current block. This product can be used as a measure for the contribution of the current block of integration points and on the basis of its magnitude one can decide whether or not it is necessary to take that block into account. In ADF, a slightly different criterion is adopted, in which the weight of the tail of a function in a certain block determines whether or not the block should be taken into account[114].

In order for this final step to be useful, the spread in the values of the operator and the AOs in a certain block should not be too large. This requires blocks which are well localized in space and do not contain too many integration points. The latter demand implies using a relatively small value for L_{block} , conflicting with the demand for efficient vectorization, which requires a large L_{block} value.

Until now, we have discussed the evaluation of matrix elements only. However, one has to take care that the evaluation of the response operator is performed in a linear scaling fashion as well. If this is not done, this part of the calculation will dominate the total CPU time. To this purpose one can use several techniques, such as a multipole expansion for the Coulomb potential[114], but the discussion of these falls outside the scope of the present article.

Only a limited number of techniques which make use of distance effects have been implemented in the ADF-RESPONSE code[88] at present. The full implementation of linear scaling techniques and distance effects is left for future work, and will be performed along similar lines as the linear scaling implementation for the ground-state KS equations in ADF[114].

2.7 Selected molecular applications

In the following sections some of the results which have been obtained by ourselves and by others are discussed in order to highlight certain points which are important for practical applications, and to show what type of calculations are feasible with the present method and what accuracy can typically be reached.

2.7.1 Influence of asymptotic behavior of v_{xc}

The approximation which is made for the xc potential v_{xc} is very important for the accuracy of response calculations, as it determines the KS orbital energy differences and the KS orbitals, which provide the starting point for the response calculation. Apart from this approximation, the xc kernel f_{xc} has to be approximated, which can be chosen independently from the xc potential. In our applications described here, the ALDA was used for the xc kernel and various xc potentials were used in the ground-state calculation.

It is known that both LDA and GGA xc potentials possess undesirable properties, of which their behavior in the outer region of the molecule is of crucial importance for response calculations. As the GGA and LDA xc potentials do not possess the correct Coulombic tail ($v_{\text{xc}} \rightarrow -1/r$), they systematically overestimate molecular polarizabilities. This overestimation increases if the outer region is more important for a particular system or for a particular

effect. For this reason, the LDA works quite poorly for hyperpolarizabilities[120], higher multipole polarizabilities[77], high-lying excitation energies[82], and for small systems such as atoms. For large molecules, dipole polarizabilities, and low-lying excitation energies the LDA and GGA failure due to the incorrect asymptotics is less pronounced.

Substantial improvements can be obtained if the potentials are corrected in such a way that the proper asymptotic $-1/r$ behavior is restored. This can be done by using self-interaction correction (SIC) schemes, which has the disadvantage of making the potential orbital-dependent. A more popular choice has been the Van Leeuwen–Baerends model xc potential (LB94)[121], in which a simple local correction to the LDA potential is suggested. In spite of its simplicity, it corrects the LDA results in several important ways. An example of the influence of the correct asymptotics is given in Figure 2.1, where the frequency-dependent quadrupole polarizability of Helium is plotted. Except for the benchmark *ab initio* curve, both the LDA/ALDA and LB94/ALDA results are shown. The LDA curve displays a clear overestimation of the static quadrupole polarizability, as well as a too steep frequency dependence, which is indicative of a too small value for the first relevant excitation energy. The LB94 curve shows important improvements in both the static value and in the frequency dependence.

These trends are by no means restricted to Helium. As demonstrated in Ref [74], the LB94 potential removes the systematic LDA overestimation of molecular polarizabilities, as well as the LDA overestimation of the frequency dependence of these polarizabilities. In Ref.[77] it was shown that similar improvements are even more pronounced for the higher multipole polarizabilities and dispersion coefficients, which is also the case for frequency-dependent hyperpolarizabilities[120]. Casida *et al.*[82] have recently shown that high-lying excitation energies are improved with respect to the LDA values if the LB94 potential is used.

In a recent study[78] in which we used very accurate exchange correlation potentials, constructed from *ab initio* densities, it appeared that additional improvements for excitation energies and polarizabilities for atoms and small molecules can be expected from approximations to v_{xc} which are more accurate than the LB94 potential. In view of the relative simplicity of the LB94 potential, the construction of such an improved potential may be quite feasible. In fact, next to orbital-dependent functionals with correct asymptotics, such as the Krieger-Li-Iafrate (KLI) potential[122, 123], new density functionals for accurate exchange-correlation potentials with correct asymptotics were recently proposed[124, 125], and are awaiting to be tested in response calculations.

2.7.2 Excitation energies of small molecules

The first excitation energy calculations in TDDFT were performed by Petersilka and Gross [126, 101, 105, 127] for atomic systems, and Jamorski *et al.*[35] and Bauernschmitt and Ahlrichs[86, 87] for molecules. As an example for the excitation energies of small molecules we give the results by Bauernschmitt and Ahlrichs for the lowest singlet and triplet excitation energies of the formaldehyde molecule in Table 2.1. Bauernschmitt and Ahlrichs[86] studied a set of several small molecules and concluded that the B3LYP[128, 129] functional gave the best performance of the methods studied (the LDA and Becke–Perdew potentials

were slightly inferior, while the singles-CI and RPA results were clearly worse). The results in the table are typical in the sense that Bauernschmitt and Ahlrichs reported a systematic underestimation for the DFT excitation energies, with typical errors of 0.4 eV. Although these results provide clear improvements with respect to RPA or TDHF, it is still important to consider the origin of this underestimation, which incidentally corresponds to the overestimation in the polarizabilities. Bauernschmitt and Ahlrichs speculate that the adiabatic approximation may be largely responsible for this underestimation. This is contradicted however by the recent results of Casida *et al.*[82], which show that the use of the LB94 potential leads to much better values for high-lying excitation energies and to *overestimations* for low-lying molecular excitation energies. This shows at the same time that the LB94 potential needs to be improved upon and that the form of the xc potential, in particular its asymptotic behavior, is of considerable influence on the results for low-lying excitation energies as well.

In a more recent paper Bauernschmitt *et al.*[87] have shown that excitation energies of large molecules can efficiently be obtained from a TDDFT approach. They provide timing results for calculations on molecules with up to about 80 atoms and 800 basis functions, which might be a good indication of what will be the magnitude of a standard calculation in the very near future, and is in agreement with our own experience for the C₆₀ molecule[76] and polyene chains[130].

Apart from the TDDFT approach, excitation energies can also be calculated using ordinary ground-state DFT, through the so-called Δ SCF approach[63, 64, 65, 66]. It is important to understand the characteristics of and differences between both types of calculation. For this reason, we have compared our own TDDFT calculations[118, 131] for the prototype Cr(CO)₆ molecule to Δ SCF results which have appeared in the literature earlier. In Table 2.2, these DFT results are compared to experimental and *ab initio* complete active space second-order perturbation theory (CASPT2) results, which can be considered as the benchmark values in this case. All three theoretical approaches are in agreement about the assignment of the lowest excitation energies. They are of the charge transfer (CT) type, in disagreement with the longstanding accepted experimental assignment to the ligand field (LF) excitation[132], which therefore has to be reconsidered. In many cases, the Δ SCF and TDDFT results are (very) close to each other, but for some excitations there are remarkable differences of more than 1 eV, which cannot be attributed to basis set differences, as we have checked by performing TDDFT test calculations in identical basis and fit sets as were used in the Δ SCF calculations of Ref.[133] in which the ADF program was also used.

For example, the two CT excitations for which experimental numbers are available are predicted to be much lower by the TDDFT calculation than by the Δ SCF calculation. The TDDFT results are in much better agreement with the experimental and CASPT2 values than the Δ SCF values are.

We have found [118, 131] that typically the Δ SCF and TDDFT results are close to each other in case the transition is dominated by one particular KS orbital replacement. In other words, if the eigenvector \mathbf{F}_i in Equation (2.24) belonging to the excitation energy has one dominant component, the Δ SCF and TDDFT approaches will yield very similar results. This is due to the fact that in the Δ SCF approach one can only consider a single orbital transition, and configuration interaction falls outside the scope of this approach, while it is

included in a natural way in the TDDFT calculations. To give some numerical examples, we quote our results for the major components of the eigenvector for a few transitions. For the experimentally observed a^1T_{1u} and b^1T_{1u} transitions, the contribution of the major orbital transition is no larger than 64% and 58% respectively, if Casida's approximate assignment scheme is used[37]. In such cases, where there is considerable mixing between the orbital transitions, the Δ SCF results can deviate considerably. This observed trend needs to be investigated in more detail and should, at the moment, not be attributed more significance than a rule of thumb.

2.7.3 Frequency-dependent hyperpolarizabilities

TDDFT calculations may become particularly important for hyperpolarizabilities, as the frequency dependence is known to be large for this property. Atomic calculations for frequency-dependent hyperpolarizabilities were already performed a decade ago by Senatore and Subbaswamy[71, 72]. More recently, analytic molecular calculations of static hyperpolarizabilities appeared[134, 135]. Until now, only a single example[76] exists of a TDDFT calculation of a frequency-dependent hyperpolarizability of a molecular system, although a larger calibration study is in progress[120], as well as an application to the NLO response of polyene chains[130]. We have recently treated the C_{60} molecule in this approach[76], for which the first hyperpolarizability β is zero because of the high symmetry, making the second hyperpolarizability tensor γ the first nonvanishing nonlinear contribution.

The C_{60} molecule is an interesting case, because of its delocalized π -system, which led to speculations about its possibly huge hyperpolarizability, which would make it an interesting candidate for application in nonlinear optical devices. Our results[76], as well as various experimental and semiempirical results have been gathered in Table 2.3. The disagreement between the experimental results is huge, and would be even larger if the older experimental results would have been included in the table. The semiempirical results seem to support the larger (and older) experimental values, although they are also very diverse. Both our LDA/ALDA and LB94/ALDA results give quite small values for the static hyperpolarizability tensor component γ_{zzzz} (which at zero frequency is equal to the average hyperpolarizability γ , because of the high symmetry of the molecule), which support the more recent experimental results by Geng and Wright[136], who could only estimate an upper limit for the hyperpolarizability. In addition, the frequency dependence we found was relatively small and could not explain the discrepancy with most experimental values. Very soon after the publication of our results, a static HF calculation on the hyperpolarizability appeared[137], which was in qualitative agreement with our results, thus providing strong support for both the DFT and HF calculations. Remaining differences between the experimental and theoretical values are in the neglect of solvent and vibrational effects in the theoretical description and form interesting subjects for future research.

2.7.4 Van der Waals dispersion coefficients

As mentioned before, the calculation of frequency-dependent multipole-multipole polarizabilities gives access to the Van der Waals dispersion coefficients which determine the long-range

dispersion part of a potential energy surface of two interacting (distant) molecules. This is due to the fact that these dispersion coefficients can be calculated from an integral involving the polarizabilities at imaginary frequencies of the two monomers. If the distance R between the two subsystems becomes very large, the dominating term in the dispersion energy is of the form $-C_6/R^6$, where C_6 is the Van der Waals dispersion coefficient which can be calculated from the dipole-dipole polarizabilities of the monomers. At smaller distances, also the C_7 and C_8 coefficients become important, governing respectively the $-1/R^7$ and $-1/R^8$ behavior. For these coefficients, one needs, in addition to the dipole-dipole polarizabilities of the monomers, the dipole-quadrupole, and quadrupole-quadrupole polarizabilities. For the interaction between two centrosymmetric molecules, the C_7 coefficient vanishes because it depends on the vanishing dipole-quadrupole polarizability. In Table 2.4 we show results which we have obtained previously[77] for the C_8^0 coefficient, which governs the isotropic part of the $-1/R^8$ interaction between, in this case, a diatomic molecule and a rare gas atom. The basis sets which were used[77] were very large containing several diffuse functions, for which reason the results can be expected to be close to the basis set limit.

The LDA/ALDA and GGA/ALDA [using the Becke[138]-Perdew[139](BP) potential] results show the usual overestimations, which finally leads to average systematic errors of 20.5% and 13.2% with respect to the many-body perturbation theory (MBPT) values. The asymptotically correct LB94 potential largely corrects this, resulting in a much smaller error of 4.2%. The difference between the average and average absolute errors for the LB94 potential shows that for this potential the errors are not systematic.

For the relative anisotropy in the dispersion coefficients, satisfactory results were obtained with all three potentials mentioned above[77]. This implies that the difficult dispersion part of long-range potential energy surfaces can be constructed with useful accuracy from the described TDDFT approach.

2.8 Conclusions

After a brief summary of the key equations of time-dependent density functional response theory, we have described how the efficient solution of these response equations can take place. An efficient implementation rests on the iterative solution of the relevant equations for the polarizability and the excitation energies. The most time consuming part of such an iterative solution is formed by the repeated matrix-vector multiplications of the coupling matrix K with trial-vectors. Four important ingredients for the efficient evaluation of this matrix-vector multiplication have been discussed: the use of a density fit for the evaluation of the induced potential, the use of the molecular symmetry through the Wigner-Eckart theorem, the parallelization of the code, and the use of distance effects. With these techniques an efficient implementation of the time-dependent density functional response equations can be realized. Such an implementation allows for a first principles determination of excitation energies, frequency-dependent (hyper)polarizabilities, and related properties of large molecules. Work performed in other groups and by ourselves has shown that such calculations are usually of very satisfactory accuracy. A few calculations on polarizabilities, hyperpolarizabilities, excitation energies, and dispersion coefficients have been reviewed in order to give examples of what the theory can typically be used for, and what accuracy can

2.9 Acknowledgements

We would like to thank J. A. Groeneveld, F. Kootstra, and V. P. Osinga for the sizable contribution they have made to the implementation described in this work. SvG gratefully acknowledges financial support from the Netherlands organization for scientific research (NWO), through its foundations SON and NCF.

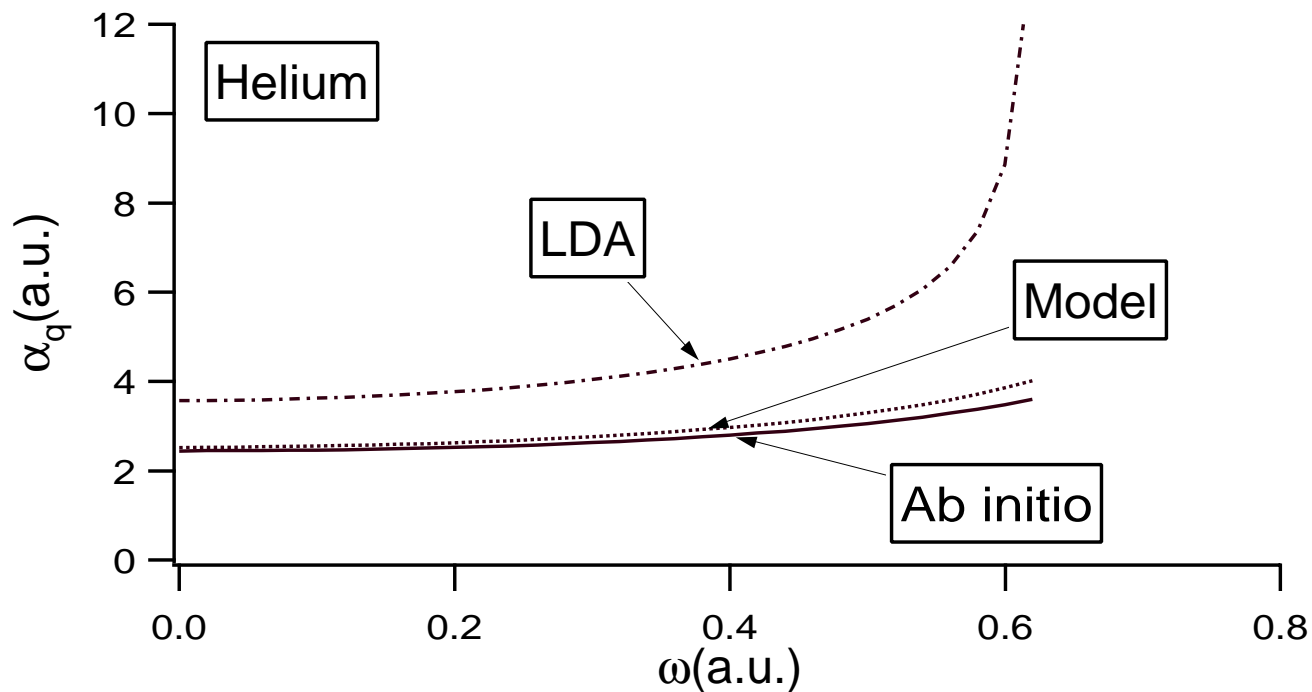


Figure 2.1: The frequency-dependent quadrupole polarizability of He. Comparison of results with the LDA and LB94 potentials to benchmark *ab initio* results.

Table 2.1: Excitation energies of CH₂O (in eV)

Transition		Excitation energy		
		LDA ^a	B3LYP[128, 129] ^a	Expt.
¹ B ₁	$\sigma \rightarrow \pi^*$	8.70	8.93	9.0
¹ A ₁	n → 3p	6.79	7.30	8.14
¹ B ₂	n → 3s	5.93	6.45	7.13
¹ A ₂	n → π^*	3.64	3.88	4.1
³ B ₂	n → 3s	5.86	6.32	7.09
³ A ₁	$\pi \rightarrow \pi^*$	6.11	5.32	6.0
³ A ₂	n → π^*	3.02	3.14	3.5
mean dev.		-0.70	-0.52	
mean abs. dev.		0.74	0.52	

^aResults taken from Ref.[86]. The CH₂O molecule has also been treated by Casida *et al.*[82].

Table 2.2: Comparison of TDDFT and Δ SCF excitation energies of Cr(CO)₆ (in eV)

Symmetry	Transition ^a	Expt. ^b	Δ SCF ^c	TDDFT ^d	CASPT2 ^e
Charge transfer excitations					
a ¹ T _{2u}	2t _{2g} → 9t _{1u}		4.0	4.11	3.70-3.56
a ¹ E _u	2t _{2g} → 9t _{1u}		4.0	4.08	3.41-3.59
a ¹ A _{2u}	2t _{2g} → 9t _{1u}		4.2	4.56	3.58-3.58
b ¹ E _u	2t _{2g} → 2t _{2u}		4.5	4.62	3.97-4.05
a ¹ A _{1u}	2t _{2g} → 2t _{2u}		4.5	4.20	4.15-4.10
b ¹ T _{2u}	2t _{2g} → 2t _{2u}		5.0	4.62	4.32-4.43
a ¹ T _{1u}	2t _{2g} → 9t _{1u}	4.43	5.6	4.28	4.54-4.11
b ¹ T _{1u}	2t _{2g} → 2t _{2u}	5.41	6.5	5.87	5.07-5.20
Ligand field excitations					
¹ T _{1g}	2t _{2g} → 6e _g		5.2	5.47	4.85
¹ T _{2g}	2t _{2g} → 6e _g		6.3	5.90	5.08

^aFor details about the orbital configuration, see Ref.[133]

^bExperimental results from Ref.[140]

^cPollak *et al.*[133]

^dSame basis sets were used as for Δ SCF calculations, BP potential[138, 139] was used for ground-state calculation as in Ref.[133]. Results with larger basis sets or with the LDA potential differ by very small amounts[118].

^eComplete active space second-order perturbation theory results with two different active spaces by Pierloot *et al.*[141]

Table 2.3: Experimental and theoretical results for γ of C_{60}

Method	ω (eV)	property	$\gamma(10^{-36}$ esu)
LB94 ^a	0	static	5.50
LB94 ^a	1.50	EOKE	6.69
LB94 ^a	0.65	EFISH	6.04
LDA ^a	0	static	7.34
LDA ^b	0	static	7.0
INDO-TDHF ^c	0	static	4.95
INDO-TDHF ^c	0.905	EFISH	5.49
INDO/SDCI-SOS ^d	0.65	EFISH	690
CNDO/S ^e	0.94	THG	654.8
CNDO/SCI-SOS ^f	0	static	-458
Expt., in film ^g	0.68	THG	430
Expt., in toluene ^h	0.65	EFISH	750
Expt., in benzene ⁱ	1.17	DFWM	$<60 \times \gamma(\text{benzene})$
Expt. ^j	various	Non-deg. FWM	<37

^aRef.[76]^bQuong and Pederson[142]^cTalapatra et al.[143]^dLi et al.[144]^eHara et al.[145]^fFanti et al.[146]^gMeth et al.[147]^hWang and Cheng[148]ⁱTang et al.[149], $\gamma^{\text{LDA}}(\text{benzene}) \approx 1.85 \times 10^{-36}$ esu[142]^jGeng and Wright[136], nondegenerate Four Wave Mixing experiment in 1,2-dichlorobenzene

Table 2.4: C_8^0 - Van der Waals coefficients for diatomic - rare gas interaction

diatomic	rare gas	LDA	BP	LB94	MBPT ^a	SoS ^b
H ₂	He	77.31	67.13	59.74	53.60	55.38
H ₂	Ne	167.6	153.5	133.7	128.4	
H ₂	Ar	720.7	663.2	644.0	576.5	
H ₂	Kr	1135	1051	989.5	953.6	
N ₂	He	284.3	259.7	222.4	219.7	
N ₂	Ne	599.1	574.2	481.4	498.7	
N ₂	Ar	2334	2240	2068	1986	
N ₂	Kr	3552	3429	3074	3145	
CO	He	334.0	304.9	257.9	262.7	
CO	Ne	693.6	664.2	548.9	588.9	
CO	Ar	2689	2576	2348	2355	
CO	Kr	4072	3923	3474	3726	
HCl	He	364.9	332.2	298.5	284.1	
HCl	Ne	764.5	730.6	639.8	643.7	
HCl	Ar	3048	2914	2815	2638	
HCl	Kr	4667	4487	4201	4219	
Cl ₂	He	1026	946.1	849.4	810.3	
Cl ₂	Ne	2086	2013	1758	1770	
Cl ₂	Ar	7758	7479	7186	6764	
Cl ₂	Kr	11539	11184	10439	10505	
Av. abs. error wrt MBPT		20.5%	13.2%	4.2%	-	
Av. error wrt MBPT		20.5%	13.2%	1.8%		

^aReference [150] Many body perturbation theory, results were linearly interpolated

^bReference [151] Sum-over-states with explicitly electron-correlated wave functions (SoS)

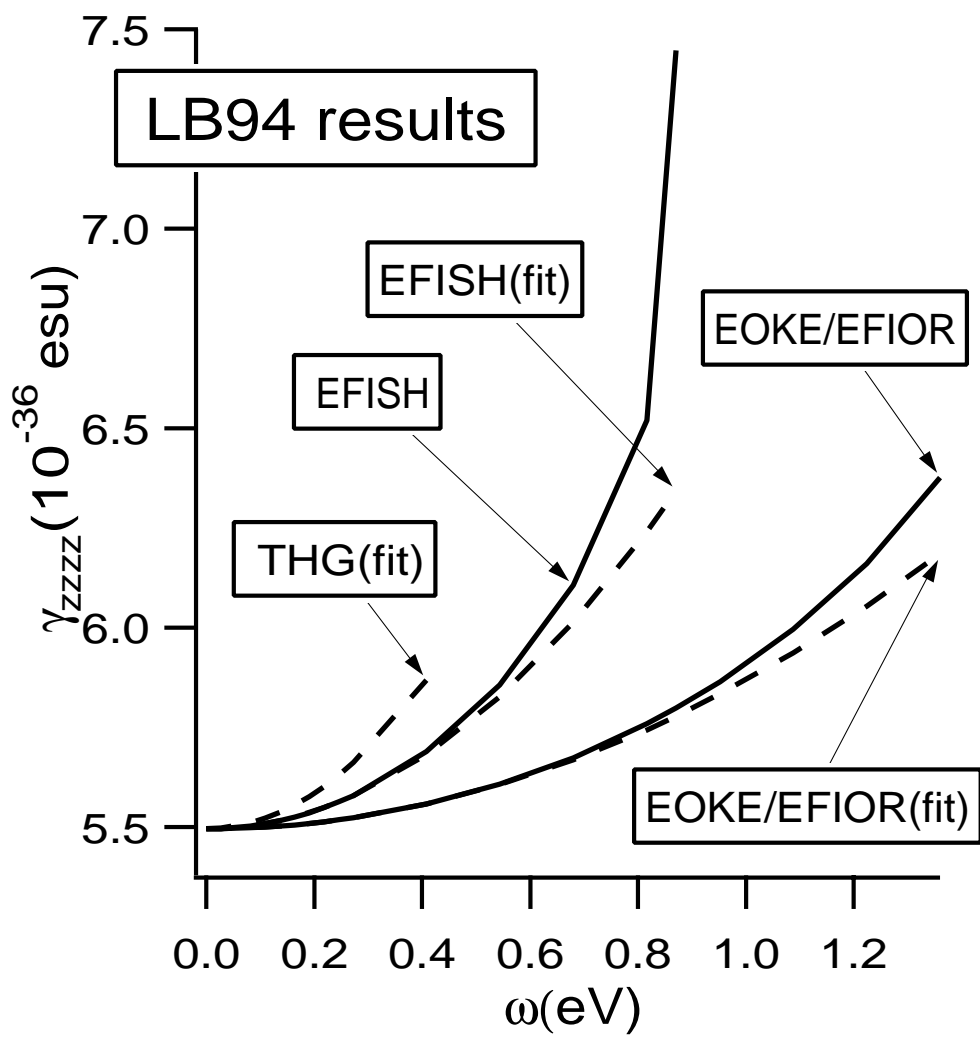


Figure 2.2: LB94 results for γ of C_{60}

Chapter 3

A density functional theory study of frequency-dependent polarizabilities and Van der Waals dispersion coefficients for polyatomic molecules

3.1 Abstract

A method for calculating frequency-dependent polarizabilities and Van der Waals dispersion coefficients, which scales favorably with the number of electrons, has been implemented in the Amsterdam Density Functional package. Time-dependent Density Functional Theory is used within the Adiabatic Local Density Approximation (ALDA). Contrary to earlier studies with this approximation, our implementation applies to arbitrary closed-shell molecular systems. Our results for the isotropic part of the Van der Waals dispersion energy are of comparable quality as those obtained in TDCHF calculations. The ALDA results for the relative anisotropy of the dipole dispersion energy compare favorably to TDCHF and MBPT results. Two semiempirical ways to calculate the dispersion energy anisotropy are evaluated. Large bases which include diffuse functions are necessary for a good description of the frequency-dependent properties considered here.

3.2 Introduction

In recent years there have been several Density Functional Theory (DFT) studies on the quality of static polarizabilities and hyperpolarizabilities. These are either finite field calculations [152, 153, 154, 155] or an implementation of the coupled Kohn–Sham equations [134, 135].

To the best of our knowledge, all the calculations of frequency-dependent (hyper)polarizabilities in DFT until now, have made use of time-dependent DFT in which the Adiabatic Local Density Approximation (ALDA) is used. However, these studies are either restricted to atomic systems [9, 16, 72, 11] or to a single center expansion [19] which is unsuitable for

general molecules. An alternative DFT method for calculating frequency-dependent response properties has been developed by Colwell et al.[134]. No results have yet been reported.

The articles cited above show that the LDA results for static polarizabilities are good, though generally somewhat too high ($\sim 5\%$). This is due to the fact that the LDA density falls off too slowly, which means that the deformability of the electron cloud becomes too high.

We are interested in frequency-dependent properties for two main reasons. The first reason is that there is an interesting link between Van der Waals dispersion coefficients and multipolar polarizabilities at imaginary frequencies [48, 156]. This opens up a route to constructing the long range part of potential energy surfaces for Van der Waals complexes within DFT. The present day local and nonlocal functionals do not seem to give satisfactory results for such complexes in supermolecule calculations [157, 158].

For small molecules often satisfactory isotropic Van der Waals coefficients can be obtained with correlated ab initio methods such as many-body perturbation theory (MBPT) [159], but these methods are restricted to small molecules because of their unfavorable scaling behavior (N^m , $m \geq 5$). Our implementation provides a tractable alternative for medium-sized molecules, because it scales like N^3 .

The second reason for our interest in frequency-dependent polarizabilities is the fact that much experimental work is done at nonzero frequency. Now, a more direct comparison with experiment becomes possible and an alternative is provided for frequency ranges which cannot be reached easily in an experiment.

3.3 The model

After some pioneering works by, among others, Zangwill and Soven [9], Ghosh and Deb [11], Bartolotti [16], and Stott and Zaremba [23], the rigorous foundation for time-dependent DFT was given by Runge and Gross [38] who formulated a time-dependent version of the Kohn–Sham scheme[1, 3]. Refs.[32] and [31] provide excellent reviews of time-dependent DFT. In the following, we will basically follow these reviews.

The Fourier transforms of the first order change in the density $\delta\rho(\mathbf{r}, \omega)$, and of a scalar time-dependent change in the external potential $\delta v_{\text{ext}}(\mathbf{r}, \omega)$ can be related by the full linear response function $\chi(\mathbf{r}, \mathbf{r}', \omega)$:

$$\delta\rho(\mathbf{r}, \omega) = \int d\mathbf{r}' \chi(\mathbf{r}, \mathbf{r}', \omega) \delta v_{\text{ext}}(\mathbf{r}', \omega). \quad (3.1)$$

However, it is very difficult to find good approximations for this linear response function, since it requires in principle the knowledge of all exact eigenfunctions and excitation energies of the system. The time-dependent DFT alternative is to use the response function $\chi_s(\mathbf{r}, \mathbf{r}', \omega)$ of the noninteracting Kohn–Sham system, in combination with an effective or screened potential $\delta v_{\text{eff}}(\mathbf{r}, \omega)$:

$$\delta\rho(\mathbf{r}, \omega) = \int d\mathbf{r}' \chi_s(\mathbf{r}, \mathbf{r}', \omega) \delta v_{\text{eff}}(\mathbf{r}', \omega). \quad (3.2)$$

This response function requires the knowledge of the occupied and virtual Kohn–Sham orbitals $\{\phi\}$ and energies $\{\varepsilon\}$, as well as the occupation numbers n , which are all obtained

in a standard DFT calculation:

$$\chi_s(\mathbf{r}, \mathbf{r}', \omega) = \sum_i^{\text{occ}} \sum_m^{\text{virt}} n_i \phi_i(\mathbf{r}) \phi_m(\mathbf{r}) \phi_m(\mathbf{r}') \phi_i(\mathbf{r}') \left(\frac{1}{(\varepsilon_i - \varepsilon_m) + \omega} + \frac{1}{(\varepsilon_i - \varepsilon_m) - \omega} \right). \quad (3.3)$$

The change in the effective potential $\delta v_{\text{eff}}(\mathbf{r}, \omega)$, which depends upon the density change $\delta\rho(\mathbf{r}, \omega)$ is given by:

$$\delta v_{\text{eff}}(\mathbf{r}, \omega) = \delta v_{\text{ext}}(\mathbf{r}, \omega) + \int d\mathbf{r}' \frac{\delta\rho(\mathbf{r}', \omega)}{|\mathbf{r} - \mathbf{r}'|} + \delta v_{\text{xc}}(\mathbf{r}, \omega). \quad (3.4)$$

The change in the exchange correlation potential is given in terms of the Fourier transform of the so-called exchange correlation kernel $f_{\text{xc}}(\mathbf{r}, \mathbf{r}'; \omega)$:

$$\delta v_{\text{xc}}(\mathbf{r}, \omega) = \int d\mathbf{r}' f_{\text{xc}}(\mathbf{r}, \mathbf{r}'; \omega) \delta\rho(\mathbf{r}', \omega). \quad (3.5)$$

The exchange correlation kernel is the functional derivative of the exchange correlation potential with respect to the time-dependent density. In the ALDA this kernel is local, both in space and time. Most applications of time-dependent DFT have used the ALDA so far [9, 72, 19, 67].

$$f_{\text{xc}}^{\text{ALDA}}(\mathbf{r}, \mathbf{r}'; \omega) = \delta(\mathbf{r} - \mathbf{r}') \frac{d^2}{d\rho^2} [\rho \varepsilon_{\text{xc}}(\rho)] |_{\rho=\rho_0(\mathbf{r})}, \quad (3.6)$$

where $\rho_0(\mathbf{r})$ is the converged SCF density. The Vosko Wilk Nusair [4] parametrization for the exchange correlation energy density ε_{xc} of a homogeneous electron gas is used. Although the ALDA can only be expected to be a good approximation for slow time-dependent processes, it appears to work well even outside this region [9].

A frequency-dependent extension, based upon a Padé-like interpolation between high and low frequency limits of the homogeneous electron gas, has been derived by Gross and Kohn [160]. However, the main deficiency of the ALDA seems to be in the spatial part rather than in the lack of frequency dependence [31, 72, 9].

The set of equations (3.2), (3.3), (3.4) and (3.5) must be solved self-consistently. After this has been done, the frequency-dependent polarizability $\alpha(\omega)$ is directly available, for a density change $\delta\rho_i(\mathbf{r}, \omega)$ due to an external potential $\delta v_{\text{ext},i}(\mathbf{r}, t) = E r_i \cos(\omega t)$:

$$\alpha_{ij}(\omega) = -\frac{2}{E} \int d\mathbf{r} \delta\rho_i(\mathbf{r}, \omega) r_j, \quad (3.7)$$

where i and j denote the Cartesian directions x, y, z . There is an interesting relation between multipolar polarizabilities at imaginary frequencies and Van der Waals dispersion coefficients [48, 45, 156]. The most general formulation [156, 161] involves a double spherical harmonics expansion.

In the present paper, we will restrict ourselves to the R^{-6} term of the dispersion interaction energy between two linear molecules, for which expressions are given in Refs. [151] and [162]. The R^{-6} term involves dipole polarizabilities only. It is governed by the isotropic coefficient C_6 and by two anisotropic coefficients: C_6' and C_6'' , which control the orientation-dependent part of the long-range interaction. The average polarizability α and the anisotropy

κ are defined with respect to the polarizability tensor components parallel and perpendicular to the main molecular symmetry axis:

$$\alpha = \frac{\alpha_{\parallel} + 2\alpha_{\perp}}{3}, \quad (3.8)$$

$$\kappa = \alpha_{\parallel} - \alpha_{\perp}. \quad (3.9)$$

The dispersion coefficients between linear molecules A and B are related to these properties at imaginary frequencies, by the following integral relations [151] (Hartree atomic units are used throughout the article, unless otherwise stated):

$$C_6(A, B) = \frac{3}{\pi} \int_0^{\infty} \alpha_A(i\omega) \alpha_B(i\omega) d\omega \quad (3.10)$$

$$C'_6(A, B) = \frac{1}{\pi} \int_0^{\infty} \kappa_A(i\omega) \alpha_B(i\omega) d\omega \quad (3.11)$$

$$C''_6(A, B) = \frac{1}{3\pi} \int_0^{\infty} \kappa_A(i\omega) \kappa_B(i\omega) d\omega \quad (3.12)$$

These equations can also be used for the symmetrical top molecules NH_3 , C_2H_6 , and $\text{c-C}_3\text{H}_6$ [162]. We further use the relative anisotropies $\Gamma(A, B)$ and $\Delta(A, B)$, defined by [163]:

$$\Gamma(A, B) = \frac{C'_6(A, B)}{C_6(A, B)} \quad (3.13)$$

$$\Delta(A, B) = \frac{C''_6(A, B)}{C_6(A, B)} \quad (3.14)$$

3.4 Implementation

The ADF program ([89, 164, 115, 90, 165]) makes use of STO basis and fit sets. Further characteristics include the use of an accurate numerical integration scheme [115, 90] and the possibility to apply a frozen core approximation.

The fit set $\{f_i\}$ employed in ADF is used to approximate the first order density change by:

$$\delta\rho(\mathbf{r}, \omega) = \sum_i^{\text{nfit}} C_i(\omega) f_i(\mathbf{r}), \quad (3.15)$$

where the coefficients $C_i(\omega)$ are real numbers. This enables one to do the integration involved in the Coulomb term of Eq. (3.4) analytically. Because of the local form of the exchange correlation kernel f_{xc} , the integration in Eq. (3.5) is trivial and one obtains:

$$\begin{aligned} \delta v_{\text{eff}}(\mathbf{r}, \omega) &= \delta v_{\text{ext}}(\mathbf{r}, \omega) + \sum_i^{\text{nfit}} C_i(\omega) \left(\int d^3\mathbf{r}' \frac{f_i(\mathbf{r}')}{|\mathbf{r} - \mathbf{r}'|} + f_i(\mathbf{r}) \frac{d^2}{d\rho^2} [\rho \varepsilon_{\text{xc}}(\rho)] \Big|_{\rho=\rho_0(\mathbf{r})} \right) \\ &\equiv \delta v_{\text{ext}}(\mathbf{r}, \omega) + v_{\text{ind}}(\mathbf{r}, \omega). \end{aligned} \quad (3.16)$$

The Coulomb and exchange correlation term are combined into an induced potential v_{ind} which is known in all the integration points of the numerical integration grid.

Substituting Eqs. (3.16) and (3.3) into Eq. (3.2) yields:

$$\delta\rho(\mathbf{r}, \omega) = \sum_i^{\text{occ}} \sum_m^{\text{virt}} n_i \phi_i(\mathbf{r}) \phi_m(\mathbf{r}) \left(\frac{1}{(\varepsilon_i - \varepsilon_m) + \omega} + \frac{1}{(\varepsilon_i - \varepsilon_m) - \omega} \right) \times \int d^3\mathbf{r}' \phi_i(\mathbf{r}') \phi_m(\mathbf{r}') [\delta v_{\text{ext}}(\mathbf{r}', \omega) + v_{\text{ind}}(\mathbf{r}', \omega)]. \quad (3.17)$$

For real orbitals ϕ the density change is given by:

$$\delta\rho(\mathbf{r}, \omega) = \sum_i^{\text{occ}} \sum_m^{\text{virt}} n_i P_{im}(\omega) \phi_i(\mathbf{r}) \phi_m(\mathbf{r}) \quad (3.18)$$

Combining the last two equations gives

$$P_{im}(\omega) = \left(\frac{1}{(\varepsilon_i - \varepsilon_m) + \omega} + \frac{1}{(\varepsilon_i - \varepsilon_m) - \omega} \right) \int d^3\mathbf{r}' \phi_i(\mathbf{r}') \phi_m(\mathbf{r}') [\delta v_{\text{ext}}(\mathbf{r}', \omega) + v_{\text{ind}}(\mathbf{r}', \omega)] \quad (3.19)$$

The coefficients $\{P_{im}\}$ are found by a self-consistent procedure. Starting with the uncoupled case ($v_{\text{ind}}(\mathbf{r}, \omega) = 0$), one obtains an initial set $\{P_{im}\}$. Then the density is fitted in order to obtain the coefficients $\{C_i\}$. These result in a new potential v_{ind} , which results in new coefficients $\{P_{im}\}$. This is repeated until the change in the coefficients becomes negligible. In order to speed up the convergence, the Direct Inversion in the Iterative Subspace (DIIS) method originating from Pulay [95, 96] is used. The expensive steps in the procedure are the integrations of Eq. (3.19), which are evaluated with an accurate numerical integration procedure [115, 90], and the density fit [89]. The use of atom-centered basis functions allows to break up the density in one- and two-center charge distributions. A least squares fit of each atom-atom charge distribution is performed with fitting functions on the two atoms. This procedure avoids the increase of the dimension of the fitting problems with system size.

3.5 Description of basis sets and parameters in the calculations

For first row atoms, the largest standard STO basis set in ADF is a triple zeta s, p basis to which a 3d and a 4f polarization function are added. For the H-atom, this basis consists of a triple zeta s basis, extended with a 2p and 3d polarization function. This basis will be called 3Z2P in this paper. For the correct description of such sensitive properties as polarizabilities, it is mandatory to add diffuse functions to the basis. Our first extension of the 3Z2P basis, which we will denote by 3Z2P*, adds the diffuse s, p, and d functions with exponents recommended by Zeiss et al. [166, 155] in the case of the H, F, N, O, and C atoms. For the rare gas atoms we follow Colwell et al. [134], by adding diffuse s, p, and d functions with exponents which were one third of the smallest exponents used in the standard 3Z2P basis.

40 POLARIZABILITIES AND VAN DER WAALS COEFFICIENTS

Because the results with this basis are still not close enough to the basis set limit, we use a basis 3Z2P**¹, in which each diffuse function of the 3Z2P* basis was replaced by two diffuse functions, one with a lower and one with a higher exponent.

After some tests with even larger basis sets and by comparison to basis set free methods (see later), the results with the 3Z2P** basis were found to be close to the basis set limit, being still slightly too low. We estimate our results to be within 3% of the basis set limit. We have employed the 3Z2P** basis for all calculations in this work, unless otherwise stated.

The influence of the fit set was minimized by taking almost saturated fit sets, without letting the overlap between different fit functions become too large.

The accuracy of the numerical integration was set such that several standard integrals are evaluated with at least five digit accuracy, enough to neglect remaining errors.

The integrals in Eqs. (3.10), (3.11) and (3.12) are solved by the twenty point Gauss–Chebyshev quadrature described in Ref.[156]. The error made by using this approximation is smaller than errors caused by basis set or fit set effects.

In most tables, the estimated computational accuracy is given. These estimates do not include basis set effects. They were made by comparing to results with somewhat smaller fit sets.

The core of all atoms except He and H was kept frozen. The outermost frozen shell was 1s for Ne, N, O, F, C, 2p for Ar and 3d for Kr. The effect of the frozen core for the polarizability of the rare gases was 1.1% for Ar and less than 0.2% for the other atoms. The effect of the frozen core approximation on molecular polarizabilities is expected to be smaller in the relative sense.

The experimental equilibrium geometries were used for all our calculations [167].

The number of iterations needed in order to solve the set of equations (3.2), (3.3), (3.4) and (3.5) for one frequency, varies between 3 and 10. A few hours on an IBM RS6000/550 workstation are needed to calculate the full polarizability tensor for c-C₃H₆ at ten imaginary frequencies, with the largest basis and fit sets and the biggest numerical integration grid used. These numbers should give an impression of the efficiency of the implementation.

3.6 Comparison with other theoretical methods

3.6.1 Static and frequency-dependent polarizabilities

As a first test of our implementation, we reproduced our finite field calculations on polarizabilities for several systems. The relative deviations found lie between 0.002 for H₂O and $3 \cdot 10^{-6}$ for Ne. This is satisfactory because in the case of H₂O the finite field result still contains some higher order effects.

We calculated the frequency-dependent polarizabilities of several rare gas atoms, in order to assess the quality of our basis sets and to compare our results to those obtained by Senatore and Subbaswamy [72], whose ALDA solution method is basis set free. They fitted the experimental data [168] and their own result for the frequency-dependent polarizability

¹A more standard notation would be 3Z2P++

$$\alpha(\omega) = \alpha_0(1 + C_2\omega^2). \quad (3.20)$$

Table 3.1: Comparison of the frequency dependence of the polarizability of rare gas atoms with basis set free ALDA results [72] and with experiment. The results are fitted according to Eq. (3.20).

Atom		He	Ne	Ar	Kr
This work 3Z2P	α_0	1.65	2.28	9.32	13.32
This work 3Z2P*	α_0	1.65	2.77	11.07	15.68
This work 3Z2P**	α_0	1.65	3.02	11.94	17.67
PZ ALDA ^a	α_0	1.66	3.05	12.01	18.02
Other LDA [30]	α_0		2.99 ^b , 3.15 ^c	11.80 ^b , 12.48 ^c	17.70 ^b , 18.86 ^c
Expt.[168]	α_0	1.38	2.67	11.07	16.74
This work 3Z2P	C_2	1.40	0.60	2.02	1.89
This work 3Z2P*	C_2	1.39	1.44	3.03	3.34
This work 3Z2P**	C_2	1.46	1.49	3.07	4.02
PZ ALDA ^a	C_2	1.49	1.49	3.13	4.10
Expt.[168]	C_2	1.16	1.11	2.60	3.61

^aNumerical ALDA results [72] according to the Perdew Zunger [169] parametrization of the homogeneous electron gas exchange correlation functional.

^bGunnarsson Lundqvist representation of exchange correlation potential [170].

^cCeperley Alder [5] exchange correlation data for the homogeneous electron gas, as used by Mahan and Subbaswamy [30].

The results are given in Table 3.1. In this table, the differences between our results and those obtained by Senatore and Subbaswamy [72] are small. Our results are clearly closer to Senatore and Subbaswamy’s results than to the experimental values, being always in between the two. Taking even bigger basis sets does not change the results significantly. From this fact and from the small differences between our results and those obtained by Senatore and Subbaswamy, we conclude that our basis and fit sets are of high quality and that our results are close to the basis set limit. The remaining differences can partially be attributed to the different parametrizations used for the numerical Ceperley and Alder electron gas results [5], because Senatore and Subbaswamy use the Perdew Zunger parametrization [169], where we employ the Vosko Wilk Nusair [4] parametrization.

In Table 3.1 also some LDA results for α_0 using different methods and different parametrizations for the exchange correlation potential are reported. The results show considerable variation, which puts the (small) differences which we obtain with respect to Ref.[72] in perspective.

The behavior of the frequency-dependent polarizability of Kr at imaginary frequencies is shown in Figure 3.1. Our result is compared to the ALDA result given on page 111 of Ref.[30], where the Gunnarsson–Lundqvist [170] expression for the exchange correlation potential has apparently been used.

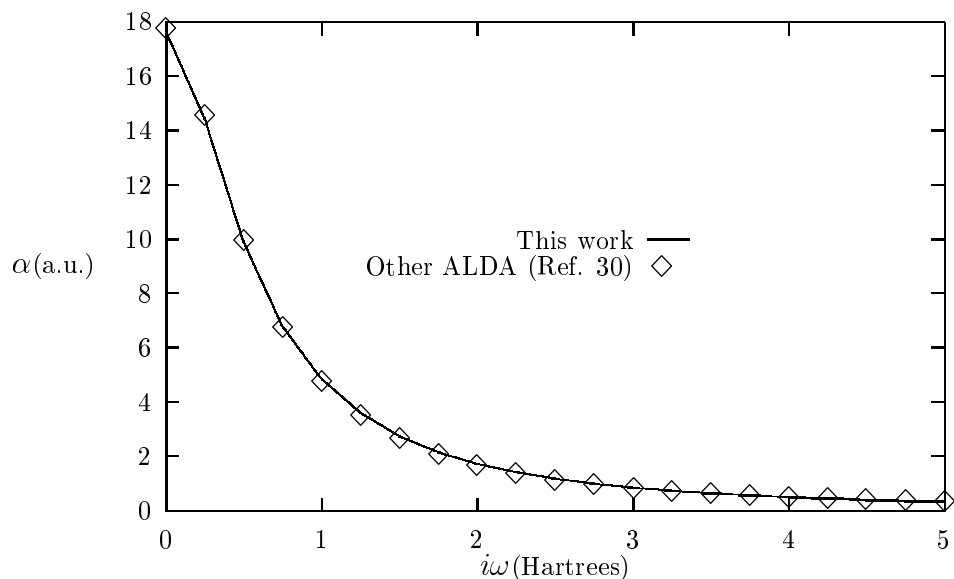


Figure 3.1: The polarizability of Kr at imaginary frequencies.

The good agreement of the zero frequency result is somewhat fortuitous, but the figure does show that the description of the frequency dependence agrees very well too. For Ne and Ar we find similar results.

In Table 3.2, we compare our results for the static polarizability of several molecules with experimental and theoretical results². These results can be used to estimate the reliability of the dispersion coefficients which will be presented in the remainder of the article. In agreement with previous work[152, 153, 154, 155], we note that the average polarizability α_0 is generally satisfactory, but somewhat too high. The anisotropies κ_0 do not show clear systematic deviation. They are of similar quality as α_0 , except for NH_3 , where there is considerable spread in the results anyway.

The reference values in Table 3.2 and the rest of this article are reliable constrained Dipole Oscillator Strength Distribution (DOSD) results, obtained through the use of experimental and theoretical dipole oscillator strength data and a system of quantum mechanical sum rule constraints.

3.6.2 Isotropic dispersion coefficients

In this paper we are primarily interested in the quality of C_6 Van der Waals dispersion coefficients for medium-sized molecules, calculated within the ALDA. The study of Bartolotti[16] for the rare gases was promising in this respect.

In Table 3.3 our values with basis set 3Z2P** are compared to time-dependent coupled Hartree-Fock (TDCHF) and MBPT results close to the basis set limits. The reference values are the DOSD results.

A few important trends can be derived from Table 3.3.

²A strange geometry was inadvertently used for H_2 in this paper. See Chapter 4 for details.

Table 3.2: Static polarizabilities.

Mol.	comp.	Experiment / DOSD	Hohm [162]	This work	Other LDA results
H ₂	α_0	5.433 ^c ; 5.53 ^a	5.43	6.10	6.13 ^f
H ₂	κ_0	2.042 ^c ; 2.12 ^a	2.04	2.15	2.09 ^f
N ₂ O	α_0	19.77 ^b ; 20.3 ^a	19.70	19.80	
N ₂ O	κ_0	19.10 ^b ; 20.0 ^a	19.10	18.44	
CO ₂	α_0	17.48 ^b ; 17.75 ^a	17.50	17.74	17.80 ^e
CO ₂	κ_0	13.70 ^b ; 14.2 ^a	13.72	13.61	13.96 ^e
NH ₃	α_0	15.0 ^a	14.56	15.62	15.57 ^e ; 15.44 ^f
NH ₃	κ_0	1.94 ^a	1.04	3.08	2.67 ^e ; 1.85 ^f
C ₂ H ₆	α_0	30.2 ^a	29.54	30.70	
C ₂ H ₆	κ_0	5.2 ^a	4.19	4.32	
c-C ₃ H ₆	α_0	38.0 ^a	37.30	39.25	
c-C ₃ H ₆	κ_0	-5.4 ^a	-4.79	-5.09	
N ₂	α_0	11.74 ^c ; 11.74 ^b		12.30	11.84 ^f
N ₂	κ_0	4.45 ^b		4.68	5.36 ^f
CO	α_0	13.08 ^d		13.68	13.41 ^f
CO	κ_0	3.567 ^d		3.30	3.90 ^f

^aRef.[171], measurements at 6328 Å ^bRef.[172] ^cRef.[173] ^dRef.[163] ^eRef.[152] ^fRef.[153]

- The ALDA results for frequency-dependent polarizabilities and isotropic C_6 Van der Waals dispersion coefficients are generally too high. This was to be expected, since the aforementioned studies on static polarizabilities show the same trend.
- The ALDA results involving He or H₂, or other small systems are relatively poor. They are approximately 15 to 20% too high. Going towards bigger systems, the results tend to improve (1 to 10% too high). This is interesting, because MBPT calculations are not feasible anymore for larger systems. The ALDA offers a parameter-free alternative.
- The ALDA results are of similar quality as the TDCHF results. They are slightly worse for small systems and somewhat better for larger systems.

3.6.3 Anisotropic dispersion coefficients

An interesting application of the presented theory is the calculation of the anisotropic Van der Waals dispersion coefficients C'_6 and C''_6 of Eqs. (3.11) and (3.12). Due to the scarceness of experimental data on the polarizability anisotropy, accurate constrained DOSD [163, 173] calculations are available for a few small molecules only. Ab initio TDCHF and MBPT calculations are possible, but not uniformly reliable as shown by Tables 3.4 and 3.5, which contain DOSD data from Refs.[163] and [173].

We have added our own ALDA results to these tables. The relative anisotropies obtained with the ALDA are at least of comparable quality as the TDCHF and MBPT results and sometimes markedly superior (the TDCHF results for CO-He and CO-Ne in Table 3.4 provide examples). It has to be remarked that the MBPT calculations of Ref.[150] clearly

improve earlier MBPT result of Ref.[156]. Hettema states in his thesis [159] that the MBPT relative anisotropies of N₂ with the rare gases which he obtains, are roughly 35% too low. He concludes that his MBPT approach is not sufficient to deal with the strong electron correlation associated with the triple bonds in N₂ and CO. Maybe the most important result from Tables 3.4 and 3.5 is that the ALDA results never differ from the accurate DOSD results by more than 18% (in the case of CO-CO, in Table 3.5). The average deviation from the DOSD values is about 6% in Table 3.4 and about 9% in Table 3.5.

We conclude that at present, the ALDA method is the most reliable method for calculating anisotropic dispersion interaction coefficients for molecules for which insufficient accurate experimental data exist in order to perform a DOSD calculation. This conclusion is supported by the fact that LDA predicts the static polarizability anisotropy better than Hartree–Fock calculations do[152].

3.7 Evaluation of two semiempirical methods

In an interesting article, Hohm [162] recently calculated anisotropic dispersion coefficients for several molecules by two semiempirical methods. In the first place he used the two traditional approximate formulas, which involve some mean excitation energy $\bar{\omega}_{AB}$ and the static polarizability tensor:

$$C'_6(A, B) \approx \frac{\bar{\omega}_{AB}}{2} \kappa^A(0) \alpha^B(0), \quad (3.21)$$

$$C''_6(A, B) \approx \frac{\bar{\omega}_{AB}}{6} \kappa^A(0) \kappa^B(0). \quad (3.22)$$

Contrary to Hohm, we use the factor $\frac{1}{6}$ in Eq. (3.22), in agreement with Ref.[181]. Hohm's own approach is to fit the average polarizability and the polarizability anisotropy to functions of the form:

$$\alpha(\omega) = \frac{1}{3} \left(\frac{f_{\parallel}}{\omega_{\parallel}^2 - \omega^2} + \frac{2f_{\perp}}{\omega_{\perp}^2 - \omega^2} \right) \quad (3.23)$$

$$\kappa(\omega) = \frac{f_{\parallel}}{\omega_{\parallel}^2 - \omega^2} - \frac{f_{\perp}}{\omega_{\perp}^2 - \omega^2}, \quad (3.24)$$

and to perform the integrations of Eqs. (3.10), (3.11) and (3.12). The differences he found between these two semiempirical approaches are quite substantial. Sometimes discrepancies of an order of magnitude or sign differences were encountered. Hohm expresses no clear preference for either method. As we have shown the validity of our approach in the beginning of the article, we can now use our method to compare the semiempirical values given by Hohm to our own values and to discuss the peculiarities of the semiempirical approaches.

In Tables 3.6, 3.7, and 3.8, our results are compared to the results given by Hohm. In the first rows of these tables, our values are given in bold face.

Considering the isotropic dispersion coefficients C_6 in Table 3.6, there is qualitative agreement between the different methods. Hohm's semiempirical method yields values (in the second row) which are too low compared to the benchmark theoretical (DOSD) values in the

third row, while our results are a bit too high. Both Hohm’s method and the mixture rule [162], which was used to calculate the values in parentheses, provide reasonable results.

In Table 3.7 results for the anisotropic dispersion coefficient C'_6 are given. The second row gives Hohm’s own results, while the third row refers to the results obtained with the approximate formula (3.21). The striking feature of this table is the disagreement between the values in the second row and the other values, where the anisotropy of NH_3 , C_2H_6 or $\text{c-C}_3\text{H}_6$ is concerned. Clearly, Hohm’s fit describes the frequency dependence of the polarizability anisotropies of these molecules incorrectly. This may be due to the fact that only a small number of data on the polarizability anisotropy were available (only for one frequency in the case of NH_3), which may have caused erroneous fit parameters. There is qualitative agreement between our results and the traditional semiempirical results in the third row. These semiempirical results are generally higher than ours. In the cases where Hohm’s results are close to the other results (H_2 , N_2O , and CO_2), his values are too low, as in Table 3.6.

In Table 3.8 the results for C''_6 are presented. As in the previous table, the second row gives Hohm’s own results, while the third row gives the results with Eq. (3.22). The results for C''_6 in our table differ from those in Hohm’s paper due to our use of the factor $\frac{1}{6}$ in Eq. (3.22), while Hohm used $\frac{1}{8}$ in his table [182]. The features of Table 3.7 are magnified here. Hohm’s results are unsatisfactory for NH_3 , C_2H_6 , and $\text{c-C}_3\text{H}_6$. The results in the third row are too large in absolute value. Hohm’s results for H_2 , N_2O , and CO_2 are too small.

The approximation that the average polarizability and the polarizability anisotropy have the same frequency dependence, which has implicitly been made in Eqs. (3.21) and (3.22), is not always a good approximation. The overestimation in the results of Tables 3.7 and 3.8 with the traditional semiempirical formulas may be largely due to this approximation.

Table 3.2 gives an impression of the quality of our dispersion coefficients in Tables 3.6, 3.7, and 3.8. For example, the polarizability anisotropy of NH_3 is too high in Table 3.2, which leads to the value of 0.118 in Table 3.8. This value is too high. On the other hand, our static polarizability values for N_2O and CO_2 are close to the experimental values, which suggests that the calculated dispersion coefficients are accurate for these molecules.

Summing up the results of Tables 3.6, 3.7, and 3.8, we can say that our results always agree qualitatively with the traditional semiempirical formulas. The results of Hohm’s approach which involve the anisotropy of NH_3 , C_2H_6 or $\text{c-C}_3\text{H}_6$ are unsatisfactory. In the case of the other molecules (H_2 , N_2O , and CO_2), the situation is less clear cut, which seems to imply that the lack of data for $\kappa(\omega)$ is mainly responsible for Hohm’s erroneous results for the larger molecules. Our results involving anisotropies are always in between the two semiempirical results. We believe that our own values are the most reliable ones.

3.8 Conclusions

An efficient way for calculating frequency-dependent polarizabilities and C_6 Van der Waals dispersion coefficients has been implemented in the ADF program using the Adiabatic Local Density Approximation. The results involving average polarizabilities are of similar quality as TDCHF calculations. The isotropic dispersion coefficients show a clear tendency to be too large, due to the overestimation of α_0 . If polarizability anisotropies are concerned, our results

compare favorably to both TDCHF and MBPT results. We used our results to compare two semiempirical ways to calculate anisotropic Van der Waals dispersion coefficients.

The extension of the ALDA to arbitrary closed-shell molecules opens up the possibility to investigate molecular properties such as photoabsorption, frequency-dependent linear response and long-range Van der Waals interactions within DFT for general medium-sized molecules.

Extensions to nonlocal or frequency-dependent functionals and to frequency-dependent hyperpolarizabilities seem feasible.

3.9 Acknowledgements

We would like to thank Dr. P. Wormer for useful discussions. G. Wiesenekker and P. Philipsen are thanked for helping with the DIIS procedure. The financial support by the Dutch Foundation for Chemical Research (S.O.N.) is gratefully acknowledged.

Table 3.3: Isotropic dispersion coefficients $C_6(A, B)$. The computational accuracy for our results is estimated to be 1%.

A	B	MBPT	TDCHF	This work	DOSD
He	He	1.431 ^c	1.375 ^c	1.82	1.458 ^g
He	Ne	3.0712 ^a	2.697 ^c	3.60	3.029 ^g
He	Ar	9.5667 ^a		11.2	9.538 ^g
He	Kr	13.652 ^a		15.4	13.40 ^g
Ne	Ne	6.5527 ^a	5.392 ^f ; 5.5136 ^a	7.26	6.383 ^g
Ne	Ar	19.753 ^a	17.641 ^a	21.8	19.50 ^g
Ne	Kr	28.009 ^a	24.802 ^a	29.9	27.30 ^g
Ar	Ar	64.543 ^a	61.833 ^a	69.9	64.30 ^g
Ar	Kr	93.161 ^a	88.563 ^a	97.1	91.13 ^g
Kr	Kr	135.08 ^a	127.41 ^a	135	129.6 ^g
H ₂	H ₂	12.62 ^c	12.30 ^c	14.3	12.09 ⁱ
H ₂	N ₂	30.54 ^c	29.28 ^f	32.8	29.46 ⁱ
H ₂ O	H ₂ O	46.443 ^b ; 47.623 ^b ; 48.794 ^d	39.437 ^b	50.1	45.37 ^h
H ₂ O	N ₂			62.2	57.68 ^h
H ₂ O	NH ₃			68.6	63.41 ^h
NH ₃	NH ₃			94.4	89.08 ^h
NH ₃	Ar	75.216 ^b ; 78.143 ^b	69.170 ^b	81.0	
NH ₃	N ₂			85.0	80.48 ^h
N ₂	N ₂	75.63 ^c	71.46 ^f	77.2	73.43 ⁱ
Ne	N ₂	21.525 ^a ; 21.75 ^c	18.88 ^f ; 19.07 ^c	23.1	20.97 ⁱ
Ar	N ₂	69.843 ^a		73.5	68.69 ⁱ
Kr	N ₂	100.67 ^a		102	97.28 ⁱ
Ne	HF	11.502 ^a		12.7	10.87 ^g
Ar	HF	36.334 ^a		39.9	34.73 ^g
Kr	HF	52.053 ^a		55.2	49.00 ^g
Ne	CO	23.075 ^a ; 22.047 ^e ; 23.32 ^c	19.24 ^c	23.8	21.87 ^j
Ar	CO	75.806 ^a ; 73.597 ^c		76.5	72.26 ^j
Kr	CO	109.63 ^a ; 106.43 ^c		106	102.5 ^j
CO	CO	89.14 ^c	73.96 ^c	83.8	81.31 ^j
CO	N ₂	82.01 ^c	72.65 ^c	80.4	77.21 ^j
CO ₂	CO ₂			161	158.7 ^k
N ₂ O	N ₂ O			186	184.9 ^h
C ₂ H ₆	C ₂ H ₆			397	381.8 ^l

^aRef.[174] ^bRef.[175] ^cRef.[156] ^dRef.[176] ^eRef.[150] ^fRef.[161] ^gRef.[177] ^hRef.[178] ⁱRef.[173]
^jRef.[163] ^kRef.[179] ^lRef.[180]

Table 3.4: Relative anisotropy in dispersion coefficients $\Gamma(A, B)$.

A-B	DOSD [163, 173]	TDCHF [156]	MBPT[156]	MBPT [150]	This work
CO-CO	0.0940	0.0854	0.1245		0.0850
CO-H ₂	0.0949	0.0872	0.1264		0.0861
H ₂ -CO	0.0976	0.0993	0.1057		0.0950
CO-N ₂	0.0939	0.0854	0.1238		0.0848
N ₂ -CO	0.1077	0.1185	0.1306		0.1092
H ₂ -H ₂	0.1006				0.0962
H ₂ -N ₂	0.1109 ^a				0.0940
N ₂ -H ₂	0.0966 ^a				0.1119
N ₂ -N ₂	0.1068				0.1084
CO-He	0.0930	0.187	0.270	0.1036	0.0842
CO-Ne	0.0916	0.182	0.265	0.1013	0.0824
CO-Ar	0.0942			0.1067	0.0852
CO-Kr	0.0943			0.1077	0.0855
H ₂ -He	0.0924				0.0906
H ₂ -Ne	0.0901				0.0882
H ₂ -Ar	0.0971				0.0934
H ₂ -Kr	0.0986				0.0945
N ₂ -He	0.1027				0.1063
N ₂ -Ne	0.0999				0.1032
N ₂ -Ar	0.1074				0.1090
N ₂ -Kr	0.1087				0.1101

^aThese data have to be interchanged with respect to the original Reference, improving the agreement with our results.

Table 3.5: Relative anisotropy in dispersion coefficients $\Delta(A, B)$.

A-B	DOSD [163, 173]	TDCHF [156]	MBPT [156]	This work
CO-CO	0.0090	0.0075	0.0159	0.00739
CO-H ₂	0.0094	0.0089	0.0137	0.00833
CO-N ₂	0.0103	0.0105	0.0166	0.00949
H ₂ -H ₂	0.0108			0.00970
H ₂ -N ₂	0.0114			0.01098
N ₂ -N ₂	0.0121			0.01225

Table 3.6: Isotropic dispersion coefficients $C_6(A, B)$.

The computational accuracy in our results (first row, bold faced) is estimated to be 1%. The second row gives Hohm's results, according to Eqs. (3.10) and (3.23). The third row gives accurate theoretical values, where available. Except for H₂-H₂ these are DOSD values. The results in round brackets were obtained by a semiempirical mixture rule [162].

	H ₂	N ₂ O	CO ₂	NH ₃	C ₂ H ₆	c-C ₃ H ₆
H ₂	14.3	51.1	47.3	36.7	75.3	95.36
	11.051	43.81	40.24	32.90	63.46	79.60
	12.058 ^a	46.97 ^b	43.33 ^c	32.78 ^b	(67.82)	
N ₂ O		186.0	173.0	132.1	271.0	343.31
		168.02	154.54	126.79	242.08	303.87
		184.9 ^b	(171.15)	128.1 ^b	(265.43)	
CO ₂			161.1	122.6	251.5	318.68
			142.23	116.71	222.45	279.21
			158.7 ^c	(118.26)	(245.24)	
NH ₃				94.4	193.6	245.38
				96.00	182.02	228.60
				89.08 ^b	(184.39)	
C ₂ H ₆					397.4	503.5
					350.22	439.55
					381.8 ^d	
c-C ₃ H ₆						638.0
						551.26

^aRef.[151] ^bRef.[178] ^cRef.[179] ^dRef.[180]

Table 3.7: Anisotropic dispersion coefficients $C'_6(A, B)$.

The results of this work are given in the first row. The second row gives the results corresponding to Eqs. (3.11), (3.23), and (3.24), while the third row corresponds to Eq. (3.21). For H_2 an accurate theoretical value has been given in the fourth row [151]. The computational accuracy for our results is estimated to be 5% for NH_3 , 3% for $c-C_3H_6$ and 2% for the other molecules.

	H_2	N_2O	CO_2	NH_3	C_2H_6	$c-C_3H_6$
H_2	1.39	4.83	4.44	3.53	7.24	9.17
	1.22	4.59	4.20	3.42	6.72	8.42
	1.43	5.73	5.12	4.07	7.79	10.72
	1.219					
N_2O	12.7	44.3	40.9	32.2	66.1	83.79
	8.69	31.50	28.55	22.90	47.31	59.18
	14.78	59.79	53.46	42.25	80.47	111.79
CO_2	9.95	34.9	32.3	25.3	52.0	65.88
	6.82	24.92	22.65	18.21	37.22	46.56
	10.68	43.23	38.65	30.54	58.14	80.82
NH_3	0.45	1.22	1.03	1.08	2.10	2.69
	-4.86	-20.14	-18.91	-15.89	-27.45	-34.58
	0.77	3.12	2.79	2.21	4.21	5.83
C_2H_6	2.7	9.4	8.6	6.9	14.1	17.90
	-1.07	-5.21	-5.10	-4.45	-6.34	-8.03
	2.94	11.77	10.52	8.35	16.01	22.03
$c-C_3H_6$	-2.647	-8.96	-8.20	-6.66	-13.60	-17.26
	3.96	17.70	16.86	14.54	22.86	28.98
	-3.67	-14.82	-13.25	-10.48	-19.97	-27.72

Table 3.8: Anisotropic dispersion coefficients $C_6''(A, B)$.

The results in this work are given in the first row. The second row gives the results corresponding to Eqs. (3.12) and (3.24), while the third row corresponds to Eq. (3.22). For H_2 an accurate theoretical value has been given in the fourth row [151]. The computational accuracy for our results is estimated to be 10% for $c\text{-C}_3\text{H}_6$, 5% for NH_3 and 2% for the other molecules.

	H_2	N_2O	CO_2	NH_3	C_2H_6	$c\text{-C}_3H_6$
H_2	0.143	1.28	0.99	0.066	0.281	-0.282
	0.13	1.02	0.79	-0.42	-0.04	0.27
	0.18	1.85	1.34	0.10	0.37	-0.46
	0.130					
N_2O		11.5	8.97	0.53	2.51	-2.49
		8.83	6.62	-1.28	0.92	-0.69
		19.32	13.97	1.01	3.80	-4.79
CO_2			7.01	0.376	1.95	-1.92
			5.00	-1.34	0.48	-0.04
			10.10	0.73	2.75	-3.46
NH_3				0.118	0.138	-0.173
				4.58	2.27	-5.55
				0.05	0.20	-0.25
C_2H_6					0.555	-0.559
					1.43	-3.15
					0.76	-0.94
$c\text{-C}_3H_6$						0.577
						7.37
						1.19

Chapter 4

Improved density functional theory results for frequency-dependent polarizabilities, by the use of an exchange-correlation potential with correct asymptotic behavior

4.1 Abstract

The exchange-correlation potentials v_{xc} which are currently fashionable in Density Functional Theory (DFT), such as those obtained from the Local Density Approximation (LDA) or Generalized Gradient Approximations (GGAs), all suffer from incorrect asymptotic behavior. In atomic calculations, this leads to substantial overestimations of both the static polarizability and the frequency dependence of this property. In the present paper, it is shown that the errors in atomic static dipole and quadrupole polarizabilities are reduced by almost an order of magnitude, if a recently proposed model potential with correct Coulombic long-range behavior is used. The frequency dependence is improved similarly. The model potential also removes the overestimation in molecular polarizabilities, leading to slight improvements for average molecular polarizabilities and their frequency dependence. For the polarizability anisotropy we find that the model potential results do not improve over the LDA and GGA results. Our method for calculating frequency-dependent molecular response properties within time-dependent DFT, which we described in more detail elsewhere, is summarized.

4.2 Introduction

In recent years there has been a growing interest in Density Functional Theory (DFT)[1, 3] from the quantum chemistry community. Its time-dependent extension, time-dependent DFT [31, 32, 37] is not yet that well explored. It was given a firm theoretical basis in 1984,

60 IMPROVED POLARIZABILITIES THROUGH CORRECT ASYMPTOTICS

by Runge and Gross [38] and offers the possibility to calculate frequency-dependent response properties, whereas finite field calculations [155, 153, 154, 183, 152] only give access to static properties. Most calculations with time-dependent DFT have been restricted to atoms [9, 23, 11, 16, 72, 30, 24, 184]. Molecular calculations were, amongst others, performed by Levine and Soven [19], in a single-center expansion. As this approach seems impractical for general systems, we recently developed a method which can be used for general molecules, although our present implementation can only handle closed-shell molecules. Our previous calculations with this method [34], using the Local Density Approximation (LDA) yielded satisfactory results for polarizabilities and Van der Waals dispersion coefficients. However, the results for the atoms showed a clear overestimation of both the static polarizability and the frequency dependence, in agreement with results from previous papers [9, 23, 11, 16, 72, 30, 24]. The molecular results were more satisfactory, though the average polarizability is systematically overestimated here too, as is also well-known [152, 34]. The overestimation seems more pronounced in lighter systems (He can serve as an example) than in heavy molecules.

In atomic calculations on properties which are even more sensitive to the outer region, such as quadrupole polarizabilities [68] and hyperpolarizabilities [72, 67, 71, 135] the LDA error is more pronounced. The static quadrupole polarizabilities of the rare gases are overestimated by the LDA by about 25% on average. The static second hyperpolarizability γ is overestimated by a factor of 2 approximately. The source of this error is well-known. The LDA potential is not attractive enough in the outer region, due to spurious self-interaction. This leads to valence electrons which are too loosely bound.

These results made it worthwhile to test a potential which has correct asymptotic behavior. There have been previous attempts to improve upon the LDA results for atomic response properties. In the book by Mahan and Subbaswamy [30] results for the static (hyper)polarizabilities with so-called self-interaction correction (SIC) [169] and partial self-interaction correction (PSIC) potentials are given. The disadvantage of this approach, is that the potential becomes orbital-dependent, which makes all calculations significantly more time consuming.

Zhong *et al.*[24] have considered the frequency dependence of the atomic polarizabilities in LDA. We agree with these authors upon the fact that occupied and unoccupied eigenvalues are too close together in LDA, which causes a too high frequency dependence. Their solution of this problem is inspired by the GW method [185, 186], which is popular in solid state physics. Their approach is simply to shift the unoccupied energies by a constant. The shift is obtained from a simple model or fitted in order to obtain the experimental static polarizability. This method is reminiscent of the more recent work of Malkin *et al.* [187], who used a comparable procedure for the calculation of NMR shielding tensors. We will compare our results to the papers mentioned above, and show that our results are at least of comparable quality, but are obtained in a more tractable or theoretically more satisfactory way.

First we will give a short outline of our implementation of the linear response equations of time-dependent DFT, which has been described in more detail elsewhere [34]. Then the model potential with correct asymptotic behavior, proposed by two of the authors in Ref.[121], will be presented. After this theoretical introduction, we present our atomic and molecular results in the next section, and we end with some concluding remarks.

4.3 Theoretical introduction

4.3.1 Frequency-dependent linear response in DFT

We will use time-dependent DFT for our calculations in this paper. For reviews on time-dependent DFT we refer to Refs.[31, 32, 37]. Many atomic results are given in the book by Mahan and Subbaswamy [30]. A more detailed description of our approach has been given elsewhere [34].

In time-dependent DFT, the frequency-dependent linear density response $\delta\rho(\mathbf{r},\omega)$ due to a scalar electric external field $\delta v_{\text{ext}}(\mathbf{r},\omega)$ is given in terms of a single particle response function $\chi_s(\mathbf{r},\mathbf{r}',\omega)$ acting on an effective field $\delta v_{\text{eff}}(\mathbf{r}',\omega)$ (atomic units are used throughout the article):

$$\delta\rho(\mathbf{r},\omega) = \int \chi_s(\mathbf{r},\mathbf{r}',\omega)\delta v_{\text{eff}}(\mathbf{r}',\omega)d\mathbf{r}'. \quad (4.1)$$

The Kohn–Sham response function $\chi_s(\mathbf{r},\mathbf{r}',\omega)$ is constructed from (real) orbitals, occupation numbers and one-electron energies, obtained in an ordinary DFT calculation:

$$\chi_s(\mathbf{r},\mathbf{r}',\omega) = \sum_i^{\text{occ.}} \sum_m^{\text{virt.}} n_i \phi_i(\mathbf{r})\phi_m(\mathbf{r})\phi_m(\mathbf{r}')\phi_i(\mathbf{r}') \left(\frac{1}{(\varepsilon_i - \varepsilon_m) + \omega} + \frac{1}{(\varepsilon_i - \varepsilon_m) - \omega} \right). \quad (4.2)$$

Because of screening effects, the effective field in Eq. (4.1) is not equal to the external field. It contains a Hartree and an exchange-correlation term due to the induced density:

$$\delta v_{\text{eff}}(\mathbf{r},\omega) = \delta v_{\text{ext}}(\mathbf{r},\omega) + \int d\mathbf{r}' \frac{\delta\rho(\mathbf{r}',\omega)}{|\mathbf{r} - \mathbf{r}'|} + \delta v_{\text{xc}}(\mathbf{r},\omega), \quad (4.3)$$

where the last term is given by

$$\delta v_{\text{xc}}(\mathbf{r},\omega) = \int d\mathbf{r}' f_{\text{xc}}(\mathbf{r},\mathbf{r}';\omega)\delta\rho(\mathbf{r}',\omega). \quad (4.4)$$

Here the exchange-correlation kernel f_{xc} has been introduced. It is the functional derivative of the exchange-correlation potential with respect to the time-dependent density. As in our previous work [34], we use the frequency-independent adiabatic LDA (ALDA) form of this kernel [31] for all our calculations. In this way we can assess the quality of different potentials, irrespective of the quality of their functional derivatives.

It should be noted that such a mixed scheme, where a different approximation for f_{xc} is made than for v_{xc} , has been used before. Mahan and Subbaswamy [30] prefer the partial SIC, which uses the self-interaction correction only for v_{xc} and not for f_{xc} , to full SIC, because the latter involves unphysical singularities. Stener *et al.* [184] have used the model potential, which we employ here and which they called VLB-potential, in combination with time-dependent DFT to calculate autoionization resonances in noble gases. They used the simple X- α form for f_{xc} , claiming that the Coulombic term in Eq. (4.3), which is the second term on the right-hand side, is much more important for the screening than the exchange-correlation term. We agree with this in general, though it should be observed that the last term is certainly not negligible. For this reason the exchange-correlation kernel has to be chosen with care.

We see no theoretical reason to prefer an f_{xc} derived from a GGA potential or the model potential to the ALDA expression for f_{xc} . In the case of the GGAs, the energy functional E_{xc} is clearly superior to that of the LDA, but the functional derivative of this functional (v_{xc}) is not improved [121]. Because of this, there seems to be no reason to prefer the second functional derivative of a GGA energy functional to the ALDA kernel f_{xc} . On similar grounds, the model potential is not *a priori* expected to give an improvement, because it was obtained with some amount of fitting without considering the quality of the derivative of the potential. It should be noted that finite field calculations can only be compared to schemes in which the exchange-correlation kernel f_{xc} is the functional derivative of the potential which is used.

The given set of Eqs. (4.1, 4.2, 4.3, 4.4) is solved iteratively for a certain external potential v_{ext} , until self-consistency is reached. Then the first order frequency-dependent density change according to the external potential is known. By choosing the appropriate external field, one can calculate dipole, quadrupole, and higher multipole polarizabilities [31, 30, 34].

4.3.2 A model potential with correct asymptotic behavior

Recently, there has been much interest in constructing nearly exact exchange-correlation potentials from highly accurate *ab initio* densities [121, 188, 189, 190, 191, 192]. The model potential used in this article is supposed to approximate such an accurate exchange-correlation potential better than the GGA and LDA potentials do. It was recently proposed by two of the present authors [121]. It yields accurate values for the eigenvalue of the highest occupied Kohn–Sham orbital. This corrects the LDA and GGA values, which are typically several eV too high, causing the density to decrease too slowly in the outer region and the electrons to be too loosely bound. However, one should not look solely at this eigenvalue. We consider the difference between the highest occupied and lowest unoccupied eigenvalue to be a more important quantity for response properties. This can already be understood from Eq. (4.2) for the response function, where only energy differences between occupied and unoccupied orbitals appear. In the work by Zhong *et al.*[24] this gap is also the main quantity.

One of the motivations for the direct modeling of the exchange-correlation potential, instead of taking the functional derivative of an energy functional, is that any exchange energy functional (the Becke functional[138] for example) of the form

$$E_x[\rho] = \int \rho^{\frac{4}{3}}(\mathbf{r}) f(x(\mathbf{r})) d\mathbf{r}, \quad (4.5)$$

with

$$x = \frac{|\nabla\rho|}{\rho^{\frac{4}{3}}}, \quad (4.6)$$

which satisfies the requirement that the exchange energy density per electron ε_x should behave asymptotically as

$$\varepsilon_x(\mathbf{r}) \sim -\frac{1}{2r} \quad (r \rightarrow \infty), \quad (4.7)$$

does not satisfy the requirement

$$v_x(\mathbf{r}) = \frac{\delta E_x[\rho]}{\delta\rho(\mathbf{r})} \sim -\frac{1}{r} \quad (r \rightarrow \infty). \quad (4.8)$$

The proof for this is given in Refs.[193, 121]. The form of the model potential we use here is analogous to Becke's functional for the exchange energy density [138]. In spin-restricted form it is given by [121]:

$$v_{\text{model}}(\mathbf{r}) = -\beta\rho^{\frac{1}{3}}\frac{x^2}{1 + 3\beta x \sinh^{-1}(x)}, \quad (4.9)$$

where β has the value 0.05, which is an order of magnitude larger than the value used by Becke in his energy functional [138]. This potential is a correction to the normal LDA potential, for which we use the Vosko–Wilk–Nusair parametrization [4]. This form of the model potential ensures the correct Coulombic decay at large distances. Furthermore, it reduces to the LDA potential in the weak inhomogeneity limit ($x \rightarrow 0$).

Most exchange-correlation potentials do not show the correct asymptotic behavior. In fact, the only examples known to us which have not yet been mentioned, are a potential based upon the computationally expensive weighted density approximation (WDA) [194, 195], and another model potential developed by some of us [196, 197]. We will make some comments on our results with the latter potential in the final section of the paper.

A comparison of the accurate exchange-correlation potential and the model potential from Ref.[121] with the LDA potential shows the erroneous behavior of the LDA potential in the outer region. These potentials are compared in Figure 4.1 for the neon atom. In the outer region, the model potential is clearly much closer to the accurate potential than the LDA potential is. In the core region there is room for improvement, because the model potential does not exhibit the peak at the boundary of the 1s and 2s shells. The relatively poor quality of the model potential near the nucleus might be the reason why the results for geometries obtained with the model potential are not so good, as was recently shown by Neumann *et al.*[198].

For polarizabilities, the outer region is of greater importance however, and in this region the LDA potential is not attractive enough. This leads to too high values for the eigenvalue of the highest occupied orbital and overestimation of polarizabilities. The characteristics of Figure 4.1 also appear for other atoms.

4.4 Details of calculation and atomic results

4.4.1 Description of the program and details of the calculations

All calculations were performed with the Amsterdam Density Functional (ADF) package [89, 164, 115, 90, 165]. Its characteristics include the use of Slater type orbitals, the possibility to use a frozen core approximation, the use of fit functions (also called auxiliary basis functions) for the density and an accurate numerical integration scheme [115, 90]. The basis sets we use for our calculations are at least as extensive as those we used previously [34]. These basis sets consisted of a valence triple zeta basis with two polarization functions, augmented with two s, two p, and two d functions, all with diffuse exponents. These diffuse functions are essential in obtaining results which are close to the basis set limit. The basis sets for atoms which we did not include in our previous publication were constructed in a similar fashion.

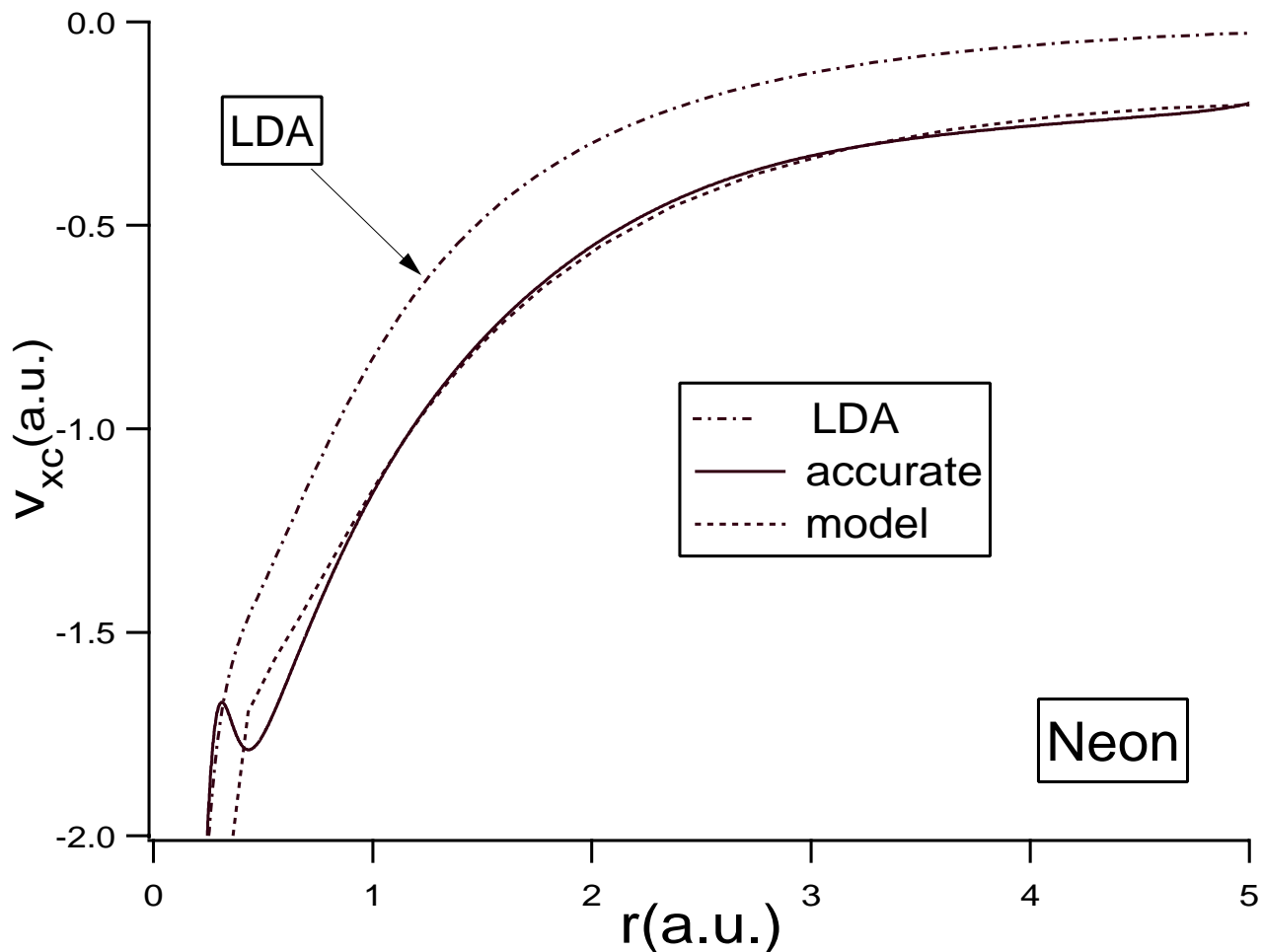


Figure 4.1: A comparison, for the neon atom, of the model potential and the LDA potential to an accurate potential, constructed from a high quality CI density.

For most molecules (H_2 , HF , F_2 , N_2 , CO , Cl_2 , HCl , CO_2 , N_2O , SO_2 , CH_4) we have added diffuse f functions to the basis sets. A comparison with the results with slightly smaller basis sets shows, that in most (but not all) cases this addition causes only very small changes in the dipole polarizabilities. For the other molecules we did not include the diffuse f functions in the bases, because of technical problems due to linear dependencies in the basis sets. Because of the large basis sets we use, we can expect to be close to the basis set limit in all the calculations presented in this paper. This is also shown by the fact that our atomic and molecular results are close to those obtained with basis set free methods [30] and to other results with high quality basis sets [152].

We made sure that all our fit sets were nearly saturated and that the integration accuracy was sufficiently high. We used the frozen core approximation for most of the atoms. The outermost frozen shell was 3d for Kr, 2p for Si, P, S, Cl, Ar, and 1s for C, N, O, F, Ne. This approximation is assumed to change the results only insignificantly, especially for molecules.

We have tested this before [34]. We demanded at least six significant digits for a set of test integrals from the numerical integration routine, which is more than sufficient.

4.4.2 Atomic results

Table 4.1: Static atomic dipole polarizabilities (in a.u.), calculated with various exchange-correlation potentials.

Atom	LDA ^a	LDA (lit)	BP ^b	PSIC ^c	model ^d	Expt. ^e
He	1.65	1.67 ^f	1.59	1.32	1.40	1.38
Ne	3.02	3.05 ^f	2.98	2.56	2.55	2.67
Ar	11.94	12.01 ^f	11.66	11.67	11.40	11.07
Kr	17.67	18.02 ^f , 17.88 ^g	17.39	17.95	16.48	16.74

^aRef.[34]

^bRef.[138, 139]

^cRef.[71, 30]

^dRef.[121]

^eRef.[168]

^fRef.[30]

^gRef.[24]

In Table 4.1 we compare the static dipole polarizability for the rare gases, calculated with different potentials. Our LDA results are close to accurate literature values, testifying to the quality of our basis and fit sets. The LDA values are substantially larger than the experimental values. The literature LDA values [30] are on average 12.8% too high. Compared to this, the results with the model potential are excellent. They differ on average only 2.6% from the experimental values. Results with the partial SIC method [30], another scheme to remove the LDA self-interaction, are worse than our results with the model potential. The average deviation from experiment is 5.3% in this case. Using full SIC (not shown in the table) hardly improves this (4.7% average deviation). Another interesting result is that the Becke–Perdew (BP) [138, 139] generalized gradient potential overestimates the polarizability somewhat less (9.0%) than the LDA potential does.

The frequency dependence of the dipole polarizability of the rare gases is sometimes given in the form [30]

$$\alpha(\omega) = \alpha_0(1 + C_2\omega^2). \quad (4.10)$$

In this formulation, which is only applicable for small values of ω , the coefficient C_2 is a measure for the frequency dependence which is independent from the static value. Zhong *et al.* [24] have devoted an article to the problem of the overestimation of the frequency dependence in atomic time-dependent LDA (TDLDA) calculations. They use two semiempirical models to increase the gap between occupied and unoccupied Kohn–Sham energies. They call this the modified TDLDA approach. One model is based on a single-oscillator model, the other one simply applies a scissors operator to the gap. In both cases one imposes that the static polarizability should equal the experimental value. Their results have

Table 4.2: Frequency dependence C_2 of atomic dipole polarizability, as defined by Eq. (4.10).

Atom	TDLDA ^a	TDLDA Lit. ^e	mod. TDLDA ^b Scissors	mod. TDLDA ^b Single Oscil.	model ^c	Expt. ^d
He	1.46	1.49	0.94	1.01	1.11	1.16
Ne	1.49	1.49	0.95	1.10	1.05	1.11
Ar	3.07	3.13	2.35	2.62	2.63	2.60
Kr	4.02	4.10	3.28	3.52	3.35	3.61

^aRef.[34]

^bModified time-dependent LDA approach, as described in the text, Ref.[24]

^cRef.[121]

^dRef.[168]

^eRef.[72]

been included in Table 4.2. In this table, our LDA values are again close to the basis set free results. These LDA results show a large overestimation of the C_2 -coefficient (24%). The semiempirical values obtained with the scissors operator are already much closer to experiment (12%), but they show a systematic underestimation of the frequency dependence. Both the single-oscillator model and the use of the model potential increase the agreement with experiment significantly. They respectively differ by only 4.3% and 4.5% from the experimental numbers. However, we stress that our results were obtained without any fitting or modeling. Merely the quality of the model potential in the outer region of the atom assures the good description of the frequency dependence.

We have also performed calculations on atomic quadrupole polarizabilities. For these calculations the inclusion of the diffuse f functions to the basis sets was much more important than for dipole polarizabilities and had a significant influence on the results. The calculations can be assumed to be equally close to the basis set limit as the calculations for dipole polarizabilities. The static results are given in Table 4.3. Again, the LDA values severely

Table 4.3: Atomic quadrupole polarizabilities (in a.u.) with different potentials.

Atom	LDA	LDA (lit.) ^a	model ^b	<i>ab initio</i>
He	3.56	3.35	2.52	2.445 ^c
Ne	9.47	9.35	7.12	7.52 ^d , 7.3276 ^e
Ar	61.81	59.6	55.61	53.58 ^f , 51.862 ^e
Kr	111.42	108.5	96.53	99.86 ^g , 99.296 ^e

^aRef.[68, 30]

^bRef.[121]

^cRef.[151]

^dCCSD(T), Ref.[199]

^eMBPT, Ref.[174]

^ffinite field MP4, Ref.[200]

^gfinite field MP4, Ref.[201]

overestimate the results from reliable *ab initio* calculations. They are on average 25% too large, with He as the worst case. The model potential brings major improvement for this property too. The results are only about 5% from the *ab initio* reference values, on average.

One of the major advantages of the model potential is that the one-electron energies of the highest occupied [121] and lowest unoccupied orbital are quite well predicted. Only the highest occupied eigenvalue has strict physical significance (it should equal minus the ionization potential), but the gap between the highest occupied and lowest unoccupied orbital determines the frequency dependence to a great extent. Especially in the region near the first excitation energy this plays an important role.

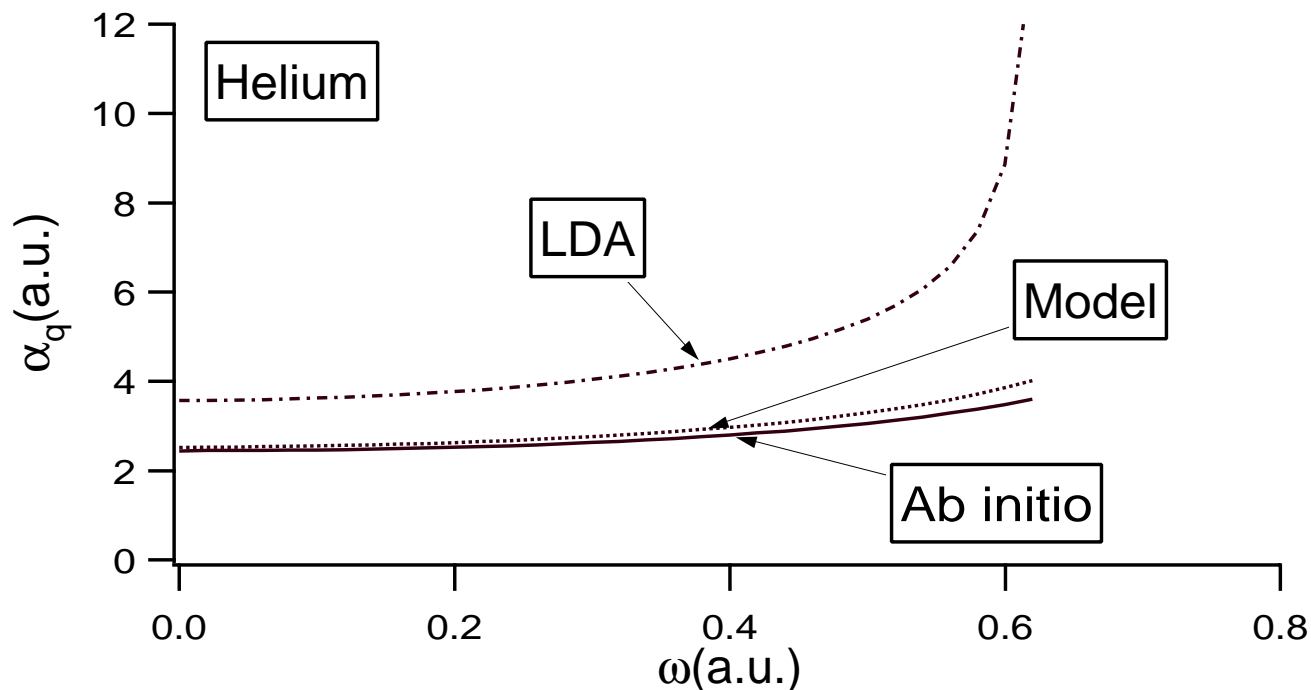


Figure 4.2: The frequency-dependent quadrupole polarizability of He. Comparison of results with the LDA and model potentials to benchmark *ab initio* results.

This can clearly be seen from Figure 4.2, where the quadrupole polarizability of He has been calculated on a wide range of real frequencies. The time-dependent LDA result and the result with the model potential are compared to an extremely accurate *ab initio* calculation [151]. It was already known from Table 4.3 that the static LDA value for the quadrupole polarizability was not very good. In addition to this, Figure 4.2 shows that the LDA result has a much too high frequency dependence and that the first excitation energy lies too low (these facts are of course interrelated). In comparison, the model potential performs quite well. It follows the accurate theoretical curve closely, along the entire frequency range. Note that this frequency range extends to 0.6 hartree!

4.5 Molecular results

4.5.1 Average polarizabilities

It has been remarked many times that both the LDA and the GGAs systematically overestimate polarizabilities. Because the atomic results with the model potential are promising, we are now going to study molecular polarizabilities. We remark that the overestimation of the polarizability is less pronounced in molecules than in atoms. Other effects, such as charge transfer from one atom to another, become important, which makes the asymptotic behavior of the potential less crucial. In order to be able to draw reliable conclusions from our calculations, we decided to perform calculations on a fairly large number (19) of small and medium-sized molecules. We took the molecules we already performed calculations on previously [34] and added those from Ref.[152]. This should yield a list of molecules which is representative and large enough.

We performed our calculations at the experimental geometries, gathered from different sources, such as Refs.[202, 167]. For the sake of reproducibility and for ease of reference, we listed the used geometries in Table 4.4. In our previous work [34], we used the same

Table 4.4: Molecular geometries used in this paper.

Molecule	bond length(Å)	Angle(degrees)
H ₂	r(HH) = 0.7461	
HF	r(HF) = 0.917	
HCl	r(HCl) = 1.2746	
N ₂	r(NN) = 1.0976	
CO	r(CO) = 1.1283	
F ₂	r(FF) = 1.417	
Cl ₂	r(ClCl) = 1.9871	
H ₂ O	r(OH) = 0.957	∠(HOH) = 104.5
H ₂ S	r(SH) = 1.3455	∠(HSH) = 93.3
CO ₂	r(CO) = 1.160	
N ₂ O	r(NO) = 1.186, r(NN) = 1.1257	
SO ₂	r(SO) = 1.4321	∠(OSO) = 119.54
NH ₃	r(NH) = 1.008	∠(HNH) = 107.3
PH ₃ ^a	r(PH) = 1.4166	∠(HPH) = 93.1
PH ₃ ^b	r(PH) = 1.437	∠(HPH) = 91.5
CH ₄	r(CH) = 1.091	
SiH ₄	r(SiH) = 1.4798	
C ₂ H ₄	r(CH) = 1.071, r(CC) = 1.344	∠(HCH) = 119.9
C ₂ H ₆	r(CH) = 1.107, r(CC) = 1.533	∠(HCH) = 109.3
c-C ₃ H ₆	r(CH) = 1.089, r(CC) = 1.510	∠(HCH) = 115.0

^aExperimental geometry

^bBecke–Perdew optimized geometry

geometries, except for H₂, for which we used the optimized geometry of r(HH) = 0.767 Å.

For PH₃ we listed both the experimental geometry and the geometry which was optimized with the Becke–Perdew potential. We performed calculations at the optimized geometry as well, in order to be able to explain a discrepancy between our results and the results obtained by McDowell *et al.*[152] for the same molecule.

Table 4.5: Average molecular polarizabilities calculated with different potentials.

Molecule	LDA	LDA (lit) ^a	BP ^b	BLYP ^c	model ^d	DOSD / Expt. ^e
H ₂	5.89		5.54		5.61	5.43
HF	6.20	6.17	6.08	6.26	5.31	5.60
HCl	18.63	18.43	18.09	18.54	17.86	17.39
N ₂	12.27		12.04		11.46	11.74
CO	13.87		13.36		12.62	13.08
F ₂	8.87	8.82	8.70	8.96	8.02	8.38
Cl ₂	32.00	31.70	31.29	31.97	30.96	30.35
H ₂ O	10.53	10.54	10.28	10.63	9.20	9.64
H ₂ S	26.34	26.13	25.49	25.94	25.39	24.71
CO ₂	17.72	17.80	17.46	17.97	16.63	17.51
N ₂ O	19.91		19.63		18.71	19.77
SO ₂	26.49	26.41	26.21	26.75	24.59	25.61
NH ₃	15.62	15.57	15.25	15.62	13.85	14.56
PH ₃ ^f	32.80	32.52	31.56	32.14	32.12	32.03
CH ₄	18.19	18.01	17.40	17.82	17.98	17.27
SiH ₄	34.04	34.28	32.34	33.14	33.91	31.90
C ₂ H ₄	28.30	29.10	27.77	29.31	27.12	27.70
C ₂ H ₆	30.74		29.72		30.54	29.54
c-C ₃ H ₆	39.19		38.91		37.91	38.0
Mean error	+5.3%		+2.4%		-0.9%	
Mean absolute error	5.3%		2.7%		3.5%	

^aRef.[152]

^bBecke–Perdew potential[138, 139]

^cBecke–Lee–Yang–Parr potential [138, 129], results obtained by McDowell *et al.* [152]

^dRef.[121]

^eExperimental and constrained Dipole Oscillator Strength Distribution results, as gathered in Refs.[152] and [34]

^fOptimized geometry was used in our calculations

In Table 4.5 the average polarizabilities for the molecules are presented. We show our results with the LDA potential, the BP potential and the model potential and compare them to literature values with LDA and GGAs, as well as to experimental values and values obtained with the accurate constrained Dipole Oscillator Strength Distribution (DOSD) method[173, 163].

In general, our LDA values agree well with previous work¹ in which high quality basis

¹Accurate finite field LDA values have recently been obtained in a basis set free manner by Dickson and

sets were used [152], except for our PH₃ results at the experimental geometry, which are 37.63, 36.42, and 35.44 for the LDA, BP, and model potentials respectively. In the table the results with the optimized geometry for PH₃ have been presented, which agree well with the literature values.

The LDA results are higher than the experimental ones, without exception. The average overestimation of the LDA values is 5.3%, which is close to the 5.7% overestimation found by McDowell *et al.* [152] for a subset of the molecules in our table.

Our values with the Becke–Perdew potential are not strictly comparable to GGA values in previous studies, because our mixed-scheme results need not be identical to finite field results. In fact, our results with the Becke–Perdew potential correct the LDA overestimation somewhat. The agreement with the experimental values is improved (2.7%). The values are still too high, though in three cases it is slightly lower than experiment. Finite field Becke–Lee–Yang–Parr (BLYP) [138, 129] values slightly increase the LDA overestimation [152].

The results with the model potential in table 4.5 are also slightly better than the LDA results. The average absolute error is somewhat reduced, to 3.5%. More importantly, the overestimation which is present in the LDA and GGA results, is removed. No large systematic over- or underestimation of the experimental results remains. Part of the remaining underestimation of 0.9% might be due to the fact that the basis set limit has not been fully reached.

It is well-known that LDA and GGA potentials underestimate the eigenvalue of the highest occupied Kohn–Sham orbital by typically 5 eV. This error is greatly reduced by the model potential we employ. The average error is a few tenth of an eV in this case [121]. One might wonder how it is possible that the LDA and GGA values for molecular polarizabilities are only a few percent too high, compared to experiment, when the highest eigenvalue is predicted so erroneously. In order to answer this question, we calculated the eigenvalue of the lowest unoccupied orbital as well. It appears that the gap between these eigenvalues is not so different for the three potentials considered here. Typically, they are identical to within a few tenth of an eV. The correct asymptotic behavior of the model potential affects the highest occupied and lowest unoccupied eigenvalues in similar fashion. They both become more bound, being shifted by almost the same amount. This is true for molecules, but it does not hold for atoms, as can be seen from Figure 4.2. This is due to the different nature of the lowest unoccupied orbital in the atomic and molecular cases. For a more detailed analysis, the knowledge of the exact Kohn–Sham values for these eigenvalues would be desirable. However, we presume that the model potential yields accurate values for the first unoccupied eigenvalue as well, because of its asymptotically correct behavior.

4.5.2 Anisotropy in the polarizability

Our results for the static polarizability anisotropy are presented in Table 4.6. The anisotropy γ is defined for diagonal polarizability tensors in the usual way [204] as:

$$\gamma^2 = \frac{1}{2} [(\alpha_{xx} - \alpha_{yy})^2 + (\alpha_{xx} - \alpha_{zz})^2 + (\alpha_{zz} - \alpha_{yy})^2], \quad (4.11)$$

Becke[203]. For most molecules their results are very close to ours, indicating that our basis sets are reliable.

Table 4.6: Polarizability anisotropies γ (in a.u.), as in Eq. (4.11). Comparison of results with different exchange-correlation potentials to experimental data.

Molecule	LDA	LDA (lit) ^a	BP ^b	BLYP ^c	model ^d	DOSD / Expt. ^e
H ₂	2.04		2.00		2.13	2.04
HF	0.93	1.10	0.96	1.160	1.28	1.33
HCl	1.29	1.30	1.32	1.329	2.29	1.45
N ₂	4.62		4.69		4.67	4.45
CO	3.26		3.40		3.23	3.57
F ₂	5.69	5.49	5.75	5.784	5.94	
Cl ₂	16.60	16.11	16.46	16.455	17.33	17.53
H ₂ O	0.07	0.24	0.15	0.296	1.25	0.66
H ₂ S	0.84	1.24	0.67	1.664	0.81	0.65
CO ₂	13.37	13.96	13.22	14.026	13.49	13.3
N ₂ O	18.73		18.63		18.35	19.10
SO ₂	13.36	13.16	13.35	13.427	13.02	13.0
NH ₃	3.09	2.67	3.09	2.676	0.25	1.94
PH ₃ ^f	2.25	2.38	2.03	2.337	0.76	
C ₂ H ₄	11.31		10.95		12.82	11.4
C ₂ H ₆	4.37		4.10		3.82	5.2
c-C ₃ H ₆	-5.25		-4.95		-5.52	-5.4

^aRef.[152]

^bBecke–Perdew potential[138, 139]

^cBecke–Lee–Yang–Parr potential [138, 129], results obtained by McDowell *et al.* [152]

^dRef.[121]

^eExperimental and constrained Dipole Oscillator Strength Distribution results, as gathered in Refs.[152] and [34]

^fOptimized geometry was used

where we use $\gamma = \alpha_{zz} - \alpha_{xx}$ for symmetric top molecules with their main symmetry axis along the z -axis. For this property the LDA and GGA results are more satisfactory and the model potential offers no improvement.

The results with LDA and Becke–Perdew, which are similar to each other, are slightly preferable. In most cases the different potentials yield similar results, but for a few molecules (notably HCl, H₂O, NH₃ and PH₃) the model potential gives markedly different results. (Here the results for PH₃ at the experimental geometry are 8.17, 8.07, and 3.13 respectively.)

The polarizability anisotropy suffers much less from the incorrect asymptotic behavior of the LDA and GGA potentials, because the overestimation of the different polarizability tensor components partially cancels in Eq. (4.11). This means that the correct description of the outer region is not as important as for the average polarizability. Other parts of the potential curve gain in importance. Because the model potential only improves the outer region and is not so good near the nucleus, one would not necessarily expect an improvement from this potential for the polarizability anisotropy. For this, one would need an exchange-

12 IMPROVED POLARIZABILITIES THROUGH CORRECT ASYMPTOTICS

correlation potential which improves upon the LDA near the nucleus as well.

The agreement between our LDA anisotropies and those obtained by McDowell *et al.* [152] is somewhat less than for the average polarizabilities, especially for the molecules with small anisotropies. This can be understood from the fact that the polarizability anisotropy is a more sensitive property than the average polarizability. It has been noted before [152] that LDA and GGA polarizability anisotropies are of higher quality than Hartree–Fock anisotropies.

4.5.3 Frequency dependence of molecular polarizabilities

Because the model potential improves the frequency dependence of the atomic polarizabilities remarkably, we have investigated the frequency dependence of average molecular polarizabilities as well. It is known that Hartree–Fock calculations underestimate the frequency dependence of the polarizability considerably. The Cauchy moment $S(-4)$ in the expansion $\alpha(\omega) = \sum_k S(-2k - 2)\omega^{2k}$, which dominates the frequency dependence in usual frequency ranges, was underestimated by 27.6% with respect to experiment in a study by Spackman on a large number of molecules [204]. To our knowledge, it has never been investigated how well different potentials in DFT describe this frequency dependence for molecules. For these two reasons we have calculated some frequency-dependent molecular polarizabilities with the same potentials we have used in the rest of this work. We compare to recent experimental values of high accuracy[162]. We could not perform calculations on O_2 , for which measurements were also performed[162], because it is an open-shell molecule. The results at $\omega = 0.140$ and 0.072 a.u. are shown in Table 4.7.

As was to be expected, the LDA and BP potentials tend to overestimate the frequency dependence. The LDA values differ from the experimental ones by 27.0% on average and the Becke–Perdew values differ by 21.3%. The overestimation is especially clear in the cases of ammonia and cyclo-propane. The model potential yields better results for these molecules. Its average error is 9.9%, which makes it a more reliable choice than Hartree–Fock, LDA or Becke–Perdew. The error in the model potential results seems to be less systematic, which is reflected by the fact that the mean error is about two times as small as the mean absolute error.

However, when considering the frequency dependence of the polarizability, another point is of importance. We made an adiabatic approximation for the exchange-correlation kernel f_{xc} in Eq. (4.4). This means that the exchange-correlation screening is assumed to be frequency-independent. In the present context it is relevant to assess the validity of this approximation. To this purpose, we have performed some test calculations with the frequency-dependent Gross–Kohn exchange-correlation kernel [160, 205, 206, 31], which is based upon the frequency-dependent linear response of the homogeneous electron gas. Although some principal objections can be raised against it (such as the violation of the so-called "Harmonic Potential Theorem"[207]), it provides at present the only practical way to go beyond the adiabatic approximation.

As a check on our implementation, we compared to Ref.[31] and reproduced Figures 1 and 2 of that paper. We also compared numerically to another implementation of the same kernel [208], finding agreement in the first five digits over a wide frequency range.

Table 4.7: Frequency dependence of average polarizability α , with different potentials. Here, Δ gives the difference between the results at the two different wavelengths.

Molecule	$\lambda(\text{\AA})$	ALDA	BP ^a	model ^b	Expt. ^c
H ₂	3251.3	6.44	6.02	6.06	5.86
	6329.9	6.03	5.66	5.72	5.54
	Δ	0.41	0.36	0.34	0.32
CO ₂	3251.3	18.83	18.68	17.57	18.62
	6329.9	18.00	17.85	16.85	17.78
	Δ	0.83	0.82	0.72	0.84
N ₂ O	3251.3	21.50	21.18	20.78	21.32
	6329.9	20.29	20.01	19.67	20.09
	Δ	1.21	1.17	1.11	1.23
NH ₃	3251.3	19.02	18.25	15.33	16.35
	6329.9	16.34	15.82	14.19	14.96
	Δ	2.68	2.43	1.14	1.39
C ₂ H ₆	3251.3	33.45	32.21	33.07	31.92
	6329.9	31.39	30.33	31.16	30.13
	Δ	2.06	1.88	1.91	1.79
c-C ₃ H ₆	3251.3	43.16	43.01	41.29	40.577
	6329.9	40.12	39.84	38.71	38.107
	Δ	3.04	3.17	2.57	2.47
Mean error in Δ		+26.1%	+18.9%	-4.2%	
Mean absolute error in Δ		27.0%	21.3%	9.9%	

^aBecke–Perdew potential [138, 139]

^bRef.[121]

^cRef.[162]

The Gross–Kohn parametrization of f_{xc} decreases the frequency dependence which is found in the ALDA. This is due to the fact that the exchange–correlation screening, which increases the polarizability, becomes smaller with increasing frequency in the Gross–Kohn parametrization.

In the literature [31, 72], it has been assumed that the adiabatic approximation is not a severe one. Our preliminary results for the frequency dependence of the average polarizability indicate that this is not true in general. We find that the ALDA results in Table 4.7 for the quantities Δ are reduced by roughly 15–30% with the Gross–Kohn kernel, thus increasing the agreement with experiment. This indicates that the adiabatic approximation cannot be applied thoughtlessly in the optical region and that its use will lead to a frequency dependence which is too high. It is important to note here that if the Gross–Kohn kernel is used in combination with the model potential, the resulting frequency dependence in Table 4.7 will be too low in comparison with experiment. This may be due to the fact that the Gross–Kohn kernel was derived from the frequency-dependent linear response of the homogeneous electron gas, which might not be a realistic model for the frequency dependence in molecules.

14 IMPROVED POLARIZABILITIES THROUGH CORRECT ASYMPTOTICS

We conclude that both the quality of the exchange-correlation potential in the outer region of the molecule and the frequency dependence of the exchange-correlation screening need to be considered in order to obtain accurate DFT results for frequency-dependent polarizabilities. We emphasize however, that the restricted number of molecules for which we performed these calculations does not allow definite generalizations and that more work is needed in order to further clarify the importance of the adiabatic approximation and the importance of the outer region of the exchange-correlation potential on the frequency dependence.

4.6 Concluding remarks

We have presented calculations with a model exchange-correlation potential, which possesses the correct long-range behavior. Our approach allows an analytic determination of frequency-dependent polarizabilities for closed-shell molecules. A mixed scheme was used, in which the adiabatic LDA approximation was used for the exchange-correlation kernel f_{xc} , regardless of the approximation made for the exchange-correlation potential v_{xc} . Our atomic results (static and dynamic dipole and quadrupole polarizabilities) are substantial improvements on previous results with LDA and GGA potentials. In our molecular calculations, the model potential removes the systematic overestimation in the average polarizability, which is obtained in calculations with LDA or GGA potentials. Both the results with the model potential and the results with the Becke–Perdew potential provide improvements on the LDA results. More subtle modeling for the exchange-correlation potential is needed to obtain satisfactory results for the anisotropy, for which the LDA and GGA results are slightly better.

In general, we observe that the asymptotic behavior of the potential is more critical for polarizability calculations than the correct description of the core region. This is shown by test calculations with a model potential which was introduced more recently [196, 197]. This potential gives a better description of the core region (it exhibits the required peaks between the atomic shells) and also possesses the correct long-range behavior. It yields accurate values for the highest occupied Kohn–Sham orbital as well, but it did not yield good results in preliminary calculations which we performed. The polarizabilities were consistently underestimated, thus over-correcting the LDA results. Subsequent analysis showed that the gap between the highest occupied and lowest unoccupied orbital was larger for this potential than for the model potential used in this work. This was due to the fact that the Coulombic asymptotic behavior was reached too slowly, showing that the problems in the modeling of potentials can be quite subtle.

In future work, it would seem desirable to improve the quality of the potential in the core region. This might help to improve the results for other response properties as well, such as NMR shielding tensors, in which the poor quality of the LDA or GGA eigenvalues is also important [187, 209, 210]. Furthermore, the quality of the exchange-correlation kernel is of importance, as shown by our finite field test calculations.

The frequency dependence of average molecular polarizabilities was also best described by the model potential. The LDA and Becke–Perdew potentials tend to overestimate this frequency dependence. The importance of the frequency dependence of the exchange-

correlation screening should not be underestimated, as shown by our preliminary results with the Gross–Kohn parametrization for f_{xc} . We have shown that the direct modeling of the exchange–correlation potential yields promising improvements in our calculations on response properties, and we hope to have encouraged further work in this direction.

In the final stages of this work, the work of Casida and coworkers [37, 80, 35] came to our attention. They also have an implementation capable of calculating molecular frequency-dependent linear response within DFT. They present results for the N_2 molecule for which they calculated excitation energies and the frequency-dependent average polarizability, suggesting that their results might be improved by using an accurate exchange–correlation potential. We learned very recently that Castro, Casida, and Salahub [211] obtained very similar results for polarizabilities with the model potential.

4.7 Acknowledgements

We thank the authors of Refs.[37, 35, 211] for making their work available prior to publication. One of the authors (SvG) acknowledges useful discussions with M. Petersilka on the Gross–Kohn exchange–correlation kernel and with E. van Lenthe. SvG also acknowledges financial support by the Dutch Foundation for Chemical Research (S.O.N.). OVG acknowledges financial support by the Netherlands Institution Fundamenteel Onderzoek der Materie (FOM), and RvL acknowledges support by the Swedish Natural Science Research Council (NFR).

Chapter 5

Application of time-dependent density functional response theory to Raman scattering

5.1 Abstract

Recently, the first density functional theory (DFT) calculations on Raman intensities and depolarization ratios were published. Those calculations were done in the static approximation. Here, we use time-dependent DFT in order to include the dependence of those properties on the frequency of the exciting light wave. By analytically calculating the frequency-dependent polarizability at different nuclear positions, our approach is closer to a fully analytic one than the previous DFT studies. Our results for five diatomics improve upon previous TDHF and SOPPA *ab initio* results and show that the frequency dependence cannot be ignored in quantitative comparisons to experiment. Our results for the important Q-branch differential Raman cross section of N₂ are closer to the experimental value than previously reported results. Inclusion of the frequency dependence has hardly any effect on the depolarization ratios, but improves the results for the cross sections obtained in static DFT calculations. Our results obtained with three different exchange-correlation potentials yield similar results in all cases.

5.2 Introduction

According to Placzek's polarizability theory [212, 213], Raman scattering intensities, differential cross sections and depolarization ratios can be obtained from the geometrical derivative of the frequency-dependent polarizability. In many studies on Raman scattering, the frequency dependence is neglected, which considerably simplifies the calculations. However, it is known from previous *ab initio* work [214, 215, 216], that the frequency dependence can have significant effects. In spite of this fact, very little frequency-dependent work has been done beyond the time-dependent Hartree–Fock (TDHF) level. Time-dependent density functional theory (DFT) [38, 31, 37, 33] offers a cheap way to treat frequency-dependent re-

response properties at the correlated level. Applications in atomic and solid state physics have been numerous, but only recently have the first implementations been developed which are capable of handling molecules in an efficient way. The results for frequency-dependent polarizabilities [35, 34, 74, 211], Van der Waals dispersion coefficients[34] and excitation energies [101, 35] provide significant improvements over TDHF results. It thus seems interesting to apply time-dependent DFT to Raman scattering.

First, we will give a short outline of our method of calculating frequency-dependent polarizabilities, which has been described in more detail elsewhere [34]. Then we will present calculations on the five diatomics N₂, CO, HCl, Cl₂, and HF, comparing to the frequency-dependent first order (TDHF) and second-order polarization propagator approximation (SOPPA) results by Oddershede and Svendsen[217] and to static DFT results obtained by Johnson and Florián[218]. Other DFT results for Raman scattering (also in the static approximation) have been obtained by Stirling[219] ¹.

5.3 Description of the calculation method

Our frequency-dependent polarizabilities are obtained using time-dependent DFT. In this theory, the frequency-dependent linear density response $\delta\rho(\mathbf{r},\omega)$ due to a scalar electric external field $\delta v_{\text{ext}}(\mathbf{r},\omega)$ is given (in principle exactly) in terms of a *single-particle* response function $\chi_s(\mathbf{r},\mathbf{r}',\omega)$ acting on an effective field $\delta v_{\text{eff}}(\mathbf{r}',\omega)$ (atomic units are used):

$$\delta\rho(\mathbf{r},\omega) = \int \chi_s(\mathbf{r},\mathbf{r}',\omega)\delta v_{\text{eff}}(\mathbf{r}',\omega)d\mathbf{r}'. \quad (5.1)$$

The Kohn–Sham response function $\chi_s(\mathbf{r},\mathbf{r}',\omega)$ is constructed from (real) orbitals, occupation numbers and one-electron energies, obtained in an ordinary DFT calculation. Because of screening effects, the effective field in Eq. (5.1) is not equal to the external field. It contains a Hartree and an exchange-correlation term due to the induced density:

$$\delta v_{\text{eff}}(\mathbf{r},\omega) = \delta v_{\text{ext}}(\mathbf{r},\omega) + \int d\mathbf{r}' \frac{\delta\rho(\mathbf{r}',\omega)}{|\mathbf{r}-\mathbf{r}'|} + \delta v_{\text{xc}}(\mathbf{r},\omega), \quad (5.2)$$

where the exchange-correlation term is given by

$$\delta v_{\text{xc}}(\mathbf{r},\omega) = \int d\mathbf{r}' f_{\text{xc}}(\mathbf{r},\mathbf{r}';\omega)\delta\rho(\mathbf{r}',\omega). \quad (5.3)$$

The exchange-correlation kernel f_{xc} is the functional derivative of the exchange-correlation potential with respect to the time-dependent density. In this work, the usual Adiabatic Local Density Approximation (ALDA) [9, 31] is used. In this approximation one uses the derivative of the time-independent LDA exchange-correlation potential for f_{xc} . After Eqs. (5.1) and (5.2) have been solved self-consistently in an iterative fashion[34], the frequency-dependent polarizability tensor is immediately obtained from the first order density change $\delta\rho(\mathbf{r},\omega)$ [31, 37, 34].

¹More recently, other DFT calculations on Raman scattering appeared in the literature. In papers by Porezag and Pederson[220], using ground-state DFT, and Ioannou and Amos[85], using time-dependent DFT, small molecules such as CH₄ were considered.

In order to calculate differential Raman cross sections and depolarization ratios, the derivatives of the frequency-dependent polarizability tensor components with respect to normal coordinates are needed, in general. In this comparative study, we just consider diatomics, for which the derivative of the polarizability tensor with respect to the bond length suffices.

In terms of the derivatives $\frac{d\alpha}{dr}$ and $\frac{d\gamma}{dr}$ of the average polarizability and polarizability anisotropy with respect to the bond length, one obtains the depolarization ratio ρ_n for unpolarized (natural) light from [53, 217]:

$$\rho_n = \frac{6 (d\gamma/dr)^2}{45 (d\alpha/dr)^2 + 7 (d\gamma/dr)^2}. \quad (5.4)$$

The depolarization ratio for linearly polarized light is obtained by replacing the factors 6 and 7 in Eq. (5.4) by 3 and 4 respectively.

For diatomics, the Q-branch ($\Delta J=0$) differential Raman cross section, observed perpendicularly to the linearly polarized incoming beam, depends upon the temperature, the frequency of the vibration mode ν_1 , the laser frequency ν_0 , the reduced mass μ of the two nuclei and the polarizability derivatives, which in turn depend upon the frequency of the laser [212, 53, 217]:

$$\left(\frac{d\sigma}{d\Omega}\right)_Q(\nu_0) = \frac{(2\pi)^4}{45} \frac{h}{8\pi^2 c \nu_1 \mu} \left[\frac{(\nu_0 - \nu_1)^4}{1 - \exp[-hc\nu_1/k_B T]} \right] \left(45 \left(\frac{d\alpha(\nu_0)}{dr}\right)^2 + \frac{7}{4} \left(\frac{d\gamma(\nu_0)}{dr}\right)^2 \right). \quad (5.5)$$

In this equation the standard double harmonic approximation has been made. The non-resonance condition has also been assumed in this work. We perform our calculations with $T=300\text{K}$, which causes the temperature-dependent exponential to be very close to zero for most cases.

5.4 Details of the calculation

Our implementation in the Amsterdam Density Functional package (ADF) [221] is capable of calculating Raman scattering intensities, differential cross sections, and depolarization ratios for arbitrary closed-shell molecules. Here we compare results for diatomics only, as a first test-case for the frequency-dependent DFT results. For the sake of comparison we use the experimental geometries, given by Oddershede and Svendsen [217] for the diatomics. For the HF-molecule we use the experimental geometry $r(\text{HF}) = 0.917\text{\AA}$. Our basis sets consist of a STO valence triple zeta basis with two polarization functions. To this we added diffuse functions with exponents that were based upon the recommended values by Guan *et al.* [155]. However, instead of adding one set of s, p, and d functions as recommended in that article and used by Johnson and Florián [218], we took two sets of s, p, d, and f functions. Our test calculations for polarizabilities indicate that there are still small differences between the results with one or two sets of diffuse functions. The very large basis sets we use here yield results for polarizabilities which are very close to the basis set limit, as our previous experience shows [74]. We can thus expect the results in this work to be close to the basis set

limit as well. Bakken and Heiberg[215] have shown that for Raman scattering, such large basis sets are needed in order to get results close to the basis set limit.

We used three different exchange-correlation potentials for our calculations, the Vosko–Wilk–Nusair[4] parametrization for the LDA, the Becke–Perdew[138, 139] generalized gradient potential and a model potential due to Van Leeuwen and Baerends [121], which is called LB94-potential here. The last potential yielded better results for polarizabilities than the other two, due to its correct asymptotic behavior[74, 211].

The choice of the exchange-correlation potential affects the response calculations, because it determines the occupation numbers, orbitals and one-electron energies. These quantities determine the Kohn–Sham response function $\chi_s(\mathbf{r}, \mathbf{r}', \omega)$ in Eq. (5.1). We emphasize that in all our calculations we employed the ALDA for the exchange-correlation kernel f_{xc} in Eq. (5.3), irrespective of the exchange-correlation potential which was used.

The geometrical derivative was evaluated by calculating the polarizability at the equilibrium geometry plus and minus 0.01 bohr, which leads to a negligible error in the numerical differentiation. By demanding very high precision for the numerical integrals, the SCF solution and the polarizabilities, we made sure that the largest source of error is still in the incompleteness of the basis and auxiliary basis sets. The changes in the results which may come from a further increase in the basis set are estimated to be 1 to 5% in all cases. This means that our conclusions will remain unchanged if even larger basis than we employed will be used.

5.5 Results and discussion

We compare to the TDHF and SOPPA results of Oddershede and Svendsen[217], for the diatomics N_2 , CO, HCl, and Cl_2 . For N_2 and HF, we compare to the static DFT results of Johnson and Florián [218]. The experimental values for the cross sections were taken from Schrötter and Klöckner[222], while the experimental results for the depolarization ratios were gathered from different sources, and may be somewhat less reliable. For the vibration frequency ν_1 in Eq. (5.5), we took the experimental values from Schrötter and Klöckner[222].

In Table 5.1 our results for N_2 at $\lambda=351.1$ nm ($\nu_0=28482$ cm $^{-1}$) and 514.5 nm ($\nu_0=19436$ cm $^{-1}$) are presented. Our DFT values for the depolarization ratio and the scattering cross section obtained with the three different potentials are much closer to each other than the TDHF and SOPPA results are. They are also much closer to the experimental value for the differential cross section. The TDHF values obtained by Oddershede and Svendsen are much higher (about 50%) than the experimental value and their SOPPA values are clearly smaller ($\sim 30\%$). The LDA, BP, and LB94 results for the cross section are 17%, 14%, and 2% too large respectively, at $\lambda=351.1$ nm. The theoretical predictions for the depolarization ratio are all close, the DFT predictions being somewhat closer to the SOPPA value than to the TDHF value. The static results by Johnson and Florián[218] have also been included in Table 5.1. The difference between their Hartree–Fock result and the one obtained by Oddershede and Svendsen is much larger than can be explained from the frequency dependence. It is probable that at least one of the two results still suffers from inadequacies in the basis set, while also the somewhat different calculation method employed by Johnson and Florián may have its influence. The difference between their LDA result and ours is less dramatic and can be

Table 5.1: Results for N₂ at $\lambda=351.1$ nm and 514.5 nm. Comparison of results in this work [from Eqs. (5.4) and (5.5)] to *ab initio* and experimental results. Static results[218] have been included in parentheses. The results for the cross sections are given in units of 10^{-31} cm² sr⁻¹.

	λ (nm)	TDHF	SOPPA ^a	LDA	BPb	LB94 ^c	Expt.
ρ_n	351.1	0.16 ^a	0.18	0.176	0.183	0.195	0.14 ^d ; 0.18 ^e
ρ_n	514.5	0.16 ^a	0.18	0.173	0.179	0.192	0.14 ^d ; 0.18 ^e
$\left(\frac{d\sigma}{d\Omega}\right)_Q$	351.1	37.9 ^a	17.2	28.47	27.71	24.88	24.3±0.5 ^f
$\left(\frac{d\sigma}{d\Omega}\right)_Q$	514.5	6.26 ^a , (3.70 ^g)	2.82	4.68, (3.59 ^h)	4.56	4.11	4.32±0.09 ^f

^aOddershede and Svendsen, Ref.[217]

^bBecke–Perdew potential, Ref.[138, 139]

^cVan Leeuwen–Baerends potential, Ref.[121]

^dRef.[223], measured at $\lambda = 457.9$ nm

^eRefs.[224, 225], measured at $\lambda = 435.8$ nm

^fSchrötter and Klöckner, Ref.[222]

^gStatic HF result by Johnson and Florián, Ref.[218]

^hStatic LDA result by Johnson and Florián, Ref.[218]

explained to large extent by the static approximation and the somewhat smaller basis sets they used.

In Table 5.2, the scattering cross sections for other diatomics are presented. Again, there is little difference between the various DFT results, whereas the TDHF and SOPPA results often differ substantially. For CO, there is fairly good agreement between the DFT, TDHF and experimental values, while the SOPPA value seems to be too high. This also holds, to lesser extent, for HCl. Again the DFT and TDHF results are in fairly good agreement with each other and with experiment. The SOPPA value is somewhat larger than these results. For the HF-molecule we compare to the results obtained by Johnson and Florián[218]. Their static Hartree–Fock value is much too low, compared to experiment. The different DFT results we obtain are also lower than the experimental value, but the agreement is improved. Again, the difference between our DFT results and those obtained by Johnson and Florián can partially be explained by the fact that they neglected the frequency dependence of the Raman scattering and used different basis sets. Both factors contribute to the fact that our values for the cross sections are larger than theirs.

The depolarization ratios (mostly at $\lambda=514.5$ nm) are given in Table 5.3. Again our DFT results do not differ much among themselves. They are somewhat closer to the SOPPA results than to the TDHF results. The accuracy of the experimental numbers is not very clear. They differ considerably from one experiment to the other. The agreement between the SOPPA and DFT results is much better than the agreement between the experimental numbers and the results from any of the theoretical methods. An exception has to be made for Cl₂, where the TDHF and SOPPA results are not so good. Oddershede and Svendsen attribute this to the fact that the basis set they used for Cl may not have been sufficiently large, because there is a large separation between the two Cl-atoms.

Table 5.2: Results for Q-branch differential Raman scattering cross sections $\left(\frac{d\sigma}{d\Omega}\right)_Q$ in units of $(10^{-31}\text{cm}^{-2}\text{sr}^{-1})$ for several diatomics at different wavelengths. Comparison of results in this work to *ab initio*, experimental, and static DFT results. Static results are given in parentheses.

Molecule	λ (nm)	TDHF	SOPPA	LDA	BP ^a	LB94 ^b	Expt. ^c
CO	435.8	7.77 ^d	16.1 ^d	7.83	7.91	7.365	8.6±0.9
CO	351.1	22.0 ^d	45.9 ^d	22.03	22.17	20.93	24.5±2.5
HCl	514.5	11.5 ^d	13.5 ^d	11.7	11.5	12.2	12.1±1.2
	351.1	75.5 ^d	91.0 ^d	79.0	77.8	81.5	68±7
HF	514.5	(1.44) ^e		3.16; (2.31) ^f	2.96; (2.41) ^g	2.46	4.2±0.4
Cl ₂	514.5	37.1 ^d	27.4 ^d	15.34	18.27	18.45	15.8±1.6

^aBecke–Perdew potential, Ref.[138, 139]

^bVan Leeuwen–Baerends potential, Ref.[121]

^cCompilation by Schrötter and Klöckner, Ref.[222]. Their estimate of the experimental uncertainties (10%) has been included in the table.

^dOddershede and Svendsen, Ref.[217]

^eStatic Hartree–Fock result, Ref.[218]

^fStatic LDA result, Ref.[218]

^gStatic B-LYP[138, 129] result, Ref.[218]

Our results for the depolarization ratios at different wavelengths support the finding of Oddershede and Svendsen that this property does not depend very much upon the wavelength. This can be understood from Eq. (5.4). For the molecules considered here, the derivatives of the average polarizability and the polarizability anisotropy, $\frac{d\alpha}{dr}$ and $\frac{d\gamma}{dr}$, exhibit a similar frequency dependence. This implies that the frequency dependences of the denominator and of the numerator in Eq. (5.4) will partially cancel.

For ease of comparison with Oddershede and Svendsen’s paper, we have presented the depolarization ratios for unpolarized light in Table 5.3. However, the results presented by Johnson and Florián [218] for the depolarization ratios of N₂ and HF are for the Q-branch only and for linearly polarized light. In terms of the polarizability derivatives this depolarization ratio is given by[227]:

$$(\rho_l)_Q = \frac{\frac{3}{4} \left(\frac{d\gamma}{dr}\right)^2}{45 \left(\frac{d\alpha}{dr}\right)^2 + \left(\frac{d\gamma}{dr}\right)^2}. \quad (5.6)$$

When we put our LDA results for the polarizability derivatives at $\lambda = 514.5$ nm into this equation, we find $(\rho_l)_Q = 0.035$ for N₂, in fairly good agreement with the static result of 0.03 obtained by Johnson and Florián and the experimental result [225] of 0.03. Similarly, we find $(\rho_l)_Q = 0.038$ for HF, where Johnson and Florián’s static LDA result is 0.04 and the experimental number[228] is 0.03.

Finally, in Table 5.4, we compare the frequency dependence of the quantity $45 \left(\frac{d\alpha}{dr}\right)^2 + \frac{7}{4} \left(\frac{d\gamma}{dr}\right)^2$ obtained with the different methods. The presented numbers give the increase in this

Table 5.3: Results for Raman depolarization ratio ρ_n , for unpolarized light. The result at $\lambda=514.5$ nm is given, unless otherwise stated. Comparison of results in this work to *ab initio*, experimental, and static DFT results.

Molecule	TDHF ^a	SOPPA ^a	LDA	BP ^b	LB94 ^c	Expt.
N ₂	0.16	0.18	0.173	0.179	0.192	0.14 ^d ; 0.18 ^e
CO	0.18	0.27	0.251	0.247	0.252	0.13 ^d ; 0.30 ^e
HCl	0.31	0.26	0.261	0.260	0.271	0.4 ^e
HF			0.185	0.187	0.207	
Cl ₂	0.45	0.42	0.205	0.194	0.230	0.22 ^f

^aOddershede and Svendsen, Ref.[217]

^bBecke–Perdew potential, Ref.[138, 139]

^cVan Leeuwen–Baerends potential, Ref.[121]

^dRef.[223], measured at $\lambda = 457.9$ nm

^eRef.[225], measured at $\lambda = 435.8$ nm

^fRef.[226]

quantity (in percents) when going from $\lambda = \infty$ to $\lambda=514.5$ nm. Thus, it directly shows the order of magnitude of the error caused by the static approximation. The agreement between the *ab initio* results and the DFT results is quite satisfactory here, even for Cl₂, where the *ab initio* results may suffer from inadequacies in the basis set[217]. All results confirm that the frequency dependence cannot be ignored. The frequency dependence differs from about 10% in N₂, CO, HCl, and HF to about 35% in Cl₂. Of course, these numbers depend strongly upon the wavelength for which the calculations are performed and upon the position of the first pole (excitation energy).

All these results indicate that the Raman differential cross section is significantly influenced by the frequency dependence. This theoretical conclusion does not agree with the analysis of the experimental data by Schrötter and Klöckner. An adequate explanation of this is lacking, but the experimental error bars may still be too large to reliably identify a small deviation from the dominating $(\nu_0 - \nu_1)^4$ frequency dependence in Eq. (5.5).

5.6 Conclusions

Our approach makes it possible to calculate frequency-dependent Raman spectra at the correlated level, in a computationally cheap fashion. Our results improve upon previous theoretical values for the differential Raman cross sections of five diatomics. There is fair agreement with experiment. The inclusion of frequency dependence is necessary for a quantitative comparison with experimental values, and improves the agreement with these values. The results for the depolarization ratios are in good agreement with TDHF and SOPPA results, whereas the experimental values show considerable spread. No clear preference for either of the three exchange-correlation potentials employed here is given, as they yield similar results in all cases. In short, our results indicate that time-dependent DFT may be a useful tool in the quantitative prediction of Raman spectra.

Table 5.4: Results for frequency dependence of $45 \left(\frac{d\alpha}{dr}\right)^2 + \frac{7}{4} \left(\frac{d\gamma}{dr}\right)^2$. The increase, in terms of percentage, of the results at $\lambda=514.5$ nm with respect to the corresponding static results is given. Comparison of results in this work to TDHF and SOPPA results.

Molecule	TDHF ^a	SOPPA ^a	LDA	BP ^b	LB94 ^c
N ₂	9.1%	9.6%	9.3%	9.1%	8.9%
CO	11.9%	13.5%	10.6%	10.4%	11.5%
HCl	11.1%	13.3%	13.5%	13.9%	13.0%
HF			9.4%	9.0%	7.5%
Cl ₂	29.2%	38.4%	34.3%	32.6%	37.5%

^aOddershede and Svendsen, Ref.[217]

^bBecke–Perdew potential, Ref.[138, 139]

^cVan Leeuwen–Baerends potential, Ref.[121]

5.7 Acknowledgements

One of the authors (SvG) acknowledges useful discussions with V. Bakken, H. Heiberg, J. Olsen, and P. Taylor during the summer school ESQC-95 and thanks V. Bakken and H. Heiberg for making available their unpublished results. SvG gratefully acknowledges financial support by the Dutch Foundation for Chemical Research (S.O.N.).

Chapter 6

Density functional results for isotropic and anisotropic multipole polarizabilities and C_6 , C_7 , and C_8 Van der Waals dispersion coefficients for molecules

6.1 Abstract

The generalized gradient-approximated (GGA) energy functionals used in Density Functional Theory (DFT) provide accurate results for many different properties. However, one of their weaknesses lies in the fact that Van der Waals forces are not described. In spite of this, it is possible to obtain reliable long-range potential energy surfaces within DFT. In this paper, we use time-dependent density functional response theory to obtain the Van der Waals dispersion coefficients C_6 , C_7 and C_8 (both isotropic and anisotropic). They are calculated from the multipole polarizabilities at imaginary frequencies of the two interacting molecules. Alternatively, one might use one of the recently proposed Van der Waals energy functionals for well-separated systems, which provide fairly good approximations to our isotropic results. Results with the Local Density Approximation (LDA), Becke–Perdew (BP) GGA, and the Van Leeuwen–Baerends (LB94) exchange-correlation potentials are presented for the multipole polarizabilities and the dispersion coefficients of several rare gases, diatomics, and the water molecule. The LB94 potential clearly performs best, due to its correct Coulombic asymptotic behavior, yielding results which are close to those obtained with many-body perturbation theory (MBPT). The LDA and BP results are systematically too high for the isotropic properties. This becomes progressively worse for the higher dispersion coefficients. The results for the relative anisotropies are quite satisfactory for all three potentials, however.

6.2 Introduction

Density functional methods[1, 3] have become very popular, because of the accuracy which can be obtained at low computational cost. There are however a few situations in which the present approximate functionals for the exchange-correlation energy clearly fail. These functionals are too crude to describe the small Van der Waals interaction energies, and the region of the potential energy surface near the Van der Waals minimum is usually not very well described [157, 158]. Both the depth and the position of the well are generally not obtained with satisfactory accuracy. Secondly, the long-range part of the potential energy surface obtained with the Local Density Approximation (LDA) and Generalized Gradient Approximations (GGAs) does not behave as R^{-6} , as it should.

In order to overcome this problem, we proposed another way of constructing the long-range part of the potential energy surface within DFT[34], by calculating the Van der Waals dispersion coefficient C_6 from frequency-dependent polarizabilities calculated with time-dependent density functional theory[38].

A somewhat different DFT approach has been introduced recently. Both Andersson et al. [229, 230, 231, 232] and Dobson and Dinte[233] have considered energy functionals which approximate the Van der Waals forces for two well-separated systems. Both these approaches and our own approach address the long-range behavior only. This means that a way to calculate Van der Waals minima reliably within DFT does not yet exist. We will not be concerned with this difficult, unsolved problem here, though it should certainly be possible to devise a scheme which connects the short-range and long-range potential energy surfaces. An outline of such a scheme has been given in Ref.[33].

In this paper, we will extend our previous work by calculating not only the C_6 dispersion coefficients, but also the C_7 and C_8 coefficients. These coefficients, connected with the R^{-7} and R^{-8} behavior of the potential energy surface, determine the form of this surface closer to the Van der Waals minimum. In order to do this, the code used for calculating frequency-dependent dipole-dipole polarizabilities was extended to general multipole-multipole polarizabilities. To the best of our knowledge, the results in this paper are the first within DFT on molecular quadrupole polarizabilities and C_7 and C_8 dispersion coefficients. Atomic results for higher multipole polarizabilities and dispersion coefficients have been obtained by Bartolotti and coworkers[16, 73].

The calculations were performed with the Amsterdam Density Functional[89, 90, 91] program (ADF). Because of limitations on the maximum l value of the basis and fit sets in ADF, we restrict ourselves to the calculation of the lowest order dispersion coefficients. We emphasize that there is no fundamental problem in going beyond C_8 coefficients.

Since our implementation of the linear response equations of time-dependent DFT has already been described[34], we will concentrate in the theoretical section on the generalizations which are needed when general multipole-multipole polarizabilities are required. For the sake of completeness, the equations which link the dispersion energy to the frequency-dependent polarizabilities are also given in detail.

It is widely acknowledged that the quality of the most popular LDA and GGA exchange-correlation potentials is unsatisfactory in the outer region of a molecule. They show an exponential decay, where the exact exchange-correlation potential tends to zero as $-1/r$.

This leads to large errors in the one-electron energy of the highest occupied Kohn–Sham orbital[121] (which should be equal to the ionization potential in magnitude) and to systematic overestimations in polarizabilities[152, 74]. We have shown previously[74] that this systematic overestimation is removed for the dipole polarizability, if one uses the Van Leeuwen–Baerends (LB94) potential[121], which has the correct asymptotic $-1/r$ behavior by construction.

As the higher multipole polarizabilities are even more sensitive to the outer region, one would expect the normal exchange-correlation potentials, such as the Vosko–Wilk–Nusair (VWN)[4] parametrization of the LDA potential and the gradient-corrected Becke–Perdew (BP) [138, 139] potential, to yield a larger overestimation here. We observed this trend for the atomic polarizabilities before [74]. For this reason the LB94 potential was included in our calculations, as well as the more common VWN (simply denoted by LDA in this work) and BP potentials.

6.3 Theoretical introduction

6.3.1 Frequency-dependent linear response in DFT

We will use time-dependent DFT[38] for our calculations in this paper. Only recently, various applications of this theory in the field of quantum chemistry have appeared[34, 74, 35, 101, 86, 75]. For recent reviews on time-dependent DFT we refer to Gross et al. [33] for a general overview of the field and to Casida[37] for the perspective of a quantum chemist. The book by Mahan and Subbaswamy[30] is also a valuable source of information and contains many of the earlier references.

Our implementation of the linear response equations (we refer to Ref.[34] for more details) had to be extended in order to calculate the linear response to a general multipole field. What we need to calculate is the frequency-dependent linear density response of a molecule $\delta\rho^{(lm)}(\mathbf{r}, \omega)$ due to a scalar electric external field of general multipole form $\delta v_{\text{ext}}^{lm}(\mathbf{r}, \omega)$, labeled with the quantum numbers l and m :

$$\delta v_{\text{ext}}^{lm}(\mathbf{r}, \omega) = \sqrt{\frac{4\pi}{2l+1}} E r^l Z_{lm}(\hat{r}) \cos(\omega t), \quad (6.1)$$

where the function Z_{lm} stands for a real combination of spherical harmonics Y_{lm} . It is important to note that, for $\delta\rho$, we use parentheses around the labels l and m in order to indicate that this density change was caused by an external field of lm symmetry. The density change will in general possess components of other $l'm'$ symmetries as well.

In time-dependent density functional response theory, this density change $\delta\rho^{(lm)}$ is given (in principle exactly) in terms of a single particle Kohn–Sham response function $\chi_s(\mathbf{r}, \mathbf{r}', \omega)$ acting on an effective field $\delta v_{\text{eff}}^{(lm)}(\mathbf{r}', \omega)$ (which differs from the external field because of screening effects):

$$\delta\rho^{(lm)}(\mathbf{r}, \omega) = \int d\mathbf{r}' \chi_s(\mathbf{r}, \mathbf{r}', \omega) \delta v_{\text{eff}}^{(lm)}(\mathbf{r}', \omega), \quad (6.2)$$

where $\delta v_{\text{eff}}^{(lm)}(\mathbf{r}, \omega)$ is the effective time-dependent potential evaluated to the first order in the perturbing potential:

$$\delta v_{\text{eff}}^{(lm)}(\mathbf{r}, \omega) = \delta v_{\text{ext}}^{lm}(\mathbf{r}, \omega) + \int d\mathbf{r}' \frac{\delta \rho^{(lm)}(\mathbf{r}', \omega)}{|\mathbf{r} - \mathbf{r}'|} + \delta v_{\text{xc}}^{(lm)}(\mathbf{r}, \omega). \quad (6.3)$$

The response function $\chi_s(\mathbf{r}, \mathbf{r}', \omega)$ is written in terms of (real) occupied and virtual Kohn–Sham orbitals and their respective energies, as well as the occupation numbers n , which can all be obtained in a standard DFT calculation.

$$\chi_s(\mathbf{r}, \mathbf{r}', \omega) = \sum_i^{\text{occ.}} \sum_m^{\text{virt.}} n_i \phi_i(\mathbf{r}) \phi_m(\mathbf{r}) \phi_m(\mathbf{r}') \phi_i(\mathbf{r}') \left(\frac{1}{(\varepsilon_i - \varepsilon_m) + \omega} + \frac{1}{(\varepsilon_i - \varepsilon_m) - \omega} \right). \quad (6.4)$$

The term for the change in the exchange–correlation potential is given by

$$\delta v_{\text{xc}}^{(lm)}(\mathbf{r}, \omega) = \int d\mathbf{r}' f_{\text{xc}}(\mathbf{r}, \mathbf{r}', \omega) \delta \rho^{(lm)}(\mathbf{r}', \omega). \quad (6.5)$$

The exchange–correlation kernel $f_{\text{xc}}(\mathbf{r}, \mathbf{r}', \omega)$ is the Fourier transform of the functional derivative of the exchange–correlation potential with respect to the time-dependent density. The so-called Adiabatic Local Density Approximation (ALDA) provides the simplest approximation to this kernel. It was first employed by Zangwill and Soven[9]. It is obtained by taking the derivative of the time-independent LDA expression for v_{xc} . The result is a function which is frequency-independent and local in space:

$$f_{\text{xc}}^{\text{ALDA}}(\mathbf{r}, \mathbf{r}', \omega) = \delta(\mathbf{r} - \mathbf{r}') \frac{d^2}{d\rho^2} \left[\rho \varepsilon_{\text{xc}}^{\text{hom}}(\rho) \right] \Big|_{\rho=\rho_0(\mathbf{r})}, \quad (6.6)$$

where this function is evaluated at the converged SCF density $\rho_0(\mathbf{r})$. In this equation, $\varepsilon_{\text{xc}}^{\text{hom}}$ represents the exchange–correlation energy density for the homogeneous electron gas, in the VWN[4] parametrization.

The ALDA has been used in most of the time-dependent DFT calculations performed until now. In the low-frequency range, experience shows that it works quite well. We emphasize that we employ the ALDA for all potentials. This means that the potential which is used influences the results only through the response function and that finite field calculations may differ from the results obtained here with the Becke–Perdew and LB94 potentials. In other words, we always take the VWN expression for ε_{xc} in Eq. (6.6).

Using this scheme, the change in the electron density $\delta \rho^{(lm)}(\mathbf{r}, \omega)$ can be calculated by iteratively using Eqs. (6.2), (6.3), and (6.5) until self-consistency is obtained. After this has been done, the frequency-dependent polarizability $\tilde{\alpha}_{m,m'}^{l,l'}(\omega)$ is directly available. For an external potential specified by the quantum numbers l and m , as given by Eq. (6.1), one has:

$$\tilde{\alpha}_{m,m'}^{l,l'}(\omega) = -\frac{2}{E} \int d\mathbf{r} \delta \rho^{(lm)}(\mathbf{r}, \omega) r^l \sqrt{\frac{4\pi}{2l'+1}} Z_{l'm'}(\hat{r}). \quad (6.7)$$

Here, the superindices l and l' determine the type of multipole–multipole polarizability considered ($l = l' = 1$ representing the ordinary dipole–dipole polarizability), while the subindices m and m' determine the component of this polarizability tensor. The indices m and m' range from $-l$ to l and $-l'$ to l' respectively. In the practical implementation

the polarizability is calculated by taking the trace of the product of the multipole moment matrix and the first order density matrix, which is a transcription of Eq. (6.7).

The tilde which has been attached to the polarizability tensor indicates that the multipole operators are based on real spherical harmonics $Z_{L,M}$, where we adopt the convention that a negative sign for the angular momentum quantum number M refers to the sine combination of two spherical harmonics. Explicit expressions can be found in Stone's book on intermolecular forces[234]. Stone also gives conversion tables which can be used for converting our results into those obtained by using other conventions (based on Cartesian tensors).

6.3.2 Van der Waals dispersion coefficients

There is an interesting relation between the polarizability tensors at imaginary frequencies and Van der Waals dispersion coefficients. The equations presented here exploit this relationship in order to obtain the dispersion coefficients. The equations have been derived and extensively used by Wormer and coworkers [49, 50, 156, 176, 175, 150]. A detailed derivation of the equation for the dispersion energy [235] (which is given below) is also available from the authors.

One starts by considering molecules A and B with orientations in space determined by the sets of Euler angles ω_A and ω_B . Their position relative to each other is given by the vector \mathbf{R} . For this system one can write the dispersion energy in terms of a complete set of scalar-coupled functions:

$$E_{\text{disp}} = \sum_{n \geq 6} \sum_{L_A, L_B, L} \sum_{K_A, K_B} C_n^{(L_A, K_A, L_B, K_B, L)} R^{-n} \times \sum_{M_A, M_B, M} \begin{pmatrix} L_A & L_B & L \\ M_A & M_B & -M \end{pmatrix} [D_{K_A M_A}^{L_A}(\omega_A)]^* [D_{K_B M_B}^{L_B}(\omega_B)]^* \times \sqrt{\frac{4\pi}{2L+1}} Y_{L,-M}(\hat{\mathbf{R}}). \quad (6.8)$$

Here the coefficients $C_n^{(L_A, K_A, L_B, K_B, L)}$ are the Van der Waals dispersion coefficients which we want to calculate. For large separations ($R \gg 1$), only the $n = 6$ term remains, yielding the R^{-6} behavior. In this paper we will also be concerned with the terms $n = 7$ and $n = 8$. The quantity between brackets is a $3j$ -symbol, while the matrices D are the Wigner rotation matrices. More details and further references can be found elsewhere[49, 50].

The dispersion coefficients are the only quantities in this equation which are unknown. They can be calculated from the multipole-multipole polarizabilities of the monomers, which appear in the so-called Casimir-Polder integrals [48]. The final expression is based upon a double spherical harmonics expansion of the $1/r_{12}$ operator:

$$C_n^{(L_A, K_A, L_B, K_B, L)} = \sum_{l_A, l'_A, l_B, l'_B}^{l_A + l'_A + l_B + l'_B + 2 = n} \zeta_{l_A, l'_A, l_B, l'_B}^{L_A, L_B, L} \sum_{m_A = -l_A}^{l_A} (-1)^{K_A} \begin{pmatrix} l_A & l'_A & L_A \\ m_A & K_A - m_A & -K_A \end{pmatrix} \sum_{m_B = -l_B}^{l_B} (-1)^{K_B} \begin{pmatrix} l_B & l'_B & L_B \\ m_B & K_B - m_B & -K_B \end{pmatrix} \times 8\pi \int_0^\infty \alpha_{m_A, K_A - m_A}^{l_A, l'_A}(i\omega) \alpha_{m_B, K_B - m_B}^{l_B, l'_B}(i\omega) d\omega. \quad (6.9)$$

Here, the coefficients ζ are given by:

$$\zeta_{l_A, l'_A, l_B, l'_B}^{L_A, L_B, L} = (-1)^{L_A + L_B + L} (-1)^{l_A + l'_A} \left[\frac{(2l_A + 2l_B + 1)!(2l'_A + 2l'_B + 1)!}{(2l_A + 1)!(2l'_A + 1)!(2l_B + 1)!(2l'_B + 1)!} \right]^{1/2} \times \\ [(2L_A + 1)(2L_B + 1)(2L + 1)] \begin{pmatrix} l_A + l_B & l'_A + l'_B & L \\ 0 & 0 & 0 \end{pmatrix} \begin{Bmatrix} l_A & l'_A & L_A \\ l_B & l'_B & L_B \\ l_A + l_B & l'_A + l'_B & L \end{Bmatrix}, \quad (6.10)$$

where the quantity between curly brackets is the Wigner $9j$ -symbol. We note that our expression contains a phase factor $(-1)^{(L_A + L_B + L)}$, which was inadvertently [236] omitted in the review paper of Ref.[49]. However, in the calculations of this paper, we always have that $L_A + L_B + L$ is even, which makes the difference in phase irrelevant.

As l_A and l'_A are combined to L_A , the last quantity is limited in the following way (similarly for L_B and L):

$$\begin{aligned} L_A &= |l_A - l'_A|, |l_A - l'_A| + 1, \dots, l_A + l'_A \\ L_B &= |l_B - l'_B|, |l_B - l'_B| + 1, \dots, l_B + l'_B \\ L &= |L_A - L_B|, |L_A - L_B| + 1, \dots, L_A + L_B \end{aligned} \quad (6.11)$$

As the polarizabilities α in these formulas are based on spherical harmonics $Y_{L,M}$ while the calculated $\tilde{\alpha}$'s are based on real spherical harmonics $Z_{L,M}$ and include the Racah renormalization factor $\sqrt{4\pi/(2l+1)}$, the following conversion has to be made:

$$\alpha_{m,m'}^{l,l'} = \frac{1}{4\pi} \sqrt{(2l+1)(2l'+1)} \times \frac{1}{2} (\sqrt{2})^{\delta_{m,0} + \delta_{m',0}} (-\sigma_m)^m (-\sigma_{m'})^{m'} \\ \left\{ \tilde{\alpha}_{|m|,|m'|}^{l,l'} - (1 - \delta_{m,0})(1 - \delta_{m',0}) \sigma_m \sigma_{m'} \tilde{\alpha}_{-|m|,-|m'|}^{l,l'} \right. \\ \left. + i \left[\sigma_{m'} (1 - \delta_{m',0}) \tilde{\alpha}_{|m|,-|m'|}^{l,l'} + \sigma_m (1 - \delta_{m,0}) \tilde{\alpha}_{-|m|,|m'|}^{l,l'} \right] \right\} \quad (6.12)$$

in order to convert from (real) $Z_{L,M}$'s to $Y_{L,M}$'s. Here δ is the Kronecker delta and σ is the sign function. For the molecules considered here, the imaginary part of α vanishes on symmetry grounds.

6.4 Computational details

The calculations were performed similarly to our calculations on dipole polarizabilities [34, 74], to which we refer for further details. We repeat the most important aspects of the calculations here, for ease of reference.

All calculations were performed with the Amsterdam Density Functional (ADF) package [89, 90, 91]. Because the properties we consider are very sensitive, the use of extensive basis and fit sets (used to make the evaluation of Coulomb potential cheaper) is required. The basis sets we use consist of a valence triple zeta Slater type basis with two polarization functions, augmented with two s, two p, two d and two f functions, all with diffuse exponents.

Because none of the atoms we consider in this paper possess d-electrons (a frozen core approximation is used, which includes the 3d-shell for Kr) and we don't consider polarizabilities higher than octupole-dipole or quadrupole-quadrupole, g-functions are not essential in the basis set. The diffuse f-functions are indispensable on the other hand, as is also shown by our test calculations.

We assume that the major source of error in our calculations comes from the remaining incompleteness in the basis and fit sets. This incompleteness becomes more important for the higher multipole polarizabilities. Our test calculations show that the other possible sources of error (the use of a frozen core approximation, the numerical integration scheme) are smaller and can be neglected.

One more technical aspect of our calculations is worth mentioning. Because of the large basis sets with many diffuse functions which are used, problems with linear dependence in the basis sometimes occur. If this becomes a problem, the eigenvectors of the overlap matrix of the basis functions with the smallest eigenvalue are removed from the basis set. This is a standard method for solving this problem, and has been applied before by others[237, 238] in similar situations.

In our calculations on water it was absolutely necessary to use this method, while the removal of dependent basis functions also affected the $C_8^{4,0,0,0,4}$ results for the diatomic-rare gas interactions. As the linear combinations of basis functions which are removed are close to being superfluous, the quality of the results is not expected to suffer much from this.

The criterion for the smallest eigenvalue in the overlap matrix was taken to be 10^{-4} for the H_2O , H_2 , N_2 and 10^{-3} for Cl_2 , CO , and HCl . This led to the removal of 7 functions for H_2O , and 4 functions for each of the diatomics. Considering the total number of basis functions (156 Slater type orbitals for H_2O , and at least 100 for all diatomics) this reduction in the basis is not very severe. Some results were insufficiently stable with respect to the criterion for removal of basis functions. These have either been left out of the tables or given in parentheses.

All in all, we believe our results to be close to the basis set limits in general. This is supported by the fact that the LB94 results are close to those obtained with MBPT. There are a few exceptions in which the agreement is less satisfactory. These will be discussed in more detail.

6.5 Polarizability results

In a previous paper[74], atomic quadrupole polarizabilities for the rare gases were presented. Here, the quadrupole-quadrupole polarizability tensors $\alpha_{m,m'}^{2,2}$ for the diatomics H_2 , N_2 , CO , HCl , and Cl_2 are given. We use the following definitions of the mean quadrupole-quadrupole polarizability ($\bar{\alpha}^{2,2}$) and the relative first ($\gamma_{\Delta_{1,2}}$) and the second ($\gamma_{\Delta_{2,2}}$) anisotropy in the quadrupole-quadrupole polarizability:

$$\begin{aligned}\bar{\alpha}^{2,2} &= (\alpha_{0,0}^{2,2} + 2\alpha_{1,1}^{2,2} + 2\alpha_{2,2}^{2,2})/5 \\ \Delta_1\alpha^{2,2} &= \alpha_{0,0}^{2,2} + \alpha_{1,1}^{2,2} - 2\alpha_{2,2}^{2,2} \\ \Delta_2\alpha^{2,2} &= (3\alpha_{0,0}^{2,2} - 4\alpha_{1,1}^{2,2} + \alpha_{2,2}^{2,2})/4\end{aligned}$$

$$\begin{aligned}\gamma_{\Delta_{1,2}} &= \frac{\Delta_1 \alpha^{2,2}}{\bar{\alpha}^{2,2}} \\ \gamma_{\Delta_{2,2}} &= \frac{\Delta_2 \alpha^{2,2}}{\bar{\alpha}^{2,2}}.\end{aligned}\tag{6.13}$$

Table 6.1: Mean quadrupole polarizability $\bar{\alpha}^{2,2}$ [cf. Eq. (6.13)] for diatomics using the LDA, BP, and LB94 potentials

Molecule	LDA	BP	LB94	<i>ab initio</i>
H ₂	21.92	19.73	18.86	16.11 ^a , 15.4122 ^b
N ₂	91.83	88.37	80.20	78.22 ^a , 80.74 ^c
CO	124.9	119.8	106.9	106.8 ^a , 112.1 ^d , 110.24 ^e , 102.52 ^f
HCl	128.2	122.2	117.8	106.1 ^a
Cl ₂	402.4	390.6	371.1	345.2 ^a , 339.0 ^g

^aRef.[150] Many-Body Perturbation Theory

^bRef.[151] Sum-over-States with explicitly correlated wave functions (SoS)

^cRef.[201] Finite field fourth order Singles Doubles Quadruples-MBPT (SDQ-MBPT)

^dRef.[239] Finite field coupled-cluster doubles (FF-CCD)

^eRef.[240] Singles doubles quadruples MBPT

^fRef.[241] Finite field HF

^gRef.[242] Finite field fourth order MBPT

In Tables 6.1, 6.2, and 6.3 the mean quadrupole polarizability and the relative first and the second anisotropies are given. As the quadrupole polarizabilities depend upon the choice of the origin, one has to specify the geometry. We have performed all our calculations (also for the dispersion coefficients) with respect to the center of mass, which is the usual choice.

For the anisotropies we present the relative numbers in order to emphasize that the quality of the polarizability anisotropies is not bad for the LDA and BP polarizability tensor components. In this way the clear overestimation, which is present in all calculations with the LDA and BP potentials, is divided out. The results of Ref.[159] were linearly interpolated because they were given at several bond distances, but not at the experimental ones used in this work and in our previous work [74].

In Table 6.1, our results for the mean quadrupole polarizabilities of the diatomics are given. The LB94 potential gives the best results of the three potentials used in this work, although the values of H₂, HCl, and Cl₂ are a bit higher than the literature values. The LDA yields overestimations from 10 to 40%, while the BP result is slightly better with overestimations of 5 to 30%. These results confirm the trends which were observed in our earlier comparison of these three potentials[74]. The trends are more pronounced in the case of quadrupole polarizabilities than for dipole polarizabilities.

The results for the relative first and the second anisotropies (given in Tables 6.2 and 6.3) obtained with the different potentials are of comparable quality. The results for diatomics containing a Chloride-atom are somewhat worse than the others. Most of the results for the relative anisotropies of all the three methods are comparable to the *ab initio* literature values.

Table 6.2: Relative first anisotropy $\gamma_{\Delta_{1,2}}$ [cf. Eq. (6.13)] in the quadrupole polarizability for diatomics using the LDA, BP, and LB94 potentials

Molecule	LDA	BP	LB94	<i>ab initio</i>
H ₂	0.479	0.485	0.498	0.474 ^a , 0.527 ^b
N ₂	1.388	1.391	1.456	1.388 ^a , 1.562 ^c
CO	1.511	1.522	1.601	1.567 ^a , 1.606 ^d , 1.611 ^e , 1.594 ^f
HCl	0.321	0.318	0.474	0.271 ^a
Cl ₂	1.788	1.811	1.835	1.781 ^a , 1.822 ^g

^aRef.[150] Many-Body Perturbation Theory

^bRef.[151] Sum-over-States with explicitly correlated wave functions (SoS)

^cRef.[201] Finite field fourth order Singles Doubles Quadruples-MBPT (SDQ-MBPT)

^dRef.[239] Finite field coupled-cluster doubles (FF-CCD)

^eRef.[240] Singles doubles quadruples MBPT

^fRef.[241] Finite field HF

^gRef.[242] Finite field fourth order MBPT

We also performed quadrupole polarizability calculations on water. Their results are shown in Table 6.4. Because of the lower symmetry of this molecule, its dipole-quadrupole polarizability does not vanish and off-diagonal elements are allowed for the quadrupole-quadrupole tensor. For the dipole-quadrupole tensor the LB94 and MBPT values are very close to each other, the values of LDA and BP being somewhat higher and the values for the Hartree-Fock method of Ref. [175] somewhat lower. Considering the excellent agreement between the LB94 and MBPT results, the CI values of Ref. [243] seem to be less accurate than either of these.

The LB94 results for the quadrupole-quadrupole polarizability are also in very good agreement with the MBPT results, except for the $\alpha_{2,0}^{2,2}$ -component. The DFT results for this component have been given in parentheses, as test calculations have shown that our results for this component are unstable with respect to small changes in the basis set. We performed a calculation where extra basis and fit functions were added on the symmetry axis at 0.27Å from the O-atom in the direction of the hydrogen atoms (with the same criterion for the removal of basis functions). This yielded a value for the LB94 potential of $\alpha_{2,2}^{2,0} = 1.38$, in much better agreement with the other values. The other components are much more stable with respect to changes in the basis set or in the criterion for removal of basis functions and can be considered reliable. It is not completely clear, why this component is less stable than the other ones. The sole fact that it is small in magnitude, is not satisfactory as an explanation.

6.5.1 Results for Van der Waals coefficients

The dispersion coefficients were calculated from Eq. (6.9), using a stand-alone program called 'disper', which was based upon a similar program by Dr./ P.E.S. Wormer and coworkers. The program uses the output of polarizability calculations with the ADF program. The

Table 6.3: Relative second anisotropy $\gamma_{\Delta_{2,2}}$ [cf. Eq. (6.13)] in the quadrupole polarizability for diatomics using the LDA, BP, and LB94 potentials

Molecule	LDA	BP	LB94	<i>ab initio</i>
H ₂	0.0217	0.0145	0.0114	0.0119 ^a , 0.1367 ^b
N ₂	-0.206	-0.208	-0.222	-0.223 ^a , -0.234 ^c
CO	-0.261	-0.266	-0.285	-0.293 ^a , -0.292 ^d , -0.294 ^e , -0.319 ^f
HCl	0.148	0.150	0.171	0.144 ^a
Cl ₂	-0.402	-0.398	-0.383	-0.395 ^a , -0.390 ^g

^aRef.[150] Many-Body Perturbation Theory

^bRef.[151] Sum-over-States with explicitly correlated wave functions (SoS)

^cRef.[201] Finite field fourth order Singles Doubles Quadruples-MBPT (SDQ-MBPT)

^dRef.[239] Finite field coupled-cluster doubles (FF-CCD)

^eRef.[240] Singles doubles quadruples MBPT

^fRef.[241] Finite field HF

^gRef.[242] Finite field fourth order MBPT

Casimir-Polder integrals, which appear in Eq. (6.9), are evaluated by Gauss-Chebyshev quadrature[156] in twenty frequency points. Because the Casimir-Polder integrals are even functions of the frequency ω , the frequency-dependent polarizabilities are needed in ten frequencies only. Test calculations with a larger number of integration points have shown that the resulting changes are minimal.

All the calculations were done for LDA, BP, and the LB94 potentials. Although the program *disper* is able to calculate the C_n Van der Waals coefficients up to arbitrary n , only the results up to C_8 are given. Higher order dispersion coefficients would not be reliable due to the limitations in basis and fit sets. The results given in this section will be concentrated on the coefficients for which literature values exist.

First we will consider C_8 -coefficients for interactions between rare gases in Table 6.5. The BP and LDA potentials overestimate this coefficient in all cases with respect to the *ab initio* values, while the Hartree-Fock values are consistently too low. The LB94 potential gives good results, though the results involving Kr are somewhat too low. This is due to the underestimation of the quadrupole polarizability of Kr by the LB94 potential[74].

The average errors and average absolute errors with respect to the MBPT values have been included in the table. The first one gives an impression of the general quality of the results, while the second gives information about the nature of the error. Clearly, the LB94 results are superior to the BP results, which are in turn better than the LDA results. The error in the LDA and BP results is very systematic, while the errors in the LB94 results are of a more random nature.

After the rare gas-rare gas interactions, the interactions between diatomics and rare gases were considered. Because the number of independent components is greatly reduced in this case, a more compact notation for the dispersion coefficients is used in the literature, based on Legendre polynomials $P_{L,M}$. In the Legendre convention one has coefficients C_n^L which

Table 6.4: Polarizability tensor elements for water, using LDA, BP, and LB94.

Tensor component	LDA	BP	LB94	TDCHF ^a	MBPT ^a	CI value ^b
$\alpha_{0,0}^{2,1}$	-3.44	-3.30	-2.70	-1.959	-2.633	-2.194
$\alpha_{2,0}^{2,1}$	-2.75	-2.88	-2.73	-2.717	-2.853	-3.433
$\alpha_{1,1}^{2,1}$	-8.11	-8.22	-7.87	-7.143	-7.843	-7.785
$\alpha_{-1,-1}^{2,1}$	-3.60	-3.39	-2.56	-1.822	-2.509	-2.062
$\alpha_{2,2}^{2,2}$	59.7	57.9	46.4	40.732	45.947	
$\alpha_{2,0}^{2,2}$	(3.9) ^c	(3.6) ^c	(0.06) ^c	1.228	1.843	
$\alpha_{1,1}^{2,2}$	64.7	62.8	54.9	46.425	51.375	
$\alpha_{0,0}^{2,2}$	55.8	53.7	43.3	37.149	42.368	
$\alpha_{-1,-1}^{2,2}$	58.4	55.9	42.8	38.043	43.398	
$\alpha_{-2,-2}^{2,2}$	58.6	56.4	44.0	37.604	42.809	

aRef.[175]

bRef.[243]

cValues in parentheses are unstable with respect to basis changes.

are related to the coefficients $C_n^{L,0,0,L}$ by[176]:

$$C_n^L = \frac{C_n^{L,0,0,L}}{(-1)^L \sqrt{2L+1}}. \quad (6.14)$$

The diatomic-rare gas interactions are completely determined by the C_n^L coefficients. All the results for the diatomic-rare gas interactions are given in the Legendre convention. Some of the LDA dispersion coefficients presented here in Tables 6.6 and 6.8, were calculated by us before[34]. In these cases very small differences occur, mainly due to the fact that we use somewhat larger basis sets in the present work. The present values have to be considered slightly more accurate for this reason.

First the isotropic dispersion coefficients will be discussed. The C_6^0 -coefficients are given in Table 6.6. For these coefficients accurate constrained Dipole Oscillator Strength Distribution (DOSD) results[173, 163, 177] are available. These are obtained by the use of available oscillator strength data and a system of quantum mechanical sum rule constraints and can be used as reference values, where these results are available.

In Table 6.6, we have given the average absolute error and average error of our results with respect to both the DOSD and the MBPT results. This has been done, because the DOSD results can be considered the benchmark, but the MBPT results are available for all the molecules. The previously noted general trend of an overestimation for LDA and BP potentials and results closer to the literature values for the LB94 potential can again be observed for these Van der Waals coefficients. Looking at the potentials individually, several trends can be noted.

For the LDA and BP potentials most values give the expected overestimation, but the overestimation is lower for the C_6 -coefficients involving Kr. This can be explained from the LDA and BP values for the dipole polarizability of Kr, which also show a smaller overestimation. The general overestimation of BP is smaller than the one of LDA (4.7% versus

Table 6.5: C_8 Van der Waals coefficients for the rare gases

Atom-Atom	LDA	BP	LB94	<i>ab initio</i>	TDCHF ^a
He - He	20.97	18.13	14.15	14.1179 ^b	
He - Ne	48.20	44.01	34.32	36.175 ^c	
He - Ar	215.0	197.2	171.8	167.47 ^c	
He - Kr	344.0	317.5	268.8	279.99 ^c	
Ne - Ne	109.6	105.2	82.02	90.344 ^c	73.458
Ne - Ar	461.5	444.3	379.5	390.12 ^c	344.51
Ne - Kr	726.4	703.1	583.0	638.14 ^c	560.17
Ar - Ar	1877	1808	1709	1623.2 ^c	1553.0
Ar - Kr	2904	2811	2578	2616.7 ^c	2487.3
Kr - Kr	4455	4337	3862	4187.3 ^c	3953.0
Av. abs. error wrt MBPT	18.9%	12.8%	5.1%		
Av. error wrt MBPT	18.9%	12.8%	-3.5%		

aRef.[174] TDCHF

bRef.[151] Sum-over-states with explicitly electron-correlated wave functions (SoS)

cRef.[174] Many-Body Perturbation Theory (MBPT)

9.8%).

With an average absolute error of 3.2%, the LB94 results approach the DOSD values best of the three exchange-correlation potentials. The MBPT results are even better, with an average absolute error of 2.0%. The average errors show that the LDA and BP errors are clearly of a systematic nature, which is not true for the LB94 and MBPT results. The errors with respect to the MBPT results show that the picture does not change if the Cl_2 molecule is taken into account as well.

In Table 6.7 the C_8^0 results are presented. The trends are the same as in the previous tables. Taking the MBPT results as a reference, the average LDA, BP, and LB94 errors are 20.5%, 13.2%, and 4.2% respectively. For the LDA and BP results, these errors are clearly larger than those for the C_6^0 results. This was to be expected, since the C_8^0 coefficients are more sensitive to the description of the outer region of the molecule. The errors are quite similar to those of the rare gases in Table 6.5.

Now we turn to the anisotropies in the dispersion coefficients. In Table 6.8, the relative anisotropic dispersion coefficients γ_6^2 are shown. They are defined by:

$$\gamma_6^2 = \frac{C_6^2}{C_6^0}. \quad (6.15)$$

In our earlier work[34] we used the symbol Γ for γ_6^2 . Similarly, we define

$$\begin{aligned} \gamma_8^2 &= \frac{C_8^2}{C_8^0}, \\ \gamma_8^4 &= \frac{C_8^4}{C_8^0}, \end{aligned}$$

$$\gamma_7^3 = \frac{C_7^3}{C_7^1}. \quad (6.16)$$

In Table 6.8, the DOSD values can again be considered the reference. Unfortunately, they are only available for H₂, N₂, and CO. The errors with respect to the DOSD values (5.9%, 4.2%, 4.1% and 11.1% for the LDA, BP, and LB94 potentials and for the MBPT results respectively) show that, for the molecules considered here, our results are in better agreement with the DOSD results than the MBPT results are. The quality of the LDA, BP, and LB94 results is very similar. This implies that reliable estimates for the *relative* anisotropies can be obtained at the LDA or BP level, because the overestimations affect the different polarizability tensor components in similar fashion.

Table 6.9 gives the results for the relative anisotropic dispersion coefficients γ_8^2 . We have calculated the average absolute errors with respect to the MBPT results. The DFT anisotropies are slightly higher than the MBPT anisotropy for Cl₂. The average errors show that the LDA and BP values tend to be very similar to each other and slightly lower than those obtained with MBPT, while the LB94 values are slightly higher. In general the agreement between the DFT results and the MBPT results is very satisfactory in this table.

Though the results for the isotropic dispersion coefficients calculated at the MBPT level are of higher quality than our DFT results, the errors of Table 6.8 indicate that the MBPT results for the relative anisotropies need not necessarily be better than ours. As still higher level calculations are lacking, it remains unclear which of the columns in Table 6.9 gives the most reliable results.

Table 6.10 contains the results for γ_8^4 . We have chosen not to include results for Cl₂, as we were unable to obtain converged results. The changes resulting from the removal of one or a few basis functions were too large to allow for a reliable quantitative estimate of this coefficient. The other dispersion coefficients and other molecules were much more stable with respect to small changes in the basis.

Once again, the agreement between the DFT results and the MBPT results is very good, considering the highly anisotropic character of this coefficient. The DFT values tend to be somewhat lower than the MBPT values. The average absolute errors are comparable for the three exchange-correlation potentials.

Finally, we come to our results for the C_7 -coefficients. As these are zero for the centrosymmetric molecules, only results for HCl-rare gas and CO-rare gas interactions are presented in Table 6.11, where the coefficient C_7^1 is considered. Once again, the LDA values are too high. To lesser extent, this also holds for the BP values, though the BP coefficient for HCl-Kr is slightly lower than the MBPT value. The LB94 and MBPT results are in good agreement, though the MBPT values are slightly higher than the LB94 values for CO.

Table 6.12 is the last table on the diatomic-rare gas interactions. It contains the relative anisotropic coefficient γ_7^3 . Very good agreement between the LDA, BP, LB94, and MBPT results is obtained for the interactions involving HCl. This is not the case for those involving CO, where the DFT results are in very good mutual agreement, but in disagreement with the MBPT results. These results represent the largest differences we found between all the DFT and MBPT results in this paper. It is not *a priori* clear which results should be more trustworthy, and more advanced calculations are needed in order to draw definite

conclusions¹. However, the fact that the DFT results are in very good mutual agreement (which might be expected only for the LDA and BP results), as well as the fact that the DFT results for CO are in better agreement with the DOSD results for γ_6^2 speak in favor of the DFT numbers.

Summing up the results for the anisotropic parts of the diatomic-rare gas interactions, one can say that the DFT and MBPT results are in very satisfactory agreement for the relative anisotropic dispersion coefficients (except for the case just mentioned).

The final results obtained for this work are the Van der Waals coefficients for the water-water interaction, presented in Table 6.13. Only those coefficients are shown for which comparison to MBPT literature values was possible. This means that very small dispersion coefficients are not included in the table. The results for the coefficients $C_6^{0,0,0,0,0}$, $C_7^{1,0,0,0,1}$, and $C_8^{0,0,0,0,0}$ once again show the overestimation in the LDA and BP results. The other components have been given relative to these values and are denoted by γ . One has, for example, that $\gamma_7^{3,2,0,0,3} = C_7^{3,2,0,0,3}/C_7^{1,0,0,0,1}$. The DFT results for $\gamma_8^{2,0,0,0,2}$ and $\gamma_8^{2,2,0,0,2}$ have been given in parentheses, as they depend strongly upon the quadrupole-quadrupole polarizability tensor component $\alpha_{2,0}^{2,2}$ of Table 6.4. The instability of this polarizability component clearly influences these dispersion coefficients. We performed some test calculations which show that the other components are influenced far less. Consequently, both the good agreement between the LB94 and MBPT results for $\gamma_8^{2,0,0,0,2}$ and the bad agreement for $\gamma_8^{2,2,0,0,2}$ should be considered accidental. The test calculation with extra diffuse functions in the center of the molecule, to which we referred earlier, yielded values of 0.052 and 0.162 for the $\gamma_8^{2,0,0,0,2}$ and $\gamma_8^{2,2,0,0,2}$ components for the LB94 potential.

In general, the LB94 potential clearly gives the best agreement with the *ab initio* values, in this case also for the relative anisotropies. This agreement can be considered very satisfactory.

It holds for all dispersion coefficients that all the discrepancies in the results can be explained by looking at the differences in the polarizability results. The frequency dependence is not of decisive importance, because it is similar for all the used methods.

6.6 Concluding remarks

We have presented calculations with three different exchange-correlation potentials within time-dependent DFT on molecular quadrupole polarizabilities and Van der Waals coefficients. These are the first such calculations within DFT. By comparing to *ab initio* literature values we have been able to analyze the strengths and weaknesses of these potentials. The LB94 results for the isotropic properties are superior to the LDA and Becke–Perdew results, which overestimate the isotropic coefficients. This is due to the fact that the LB94 potential exhibits the correct Coulombic asymptotic behavior, which the ordinary LDA and GGA potentials do not. For the relative anisotropies, the results obtained with the three

¹Such advanced calculations have recently been performed by Hättig and Hess[244]. Their time-dependent MP2 results for γ_7^3 , obtained in very large basis sets, are in excellent agreement with our DFT results. In particular, they obtained -0.044 for CO-He, -0.0415 for CO-Ne, -0.0483 for CO-Ar, and -0.0500 for CO-Kr.

potentials are of similar quality. The anisotropic DFT results are in good agreement with the MBPT values, and seem to be of competitive quality.

Our results indicate that it is possible to obtain reliable long-range potential energy surfaces within the framework of density functional theory. An important next step would be to link this long-range potential energy surface with the short-range part, in order to obtain a reliable description of Van der Waals minima.

6.7 Acknowledgments

We would like to thank Dr. P.E.S. Wormer from the University of Nijmegen for useful discussions concerning Eqs. (6.8), (6.9), and (6.10), and for providing the program DISPER upon which our own implementation is based. One of the authors (SvG) acknowledges financial support by the Dutch Foundation for Chemical Research (S.O.N.).

Table 6.6: C_6^0 - Van der Waals coefficients for diatomic - rare gas

diatomic	rare gas	LDA	BP	LB94	MBPT ^a	DOSD ^b	SoS ^c
H ₂	He	4.789	4.327	4.102	3.913	4.007 ^d	4.01281
H ₂	Ne	9.187	8.679	7.961	8.027	8.091 ^d	
H ₂	Ar	30.36	28.54	28.84	27.12	27.64 ^d	
H ₂	Kr	42.46	40.13	39.59	39.47	39.44 ^d	
N ₂	He	11.77	11.00	9.939	9.773	10.23 ^d	
N ₂	Ne	23.01	22.43	19.73	20.25	20.97 ^d	
N ₂	Ar	73.22	71.16	68.23	65.60	68.69 ^d	
N ₂	Kr	101.6	99.32	93.00	94.52	97.28 ^d	
CO	He	12.23	11.39	10.21	10.83	10.69 ^e	
CO	Ne	23.80	23.16	20.18	22.34	21.87 ^e	
CO	Ar	76.47	74.15	70.52	73.36	72.26 ^e	
CO	Kr	106.4	103.7	96.32	106.1	102.5 ^e	
HCl	He	15.44	14.31	13.36	13.33	13.33 ^f	
HCl	Ne	29.71	28.77	26.02	27.34	27.05 ^f	
HCl	Ar	97.57	94.18	93.56	91.48	91.21 ^f	
HCl	Kr	136.3	132.3	128.3	132.9	129.9 ^f	
Cl ₂	He	26.75	24.90	23.04	23.48		
Cl ₂	Ne	51.47	50.04	44.88	47.98		
Cl ₂	Ar	169.0	163.8	161.5	161.5		
Cl ₂	Kr	236.2	230.2	221.6	234.8		
Av. abs. error wrt DOSD		9.8%	4.7%	3.2%	2.0%		
Av. error wrt DOSD		9.8%	4.7%	-2.0%	-0.5%		
Av. abs. error wrt MBPT		9.7%	5.2%	3.8%			
Av. error wrt MBPT		9.7%	4.8%	-1.8%			

^aRef.[150] MBPT, results were linearly interpolated^bConstrained dipole oscillator strength distribution results^cRef.[151] Sum-over-states with explicitly electron-correlated wave functions (SoS)^dRef.[173]^eRef.[163]^fRef.[177]

Table 6.7: C_8^0 - Van der Waals coefficients for diatomic - rare gas

diatomic	rare gas	LDA	BP	LB94	MBPT ^a	SoS ^b
H ₂	He	77.31	67.13	59.74	53.60	55.38
H ₂	Ne	167.6	153.5	133.7	128.4	
H ₂	Ar	720.7	663.2	644.0	576.5	
H ₂	Kr	1135	1051	989.5	953.6	
N ₂	He	284.3	259.7	222.4	219.7	
N ₂	Ne	599.1	574.2	481.4	498.7	
N ₂	Ar	2334	2240	2068	1986	
N ₂	Kr	3552	3429	3074	3145	
CO	He	334.0	304.9	257.9	262.7	
CO	Ne	693.6	664.2	548.9	588.9	
CO	Ar	2689	2576	2348	2355	
CO	Kr	4072	3923	3474	3726	
HCl	He	364.9	332.2	298.5	284.1	
HCl	Ne	764.5	730.6	639.8	643.7	
HCl	Ar	3048	2914	2815	2638	
HCl	Kr	4667	4487	4201	4219	
Cl ₂	He	1026	946.1	849.4	810.3	
Cl ₂	Ne	2086	2013	1758	1770	
Cl ₂	Ar	7758	7479	7186	6764	
Cl ₂	Kr	11539	11184	10439	10505	
Av. abs. error wrt MBPT		20.5%	13.2%	4.2%		
Av. error wrt MBPT		20.5%	13.2%	1.8%		

^aRef.[150] MBPT, results were linearly interpolated

^bRef.[151] Sum-over-states with explicitly electron-correlated wave functions (SoS)

Table 6.8: γ_6^2 - Van der Waals coefficients for diatomic - rare gas

diatomic	rare gas	LDA	BP	LB94	MBPT ^a	DOSD ^b	SoS ^c
H ₂	He	0.0875	0.0915	0.0931	0.0902	0.0924 ^d	0.0946
H ₂	Ne	0.0852	0.0893	0.0902	0.0883	0.0901 ^d	
H ₂	Ar	0.0905	0.0947	0.0971	0.0946	0.0971 ^d	
H ₂	Kr	0.0917	0.0960	0.0984	0.0961	0.0986 ^d	
N ₂	He	0.1040	0.1064	0.1107	0.0824	0.1027 ^d	
N ₂	Ne	0.1010	0.1034	0.1068	0.0803	0.0999 ^d	
N ₂	Ar	0.1068	0.1095	0.1145	0.0857	0.1074 ^d	
N ₂	Kr	0.1079	0.1108	0.1157	0.0870	0.1087 ^d	
CO	He	0.0833	0.0856	0.0884	0.1023	0.0930 ^e	
CO	Ne	0.0814	0.0837	0.0860	0.1001	0.0916 ^e	
CO	Ar	0.0842	0.0868	0.0899	0.1054	0.0942 ^e	
CO	Kr	0.0845	0.0873	0.0903	0.1064	0.0943 ^e	
HCl	He	0.0330	0.0337	0.0431	0.0368		
HCl	Ne	0.0324	0.0332	0.0419	0.0361		
HCl	Ar	0.0329	0.0337	0.0440	0.0375		
HCl	Kr	0.0328	0.0337	0.0443	0.0378		
Cl ₂	He	0.1323	0.1334	0.1346	0.1355		
Cl ₂	Ne	0.1281	0.1295	0.1294	0.1310		
Cl ₂	Ar	0.1374	0.1390	0.1415	0.1437		
Cl ₂	Kr	0.1395	0.1412	0.1437	0.1469		
Av. abs. err. wrt DOSD		5.9%	4.2%	4.1%	11.1%		
Av. abs. err. wrt MBPT		12.7%	11.6%	13.8%			

^aRef.[150] MBPT, results were linearly interpolated^bConstrained dipole oscillator strength distribution results^cRef.[151] Sum-over-states with explicitly electron-correlated wave functions (SoS)^dRef.[173]^eRef.[163]

Table 6.9: γ_8^2 - Van der Waals coefficients for diatomic - rare gas

diatomic	rare gas	LDA	BP	LB94	MBPT ^a	SoS ^b
H ₂	He	0.2786	0.2870	0.3064	0.2950	0.3080
H ₂	Ne	0.2520	0.2588	0.2739	0.3233	
H ₂	Ar	0.2161	0.2197	0.2290	0.2184	
H ₂	Kr	0.2016	0.2049	0.2138	0.2018	
N ₂	He	0.8864	0.8944	0.9465	0.9227	
N ₂	Ne	0.8270	0.8353	0.8748	0.8488	
N ₂	Ar	0.6927	0.6931	0.7228	0.7003	
N ₂	Kr	0.6399	0.6402	0.6708	0.6428	
CO	He	0.9932	1.0046	1.0637	1.0424	
CO	Ne	0.9279	0.9352	0.9841	0.9600	
CO	Ar	0.7936	0.7970	0.8322	0.8151	
CO	Kr	0.7375	0.7406	0.7764	0.7553	
HCl	He	0.1615	0.1671	0.2127	0.1861	
HCl	Ne	0.1546	0.1590	0.1997	0.1744	
HCl	Ar	0.1236	0.1268	0.1630	0.1397	
HCl	Kr	0.1132	0.1161	0.1515	0.1277	
Cl ₂	He	1.5042	1.5389	1.4979	1.4946	
Cl ₂	Ne	1.4301	1.4595	1.4170	1.4060	
Cl ₂	Ar	1.2751	1.2994	1.2588	1.2497	
Cl ₂	Kr	1.2046	1.2279	1.1951	1.1778	
Av. abs. error wrt MBPT		5.5%	5.0%	6.5%		
Av. error wrt MBPT		-4.9%	-3.3%	4.5%		

^aRef.[150] MBPT, results were linearly interpolated

^bRef.[151] Sum-over-states with explicitly electron-correlated wave functions (SoS)

Table 6.10: γ_8^4 - Van der Waals coefficients for diatomic - rare gas

diatomic	rare gas	LDA	BP	LB94	MBPT ^a	SoS ^b
H ₂	He	0.0098	0.0092	0.0082	0.0091	0.0099
H ₂	Ne	0.0092	0.0085	0.0074	0.0076	
H ₂	Ar	0.0063	0.0058	0.0052	0.0062	
H ₂	Kr	0.0055	0.0051	0.0046	0.0055	
N ₂	He	-0.0208	-0.0212	-0.0200	-0.0217	
N ₂	Ne	-0.0176	-0.0180	-0.0163	-0.0179	
N ₂	Ar	-0.0181	-0.0183	-0.0177	-0.0192	
N ₂	Kr	-0.0174	-0.0176	-0.0171	-0.0187	
CO	He	-0.0392	-0.0402	-0.0361	-0.0379	
CO	Ne	-0.0345	-0.0354	-0.0308	-0.0322	
CO	Ar	-0.0337	-0.0345	-0.0315	-0.0334	
CO	Kr	-0.0323	-0.0330	-0.0303	-0.0325	
HCl	He	0.0621	0.0658	0.0768	0.0777	
HCl	Ne	0.0555	0.0586	0.0675	0.0682	
HCl	Ar	0.0483	0.0509	0.0594	0.0598	
HCl	Kr	0.0445	0.0469	0.0552	0.0552	
Av. abs. error wrt MBPT		8.6%	7.5%	6.4%		
Av. error wrt MBPT		-3.4%	-3.2%	-6.4%		

^aRef.[150] MBPT, results were linearly interpolated^bRef.[151] Sum-over-states with explicitly electron-correlated wave functions (SoS)Table 6.11: C_7^1 - Van der Waals coefficients for diatomic - rare gas

diatomic	rare gas	LDA	BP	LB94	MBPT ^a
CO	He	35.23	32.17	27.12	28.69
CO	Ne	66.12	63.04	51.06	57.25
CO	Ar	230.8	219.1	197.9	204.9
CO	Kr	325.8	312.1	274.9	302.3
HCl	He	21.33	19.57	19.23	18.54
HCl	Ne	40.95	39.28	37.30	37.72
HCl	Ar	135.2	129.1	135.4	128.0
HCl	Kr	189.2	181.6	186.0	186.5

^aRef.[150] MBPT, results were linearly interpolated

Table 6.12: γ_7^3 - Van der Waals coefficients for diatomic - rare gas

diatomic	rare gas	LDA	BP	LB94	MBPT ^a
CO	He	-0.0448	-0.0443	-0.0428	-0.0216
CO	Ne	-0.0432	-0.0430	-0.0404	-0.0191
CO	Ar	-0.0488	-0.0484	-0.0484	-0.0279
CO	Kr	-0.0504	-0.0501	-0.0502	-0.0306
HCl	He	0.2495	0.2649	0.2627	0.2669
HCl	Ne	0.2437	0.2588	0.2549	0.2615
HCl	Ar	0.2553	0.2719	0.2717	0.2759
HCl	Kr	0.2575	0.2746	0.2745	0.2792

^aRef.[150] MBPT, results were linearly interpolated

Table 6.13: Van der Waals coefficients for H₂O-H₂O

Coefficient	LDA	BP	LB94	MBPT ^a
$C_6^{0,0,0,0,0}$	50.37	48.65	43.17	46.433
$\gamma_6^{2,2,0,0,2}$	0.041	0.044	0.077	0.0647
$\gamma_6^{2,2,2,2,4}$	0.0059	0.0065	0.016	0.0112
$C_7^{1,0,0,0,1}$	113.7	111.80	96.48	102.16
$\gamma_7^{2,2,1,0,3}$	-0.027	-0.029	-0.055	-0.0460
$\gamma_7^{3,0,0,0,3}$	-0.244	-0.25	0.277	-0.2779
$\gamma_7^{3,2,0,0,3}$	0.315	0.331	0.366	0.3578
$\gamma_7^{3,0,2,2,5}$	-0.027	-0.030	-0.064	-0.0529
$\gamma_7^{3,2,2,2,5}$	0.036	0.041	0.084	0.0681
$C_8^{0,0,0,0,0}$	1426	1361	1115	1141.7
$\gamma_8^{1,0,1,0,2}$	-0.150	-0.157	-0.162	-0.1636
$\gamma_8^{2,0,0,0,2}$	(0.066) ^b	(0.064) ^b	(0.066) ^b	0.0626
$\gamma_8^{2,2,0,0,2}$	(0.040) ^b	(0.051) ^b	(0.206) ^b	0.1179
$\gamma_8^{3,2,1,0,4}$	-0.048	-0.053	-0.061	-0.0603
$\gamma_8^{3,0,3,0,6}$	-0.043	-0.048	-0.061	-0.0615
$\gamma_8^{3,2,3,0,6}$	0.055	0.063	0.080	0.0791
$\gamma_8^{3,2,3,2,6}$	-0.071	-0.082	-0.105	-0.1019
$\gamma_8^{4,0,0,0,4}$	-0.075	-0.075	-0.098	-0.0977
$\gamma_8^{4,2,0,0,4}$	0.078	0.081	0.094	0.0865

^aRef.[175]

^bValues in parentheses are unstable with respect to basis changes.

Chapter 7

Time-dependent density functional results for the dynamic hyperpolarizability of C_{60}

7.1 Abstract

The experimental, as well as theoretical, values for the frequency-dependent hyperpolarizability of C_{60} differ by orders of magnitude. We present the first density functional calculation of a molecular frequency-dependent hyperpolarizability. Our implementation is very economical, enabling the treatment of molecules of this size, in a potentially much more accurate way than can be obtained with alternative methods. Our results strongly support the recent results by Geng and Wright, who report much lower experimental values than previous authors.

7.2 Introduction

At present, there is much interest in the field of nonlinear optics. Possibly interesting technological applications for nonlinear optical materials range from optical signal-processing devices to all-optical computers. Theoretical calculations can be a useful aid in understanding relationships between molecular structure and nonlinear optical properties and in the prescreening of molecules which might exhibit large nonlinear polarizabilities (hyperpolarizabilities). The experimental determination of these properties on the other hand, is usually much more time consuming and expensive.

Organic molecules with delocalized electron systems are of particular interest, because of their potentially large nonlinear optical response. Here, we will treat one of these organic molecules for which huge hyperpolarizabilities have been reported experimentally: the Buckminster fullerene C_{60} . For this system, of great current interest, discrepancies of ten orders of magnitude[136] exist in the experimental data. An accurate theoretical determination is therefore particularly timely.

For a system of the size of C_{60} , and also for other large organic molecules such as linear

polymeric chains, it is important to have a theoretical approach which is both accurate and efficient. For hyperpolarizabilities, accuracy demands that both frequency dispersion and the effects of electron correlation are taken into account. Such an approach could also serve as a benchmark for more approximate calculations. The correlated methods conventionally used in quantum chemistry can be very useful in this respect, but they are too time consuming to be used for large molecules. On the other hand, time-dependent Hartree–Fock (TDHF) and semiempirical calculations may not always be of the desired accuracy.

In the framework of time-dependent Density Functional Theory (TDDFT) (an extensive review is provided by Ref.[33]), the frequency-dependent hyperpolarizability tensors are obtained in a formally exact manner. We have developed a scheme which uses TDDFT for the calculation of the dynamic first hyperpolarizability tensors β . Higher nonlinear polarizabilities can be obtained by finite differentiation. Our scheme applies to molecules as well as atoms and requires the solution of the first order response equations only, making it both more generally applicable and more efficient than Senatore and Subbaswamy’s approach[72]. The N^3 scaling of the computational cost of our hyperpolarizability calculations is the same as for an ordinary DFT calculation, making applications to large molecules possible. Our previous calculations on linear polarizabilities and related properties[34, 74, 75, 77] show that an accuracy is obtained which is higher than that obtained at TDHF level and often comparable to extensive correlated ab initio quantum chemical calculations.

7.3 Outline of theoretical approach

In the TDHF case, the starting point for the solution of the higher order response equations is given by[245, 104, 246]:

$$FC - i\frac{\partial}{\partial t}SC = SC\varepsilon, \quad (7.1)$$

where C is the time-dependent coefficient matrix of the orbitals expanded in a fixed atomic orbital basis set, S is the overlap matrix of the atomic orbitals, F is the Fock matrix and ε is a Lagrangian multiplier matrix, associated with the constraint that the orbitals remain orthonormal at all times:

$$\frac{\partial}{\partial t}(C^\dagger SC) = 0. \quad (7.2)$$

In TDHF theory this equation is derived from Frenkel’s principle[247]. In TDDFT, one can derive a similar equation, where the Fock matrix F is replaced by the appropriate DFT equivalent. This can be shown by considering orbital variations which minimize the action functional in TDDFT[33, 38], under the orthonormality constraint. One could choose the Lagrangian multiplier matrix ε to be identical to zero, in which case the ”canonical” time-dependent Kohn–Sham equations[33, 38] arise:

$$\left[-\frac{\nabla^2}{2} + v_s[\rho](\mathbf{r}, t) \right] \phi_i(\mathbf{r}, t) = i\frac{\partial}{\partial t}\phi_i(\mathbf{r}, t), \quad (7.3)$$

where $v_s[\rho](\mathbf{r}, t)$ is the time-dependent Kohn–Sham potential, consisting of the external potential, a Hartree term and an unknown exchange–correlation term. Eq. (7.2) could alternatively be obtained by replacing the rapidly oscillating orbitals ϕ_i in Eq. (7.3) by orbitals

which differ from these by a time-dependent phase factor $\exp[i \int^t \varepsilon_i(t') dt']$. One may thus proceed similarly in the TDDFT case as in the TDHF case. We have followed Karna and Dupuis[104], who present detailed equations for all first and second order hyperpolarizability tensors associated with external electric perturbations consisting of a static and a monochromatic part:

$$v_{\text{ext}}(\mathbf{r}, t) = \mathbf{E}(1 + e^{i\omega t} + e^{-i\omega t}). \quad (7.4)$$

They obtain their results by expanding the matrices F , C and ε of Eq. (7.1) into different orders of the external perturbation and in different frequency components (the overlap matrix S is independent of the perturbation). The density matrix D , given by:

$$D = CnC^\dagger, \quad (7.5)$$

where n is the occupation number matrix, is likewise expanded. The goal is to obtain expressions for the various first hyperpolarizability tensors, such as the tensor $\beta_{ijk}(-2\omega; \omega, \omega)$ governing the Second Harmonic Generation (SHG). This tensor is obtained by taking the trace of the product of the second order density matrix D and the dipole moment matrix H :

$$\beta_{ijk}(-2\omega; \omega, \omega) = -Tr[H^i D^{jk}(\omega, \omega)]. \quad (7.6)$$

This expression contains the second order density matrix D^{jk} . However, the so-called $(2n+1)$ -theorem of perturbation theory states that the energy can be calculated to third order if the wavefunction is known to first order only. Thus, Eq. (7.6) can be rewritten such that only first order quantities ($C^{(1)}$, $D^{(1)}$, $F^{(1)}$ and $\varepsilon^{(1)}$) appear on the right-hand side, as explicitly shown by Karna and Dupuis. In the SHG-case the first order equations need to be solved at frequencies 0 , ω and 2ω . The TDHF results[245, 104, 246] using the $(2n + 1)$ -theorem can directly be used in the DFT case. The only difference worth mentioning is that the exchange-correlation potential in the DFT case depends nonlinearly on the density, which is not true for the HF exchange term. This leads to certain extra terms in the DFT expressions, which do not pose computational problems however.

Both for the first and the second functional derivatives of the exchange-correlation potential, we apply the so-called Adiabatic Local Density Approximation (ALDA)[33], which is by far the most usual approximation and appears to work quite well[34, 74, 75, 77]. More details on our implementation will be presented elsewhere. Related DFT work has been done by Colwell et al.[134] for static hyperpolarizabilities, Dal Corso et al.[248] for the nonlinear optical susceptibility of a solid and Gonze[249], who reviews density-functional perturbation theory for static perturbations.

7.4 Frequency-dependent hyperpolarizability of C₆₀

We have calculated the frequency-dependent hyperpolarizability of C₆₀. Because of the icosahedral symmetry (I_h), the first order hyperpolarizability β of C₆₀ vanishes, making the second hyperpolarizability γ the first nonvanishing term after the linear polarizability. Our results for γ are obtained by analytically calculating the β tensors in a small electric field (0.001 a.u.), which leads to a negligible error. This approach enables us to restrict

ourselves to the solution of the first order response equations. However, it also implies a limitation to nonlinear optical effects in which no more than two time-varying fields appear. For this reason we can calculate the tensors $\gamma(-2\omega; \omega, \omega, 0)$, $\gamma(-\omega; \omega, 0, 0)$, $\gamma(0; \omega, -\omega, 0)$ and $\gamma(0; 0, 0, 0)$ governing Electric-Field Induced SHG (EFISH), the Electro-Optical Kerr Effect (EOKE), the Electric-Field Induced Optical Rectification (EFIOR), and the static second hyperpolarizability respectively. However, we can only make indirect statements about the tensors governing Third Harmonic Generation (THG), $\gamma(-3\omega; \omega, \omega, \omega)$, and Degenerate Four Wave Mixing (DFWM), $\gamma(-\omega; \omega, -\omega, \omega)$. These indirect statements are based upon the following dispersion formula[250, 251], which holds for small frequencies:

$$\gamma(-\omega_\sigma; \omega_1, \omega_2, \omega_3) = \gamma(0; 0, 0, 0) \left(1 + A\omega_L^2 + \dots \right), \quad (7.7)$$

where $\omega_L^2 = \omega_\sigma^2 + \omega_1^2 + \omega_2^2 + \omega_3^2$. We have determined the constant A by a fit to our EOKE and EFISH results, thus obtaining approximate results for THG and DFWM at small frequencies.

In the static case, the γ -tensor has only one independent component, γ_{zzzz} , which is equal to the average γ . Because this is still approximately true in the frequency-dependent case (Kleinman symmetry) in the off-resonant region, we have restricted our calculations to γ_{zzzz} . We performed our calculations at the Becke-Perdew optimized geometry, where the two different C—C bond lengths are 1.397Å(C=C) and 1.452Å(C—C) respectively, in very good agreement with experimental NMR data[252] of 1.40Å and 1.45Å.

We have tested that the accuracy for certain technical parameters (concerning numerical integration, convergence of the ordinary SCF and the iterative solution of the first order response equations) in the calculation is more than sufficient for our present purposes.

The basis set for our calculation consists of a valence triple zeta Slater type orbital basis set with one polarization function. In order to improve the flexibility of the basis in an economic and numerically stable way, we added several diffuse functions in the center of the molecule, describing both the regions inside and far outside the C₆₀ cage. Further improvements in the basis set will slightly increase our results, but probably not by more than 5 to 10 %.

We use both the LDA and LB94[121] exchange-correlation potentials in our calculations, using the ALDA for its derivatives. The LB94 potential substantially improves the LDA results in linear response calculations[74, 77], due to its correct Coulombic asymptotic behavior. The LDA potential decays exponentially, resulting in overestimations for polarizabilities (~5%) and hyperpolarizabilities (a factor 2 for the rare gases[72]). For this reason, we focus on the LB94 results and expect them to be lower and more reliable than our LDA results.

We fitted our linear polarizability results to the expression $\alpha(\omega) = \alpha(0) + C\omega^2$, obtaining $543.7 + 6890 \omega^2$ for LB94 and $556.7 + 7020 \omega^2$ for LDA (α and ω in a.u.). The static polarizabilities are in good agreement with previous theoretical results as gathered in Ref.[253]. Our results show a higher frequency dispersion than the TDHF values of Ref.[253], which is the usual picture, as the TDHF values tend to be too low.

The polarizability curves show the first strong pole near 3.33 eV (LB94) or 3.42 eV (LDA), close to an approximate LDA value of 3.36 eV[254] and in much better agreement with the experimental value of 3.78 eV[255] than the TDHF value[253] of 5.5 eV. This supports our confidence in the TDDFT results.

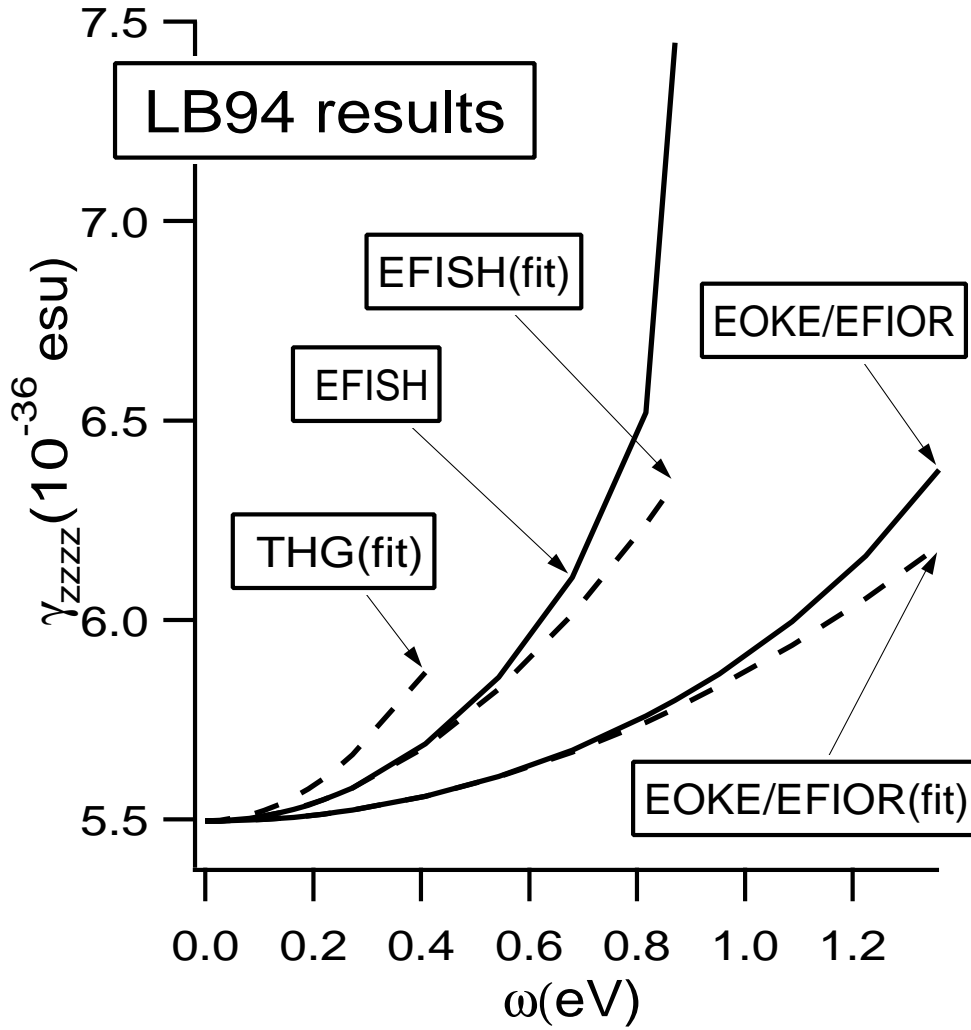


Figure 7.1: LB94 results for γ of C_{60}

The hyperpolarizability results with the LB94 potential are shown in Figure 7.1, where the EFIOR results are identical to the EOKE results. The EOKE and EFISH results at 11 frequencies from $\omega=0$ to 0.01 a.u. (0.27eV) have been fitted to Eq. (7.7). Only using frequencies up to 0.005 a.u. hardly influences the fitted value (about 1% deviation). The resulting constant A has been used to draw an estimate for the THG curve, which is reliable for small frequencies only. Both the fitted and the real curve are shown for EOKE and EFISH. They start to diverge at the point where higher order terms in ω^2 become important (in the vicinity of a pole). The EFISH curve exhibits a pole near 0.90 eV. The INDO-TDHF value of Ref.[143] is still small there, indicating a different position of the pole.

The static LB94 result is 5.50×10^{-36} esu (in the definition of γ used by experimentalists), about 34% lower than the LDA result of 7.34×10^{-36} esu. This is in good agreement with Quong and Pederson's static LDA result[142] of 7.0×10^{-36} esu. The difference between the

LDA and LB94 result shows the large influence of the asymptotic behavior of the potential on properties which depend strongly upon the density in the outer region of the molecule.

The fitted lines in Figure 7.1 correspond to a value of the constant A of (25.1 ± 0.2) a.u. [LDA yields $A = (23.0 \pm 0.2)$ a.u.]. As in the linear polarizability case, the two potentials yield similar results for the frequency dependence.

7.5 Comparison with experimental and theoretical results

Table 7.1: Experimental and theoretical results for γ of C₆₀

Method	ω (eV)	property	$\gamma(10^{-36}$ esu)
LB94 ^a	0	static	5.50
LB94 ^a	1.50	EOKE	6.69
LB94 ^a	0.65	EFISH	6.04
LDA ^a	0	static	7.34
LDA ^b	0	static	7.0
INDO-TDHF ^c	0	static	4.95
INDO-TDHF ^c	0.905	EFISH	5.49
INDO/SDCI-SOS ^d	0.65	EFISH	690
CNDO/S ^e	0.94	THG	654.8
CNDO/SCI-SOS ^f	0	static	-458
Expt., in film ^g	0.68	THG	430
Expt., in toluene ^h	0.65	EFISH	750
Expt., in benzene ⁱ	1.17	DFWM	$<60 \times \gamma(\text{benzene})$
Expt. ^j	various	Non-deg. FWM	<37

^aThis work

^bQuong and Pederson[142]

^cTalapatra et al.[143]

^dLi et al.[144]

^eHara et al.[145]

^fFanti et al.[146]

^gMeth et al.[147]

^hWang and Cheng[148]

ⁱTang et al.[149], $\gamma^{\text{LDA}}(\text{benzene}) \approx 1.85 \times 10^{-36}$ esu[142]

^jGeng and Wright[136], nondegenerate Four Wave Mixing experiment in 1,2-dichlorobenzene

Some theoretical and experimental results for the hyperpolarizability of C₆₀ have been collected in Table 7.1. Large values are obtained in the older experiments and in the semiempirical calculations. The newer experimental data give upper bounds, which are more than an order of magnitude lower. Those results are supported by static LDA values such as the one of Ref.[142]. However, very large enhancements due to frequency dispersion were found

COMPARISON WITH OTHER RESULTS 115

in terms of a simple three-level model[256], questioning the relevance of static calculations. Our results on the contrary, show that there is only a moderate frequency dispersion effect in the off-resonant region.

Geng and Wright [136] list several difficulties, circumvented in their approach, in the experimental determination of γ , such as the need to perform absolute intensity measurements. In the semiempirical sum-over-states (SOS) calculations, the results may be artificially large due to the limited number of states taken into account. A further uncertainty is the level of configuration interaction (CI) which is needed for a converged result. The singles CI approximation seems to be insufficient[145].

In our calculations, we have neglected vibrational and solvent effects, which may be important. The vibrational effects are usually small when optical fields are involved, leaving solvent effects as the probably largest source of error when comparing to experimental values. The solvent can increase both the static hyperpolarizability and its frequency dependence considerably. It will have to be considered when excellent agreement between theory and experiment is required.

On the basis of our gas phase results for γ of C_{60} , in which frequency dispersion, screening, and electron correlation effects are (approximately) taken into account, we confirm the experimental upper bounds for γ which were recently presented in the literature ¹.

S. v. G. acknowledges useful discussions with Robert van Leeuwen and financial support from the Netherlands organization for scientific research (NWO) through its foundations SON and NCF.

¹Only a few months after our work was published, a static Hartree–Fock calculation by Norman *et al.*[137] appeared in the literature. Their value of $\gamma(0; 0, 0, 0) = 9.6 \times 10^{-36}$ esu is in fairly good agreement with our values. Even more recently, a new experimental result appeared[257], which also gives a low upperbound of 9.0×10^{-35} esu for the hyperpolarizability of C_{60} , because the optical nonlinearity of C_{60} was too low to be detected. Consequently, both recent theoretical and recent experimental papers provide support for our conclusion.

Chapter 8

Density functional theory response property calculations with accurate exchange-correlation potentials

8.1 Abstract

Response calculations in the framework of time-dependent density functional theory (TDDFT) have by now been shown to surpass time-dependent Hartree–Fock (TDHF) calculations in both accuracy and efficiency. This makes TDDFT an important tool for the calculation of frequency-dependent (hyper)polarizabilities, excitation energies and related properties of medium-sized and large molecules. Two separate approximations are made in the linear DFT response calculations. The first approximation concerns the exchange-correlation (xc) potential, which determines the form of the Kohn–Sham orbitals and their one-electron energies, while the second approximation involves the so-called xc kernel f_{xc} , which determines the xc contribution to the frequency-dependent screening. By performing calculations on small systems with accurate xc potentials, constructed from *ab initio* densities, we can test the relative importance of the two approximations for different properties and systems, thus showing what kind of improvement can be expected from future, more refined, approximations to these xc functionals. We find that in most, but not all, cases, improvements to v_{xc} seem more desirable than improvements to f_{xc} .

8.2 Introduction

Several reliable quantum chemical *ab initio* methods have become available over recent years for the accurate determination of such molecular properties as excitation energies, frequency-dependent polarizabilities, and frequency-dependent hyperpolarizabilities. In particular, we mention coupled-cluster response theory [258, 259], multiconfiguration time-dependent Hartree–Fock (MCTDHF)[260], and time-dependent MP2[261, 262, 263, 244] which have, among other things, been used for the calculation of hyperpolarizabilities and excitation energies.

However, because they are computationally intensive, these methods are restricted to small or medium-sized systems. For systems where the cost of the most reliable of these *ab initio* methods becomes prohibitive, a computationally more efficient method is required, which is accurate at the same time. Density-Functional Theory (DFT) provides such a method through its time-dependent extension (TDDFT).

Almost two decades ago, Zangwill and Soven[9] were among the first to apply this theory in the linear response regime. They calculated photoabsorption cross sections of rare gases in the local density approximation (LDA). Only a few years later did the rigorous justification of their approach appear, with the work of Runge and Gross[38], who proposed a set of time-dependent Kohn–Sham (KS) equations. For a recent review of TDDFT and applications of it, the reader is referred to Ref.[33].

The first response calculations on molecules in this framework appeared only recently (after an initial attempt by Levine and Soven, [19] whose approach was based on a single-center expansion which made it impractical for general molecules). At the moment several groups have performed (molecular) response calculations using TDDFT. Calculations on frequency-dependent multipole polarizabilities[74, 35, 77, 264], excitation energies [101, 105, 127, 37, 35, 81, 86, 87, 265], frequency-dependent hyperpolarizabilities[76], Van der Waals dispersion coefficients[34, 77] and Raman scattering [75] have appeared until now. From the data in these papers it appears that the TDDFT results are usually superior to their TDHF counterparts, and in many cases competitive with correlated *ab initio* results at the TDMP2 level. At the same time, implementations of the TDDFT linear response equations using auxiliary basis functions (fit functions) [34, 81, 87] have been reported to scale as N^3 (N being the number of atoms in the calculation), which is even more favorable than the nominal N^4 scaling of TDHF. TDDFT thus surpasses TDHF both in the accuracy of the results and in the efficiency of the calculations.

Now that the usefulness of TDDFT in this regime has been firmly established and many different properties can be routinely obtained, it is of importance to know which factors restrict the accuracy of the TDDFT calculations. If an even higher quality in the results is required than is attainable with the approximations that are presently used in these calculations, it will be important to know which approximations have the largest influence on the various properties that are accessible.

Apart from practical limitations in accuracy due to the use of finite basis sets, two approximations are made in the TDDFT linear response calculations: one for the usual xc potential v_{xc} and one for the less common xc kernel f_{xc} . Our aim is to estimate the importance of the two approximations by performing calculations using accurate xc potentials constructed from essentially exact *ab initio* densities. If such a density is available, one can construct an xc potential which yields this target density, by iteratively adapting the xc potential until the target density is finally obtained within satisfactory accuracy, in a KS calculation with this potential. In this manner, the approximation for v_{xc} is basically removed. By increasing the technical accuracy of the calculations to the limit (we are referring to basis and fit set size, integration accuracy, convergence criterion for the iterative solution of the KS equations and so on), we can be sure that the bulk of the remaining deviations from the experimental values is due to deficiencies in the second approximation: the approximation to f_{xc} .

Unfortunately, the reliable xc potentials which are needed for these calculations are avail-

able for a few small systems only: the He, Be, and Ne atoms. The reason for this is that virtually all accurate densities are obtained from *ab initio* programs using Gaussian type orbitals (GTOs). Constructing an xc potential belonging to such a density leads to certain anomalies in the potential which are due to the specific properties of the GTOs. The anomalies include an incorrect asymptotic behavior and spurious oscillations in the potential[266]. The exact xc potential should asymptotically display a $-1/r$ behavior, but a Gaussian density results in a potential which diverges quadratically at infinity. Furthermore, the potential exhibits oscillations which are also due to the use of Gaussian basis functions. Although these oscillations should disappear in the basis set limit, they form a practical problem even for very large GTO basis sets.

This problem can be circumvented by using accurate densities based on Slater type orbitals (STOs) or densities which have not been expanded in a basis set at all. Such densities, however, are rare. Accurate densities based on STOs are, to the best of our knowledge, only available for Be and Ne. These densities were obtained by Bunge and Esquivel from a CI calculation using large STO basis sets [267, 268]. For He and Be, accurate xc potentials have been constructed by Umrigar and Gonze[269, 270]. They numerically generated essentially exact densities for these systems by integrating very accurate wave functions[269] (for He) or by employing various Monte Carlo techniques[270] (for Be).

For these atomic systems, we have calculated several response properties, such as static dipole and quadrupole polarizabilities, the frequency dependence of the dipole polarizability, singlet and triplet excitation energies, and oscillator strengths, using approximations of varying quality for both the xc potential and the xc kernel. This provides useful information on the appropriateness of the respective approximations for these systems.

In order to check whether or not the conclusions we draw from these atomic cases hold for molecules as well, we also consider some small molecules in the final part of the paper. Here we have to cope with the problem indicated above, that very accurate xc potentials do not exist for these systems. However, as will be explained later, we have constructed xc potentials which can be expected to improve upon existing approximate xc potentials for these systems, such as the LDA, generalized gradient approximated (GGA) and van Leeuwen–Baerends (LB94) potentials.

It can be expected that the improved potentials will yield improved results. However, the results with the usual potentials (especially the LB94 potential) are already quite satisfactory. It is therefore an open question whether much further improvement can be obtained by improving the xc potential, or that improvements to the xc kernel are more important. This is the question that will be addressed in the part of the paper dealing with the molecular case.

In the following section, the most important equations for the DFT linear response calculations will be repeated and the relevant terms and equations will be introduced. After that, the technical details of the calculations will be given as well as the indications that our basis sets are very accurate. After this, our results will be discussed. First, the atomic polarizability results are treated. Then the excitation energies are discussed and compared to similar calculations which have very recently been performed by Petersilka *et al.*[127] and by Filippi *et al.*[271]. Finally, we present our molecular results and we end with some conclusions and suggestions for future work.

8.3 Outline of the theory

DFT is based on the papers by Hohenberg and Kohn[1] and by Kohn and Sham[3]. The main result is that the density of a system is identical to the density of an associated noninteracting particle system, defined by the Kohn–Sham equations (atomic units are used throughout):

$$\left[-\frac{\nabla^2}{2} + v_s[\rho](\mathbf{r}) \right] \phi_i(\mathbf{r}) = \varepsilon_i \phi_i(\mathbf{r}). \quad (8.1)$$

Here $v_s[\rho](\mathbf{r})$ is the so-called Kohn–Sham potential, consisting of the external potential v_{ext} (the Coulomb field of the nuclei), the Hartree potential v_H , which is trivially calculated from the density, and the xc potential v_{xc} , which is the only unknown part:

$$v_s(\mathbf{r}) = v_{\text{ext}}(\mathbf{r}) + v_H(\mathbf{r}) + v_{\text{xc}}(\mathbf{r}). \quad (8.2)$$

The xc potential v_{xc} , which is the functional derivative of the xc energy functional E_{xc} with respect to the density, has to be approximated in practical calculations. The most common approximations are the LDA and GGAs, although for response calculations the use of asymptotically correct xc potentials (such as the LB94 potential[121]) seems more appropriate. The xc potential determines the Kohn–Sham orbitals ϕ_i and their one-electron energies ε_i in Eq. (8.1). It also determines the density, which is obtained from the squares of the occupied Kohn–Sham orbitals times their occupation numbers f_i :

$$\rho(\mathbf{r}) = \sum_i^{N_{\text{occ}}} f_i |\phi_i(\mathbf{r})|^2. \quad (8.3)$$

The exact xc potential, which is unique, yields the exact density of the system. This fact can be exploited to find a very accurate xc potential for systems for which a very accurate density is known. After having iteratively found the xc potential which generates the very accurate target density, one immediately obtains Kohn–Sham orbitals and one-electron energies to very good accuracy.

In the time-dependent extension of the Kohn–Sham equations, as proposed by Runge and Gross[38], a time-dependent Kohn–Sham potential $v_s(\mathbf{r}, t)$ appears:

$$\left[-\frac{\nabla^2}{2} + v_s[\rho](\mathbf{r}, t) \right] \phi_i(\mathbf{r}, t) = i \frac{\partial}{\partial t} \phi_i(\mathbf{r}, t). \quad (8.4)$$

The unknown xc part of this time-dependent Kohn–Sham potential is called the time-dependent xc potential $v_{\text{xc}}(\mathbf{r}, t)$. In linear response calculations one needs the functional derivative $f_{\text{xc}}(\mathbf{r}, \mathbf{r}', t, t')$ of this time-dependent xc potential with respect to the time-dependent density $\rho(\mathbf{r}, t)$:

$$f_{\text{xc}}(\mathbf{r}, \mathbf{r}', t, t') = \frac{\delta v_{\text{xc}}(\mathbf{r}, t)}{\delta \rho(\mathbf{r}', t')}, \quad (8.5)$$

which, as it depends on $t - t'$ only, can be Fourier transformed to $f_{\text{xc}}(\mathbf{r}, \mathbf{r}', \omega)$. This functional derivative f_{xc} is called the xc kernel and constitutes the second xc functional for which

approximations have to be made in DFT response calculations. In nonlinear response calculations, higher functional derivatives of $v_{xc}(\mathbf{r}, t)$ are needed as well [33, 76, 134], but usually these do not affect the results very much[272]. In this paper, we restrict ourselves to the linear response case.

As f_{xc} is a function of two spatial variables and one frequency variable, it is rather complicated. However, the most usual and simplest approximation to it, the adiabatic LDA (ALDA), provides a very simple functional form for the xc kernel, by taking the derivative of the time-independent LDA expression for v_{xc} with respect to the density:

$$f_{xc}^{\text{ALDA}}(\mathbf{r}, \mathbf{r}', \omega) = \delta(\mathbf{r} - \mathbf{r}') \frac{d^2}{d\rho^2} \left[\rho \varepsilon_{xc}^{\text{hom}}(\rho) \right] \Big|_{\rho=\rho_0(\mathbf{r})}, \quad (8.6)$$

where $\varepsilon_{xc}^{\text{hom}}$ is the xc energy density of the homogeneous electron gas in the Vosko–Wilk–Nusair (VWN) approximation[4]. Evidently, this is a rough approximation to the exact f_{xc} as the frequency dependence is totally ignored (the adiabatic approximation assumes systems which are slowly varying in time), as is the spatial nonlocality of the kernel.

More refined approximations for the xc kernel are available. Petersilka and coworkers have introduced the time-dependent optimized effective potential (TDOEP) expression for the exchange part of the xc kernel[101, 105]. In spin-unrestricted form, it is given by[101, 127]:

$$f_{x\sigma\sigma'}^{\text{TDOEP}}(\mathbf{r}, \mathbf{r}', t, t') = -\delta(t - t') \delta_{\sigma\sigma'} \frac{|\sum_k f_{k\sigma} \phi_{k\sigma}(\mathbf{r}) \phi_{k\sigma}^*(\mathbf{r}')|^2}{|\mathbf{r} - \mathbf{r}'| n_{0\sigma}(\mathbf{r}) n_{0\sigma}(\mathbf{r}')}, \quad (8.7)$$

where $f_{k\sigma}$ is the occupation number of the KS spin orbital $\phi_{k\sigma}$ and where $n_{0\sigma}$ is the ground-state number density of the spin σ electrons. Although at present their expression still ignores the frequency dependence of f_{xc} , which is hard to model, their result should be very close to the exact exchange-only expression for the xc kernel in the limit $\omega \rightarrow 0$. A frequency-dependent extension of the ALDA expression has been provided by Gross and Kohn[160, 205, 206, 31]. In this work, we will be using the ALDA expression for f_{xc} and its exchange-only counterpart.

In a linear response calculation, we want to find the density change $\delta\rho(\mathbf{r}, \omega)$ which is induced by a frequency-dependent external electric field $\delta v_{\text{ext}}(\mathbf{r}, \omega)$. In time-dependent density-functional linear response theory, the density change does not depend on the external potential alone, but also on the potential which is induced by the density change through screening effects. The density change thus reacts to an *effective* potential δv_{eff} through the independent-particle linear response equation:

$$\delta\rho(\mathbf{r}, \omega) = \int d\mathbf{r}' \chi_s(\mathbf{r}, \mathbf{r}', \omega) \delta v_{\text{eff}}(\mathbf{r}', \omega). \quad (8.8)$$

Here, χ_s is the single-particle Kohn–Sham response function, constructed from occupied and virtual Kohn–Sham orbitals and one-electron energies[31, 34]. This means that the exact xc potential will lead to the exact χ_s . The effective potential consists of the external potential δv_{ext} and two parts which depend upon the induced density $\delta\rho(\mathbf{r}, \omega)$: the Coulomb or Hartree term and the xc term:

$$\delta v_{\text{eff}}(\mathbf{r}, \omega) = \delta v_{\text{ext}}(\mathbf{r}, \omega) + \int d\mathbf{r}' \frac{\delta\rho(\mathbf{r}', \omega)}{|\mathbf{r} - \mathbf{r}'|} + \delta v_{xc}(\mathbf{r}, \omega). \quad (8.9)$$

This implies that, if an exact xc potential is available, the only remaining unknown in Eq. (8.9) is the xc part to the screening, δv_{xc} . This xc part is given in terms of the Fourier transform of the xc kernel f_{xc} of Eq. (8.5):

$$\delta v_{xc}(\mathbf{r}, \omega) = \int d\mathbf{r}' f_{xc}(\mathbf{r}, \mathbf{r}', \omega) \delta \rho(\mathbf{r}', \omega). \quad (8.10)$$

An important advantage of the ALDA in practical applications, is that the evaluation of δv_{xc} in the integration points becomes a trivial multiplication of f_{xc} and $\delta \rho$, due to the delta function appearing in Eq. (8.6). For nonlocal kernels, such as the TDOEP kernel of Eq. (8.7), the evaluation of δv_{xc} in all integration points becomes an expensive computational task.

Equations (8.8,8.9,8.10) are solved self-consistently in an iterative fashion, starting from the uncoupled approximation ($\delta v_{\text{eff}} = \delta v_{\text{ext}}$) in Eq. (8.9). The induced density immediately yields the frequency-dependent polarizability tensor $\alpha_{ij}(\omega)$ [31, 30, 34] for a density change $\delta \rho_i(\mathbf{r}, \omega)$ due to an external potential $\delta v_{\text{ext}}(\mathbf{r}, \omega) = \mathbf{r}_i \cos(\omega t)$:

$$\alpha_{ij}(\omega) = -2 \int d\mathbf{r} \delta \rho_i(\mathbf{r}, \omega) r_j, \quad (8.11)$$

where i and j denote the Cartesian directions x, y, z . We remark that in the actual implementation the polarizability is obtained as the trace of a matrix product of the first order density matrix and the dipole moment matrix, which is equivalent to the integration in this equation.

By considering different multipole external electric fields, all multipole polarizabilities can be obtained. The excitation energies and oscillator strengths presented in this work[265] have been obtained along the lines of References[37, 35], using the same auxiliary basis functions techniques as in Reference [34].

The singlet excitation energies and oscillator strengths obtained in this manner are directly related to the frequency-dependent polarizability $\alpha(\omega)$ by the relation:

$$\alpha_{\text{av}}(\omega) = \sum_i \frac{f_i}{\omega_i^2 - \omega^2}, \quad (8.12)$$

where f_i are the oscillator strengths and ω_i the excitation energies, and where the average polarizability α_{av} is equal to $(\alpha_{xx} + \alpha_{yy} + \alpha_{zz})/3$. The frequency dependence of this average polarizability is often expressed in terms of the Cauchy coefficients S_i :

$$\alpha_{\text{av}}(\omega) = \sum_{k=1}^{\infty} S_{-2k} \omega^{2(k-1)}. \quad (8.13)$$

The Cauchy coefficients can be obtained from the excitation energies and oscillator strengths by the relation[35]:

$$S_{-2k} = \sum_i \omega_i^{-2k} f_i. \quad (8.14)$$

In the basis set limit, the Cauchy coefficient S_0 should be equal to the number of electrons. The coefficient S_{-2} is equal to the average static polarizability, as can be seen by substituting $\omega = 0$ in Eq. (8.13).

In this work, we will approximate the screening part of $\delta v_{\text{eff}}(\mathbf{r}, \omega)$ in different ways. The approximation $\delta v_{\text{eff}} = \delta v_{\text{ext}}$ is called the uncoupled approximation, as screening is fully ignored. Taking into account Coulomb screening only, is equivalent to the approximation $f_{\text{xc}} = 0$. The results arising from this approximation will be denoted by "Coulomb" in the tables. The main part of the xc screening comes from the exchange part as could be expected. This will be shown by calculations in which we take $f_{\text{c}} = 0$, effectively using an $X\alpha$ form for f_{xc} , with α equal to 2/3. This approximation will be denoted by "Coulomb + f_{x} " in the tables. The fully coupled results refer to the ALDA with the Vosko–Wilk–Nusair approximation to ε_{xc} [4]. They will be denoted by either "ALDA" or "Coulomb + f_{xc} ".

8.4 Computational details

The Amsterdam density-functional program (ADF)[89, 90, 91] has been used for all calculations. The distinctive features of this program include the use of Slater type orbitals (STOs), a well-balanced numerical integration scheme[90], a density fitting procedure for the Coulomb-type integrals using auxiliary basis functions (fit functions)[89], and a fully vectorized and parallelized code in combination with the use of symmetry [91]. The same features hold for the extension of ADF by which the response properties have been calculated[88].

8.4.1 Atomic calculations

In the atomic calculations on He, Be, and Ne, our goal has been to provide benchmark quality results with essentially exact xc potentials. For this reason we have tried to perform the calculations as accurately as possible. We included all electrons in the solution of the Kohn–Sham and the response equations. In other words, we did not use a frozen core approximation. The numerical integration accuracy was such that twelve significant digits were demanded for a representative set of test integrals (by default four significant digits are demanded). The convergence criterion in the self-consistent procedure for the solution of the Kohn–Sham equations was set to 10^{-12} (default value 10^{-6}).

We have tried to reach the basis set limit by constructing large even-tempered STO basis sets. The final results and error margins have been obtained by comparing results from various basis sets of (very) high quality. The basis sets consist of several hundreds s, p, d, and f functions (higher angular momentum values are not available yet in ADF, but they are not needed in our present calculations) with both very diffuse and very contracted functions.

A typical basis set consists of 19 s functions, 20 p functions, 21 d functions, and 21 f functions, giving a total of 331 primitive basis functions. The most contracted functions of each type are a 1s function with exponent 20, a 2p function with exponent 20, a 3d function with exponent 40 and a 4f function with exponent 60. The most diffuse functions are 6s, 6p, 6d and 6f functions with exponents of 0.17 for one particular basis set. In other basis sets even more diffuse functions have been used, without significant change in the results.

The fit sets with s, p, d, f, and g functions have also been constructed in an even-tempered fashion, the most diffuse fit function being adapted to the most diffuse product of basis functions and the most contracted fit function adapted to the product of the most contracted basis functions. With these fit sets, which are clearly larger than the associated

basis sets, typical fit errors (defined as the integral over all space of the squared difference between the exact and fitted converged SCF densities) of only 10^{-7} occurred. The most contracted fit functions possessed the smallest possible n value, while the most diffuse fit functions had an n value of 10 for all l values. The basis and fit sets are available for the interested reader[273].

For Helium and Beryllium the accuracy of our basis sets was confirmed by the fact that they reproduced the one-electron energies of References [127] and [271, 113] to all presented digits. For Neon we have adopted the same basis sets. The accuracy of the basis sets is further supported by the values for the Cauchy moment S_0 of Eq. (8.13) which we obtained. In the basis set limit, the value of S_0 (which is equal to the sum of the oscillator strengths) should equal the number of electrons. Typical deviations with our present basis sets are merely 10^{-3} to 10^{-6} , while for the largest basis sets in the ADF database, these errors are in the order of 0.1 to 1.

The accurate potentials were used in the following way. We used linear interpolation on the available accurate xc potential data, as provided by Umrigar and Gonze[269, 270], in order to find the values of these potentials in the integration points generated by ADF. Afterwards, the Kohn–Sham equations were solved in these fixed xc potentials. As the number of points in which the accurate xc potentials were generated by Umrigar and Gonze is very large, the linear interpolation scheme will not influence our results by a significant amount. This is clear from the fact that we retrieve the KS orbital energies obtained by Savin *et al.*[113].

For the Neon atom, there is no v_{xc} potential available of comparable accuracy. We have generated one from the STO CI density of Bunge and Esquivel[268]. This STO density is not sufficiently accurate in the outer region in order to allow for a straightforward determination of the xc potential in the whole \mathbf{r} range. In the iterative procedure to determine the potential (the accurate updating procedure of Schipper *et al.*[266]), the potential was fixed in the outer region of the atom for this reason, in order to obtain the correct asymptotic $-1/r$ behavior. The potential was constructed in such a way that it reached the $-1/r$ behavior at a certain cutoff point, beyond which the potential was taken identical to $-1/r$. The cutoff point was chosen in such a way that the orbital energy of the highest occupied KS orbital was very close to the experimental ionization energy (0.792 hartree). The resulting cutoff point was 6.72 au. Consequently, the accurate xc potential for Ne may be somewhat less accurate than the xc potentials for He and Be.

8.4.2 Molecular calculations

We have constructed molecular xc potentials which possess some important features which are typical of the exact xc potential and which recover our target Gaussian multireference configuration interaction (MRCI) density to reasonable accuracy. By construction, the potentials generated in our procedure will be smooth, possess the correct asymptotic $-1/r$ behavior, yield the experimental ionization potential for the highest occupied Kohn–Sham orbital and are required to recover the MRCI density to reasonable accuracy. This final requirement ensures that the intershell peaks, exhibited by the exact xc potential, are present in our constructed potential as well.

The Hartree–Fock and subsequent direct (multireference) CI calculations, at the single-double excitation level, were performed with the ATMOL[274] package. The correlation energy which was recovered was 98% for H₂, 90% for HF, 82% for N₂, and typically around 75 to 80% for the other molecules, when compared to the semiempirical correlation energy estimates of Savin *et al.*[275].

Correlation-consistent GTO basis sets of at least valence triple zeta quality were used, to which sets of diffuse functions were added. The basis set sizes were different depending on the molecule. Our aim was to take a reliable correlation-consistent basis set including diffuse functions. Typically, we took Woon and Dunning’s[276] doubly or in most cases triply augmented correlation-consistent (cc) valence triple zeta (pVTZ) basis sets denoted by d-aug-cc-pVTZ or t-aug-cc-pVTZ. We have also performed calculations with correlation-consistent quadruple zeta basis sets to which we added some diffuse functions ourselves. The total number of GTOs was typically between 100 and 150.

We have further used the straightforward scheme of Reference [121], for updating the xc potential until the density resulting from the KS calculation with that xc potential was sufficiently close to the target CI density. We used an asymptotically correct initial guess for the xc potential of the form

$$v_{xc}(\mathbf{r}) = v_{X\alpha}(\mathbf{r}) + 2\varepsilon_c^{\text{VWN}}(\mathbf{r}) + 2\varepsilon_x^{\text{Becke}}(\mathbf{r}), \quad (8.15)$$

consisting of the $X\alpha$ -potential, the Vosko–Wilk–Nusair parametrization of the LDA correlation energy density, and the Becke energy functional for the correction to the $X\alpha$ exchange. This last term ensures the correct asymptotic $-1/r$ behavior. This initial guess has been successfully employed several times before[188].

Because of the known problems[266] which arise, in case of a Gaussian CI density, if the potential is converged completely (such as spurious oscillations and incorrect asymptotic behavior), the updating scheme was changed in such a fashion that the outer region of the potential was left virtually unchanged[188], so as to retain its asymptotically correct behavior. The updating scheme slowly converges to the (undesirable) exact xc potential. After a hundred cycles, the integrated absolute density error with respect to the CI density, as defined in Reference [266], has typically dropped to a satisfactory 10^{-2} or 10^{-3} . Further convergence hardly improves this difference, but it does introduce the spurious oscillations mentioned before. For this reason we used, as recommended[266], the potentials which appeared after a hundred cycles. The parameter α of the starting $X\alpha$ potential was chosen such that the eigenvalue of the highest occupied Kohn–Sham orbital $\varepsilon^{\text{HOMO}}$, belonging to the final potential, equals minus the ionization potential, as it should.

The potentials, which have all been constructed in this manner, can certainly not be called exact, and our method of construction severely restricts the freedom of the potential. For example, the distance at which the potential gets close to the $-1/r$ behavior is predominantly determined by the start-up potential. However, our results did not change very much if another start-up potential with correct asymptotic behavior was used. On the other hand, if the α parameter in the start-up potential was not adapted in order to obtain the experimental ionization potential, relatively poor results were obtained.

Although the potentials will not be the exact ones, which belong to the exact (not the GTO-CI) correlated densities, there are good reasons to assume that the constructed poten-

tials improve upon the xc potentials which were used in previous DFT response calculations, such as the usual potentials belonging to the LDA or GGAs or the asymptotically correct Van Leeuwen–Baerends potential[121] (LB94). These potentials all exhibit one or several distinct weaknesses, such as the faster than Coulombic decay of the potential in the outer region (LDA and GGAs), inferior values for the highest occupied Kohn–Sham orbital which should equal minus the experimental ionization energy (LDA and GGAs), poor description or absence of the intershell peaks (LDA, GGAs and LB94) and poor description of the inner region of the atoms in the molecule (LB94).

8.5 Results and discussion

8.5.1 Atomic results, polarizabilities

Table 8.1: Dipole and quadrupole polarizabilities of Helium, Beryllium and Neon with various xc potentials using the ALDA for f_{xc} .

Polarizability	Atom	LDA ^a	LB94 ^b	Accurate v_{xc} ^c	Literature
dipole	He	1.6576	1.3896	1.3824	1.3832 ^d
	Be	43.79±0.02	42.87±0.01	39.57±0.01	37.73±0.05 ^e
	Ne	3.049±0.003	2.590	(2.657)	2.670 ^f
quadrupole	He	3.576	2.561	2.538	2.4451 ^d
	Be	369.9±0.5	342.4±0.5	300.4±0.5	298.8 ^g ; 298.8±2.6 ^h
	Ne	9.66±0.02	7.26±0.03	(7.52±0.02)	7.52 ⁱ ; (7.33 ^j)

^aThe VWN[4] parametrization is used.

^bThe Van Leeuwen–Baerends model potential[121].

^cAccurate xc potential due to Umrigar and Gonze[269]; for Ne, the potential constructed from the Bunge–Esquivel STO CI density was used (see text).

^dBenchmark *ab initio* calculation using explicitly correlated wave functions [151].

^eRecent basis set limit result obtained with the explicitly correlated coupled-cluster method[277].

^fValue obtained by comparison of many experimental data[168].

^gcoupled-cluster double-excitation value with fourth-order contribution from singlet and triplet excitations [278].

^hFourth-order Møller-Plesset perturbation theory value[279]

ⁱcoupled-cluster singles doubles value, with an approximate triples contribution [CCSD(T)][199]

^jsecond-order many-body perturbation theory value [174].

In Table 8.1, the dipole and quadrupole polarizabilities are presented for the three atoms which are studied here. The results for He and Ne with the LDA and LB94 potentials are somewhat more accurate than our previous results[34, 74] due to the removal of the frozen core approximation for Ne and the improvements in the basis sets. As expected,

this has led to slightly higher values for the polarizabilities. The LDA dipole polarizabilities of He and Ne are now in perfect agreement with the numerical results reported in Table 4.4 of Reference [30], showing that our results are very close to the basis set limit. The quadrupole polarizability results are not identical to those obtained by Mahan[68], because the Gunnarsson–Lundqvist parametrization[170] for v_{xc} was used in that work.

It has been emphasized several times[152, 74] that the usual xc potentials, such as the LDA potential, overestimate the polarizabilities due to their incorrect asymptotic behavior. This is obvious in Table 8.1. The LDA dipole polarizabilities are too high by 19.8%, 16.1%, and 14.2% respectively, while the LDA quadrupole polarizabilities are too high by 46.3%, 23.8% and 28.3%. The asymptotically correct LB94 potential already improves considerably upon this. The errors for this potential are +0.46%, +13.6% and -3.0% for the dipole polarizabilities. For the quadrupole polarizabilities, the numbers are +4.7%, +14.6% and -3.2% . The accurate xc potential improves upon the LDA and LB94 results in all six cases. For the dipole polarizabilities, the errors are -0.06% , +4.9% and -0.5% , while the quadrupole polarizability errors are +3.80%, +0.54%, and 0.0%, respectively.

In order to investigate how sensitive these properties are with respect to small changes in the xc potential, we have repeated the Be calculations not with the Umrigar–Gonze potential, but with another accurate xc potential, constructed from the Esquivel–Bunge CI STO density[267], in the same way as we construct our Ne potential from an STO CI density by Bunge and Esquivel[268].

The xc potential for Be by Umrigar and Gonze[269] should be considered more reliable than the present one, but these test calculations give an indication of how much our Neon results may still differ from results with the truly exact xc potential. We find a dipole polarizability of 40.01 ± 0.01 (instead of 39.57 with the Umrigar–Gonze potential) and a quadrupole polarizability of 309.2 ± 0.2 (instead of 300.4) with the xc potential constructed from the Esquivel–Bunge density for Be. The differences with respect to the results with the accurate potential by Umrigar and Gonze are considerable. For this reason we have given the Ne results in parentheses in Table 8.1, although we expect the results with the Bunge–Esquivel density for the rare gas Ne to be more reliable than those for Be.

The average absolute error for all six numbers in Table 8.1 is reduced by roughly a factor of four by going from the LDA potential to the LB94 potential. The average absolute error with the accurate xc potential is again a factor of four smaller than the average absolute LB94 error, and a factor of fifteen smaller than the LDA error. For these atomic polarizabilities it is consequently clear that improvements to the xc potential will yield the bulk of the improvement which can be obtained. The remaining errors have to be due to deficiencies in the xc kernel f_{xc} . As we are considering static polarizabilities, these deficiencies relate to the spatial variables, not to the frequency dependence.

In four cases out of six, the accurate xc potential results for the polarizabilities of these atoms can be called excellent. The errors for the quadrupole polarizability of He(+3.8%) and the dipole polarizability of Be(+4.9%) are however still substantial. Upon closer analysis, the dipole polarizability of Be appears to depend strongly on the description of the $2s \rightarrow 2p$ transition (the reason for the different dipole polarizability obtained with the Esquivel–Bunge density is also that this transition is differently described). For this analysis, it is useful to look at Eq. (8.12), which expresses the polarizability in terms of the oscillator

strengths f_i and the excitation energies ω_i . Using this equation for the present static case ($\omega=0$), we find that about 95% of the polarizability of Be is due to the (singlet) $2s \rightarrow 2p$ transition. For this transition, we obtained an oscillator strength of 1.339 au (having taken the degeneracy of the p-orbitals into account) and an excitation energy of 0.1868 hartree, as will be shown in one of the following tables. The experimental value for the excitation energy is 0.1939 hartree. Our excitation energy with the accurate xc potential is consequently too low by 3.7%. This should lead to an overestimation in the contribution of the $2s \rightarrow 2p$ transition to the polarizability of no less than 7.7%. Apparently, the oscillator strength for this transition is underestimated, leading to a fortuitous cancellation of errors. In short, the error in the predicted dipole polarizability of Beryllium, obtained with the accurate xc potential, can be fully explained from the inability of the ALDA xc kernel to describe the $2s \rightarrow 2p$ transition with sufficient accuracy. In passing, we note that the $2s \rightarrow 2p$ transition in Be is the only atomic transition we consider, which is close in energy to excitation energies normally encountered in molecules.

Table 8.2: Dipole and quadrupole polarizabilities of Helium, Beryllium and Neon with various xc kernels using the accurate xc potential.

Polarizability	Atom	uncoupled	Coulomb	Coul.+ f_x	Coul.+ f_{xc}	Literature
dipole	He	1.5158	1.2231	1.3665	1.3824	1.3832[151]
	Be	73.98	29.36	37.99	39.57	37.73 \pm 0.05[277]
	Ne	3.063	2.417	2.632	2.657	2.67[168]
quadrupole	He	2.452	2.385	2.518	2.538	2.4451[151]
	Be	283.7	251.8	291.5	300.4	298.8 \pm 2.6[279]
	Ne	7.39	6.98	7.45	7.52	7.52[199]

In Table 8.2, the importance of the various contributions to the screening is tabulated. As explained in the introductory section, the "uncoupled" results refer to a total neglect of screening, which is equivalent to the approximation $\delta v_{\text{eff}} = \delta v_{\text{ext}}$ in Eq. (8.9). The uncoupled results for the dipole polarizability are far too large in all three cases (this is also the usual case in molecular dipole polarizability calculations), while the uncoupled quadrupole polarizabilities are much closer to the experimental values. Interestingly, the uncoupled quadrupole polarizabilities are too low for Be and Ne and slightly too high for He.

In agreement with Reference [35], we find that the inclusion of the Coulomb screening in the second column (this is the approximation $f_{xc} = 0$) substantially reduces all the uncoupled polarizabilities and leads to too low values with respect to experiment in all six cases. In the column denoted by "Coulomb + f_x ", the exchange part of the screening is included, using the Vosko–Wilk–Nusair (VWN) exchange functional (which is equivalent to the $X\alpha$ parametrization with $\alpha = 2/3$). It is clear from the table that the exchange part constitutes the major part of the xc screening, as could be expected.

Finally, in the last two columns we have copied the fully coupled (both exchange and correlation screening included in the xc kernel) and experimental/*ab initio* values from Table 8.1, for ease of comparison. The inclusion of the correlation part of the screening substantially reduces the errors in four cases out of six. In the other two cases (those with the largest deviations with respect to the benchmark values) the results get somewhat worse.

In the rest of this work, it will be shown that the fully coupled calculations for the excitation energies of Helium hardly differ from the uncoupled values (the differences between occupied and virtual KS orbital energies), which are already excellent. In view of this fact, it may be somewhat surprising that the fully coupled (both Coulomb and xc screening taken into account) result for the static dipole polarizability of Helium is considerably better than the uncoupled value. This must of course be due to the improved results for the oscillator strengths which appear in Eq. (8.12).

Table 8.3: Helium oscillator strengths.

Transition	Exact ^a	ALDA ^b
1s \rightarrow 2p	0.27616	0.283 (+2.5%)
1s \rightarrow 3p	0.07343	0.0698 (-4.9%)
1s \rightarrow 4p	0.02986	0.0282 (-5.5%)
1s \rightarrow 5p	0.01504	0.0142 (-5.5%)
1s \rightarrow 6p	0.00863	0.0082 (-5.0%)

^aAccurate nonrelativistic theoretical calculations[280, 281].

^bResults with accurate xc potential and ALDA for f_{xc} .

In Table 8.3, these fully coupled oscillator strengths for He, calculated with the accurate xc potential, are compared to the literature values. Here, it becomes clear that the excellent result for the static dipole polarizability of Helium, does not hold for the individual oscillator strengths. The contribution of the 1s \rightarrow 2p transition to the dipole polarizability, using our ALDA values for the oscillator strength and the excitation energy in Eq. (8.12), is 0.471 au. The literature values for the excitation energy and the oscillator strength yield a contribution of only 0.454 au. This is counterbalanced by the other oscillator strengths, which are a bit too low. We note however, that only the exact frequency-dependent xc kernel can be expected to give the individual oscillator strengths and excitation energies correctly.

Because the static dipole polarizability of He comes out so nicely with the accurate xc potential, it is interesting to see if this remains so in the frequency-dependent case. In the static polarizability calculations, the spatial part of the xc kernel is tested. In a frequency-dependent run, one also tests the frequency dependence of this kernel. In other words, one tests how well the adiabatic approximation holds when the frequency of the external field approaches the first excitation energy with nonvanishing oscillator strength.

Our results for the frequency dependence of the dipole polarizability of He are gathered in Table 8.4, as well as in Figure 8.1. The LDA results are far too large and increase too sharply with increasing frequency. This is of course related to the position of the first pole, which appears much too early with the LDA potential. The LB94 results are already much better, but the results with the accurate xc potential are closest to the benchmark results (taken from highly accurate *ab initio* calculations with explicitly correlated wave functions[151]). This holds both for the results with the full ALDA and with the exchange-only ($X\alpha$) approximation for f_{xc} . However, the figure shows that it is not possible to ignore the xc screening altogether, as the accurate v_{xc} /Coulomb curve is quite poor. This was to be expected in view of the poor corresponding static result in Table 8.2. So it appears that

Table 8.4: Frequency dependence of the dipole polarizability of Helium with various xc potentials

Freq. (hartree)	Exact ^a	Acc/ALDA ^b	Acc/x-only ^c	Acc/Coulomb ^d	LDA ^e	LB94 ^f
0	1.383	1.382	1.366	1.223	1.658	1.390
0.1	1.399	1.398	1.382	1.236	1.682	1.406
0.2	1.448	1.448	1.431	1.276	1.763	1.456
0.3	1.541	1.542	1.522	1.350	1.921	1.551
0.4	1.698	1.701	1.677	1.475	2.219	1.713
0.5	1.970	1.979	1.946	1.686	2.883	1.996
0.6	2.508	2.537	2.480	2.090	pole ^g	2.571
0.7	4.116	4.286	4.114	3.192	pole	4.490

^aBenchmark *ab initio* calculation using explicitly correlated wave functions[151].

^bResults with accurate xc potential due to Umrigar and Gonze[269] with ALDA approximation for f_{xc} .

^cResults with accurate xc potential due to Umrigar and Gonze[269] with exchange-only ($X\alpha$) approximation for f_{xc} .

^dResults with accurate xc potential due to Umrigar and Gonze[269] with approximation $f_{xc} = 0$.

^eThe VWN parametrization is used[4].

^fVan Leeuwen–Baerends potential[121].

^gFor LDA, the first pole appears before 0.6 hartree.

both an accurate v_{xc} and a reasonable approximation for f_{xc} are needed for reliable results here.

For the accurate v_{xc} /ALDA results, the deviation in the frequency range of 0 to 0.3 hartree is less than 0.1% from the literature values. For higher frequencies, the deviations are not negligible anymore. At 0.7 hartree, in the neighborhood of the pole, the accurate v_{xc} /ALDA result overshoots by 4%. Interestingly, in this region the accurate v_{xc} /exchange-only f_{xc} are the best, in contrast to the situation at zero frequency.

One might be tempted to blame this solely on the adiabatic approximation (the neglect of frequency dependence in the xc kernel), which is supposed to break down in the vicinity of a pole. This breakdown is due to the fact that the position of this pole, which determines the polarizability in the frequency region near that pole, is only given correctly by the exact frequency-dependent xc kernel. The exact static xc kernel will give a different position of the first pole, with large effects for the frequency-dependent polarizability near the pole, as is clear from Eq. (8.12). However, this question cannot be answered unless one would know the polarizability result with the (unknown) exact static f_{xc} . This result should be equal to the experimental number at $\omega = 0$, but will differ from the ALDA result at finite frequencies, in case this static result is obtained from different values for the oscillator strengths and excitation energies (especially those belonging to the first pole). If one recalculates the polarizability with the experimental values for the excitation energy and oscillator strength of the $1s \rightarrow 2p$ transition, the result is even somewhat below the exact literature value at

$\omega = 0.7$ hartree (4.07 au). The overestimated value for the oscillator strength and the underestimated value for the first excitation energy are responsible for the overestimated polarizability at larger frequencies in roughly equal amounts.

We have checked whether the curve with the accurate xc potential improves if one employs Gross and Kohn's frequency-dependent xc kernel[160, 205, 206, 31], instead of the ALDA f_{xc} . This is not the case. The Gross–Kohn (GK) kernel indeed lowers the frequency dependence, but the correction is far too large, resulting in a curve which is too low in the whole frequency range (1.49 au at 0.3 hartree and 2.31 au at 0.6 hartree). Furthermore, an unphysical anomalous frequency dispersion appears in the very low frequency region. This behavior can be understood from the frequency dependence of the real part of the GK kernel. If the frequency becomes larger than zero, the absolute value of the real part of the GK kernel decreases. The xc screening is reduced in this way. The magnifying effect of this screening (see the results of Table 8.2) on the polarizability also reduces, leading to a polarizability which *decreases* with increasing frequency (for very small frequencies).

For the Cauchy coefficient S_{-4} , which describes the frequency dependence of the dipole polarizability in the low frequency region, we obtain 1.554 ± 0.001 with the accurate xc potential. A fit to the literature data[151] yields a value of 1.54 ± 0.01 . Apparently the fit to the experimental data[168], resulting in a value of 1.60, in Reference [72] overestimates the frequency dependence of the dipole polarizability in the low frequency region somewhat.

The LDA and LB94 results for this coefficient are 2.432 ± 0.001 and 1.573 ± 0.001 , respectively. For the coefficient S_{-6} we obtain LDA and LB94 results of 4.462 ± 0.002 and 2.127 ± 0.002 respectively. The accurate potential yields 2.086 for S_{-6} . For the higher Cauchy coefficients, the importance of the first transition with nonvanishing oscillator strength increases, as can be seen from Eq. (8.14). In view of the overestimated oscillator strength and underestimated excitation energy for this transition with the accurate xc potential, the S_{-4} and S_{-6} can be expected to be somewhat too large.

For the Cauchy coefficients of Be, we find 1.35×10^3 , 1.36×10^3 and 1.105×10^3 for S_{-4} using the LDA, LB94 and accurate xc potentials respectively. The numbers for the S_{-6} coefficient are 4.26×10^4 , 4.43×10^4 , 3.155×10^4 . These results, even those from the accurate potential, are too large because of the inaccurate description of the $2s \rightarrow 2p$ transition. A correction on these values, based upon the coupled-cluster value of the static polarizability of 37.73, and the experimental excitation energy, would yield (semiempirical) estimates of $(1.0 \pm 0.1) \times 10^3$ and $(2.6 \pm 0.2) \times 10^4$ for S_{-4} and S_{-6} , respectively.

8.5.2 Atomic results, excitation energies of Helium

In this section we discuss our results for the excitation energies. Recently, Savin, Umrigar, and Gonze have shown[113] that the exact Kohn–Sham one-electron energy differences between the highest occupied Kohn–Sham orbital and virtual orbitals provide quite satisfactory approximations to excitation energies for Helium and Beryllium. The orbital energy differences lie between the experimental singlet and triplet excitation energies, almost without exception.

Going beyond this, Filippi, Umrigar and Gonze[271] calculated excitation energies using two perturbative schemes. One of these first-order perturbative schemes, based upon Görling

and Levy's adiabatic connection approach[282, 283], improves upon the orbital energy difference approximation to the excitation energies. We have included these results in the tables. The other results obtained by Filippi *et al.* are based on ordinary perturbation theory and provide no improvement over the Kohn–Sham orbital energy differences. These results will not be discussed here.

Petersilka, Gossmann, and Gross[127] have recently calculated excitation energies for Helium with Umrigar and Gonze's accurate xc potential[269], using the TDDFT approach. They present numerical results using the ALDA and TDOEP xc kernels, both in their single-pole approximation (SPA) and by diagonalizing a matrix containing contributions from as many bound Kohn–Sham orbitals as were needed for converged results. For ease of reference we repeat their equations[127] for the SPA excitation energies here, for an excitation from occupied orbital ϕ_i to virtual orbital ϕ_a :

$$\begin{aligned}\omega_{\text{sing}} &= (\varepsilon_a - \varepsilon_i) + 2\text{Re} \int d^3\mathbf{r} \int d^3\mathbf{r}' \phi_i^*(\mathbf{r}) \phi_a^*(\mathbf{r}) \\ &\times \left(\frac{1}{|\mathbf{r} - \mathbf{r}'|} + \frac{1}{4} [f_{xc}^{\uparrow\uparrow} + f_{xc}^{\uparrow\downarrow} + f_{xc}^{\downarrow\uparrow} + f_{xc}^{\downarrow\downarrow}] \right) \phi_i(\mathbf{r}') \phi_a(\mathbf{r}'), \\ \omega_{\text{trip}} &= (\varepsilon_a - \varepsilon_i) + 2\text{Re} \int d^3\mathbf{r} \int d^3\mathbf{r}' \phi_i^*(\mathbf{r}) \phi_a^*(\mathbf{r}) \left(\frac{1}{4} [f_{xc}^{\uparrow\uparrow} - f_{xc}^{\uparrow\downarrow} - f_{xc}^{\downarrow\uparrow} + f_{xc}^{\downarrow\downarrow}] \right) \phi_i(\mathbf{r}') \phi_a(\mathbf{r}'),\end{aligned}$$

where ε_i and ε_a are KS orbital energies and where $f_{xc}^{\sigma\sigma'}$ is a shorthand notation for $f_{xc}^{\sigma\sigma'}(\mathbf{r}, \mathbf{r}', \omega_0)$, which is the Fourier transform of the functional derivative

$$f_{xc}^{\sigma\sigma'}(\mathbf{r}, t, \mathbf{r}', t') = \frac{\delta v_{xc}^\sigma(\mathbf{r}, t)}{\delta \rho^{\sigma'}(\mathbf{r}', t')}. \quad (8.16)$$

Combining these expressions yields the SPA expression for the singlet-triplet splitting

$$\omega_{\text{sing}} - \omega_{\text{trip}} = \text{Re} \int d^3\mathbf{r} \int d^3\mathbf{r}' \phi_i^*(\mathbf{r}) \phi_a^*(\mathbf{r}) \left(\frac{2}{|\mathbf{r} - \mathbf{r}'|} + f_{xc}^{\uparrow\downarrow}(\mathbf{r}, \mathbf{r}', \omega_0) + f_{xc}^{\downarrow\uparrow}(\mathbf{r}, \mathbf{r}', \omega_0) \right) \phi_i(\mathbf{r}') \phi_a(\mathbf{r}'), \quad (8.17)$$

where $f_{xc}^{\uparrow\downarrow}$ is equal to $f_{xc}^{\downarrow\uparrow}$ for closed-shell systems, as are $f_{xc}^{\uparrow\uparrow}$ and $f_{xc}^{\downarrow\downarrow}$.

Their approach should yield the same results as ours, provided that our basis set is sufficiently large. We have checked that the orbital energy differences are identical to those obtained by Petersilka *et al.*[127] for He, and those by Savin *et al.*[113] for He and Be. We have furthermore checked that we could reproduce the ALDA-SPA results by Petersilka *et al.*, by calculating the required matrix elements. The SPA results were identical, except for a single deviation of only 0.1 mhartree. We have also confirmed that the implementations of f_{xc} and G_{xc} are identical[208].

However, it appeared that our fully coupled ALDA results were not identical to those obtained by Petersilka *et al.* by diagonalizing a large matrix. The reason for this, as suggested by Petersilka[208], is that in their numerical program, continuum contributions cannot be taken into account, while our basis set program provides a (discrete) description of the continuum through the virtual orbitals with positive one-electron energies. This was verified by only taking into account virtuals with negative one-electron energies in our calculations. In this way we recovered the results obtained by Petersilka *et al.* It will be shown below that this continuum contribution considerably improves some of the results.

Table 8.5: Helium singlet excitation energies (in hartrees).

Transition	Exact ^a	KS eigenvalues ^b	ALDA,bound ^c	TDOEP-SPA/PT ^d	ALDA, full ^e
1s → 2s	0.7578	0.7460	0.7678	0.7687	0.7608
1s → 3s	0.8425	0.8392	0.8461	0.8448	0.8435
1s → 4s	0.8701	0.8688	0.8719	0.8710	0.8706
1s → 5s	0.8825	0.8819	0.8835	0.8830	0.8828
1s → 6s	0.8892	0.8888	0.8898	0.8894	0.8893
1s → 2p	0.7799	0.7772	0.7764	0.7850	0.7751
1s → 3p	0.8486	0.8476	0.8483	0.8500	0.8479
1s → 4p	0.8727	0.8722	0.8726	0.8732	0.8724
1s → 5p	0.8838	0.8836	0.8838	0.8841	0.8837
1s → 6p	0.8899	0.8898	0.8899	0.8901	0.8898
Av. abs. err. ^f		2.2	2.1	2.2	1.0

^aAccurate nonrelativistic calculations by Drake[280].

^bZeroth-order approximation provided by differences in KS eigenvalues.

^cALDA results obtained by taking into account all bound KS orbitals [127].

^dValues obtained with TDOEP kernel in the SPA[127] or by DFT perturbation theory [271]. The results for the higher transitions are given in Reference [127] only.

^eThis work, ALDA results obtained by taking into account all bound and unbound KS orbitals.

^fThe average absolute error with respect to the "exact" values is given in mhartree.

In Table 8.5, several results for the singlet excitation energies of Helium have been gathered. It is clear that the orbital energy differences in the third column already provide good approximations to the experimental excitation energies. The average absolute deviation is only 2.2 mhartree from the experimental values. Petersilka's fully coupled ALDA results with bound orbitals yield a similar deviation of 2.1 mhartree.

The best results by Filippi *et al.*[271] have been given in the fourth column. These results are in fact identical to the SPA results obtained by Petersilka *et al.* with the TDOEP approximation for f_{xc} . This can be understood from the fact that, for two-electron systems, both approaches reduce to the calculation of the same Coulomb-type matrix element (compare the appendix of Reference [271] and Eq. (8.7)). Both approaches give a first-order exchange-only correction to the orbital energy differences. The results obtained by Filippi *et al.* give no improvement over the ALDA results obtained by Petersilka *et al.*

Our fully coupled ALDA results, which have converged with respect to basis set size, are given in the last column. The deviation with respect to the experimental values drops by a factor of two in comparison to the results obtained by Petersilka *et al.* and those obtained by Filippi *et al.* The average absolute deviation is 1.0 mhartree for our results. We emphasize that the only difference between our results in the final column and those obtained by Petersilka *et al.*, is the inclusion of virtual orbitals with positive one-electron energies in our calculation[208]. It is the contribution of the continuum that ensures the improvement in the results. One can speculate that a similar improvement could be obtained for the

TDOEP kernel, if a fully coupled calculation would be performed. It is too early to conclude that the ALDA performs better than the TDOEP for these transitions.

It is interesting to note that the last three columns of Table 8.5 all correct the $s \rightarrow s$ orbital energy differences in the right direction with respect to the experimental values, but by too large amounts. For the $s \rightarrow p$ transitions, the ALDA corrections to the orbital energy differences are again in the right direction, but for these transitions the correction is not large enough. The notable exception is the $2s \rightarrow 2p$ transition. Here, the ALDA correction actually makes the result worse. The first-order exchange-only results of Filippi *et al.* are worse than the ALDA results for the singlet $s \rightarrow s$ and $s \rightarrow p$ transitions.

Table 8.6: Helium triplet excitation energies (in hartrees).

Transition	Exact ^a	KS eigenvalues ^b	ALDA,bound ^c	TDOEP-SPA/PT ^d	ALDA,full ^e
1s \rightarrow 2s	0.7285	0.7460	0.7351	0.7232	0.7334
1s \rightarrow 3s	0.8350	0.8392	0.8368	0.8337	0.8362
1s \rightarrow 4s	0.8672	0.8688	0.8679	0.8667	0.8677
1s \rightarrow 5s	0.8811	0.8819	0.8815	0.8808	0.8813
1s \rightarrow 6s	0.8883	0.8888	0.8885	0.8882	0.8885
1s \rightarrow 2p	0.7706	0.7772	0.7698	0.7693	0.7689
1s \rightarrow 3p	0.8456	0.8476	0.8457	0.8453	0.8454
1s \rightarrow 4p	0.8714	0.8722	0.8715	0.8712	0.8713
1s \rightarrow 5p	0.8832	0.8836	0.8832	0.8831	0.8831
1s \rightarrow 6p	0.8895	0.8898	0.8895	0.8895	0.8895
Av. abs. err. ^f	3.5	1.1	0.9	0.9	

^aAccurate nonrelativistic calculations by Drake[280].

^bZeroth-order approximation provided by differences in KS eigenvalues.

^cALDA results obtained by taking into account all bound KS orbitals [127].

^dValues obtained with TDOEP kernel in the SPA[127] or by DFT perturbation theory [271]. The results for the higher transitions are given in Reference [127] only.

^eThis work, ALDA results obtained by taking into account all bound and unbound KS orbitals.

^fThe average absolute error with respect to the "exact" values is given in mhartree.

In Table 8.6, the triplet excitation energies corresponding to the singlet excitation energies of Table 8.5 are presented. Here, all results clearly improve upon the orbital energy differences. Contrary to what was seen in the previous table, the two sets of ALDA results do not differ much in accuracy here. The inclusion of the continuum contribution plays less of a role than in the singlet case and also Filippi *et al.*'s exchange-only results are hardly worse than the fully coupled ALDA results. The exchange-only results again overcorrect the orbital energy differences, as in the singlet case, for the $s \rightarrow s$ transitions. The ALDA results give too small corrections for these transitions. All coupled results for the $s \rightarrow p$ transitions are quite satisfactory.

Now we turn to the singlet-triplet splittings for these transitions in Table 8.7. Here, the ALDA results are clearly better than the exchange-only results. The exchange-only results

Table 8.7: Helium singlet-triplet splittings (in millihartrees).

Transition	Exact ^a	ALDA,bound ^b	TDOEP-SPA/PT ^c	ALDA,full ^d
1s → 2s	29.3	32.7	45.5	27.4
1s → 3s	7.4	9.4	11.1	7.3
1s → 4s	2.9	4.0	4.3	2.9
1s → 5s	1.4	2.1	2.2	1.4
1s → 6s	0.8	1.3	1.2	0.8
1s → 2p	9.3	6.6	15.7	6.2
1s → 3p	2.9	2.6	4.7	2.5
1s → 4p	1.3	1.1	2.0	1.1
1s → 5p	0.6	0.6	1.0	0.6
1s → 6p	0.4	0.3	0.6	0.3
Av. abs. error ^e		1.1	3.2	0.6

^aAccurate nonrelativistic calculations by Drake[280].

^bALDA results obtained by taking into account all bound KS orbitals [127].

^cValues obtained with TDOEP kernel in the SPA[127] or by DFT perturbation theory [271]. The results for the higher transitions are given in Reference [127] only.

^dThis work, ALDA results obtained by taking into account all bound and unbound KS orbitals.

^eThe average absolute error with respect to the "exact" values is given in mhartree.

give too high splittings, as already observed by Petersilka *et al.* [105, 127]. This is due to the fact that the corrections to the orbital energy differences are too large in the exchange-only case, for both the singlet and the triplet energies.

In the ALDA results a cancellation of errors occurs, as the singlet and triplet excitation energies are both too high for the s→s transitions. For this reason, the ALDA singlet-triplet splittings come out more accurately than the excitation energies themselves. From this table, it is obvious that the continuum contribution is of importance and helps to further improve upon Petersilka's ALDA results. The final average absolute error for the fully coupled ALDA results in the last column is a very satisfactory 0.6 mhartree, which clearly improves upon both the ALDA results with bound KS orbitals only and the exchange-only values based on DFT perturbation theory (PT).

8.5.3 Atomic results, excitation energies of Beryllium

Now we turn to the excitation energies of Beryllium. The singlet excitation energies are given in Table 8.8. For the LDA potential, only the first couple of excitation energies have been given. Those are the only transitions to virtuals which are bound in the LDA potential. Not surprisingly, no reliable values for higher excitation energies could be obtained. The ordering of the excitations even differs from the experimental ordering. We can conclude that the LDA potential does not give a qualitatively correct description of all but the lowest excitations in Be.

Table 8.8: Beryllium singlet excitation energies (in hartrees), uncertainties in the final digit in parentheses.

Transition	Expt. ^a	KS eigenvalues ^b	ALDA,full ^c	PT ^d	LB94 ^e	LDA ^f
2s → 2p	0.193941	0.1327	0.1868	0.1989	0.1747(1)	0.1772(1)
2s → 3s	0.249127	0.2444	0.2495	0.2556	0.2402(2)	0.2040(5)
2s → 3p	0.274233	0.2694	0.2710	0.2741	0.2593(3)	
2s → 3d	0.293556	0.2833	0.2778	0.2852	0.2669(3)	
2s → 4s	0.297279	0.2959	0.2977(1)	0.2990		
2s → 4p	0.306314	0.3046	0.3048(1)	0.3061		
2s → 4d	0.313390	0.3098	0.3084(1)	0.3106		
2s → 5s	0.315855	0.3153	0.3160(1)	0.3166		
Av. abs. error ^g		11.0(3.9)	4.2(3.8)	3.2		

^aThe experimental excitation energies[284].

^bZeroth-order approximation provided by differences in KS eigenvalues.

^cThis work, ALDA results obtained by taking into account all bound and unbound KS orbitals.

^dValues obtained by DFT perturbation theory [271].

^eVan Leeuwen–Baerends potential[121]. The higher excitation energies are not given as they vary too much in different basis sets.

^fThe VWN parametrization is used[4]. Only the results for the transitions to bound virtual KS orbitals are given.

^gThe average absolute error with respect to the "exact" values is given in mhartree, in parentheses the value for all but the first transition.

For the LB94 potential, results for the lowest four excitation energies are given. For higher excitations, relatively large differences between results in different basis sets occurred. This is due to the long range of the LB94 potential, which leads to increased basis set effects in the very low density region. The typical magnitude of the differences is a few millihartrees. For this reason we decided not to include those numbers in this and the following tables.

The LB94 results are much better already than the LDA potential. Due to the correct asymptotics, these Rydberg-like transitions are described reasonably well, with an average error of 17.4 millihartree (this should be compared to our results with the accurate xc potential, which yields an average error of 6.6 mhartree for these transitions).

The accurate potential results are better still. The average error of 4.2 mhartree gives a factor of 2.6 improvement with respect to the LB94 results, and a factor of 2.5 improvement with respect to the orbital energy differences. However, if the 2s→2p transition is disregarded (a very large correction to the orbital energy difference is needed for this transition), the ALDA results do not improve upon the orbital energy differences at all. This is entirely due to the s→d transitions, which are poorly treated by the ALDA kernel. Not only are the ALDA results for these transitions clearly worse than both the exact exchange-only results and the orbital energy differences, they even correct the orbital energy differences in the wrong direction. The results by Filippi *et al.* do provide a correction in the right direction,

although by too small an amount.

On the other hand, the $s \rightarrow s$ and $s \rightarrow p$ transitions are treated satisfactorily by the ALDA kernel. The errors in the ALDA results for $s \rightarrow s$ transitions (0.4, 0.4 and 0.15 mhartree) are considerably lower than those for the $s \rightarrow p$ transitions (7.1, 3.2 and 1.5 mhartree), which in turn are superior to the $s \rightarrow d$ transition results with errors of 15.8 and 5.0 mhartree. The ALDA results for the $s \rightarrow s$ transitions are clearly better than the exact exchange results and the orbital energy differences, as was also the case for the singlet $s \rightarrow s$ transitions of Helium in Table 8.7.

On the whole, the perturbative values obtained by Filippi *et al.*[271] are somewhat more accurate than our ALDA results here, with an average error of 3.2 mhartree. The quality of their results does not show the same variety in errors for the different types of transitions. It has already been observed by Petersilka and Gross[105] that the singlet spectrum is reproduced at least as well by the TDOEP kernel as by the ALDA kernel, while the ALDA kernel is to be preferred for triplet excitation energies.

Table 8.9: Beryllium triplet excitation energies (in hartrees), uncertainties in the final digit in parentheses.

Transition	Expt. ^a	KS eigenvalues ^b	ALDA,full ^c	PT ^d	LB94 ^e	LDA ^f
2s \rightarrow 2p	0.100153	0.1327	0.08885	0.0629	0.07665(1)	0.08675
2s \rightarrow 3s	0.237304	0.2444	0.2382	0.2331	0.2265(1)	0.2021(4)
2s \rightarrow 3p	0.267877	0.2694	0.2647	0.2640	0.2527(2)	
2s \rightarrow 3d	0.282744	0.2833	0.2802	0.2814	0.2694(2)	
2s \rightarrow 4s	0.293921	0.2959	0.2941	0.2928		
2s \rightarrow 4p	0.300487	0.3046	0.3030	0.3029		
2s \rightarrow 4d	0.309577	0.3098	0.3085	0.3089		
2s \rightarrow 5s	0.314429	0.3153	0.3145	0.3139		
Av. abs. err. ^g		6.1	2.7	6.4		

^aThe experimental excitation energies[284].

^bZeroth-order approximation provided by differences in KS eigenvalues.

^cThis work, ALDA results obtained by taking into account all bound and unbound KS orbitals.

^dValues obtained by DFT perturbation theory [271].

^eVan Leeuwen–Baerends potential[121]. The higher excitation energies are not given as they vary too much in different basis sets.

^fThe VWN parametrization is used[4]. Only the results for the transitions to bound virtual KS orbitals are given.

^gThe average absolute error with respect to the "exact" values is given in mhartree.

The ALDA and exchange-only triplet energies for Beryllium in Table 8.9 provide corrections in the right direction with respect to the orbital energy differences for all transitions except the $2s \rightarrow 4p$ transition. The ALDA results, with an average absolute error of 2.7 mhartree, are clearly better than the exchange-only results (6.4 mhartree), which do not improve upon the orbital energy differences here (6.1 mhartree). As in the singlet case, the

LB94 and LDA results are clearly worse.

Table 8.10: Beryllium singlet-triplet splittings (in millihartrees), uncertainties in the final digit in parentheses

Transition	Expt. ^a	ALDA,full ^b	PT ^c	LB94 ^d	LDA ^e
2s \rightarrow 2p	93.8	98.0	136	98.0(1)	90.4(1)
2s \rightarrow 3s	11.8	11.3	22.5	13.7(1)	2.3(1)
2s \rightarrow 3p	6.4	6.3	10.1	6.6(1)	
2s \rightarrow 3d	10.8	-2.4	3.8	-2.5(1)	
2s \rightarrow 4s	3.4	3.6	6.2		
2s \rightarrow 4p	5.8	1.8	3.2		
2s \rightarrow 4d	3.8	-0.1	1.7		
2s \rightarrow 5s	2.4	1.5	2.7		
Av .err. (mhartree)		6.1	8.9		

^aThe experimental excitation energies[284].

^bThis work, ALDA results obtained by taking into account all bound and unbound KS orbitals.

^cValues obtained by DFT perturbation theory [271].

^dVan Leeuwen–Baerends potential[121]. The higher excitation energies are not given as they vary too much in different basis sets.

^eThe VWN parametrization is used[4]. Only the results for the transitions to bound virtual KS orbitals are given.

In Table 8.10 the singlet-triplet splittings for Beryllium are given. For the three lowest transitions, the ALDA splitting is clearly superior to the exchange-only splitting and can be considered very satisfactory. For the higher transitions, this is not the case anymore. The ALDA results for the $s \rightarrow d$ transitions are even qualitatively incorrect, as the wrong sign for the singlet-triplet splitting is predicted by the ALDA kernel. Although the exchange-only results by Filippi *et al.*[271] for these splittings are also not very impressive, they at least give the right sign. The wrong sign remains if one uses either only bound orbitals or the single pole approximation. If one uses only the exchange part of the ALDA kernel, the singlet-triplet splitting for the $2s \rightarrow 3d$ transition remains negative, but the right sign is predicted if one totally neglects the xc screening (only "Coulomb" screening).

We obtained similar inversions of the singlet and triplet levels for the $2s \rightarrow 4f$ transition in Be and the $s \rightarrow d$ and $s \rightarrow f$ transitions in Helium. For these Helium transitions, the absolute value of the splitting (which should be in the microhartree regime) is clearly overestimated as well, both in the SPA and in the full ALDA results. We do not presume that this is a basis set artifact, because it was reproduced in different basis sets of high quality. In the same basis sets, the approximation $f_{xc} = 0$ (Coulomb screening only) does lead to positive values for all splittings. As the Coulomb-type matrix elements obtained in this way determine the TDOEP exchange-only results for He, we can actually calculate the results that would be obtained by Filippi *et al.* for these transitions, or by Petersilka *et al.* in their SPA/TDOEP results. In turns out that the TDOEP kernel correctly predicts positive singlet-triplet splittings for

the $s \rightarrow d$ and $s \rightarrow f$ transitions in Helium. Even higher quality calculations than the present ones would be required to see whether these splittings are also of the correct magnitude, although our results indicate that they probably will be.

These SPA results can be understood from the SPA expression for the singlet-triplet splitting in Eq. (8.17). From that expression, it is clear that approximations for f_{xc} which are diagonal in spin space (such as the TDOEP and exchange-only ALDA kernels) yield no contribution to the singlet-triplet splitting in the SPA. Only the Coulomb term in Eq. (8.17) remains in that case. For this reason, it should not be very surprising that the ALDA results for the splittings are usually better than the TDOEP kernel results. This expression also explains why only the ALDA xc kernel can give rise to negative SPA singlet-triplet splittings. Apparently, the correlation part of the ALDA kernel, based on the homogeneous electron gas, is too crude to provide an accurate correction for this very subtle and small effect for these transitions. In short, we can state that although the correlation part of the ALDA kernel in general yields improved results with respect to the exchange-only approximations, the negative singlet-triplet splittings to which it gives rise show that it still needs to be improved upon.

The LB94 results show that the singlet-triplet splittings are more sensitive to the xc kernel than to details of the xc potential, because they are very similar to the ALDA results with the accurate potential. The LDA results, on the other hand, show that the xc potential should at least possess the correct asymptotic behavior in order to obtain reliable singlet-triplet splittings for the higher-lying excitations. Only the LDA result for the first splitting is qualitatively correct.

8.5.4 Molecular polarizability results

Table 8.11: Molecular polarizabilities with LDA, LB94, and semiaccurate potential.

Molecule	LDA	LB94	Accurate v_{xc} ^a	Acc/Expt. ^b
H ₂	5.9	5.61	5.16	5.1816 ^c
N ₂	12.27	11.46	11.68	11.74
HF	6.20	5.31	5.49	5.52 ^d
HCl	18.63	17.86	17.25	17.39
H ₂ O	10.53	9.20	9.45	9.64
CO	13.87	12.62	12.86	13.08
Av. err.	+8.8%	-0.6%	-1.0%	
Av. abs. err.	+8.8%	3.6%	-1.0%	

^aResults obtained with large GTO basis sets for the CI. The difference in the polarizability by using another large augmented GTO basis set is smaller than 1%; typically a few tenths of a percent.

^bBenchmark theoretical or experimental results.

^cVibrationless theoretical value.

^dVibrationless estimate.

We have performed polarizability calculations using xc potentials constructed from (MR)SDCI densities, as has been pointed out earlier. The results for the static average polarizabilities of some small molecules are given in Table 8.11. We used the experimental equilibrium bond distances of 1.4 bohr for H_2 (0.7408 Å), 0.917 Å for HF, 1.2746 Å for HCl, 1.12832 Å for CO, 1.09768 Å for N_2 , and 0.957 Å for the H—O distance in H_2O , with a H—O—H angle of 104.5 degrees.

As usual, the LDA results are clearly and invariably too high (on average 8.8%). The LB94 results are much better. They do not show a systematic error (the average error is only 0.6%), and the average absolute error (3.6%) is considerably lower than for the LDA results (8.8%). The results with the accurate potentials are much better still. The average absolute error reduces by almost a factor of four to 1.0% with respect to the LB94 results. This is a strong indication that improved models for v_{xc} will considerably improve molecular polarizability results. The results with the accurate potential are invariably too low with respect to the experimental or vibrationless theoretical results. Several reasons can be given for this. The most obvious one is that the CI results for the polarizabilities (which we obtained from finite field CI calculations, using the same type of CI that generated the density from which the "accurate" v_{xc} was constructed) are also invariably too low. In most cases the underestimation was even more than the result with the accurate potential; for example, we obtained from the finite field CI calculations a polarizability of 5.185 for H_2 , 16.97 for HCl, and 9.20 for H_2O (where the accurate potential results were 5.16, 17.25, and 9.45 respectively).

This implies that either the basis sets we used in the CI calculations were not large enough or the level of CI (which was SD) was insufficiently high. We expect both factors to contribute. As far as the level of correlation is concerned, it is known from coupled-cluster response calculations that CCSD(T) results are often clearly better than CCSD or CISD results. In the basis sets we used, one or more sets of augmenting functions were added, and we obtained Hartree–Fock results for the polarizabilities which were close to the basis set limit values. This does not imply that these basis sets were sufficiently large for the correlated calculations, however.

One might furthermore suspect our construction scheme for the potential to influence the polarizability results artificially. This could lead to a small (possibly systematic) error in either direction. A final suggestion that the remaining 1% error is due to the intrinsic errors of the xc kernel f_{xc} cannot be dismissed, although it is much too early on the basis of this evidence to jump to such a conclusion. Finally, a comparison of our LDA values to the basis set free values obtained by Dickson and Becke[203] shows that our basis sets in the DFT calculation are sufficiently large.

It should be emphasized that we do not suggest the present approach as a practical method for calculating polarizabilities. We have merely tried to indicate that an accurate future model for the xc potential will yield considerable improvements in molecular polarizabilities as well. Similar preliminary calculations on excitation energies and hyperpolarizability have not led to such a clear picture, however. It would be desirable to repeat a similar molecular study using a higher level correlated method than the present one, preferably in a fully numerical program, or in a large STO basis set (although in the latter case one has to make sure that the density in the outer region decays correctly). Such a study would allow

more definite statements to be made.

8.6 Conclusions and future directions

We have performed accurate atomic calculations using accurate xc potentials on excitation energies and polarizabilities of three small atoms: He, Be and Ne. Our results show that important improvements with respect to calculations using the LDA potential or LB94 potential are obtained. The use of an accurate xc potential removes the larger part of the discrepancy with respect to the experimental values. The remaining discrepancies are due to deficiencies in the ALDA xc kernel. Our results show that the ALDA kernel is at least comparable in quality to the exchange-only TDOEP kernel and that taking into account "continuum contributions" has a positive effect on the calculated excitation energies.

We believe that the major deficiencies in the xc kernels are still in the spatial part, not in the frequency dependence. Major improvements may come from a TDOEP kernel, which includes accurate correlation contributions. This correlation contribution is clearly important in the results for the singlet-triplet splittings. Further improvement should come from improved modeling of the frequency dependence of the kernel.

The benefit of more refined approximations for the xc kernel will be useful only in combination with improved xc potentials. To the very least, these potentials should be self-interaction free, or, in other words, possess the correct asymptotic behavior. Such potentials can be constructed by either adding a (semiempirical) correction to a usual xc potential as in the LB94 potential[121], or by using OEP potentials in the Krieger–Li–Iafrate[285] (KLI) approximation[286, 287, 288]. Such an xc potential has to yield accurate predictions for the experimental ionization potential in order to improve upon existing approximate xc potentials.

8.7 Acknowledgements

We are grateful to Professor Dr. Umrigar[270, 269] for providing the accurate xc potentials for He and Be, and to the authors of References [113, 271] for making their work available prior to publication. We thank Martin Petersilka for sending his work prior to publication and for many very useful discussions. SvG gratefully acknowledges financial support from the Netherlands organization for scientific research (NWO) through its foundations SON and NCF.

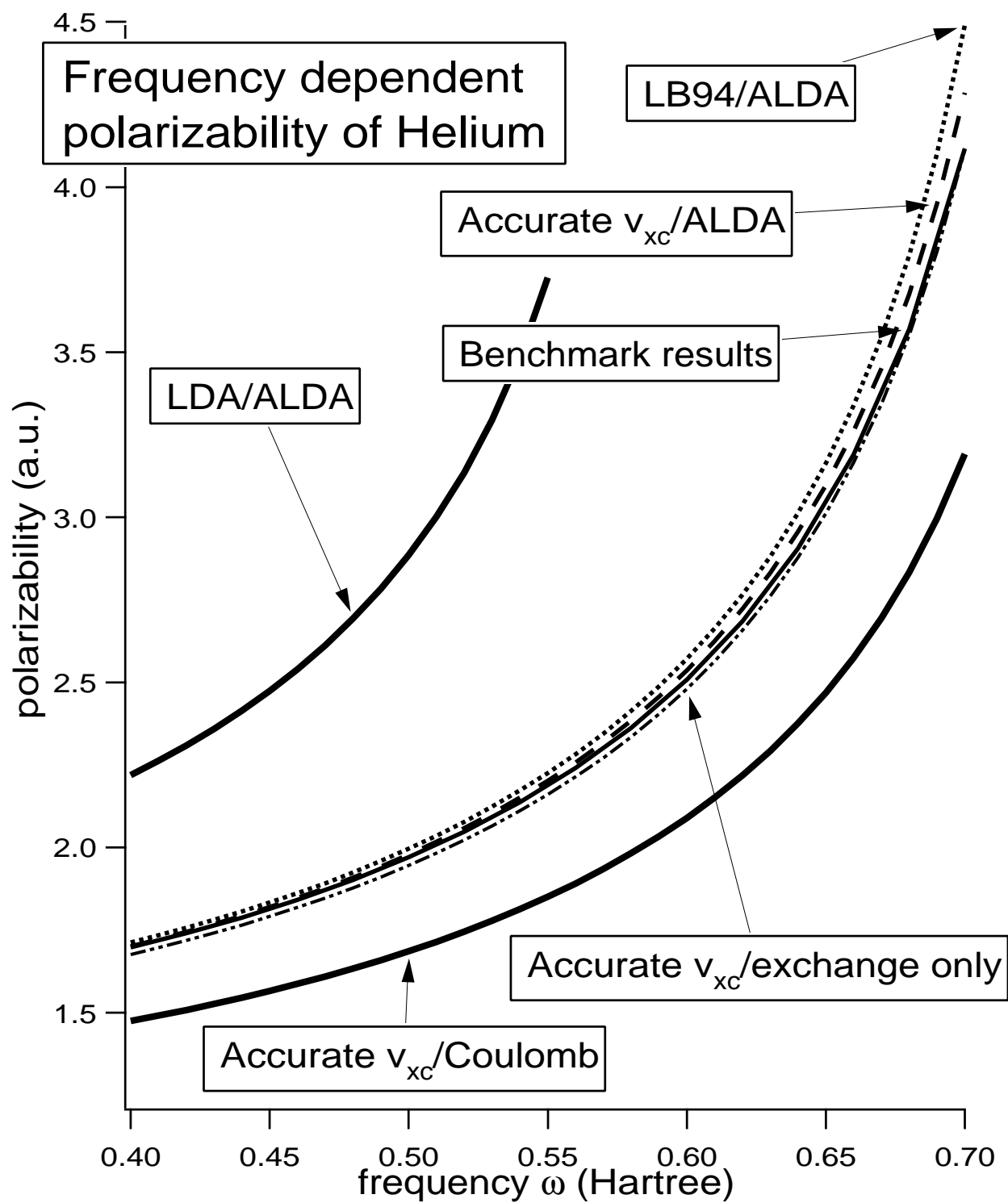


Figure 8.1: The dynamic polarizability of He calculated with different xc potentials and xc kernels.

Chapter 9

Calculating frequency-dependent hyperpolarizabilities using time-dependent density functional theory

9.1 Abstract

An accurate determination of frequency-dependent molecular hyperpolarizabilities is at the same time of possible technological importance and theoretically challenging. For large molecules, Hartree–Fock theory was until recently the only available *ab initio* approach. However, correlation effects are usually very important for this property, which makes it desirable to have a computationally efficient approach in which those effects are (approximately) taken into account. We have recently shown that frequency-dependent hyperpolarizabilities can be efficiently obtained using time-dependent density functional theory. Here, we shall present the necessary theoretical framework and the details of our implementation in the Amsterdam Density Functional program. Special attention will be paid to the use of fit functions for the density and to numerical integration, which are typical of density functional codes. Numerical examples for He, CO, and *para*-nitroaniline are presented, as evidence for the correctness of the equations and the implementation.

9.2 Introduction

In recent years there has been a growing interest in nonlinear optical (NLO) properties of molecules. NLO materials are important for optical-switching devices, applications in telecommunications, and for optical computing. Theory can play a leading role in finding suitable NLO materials if a reliable and efficient approach is available. In that case, theory can predict the NLO properties of large molecules with possibly large NLO responses. Density Functional Theory (DFT) has been shown to provide such an accurate and efficient technique for the prediction of energies and structures. It therefore seems appealing to use

DFT for the prediction of NLO properties as well.

There are basically two different ways to calculate molecular properties which can be written in terms of energy derivatives, such as the polarizabilities and hyperpolarizabilities determining the linear and nonlinear optical response of a system. The first is to use finite difference techniques, where the energy is calculated for different values of, in our case, the electric field. The derivative of the energy is then obtained from a finite differentiation. This method is perfectly viable if one carefully chooses the strengths of the perturbations. It is a convenient method because it can be applied with any program capable of calculating the energy of the perturbed system, without extra programming effort.

There are also several drawbacks to this approach however. In the first place, it requires much human time (if the process has not been automated), because one has to check the effect of varying the perturbation strengths carefully. Furthermore, one needs very well-converged energies in order to make reliable predictions, which makes the calculations much more time-consuming. Besides this, several calculations are needed in order to obtain one property. All these problems are amplified if one goes to higher (third or fourth) derivatives of the energy.

For these reasons the alternative, analytic, approach is often preferable. The desired properties are obtained from a single calculation by evaluating the derivatives of the energy analytically. The drawback is that a considerable programming effort may be required for certain properties, especially for the higher-order derivatives of the energy. However, once the programming has been done, the calculation of properties has become much more convenient and routine, as well as more accurate. One other important advantage of the analytical approach is that it gives access to time-dependent (or frequency-dependent) properties as well. There is no way to calculate properties which depend upon the frequency of the external field in the finite field (FF) approach.

In *ab initio* theoretical chemistry, the calculation of analytic derivatives has become routine for many time-dependent and time-independent properties, including higher-order properties. This is not yet the case in DFT, which has mainly been used for studying energies and geometries. The calculation of molecular response properties in DFT is relatively new, and is usually performed using FF techniques. This situation is however beginning to change. Analytic formulations and computer implementations for such diverse second-order properties as NMR parameters [187, 209, 210], ESR parameters [289, 290, 291, 292], magnetizabilities[43], and polarizabilities[34] are now available. The results are encouraging in that they are usually superior to those obtained at the Hartree–Fock (HF) level.

Higher-order properties, such as hyperpolarizabilities and Raman scattering intensities and depolarization ratios, are usually treated by finite difference techniques. In this work, on the contrary, the analytical approach will be used for calculating frequency-dependent hyperpolarizabilities within DFT. The first application of our implementation, to the C_{60} molecule, has recently been published elsewhere[76], but contains only a rough outline of the underlying theory. In the present work, which will be of a rather technical nature, we shall describe our implementation in the Amsterdam Density Functional (ADF) program[89, 90, 91, 114] in more detail. As there are many analogies to the calculation of frequency-dependent hyperpolarizabilities in time-dependent Hartree–Fock (TDHF) theory, which has become routine by now, those parts of the derivation and implementation which are typical

of time-dependent DFT (TDDFT) will be emphasized.

In particular, we will derive the starting equation of this paper (a variation on the so-called time-dependent Kohn–Sham (KS) equations of DFT), present equations for functional derivatives of the time-dependent exchange–correlation (xc) potential, which replaces the Hartree–Fock exchange operator, and present concise final DFT results, using the $(2n + 1)$ -rule, for the first hyperpolarizability tensor $\beta_{abc}(-\omega_\sigma; \omega_b, \omega_c)$ for several important NLO properties.

In a more technical sense, we will discuss the influence of using so-called auxiliary basis sets for fitting the density, which are used in most modern DFT codes. Accuracy issues related to numerical integrations, which are needed in DFT because integrals involving the complicated xc potential cannot be calculated analytically, will also be discussed. It is shown that the errors introduced through these approximations can be kept under control.

Our implementation for the calculation of frequency-dependent hyperpolarizabilities presents the first analytic implementation of a third-order time-dependent property in DFT, which is applicable to general molecules. The efficiency of the resulting implementation is similar to that of an ordinary energy calculation in DFT, namely N^3 . This, in combination with the use of symmetry, and, in future refinements to the code, of linear scaling techniques[114], as well as a fully vectorized and parallelized code, will enable one to treat large molecules (more than 100 atoms) at a level of theory which usually supersedes Hartree–Fock. Here, only numerical examples on He, CO, and *para*-nitroaniline will be presented in order to document the technical accuracy of the implementation. A comparative study on frequency-dependent hyperpolarizabilities of a set of small molecules, in which the performance of various xc potentials is compared to that of (correlated) *ab initio* methods, is in progress[272].

9.3 The basic equations

In TDHF, the starting point for the calculation of NLO properties is given by[245, 104, 246]:

$$FC - i \frac{\partial}{\partial t} SC = SC\varepsilon, \quad (9.1)$$

where F , C , S , and ε are the Fock, coefficient, overlap and Lagrangian multiplier matrices, to be specified in detail below. This equation is derived from Frenkel’s variational principle[247, 102, 293, 294] for the total wavefunction Ψ , to which the HF wavefunction is an approximation. It would be desirable to start the DFT treatment of these properties from a similar equation, because many of the well-developed TDHF techniques can be used in that case. However, the DFT wavefunction, which is the Slater determinant of the KS orbitals, is not equal to the exact wavefunction, which prohibits the use of Frenkel’s principle.

Instead, in TDDFT one searches for a stationary point of the action integral \mathcal{A} :

$$\mathcal{A} = \int_{t_0}^{t_1} dt \langle \Psi(t) | i \frac{\partial}{\partial t} - \hat{H}(t) | \Psi(t) \rangle, \quad (9.2)$$

where Ψ is the total wavefunction of the system. In view of the correspondence between the time-dependent densities and wavefunctions, this action functional can be regarded as

a density functional $\mathcal{A}[\rho]$, which must have a stationary point at the exact time-dependent density[38], which is the central quantity in TDDFT. This exact density can be found from the Euler–Lagrange equation $\delta\mathcal{A}[\rho]/\delta\rho(\mathbf{r}, t) = 0$. The action functional A is given in terms of time-dependent single-particle orbitals $\{\phi_j(\mathbf{r}, t)\}$ by[97, 33]:

$$A[\{\phi_j\}] = \sum_j^N \int_{-\infty}^{t_1} dt \int d^3\mathbf{r} \phi_j^*(\mathbf{r}, t) \left(i \frac{\partial}{\partial t} + \frac{\nabla^2}{2} \right) \phi_j(\mathbf{r}, t) - \frac{1}{2} \int_{-\infty}^{t_1} dt \int d^3\mathbf{r} \rho(\mathbf{r}, t) v_{\text{ext}}(\mathbf{r}, t) - \frac{1}{2} \int_{-\infty}^{t_1} dt \int d^3\mathbf{r} \int d^3\mathbf{r}' \frac{\rho(\mathbf{r}, t)\rho(\mathbf{r}', t)}{|\mathbf{r} - \mathbf{r}'|} - A_{\text{xc}}[\{\phi_j\}], \quad (9.3)$$

where all unknown many-body terms are hidden in the xc-part of the action functional A_{xc} , of which the functional derivative with respect to the time-dependent density is called the time-dependent xc-potential $v_{\text{xc}}(\mathbf{r}, t)$. If we explicitly demand the orbitals to remain orthonormal at all times, by adding to the action functional A the constraint term $A^{\text{constraint}}$, involving Lagrangian multipliers ε_{ij}

$$A^{\text{constraint}} = \sum_{ij} \varepsilon_{ij}(t) \left(\delta_{ij} - \int d^3\mathbf{r} \phi_i^*(\mathbf{r}, t) \phi_j(\mathbf{r}, t) \right) = 0, \quad (9.4)$$

and we demand the resulting total action functional to be stationary with respect to orbital variations $\partial A/\partial\phi_k^* = 0$, we obtain a general form of the time-dependent KS equations[295]:

$$\sum_j \varepsilon_{ij}(t) \phi_j(\mathbf{r}, t) + i \frac{\partial}{\partial t} \phi_i(\mathbf{r}, t) = \left[-\frac{\nabla^2}{2} + v_s(\mathbf{r}, t) \right] \phi_i(\mathbf{r}, t) \equiv F_s \phi_i(\mathbf{r}, t), \quad (9.5)$$

where $v_s(\mathbf{r}, t)$ is the time-dependent KS potential, and where the time-dependent density $\rho(\mathbf{r}, t)$ is obtained from the squares of the occupied orbitals

$$\rho(\mathbf{r}, t) = \sum_i^{\text{occ}} |\phi_i(\mathbf{r}, t)|^2. \quad (9.6)$$

If the orbitals ϕ_i of Equation (9.5) are expanded in a fixed, time-independent basis set of AOs $\{\chi_\mu\}$:

$$\phi_i(\mathbf{r}, t) = \sum_\mu \chi_\mu(\mathbf{r}) C_{\mu i}(t), \quad (9.7)$$

where the time-dependence of ϕ_i is completely determined by the coefficient matrix C , we obtain the desired matrix form of the time-dependent KS equations, which will form the starting point of the perturbative expansion:

$$F_s C - i \frac{\partial}{\partial t} S C = S C \varepsilon, \quad (9.8)$$

where F_s is now the AO matrix of the operator defined in Equation (9.5), and S is the overlap matrix of the AOs [$S_{\mu\nu} = \int d\mathbf{r} \chi_\mu^*(\mathbf{r}) \chi_\nu(\mathbf{r})$]. The matrix equation for the orthonormality constraint reads:

$$\frac{\partial}{\partial t} (C^\dagger S C) = 0 \quad (9.9)$$

[and $(C^\dagger S C) = 1$ at $t \rightarrow -\infty$], and the density matrix D is known from the coefficient matrix C and the occupation number matrix n :

$$D = C n C^\dagger. \quad (9.10)$$

Although all equations can be extended to the spin-unrestricted case[296], we will be dealing with closed-shell systems only in this paper, in which case the matrix n is diagonal with components either equal to 2 (occupied KS orbitals) or 0 (virtual KS orbitals).

Different choices for the Lagrangian multipliers $\varepsilon_{ij}(t)$ are allowed. The "canonical" form of the time-dependent KS equations is obtained from the choice $\varepsilon_{ij}(t) \equiv 0$, which has implicitly been made by Runge and Gross[38] in their derivation of the time-dependent KS equations. There is no objection to that particular choice because the Hermiticity of the Hamiltonian assures the orthonormality of the orbitals in that case. However, the choice $\varepsilon_{ij}(t) \equiv 0$ is not the most suitable one for our present purpose of finding higher-order perturbative solutions to the time-dependent KS equations, as was already discussed by Langhoff, Epstein, and Karplus in their review article on time-dependent perturbation theory[293]. It would lead to orbitals which vary rapidly in time, and cause so-called normalization and secular terms[293] to occur. If these terms are not dealt with properly, which is a technically cumbersome task, they may lead to unphysical divergences in the equations. These troublesome terms can be factored from the equations for all orders by making suitable choices for the Lagrangian multipliers, as will be done here. In this manner, many problems are automatically circumvented and the proper passage to the time-independent equations for static perturbations is guaranteed. This can be done, anticipating the expansion of all matrices in different orders of the external perturbation, by choosing a diagonal time-independent zeroth-order ε -matrix, resulting in the ordinary canonical KS equations of ground-state DFT for the zeroth-order equation:

$$F_s^{(0)} C^{(0)} = S^{(0)} C^{(0)} \varepsilon^{(0)}, \quad (9.11)$$

where $\varepsilon^{(0)}$ is a diagonal matrix containing the KS orbital energies. One has a freedom of choice for the Lagrangian multiplier matrix in each order of the perturbation [293, 249] (although it necessarily is block-diagonal and Hermitian[102]). In case the Lagrangian matrix is chosen diagonal in all orders, the corresponding time-dependent orbitals ϕ_i^{diag} are easily seen [from Equation (9.5)] to be identical to the canonical KS orbitals $\phi_i^{\text{can.}}$ (which correspond to $\varepsilon \equiv 0$) up to a purely imaginary time-dependent phase factor:

$$\phi_i^{\text{diag}} = \phi_i^{\text{can.}} \times \exp[i \int_{-\infty}^t \varepsilon_i(t') dt']. \quad (9.12)$$

In fact, Equation (9.8) can be obtained by inserting the definition of the "diagonal-gauge" orbitals in the canonical time-dependent KS equations. Finally, we remark that we do not use a diagonal ε -matrix, because there are technical advantages[104, 249], to be discussed below, in choosing ε nondiagonal for the higher-order equations.

9.4 Expansion of basic equations

We consider a system in external electric fields $\mathbf{E}^a(\mathbf{r}, t)$, $\mathbf{E}^b(\mathbf{r}, t)$, ... consisting of a monochromatic and a static part:

$$\mathbf{E}^a(\mathbf{r}, t) = \mathbf{E}^a(\mathbf{r}) \times [1 + e^{i\omega_a t} + e^{-i\omega_a t}], \quad (9.13)$$

labeled with the Cartesian directions a, b, \dots equal to x, y , or z . Although our approach can be used for general frequencies $\omega_a, \omega_b, \dots$, the implementation is at present restricted to frequencies which are either equal to 0 or to some common frequency ω . Most of the important NLO phenomena, such as Second Harmonic Generation (SHG), and many others, arise from interactions of multiple monochromatic and static fields and can consequently be described with the equations in this work.

In the dipole approximation, the external perturbation term \mathcal{H}' in the KS Hamiltonian becomes:

$$\mathcal{H}' = \mu \cdot \mathbf{E}(\mathbf{r}, t), \quad (9.14)$$

where μ is the dipole moment operator. The equations presented in this section until now, are identical to those used in TDHF theory[245, 246, 104]. The difference enters through the Fock or KS matrix. In TDHF theory it is given by[245, 246, 104]:

$$F = h + D \times (2J - K). \quad (9.15)$$

Here h is the one-electron integral matrix, containing the kinetic energy and the Coulomb field of the nuclei, as well as the external electric field of Equation (9.14). D is once again the density matrix, and J and K are the four-index Coulomb and exchange supermatrices. We have used a notation which slightly differs from the one used in earlier work[104] in order to make the multiplication of the two-index and four-index matrices more explicit. The KS matrix F_s is obtained by the substitution

$$D \times (K) \longrightarrow v_{xc}, \quad (9.16)$$

where v_{xc} is the matrix form of the (time-dependent) xc potential. Contrary to its HF counterpart K , the matrix v_{xc} is a two-index matrix, obtained from the local xc potential v_{xc} :

$$[v_{xc}]_{\kappa\lambda} = \int d\mathbf{r} \chi_{\kappa}(\mathbf{r}) v_{xc}(\mathbf{r}, t) \chi_{\lambda}(\mathbf{r}). \quad (9.17)$$

In this equation and the following ones, complex conjugate signs have been left out, as we are assuming real AOs and KS orbitals. Obviously, the fact that the KS xc potential is local, in contrast to the nonlocal exchange potential in HF theory, simplifies the DFT response calculations. On the other hand, because the approximations for v_{xc} are not of the same simplicity as the HF exchange potential, the integrals in which v_{xc} or related quantities occur cannot be calculated analytically and have to be obtained by numerical integration. Another important difference between the HF exchange potential and the KS xc potential is that the latter is a nonlinear functional of the density, while the exchange matrix $D \times (K)$ has a linear dependence. It will be shown in the rest of this work that, for this reason, the DFT

equations for the various NLO properties contain certain extra terms which are not present in the TDHF equations, as presented for example by Karna and Dupuis[104].

The goal is to start from the equations given above and to end up with equations for the various linear and nonlinear polarizabilities (hyperpolarizabilities), which can be defined through an expansion of the dipole moment into different orders of the external fields:

$$\mu_a = \mu_a(E^b = E^c = E^d = \dots = 0) + \sum_b \alpha_{ab} E^b + \frac{1}{2!} \sum_{bc} \beta_{abc} E^b E^c + \frac{1}{3!} \sum_{bcd} \gamma_{abcd} E^b E^c E^d. \quad (9.18)$$

The time dependence of the dipole moment can be written out explicitly[94], leading to the various frequency-dependent hyperpolarizability tensors. These tensors can be obtained from the trace of the dipole moment matrix H^a and the n -th order density matrix $D^{(n)}$ (where $n = 1$ for the linear polarizability α , $n = 2$ for the first hyperpolarizability tensor β , and so on), induced by electric fields in directions b, c, \dots of frequency $\omega_b, \omega_c, \dots$:

$$\begin{aligned} \alpha_{ab}(-\omega_\sigma; \omega_b) &= -\text{Tr} [H^a D^b(\omega_b)] \\ \beta_{abc}(-\omega_\sigma; \omega_b, \omega_c) &= -\text{Tr} [H^a D^{bc}(\omega_b, \omega_c)] \\ \gamma_{abcd}(-\omega_\sigma; \omega_b, \omega_c, \omega_d) &= -\text{Tr} [H^a D^{bcd}(\omega_b, \omega_c, \omega_d)]. \end{aligned} \quad (9.19)$$

Here, the usual convention is adopted that ω_b, ω_c and ω_d refer to the frequencies of the external fields, while ω_σ is equal to the sum of these frequencies: $\omega_\sigma = \omega_b + \omega_c + \dots$. As stated before, we will treat only those cases in which the frequencies of the external electric fields are either equal to zero or equal to ω . This gives access to such important properties as Second Harmonic Generation (SHG) [$\beta(-2\omega; \omega, \omega)$], Third Harmonic Generation (THG) [$\gamma(-3\omega; \omega, \omega, \omega)$], and the Electro-optical Kerr effect (EOKE) [$\gamma(-\omega; \omega, 0, 0)$], as well as many others[245, 104]. Some of these properties can be obtained by a combination of analytical and finite difference techniques. For example, all components of the γ -tensor governing the EOKE can be obtained from analytical time-dependent calculations on the Electro-optical Pockels Effect (EOPE) tensor $\beta(-\omega; \omega, 0)$ in various small electric fields in various directions, by the relation:

$$\gamma_{abcd}(-\omega; \omega, 0, 0) = \lim_{E^d \rightarrow 0} \frac{\beta_{abc}(-\omega; \omega, 0) |_{E=E^d}}{E^d}. \quad (9.20)$$

This means that an analytic implementation for arbitrary β -tensors gives access to certain frequency-dependent γ -tensors as well, through finite difference techniques. This was, for example, used in our first application of the present techniques, on the frequency-dependent hyperpolarizability γ of the C_{60} molecule[76].

As in the TDHF case, the main technical difficulty is to rewrite Equation (9.19) in such a way that the so-called $(2n + 1)$ -theorem is exploited. This theorem states that if the wave function is known up to order n , the energy can be obtained up to order $2n + 1$. In the present case, it means that the static first hyperpolarizability tensor β , which corresponds to the third-order term of the energy in a Taylor expansion with respect to an electric field, can be obtained from the knowledge of first-order quantities in the field only, implying that the so-called second-order perturbed equations do not have to be solved. In other words, one can rewrite Equation (9.19) for β in such a way that the second-order density matrix is not

needed. Both Karna and Dupuis[104] and Rice *et al.*[246] have explicitly shown for the TDHF case, that the $(2n+1)$ -theorem can be used for the frequency-dependent hyperpolarizabilities also. Karna and Dupuis have given explicit expressions for all major NLO properties up to third-order (γ). In this work, we follow the paper by Karna and Dupuis, and our aim is to indicate what differences with respect to their results appear in the DFT case. From these differences, one obtains the explicit expressions for all those properties in the DFT case as well. Some comments will be made about the efficient implementation of these equations.

In the DFT case, methods for calculating (frequency-dependent) β and γ 's have been given by Zangwill[67] and by Senatore and Subbaswamy[71, 72] for the atomic case, using spherical symmetry. Apart from this restriction, they do not use the $(2n+1)$ -theorem. This implies that an implementation of their equations will necessarily be less efficient than a calculation along the lines of this paper. For static first hyperpolarizabilities β , Colwell *et al.*[134, 135] have presented equations which can be used in the molecular case and which do make use of the $(2n+1)$ -theorem. Both for the case where the Local Density Approximation (LDA) is used for the xc potential and its derivatives[134] and for the case where a Generalized Gradient Approximation (GGA) is used[135], they provide expressions for $\beta_{abc}(0; 0, 0)$, with applications to CH_2O , CH_3F and CH_3CN . Their work is similar in nature to the work of Rice *et al.*[246]. This is also true for their paper on frequency-dependent polarizabilities[83], using the current-density functional theory approach. By following in the track of Rice *et al.*, their approach could be extended to the frequency-dependent hyperpolarizability case. However, as we are mainly interested in electric properties, the consideration of magnetic fields, as in current-density functional theory, is unnecessary. In any case, the effect of the current-density has been shown to be very small[84].

The way to proceed from here is to expand the equations presented above in different orders of the electric field. After that, first-order and higher-order equations are obtained in which quantities with the same frequency dependence are taken together. The solution to these equations will yield the first and higher-order density matrices which are needed for the calculation of the frequency-dependent (hyper)polarizabilities in Equation (9.19). The expansion in different orders of the electric field proceeds identically for all matrices which are involved. As an example, we give the expansion of the density matrix D [104]:

$$D = D^{(0)} + \sum_a E^a D^a + \frac{1}{2!} \sum_{a,b} E^a E^b D^{ab} + \frac{1}{3!} \sum_{a,b,c} E^a E^b E^c D^{abc} + \dots \quad (9.21)$$

By combining all terms of a certain order in one symbol, irrespective of their frequency dependencies, we have adopted the same shorthand notation as Karna and Dupuis, which also implies that, here and in the following, the number of indices a, b, \dots indicates the order of the associated matrix. For example, the symbol D^{ab} is short for:

$$D^{ab} = e^{+2i\omega t} D^{ab}(+\omega, +\omega) + e^{+i\omega t} [D^{ab}(0, +\omega) + D^{ab}(+\omega, 0)] + D^{ab}(+\omega, -\omega) \\ + D^{ab}(-\omega, +\omega) + D^{ab}(0, 0) + e^{-i\omega t} [D^{ab}(0, -\omega) + D^{ab}(-\omega, 0)] + e^{-2i\omega t} D^{ab}(-\omega, -\omega). \quad (9.22)$$

The matrices F , C , S , and ε can be expanded in a similar fashion[104]. However, as we are using a fixed AO basis set, the overlap matrix S is independent of the field ($S = S^{(0)}$), resulting in vanishing terms above zeroth-order. The same holds for the Coulomb supermatrix

J and the Hartree-Fock exchange matrix K , but not for its DFT equivalent v_{xc} . As the most important difference between the TDHF equations and the time-dependent DFT equations arises from this difference between the HF exchange potential and the xc potential in DFT, we will show in the next section how the xc potential is expanded in different orders of the electric field.

9.5 Expansion of xc potential

In this section, we show what a functional Taylor expansion of the time-dependent xc potential with respect to external electric perturbations looks like. We use the compact four-vector notation $\mathbf{x} = (\mathbf{r}, t)$ as in Reference [33] and start from the formula for a functional Taylor expansion[297] of a functional v_{xc} in the space-time point x , with a functional dependence on the total external potential v_{ext} (which includes the interaction with the nuclei, etcetera). If this external potential is slightly perturbed by the electric field E , we have:

$$\begin{aligned} v_{\text{xc}}[v_{\text{ext}} + \mu \cdot E](\mathbf{x}) &= v_{\text{xc}}[v_{\text{ext}}](\mathbf{x}) + \int \frac{\delta v_{\text{xc}}(\mathbf{x})}{\delta v_{\text{ext}}(\mathbf{y})} \Big|_{E=0} \mu \cdot E(\mathbf{y}) d\mathbf{y} \\ &+ \frac{1}{2!} \int \int \frac{\delta^2 v_{\text{xc}}(\mathbf{x})}{\delta v_{\text{ext}}(\mathbf{y}) \delta v_{\text{ext}}(\mathbf{y}')} \Big|_{E=0} \mu \cdot E(\mathbf{y}) \mu \cdot E(\mathbf{y}') d\mathbf{y} d\mathbf{y}' + \dots, \end{aligned} \quad (9.23)$$

where all functional derivatives are to be evaluated at the unperturbed external potential ($E = 0$). Splitting the electric perturbation in its Cartesian components $\mu_a E^a, \mu_b E^b, \dots$ as in Equation (9.13), this becomes:

$$\begin{aligned} v_{\text{xc}}[v_{\text{ext}} + \sum_a \mu_a E^a](\mathbf{x}) &= v_{\text{xc}}[v_{\text{ext}}](\mathbf{x}) + \sum_a \int \frac{\delta v_{\text{xc}}(\mathbf{x})}{\delta v_{\text{ext}}(\mathbf{y})} \Big|_{\rho=\rho^{(0)}} \mu_a E^a(\mathbf{y}) d\mathbf{y} \\ &+ \frac{1}{2!} \sum_a \sum_b \int \int \frac{\delta^2 v_{\text{xc}}(\mathbf{x})}{\delta v_{\text{ext}}(\mathbf{y}) \delta v_{\text{ext}}(\mathbf{y}')} \Big|_{\rho=\rho^{(0)}} \mu_a E^a(\mathbf{y}) \mu_b E^b(\mathbf{y}') d\mathbf{y} d\mathbf{y}' + \dots, \end{aligned} \quad (9.24)$$

where the derivatives are evaluated at the converged SCF density $\rho^{(0)}$ (equivalent to $E = 0$). Although all results can be generalized to higher order, we will restrict ourselves to two fields here, as this is sufficient for our present purposes.

Instead of the functional derivatives with respect to external perturbations in Equation (9.24), we require derivatives with respect to perturbed densities. Similar derivatives have been considered in Ref.[33], and by direct analogy to Equation (179) in section 5.2 of that work, we get:

$$\frac{\delta^2 v_{\text{xc}}(\mathbf{x})}{\delta v_{\text{ext}}(\mathbf{y}) \delta v_{\text{ext}}(\mathbf{y}')} = \int d\mathbf{z} \int d\mathbf{z}' \frac{\delta^2 v_{\text{xc}}(\mathbf{x})}{\delta \rho(\mathbf{z}') \delta \rho(\mathbf{z})} \frac{\delta \rho(\mathbf{z}')}{\delta v_{\text{ext}}(\mathbf{y})} \frac{\delta \rho(\mathbf{z})}{\delta v_{\text{ext}}(\mathbf{y}')} + \int d\mathbf{z} \frac{\delta v_{\text{xc}}(\mathbf{x})}{\delta \rho(\mathbf{z})} \frac{\delta^2 \rho(\mathbf{z})}{\delta v_{\text{ext}}(\mathbf{y}) \delta v_{\text{ext}}(\mathbf{y}')} \quad (9.25)$$

with a similar expression for the first functional derivative. Here, all functional derivatives are again to be evaluated at $\rho = \rho^{(0)}$. We employ the usual notation[33] for the functional derivatives of the time-dependent xc potential with respect to the time-dependent density (or

densities). These functional derivatives f_{xc} and g_{xc} are the so-called xc kernels of TDDFT:

$$\begin{aligned} f_{\text{xc}}(\mathbf{z}, \mathbf{z}') &\equiv \frac{\delta v_{\text{xc}}(\mathbf{z})}{\delta \rho(\mathbf{z}')} \Big|_{\rho=\rho^{(0)}} \\ g_{\text{xc}}(\mathbf{z}, \mathbf{z}', \mathbf{z}'') &\equiv \frac{\delta^2 v_{\text{xc}}(\mathbf{z})}{\delta \rho(\mathbf{z}') \delta \rho(\mathbf{z}'')} \Big|_{\rho=\rho^{(0)}}. \end{aligned} \quad (9.26)$$

The functional derivatives $\delta \rho(\mathbf{x})/\delta v_{\text{ext}}(\mathbf{y})$ and $\delta^2 \rho(\mathbf{x})/\delta v_{\text{ext}}(\mathbf{y})\delta v_{\text{ext}}(\mathbf{y}')$ are in fact the exact first- and second-order response functions, which relate the perturbations $\mu_a E^a, \mu_b E^b, \dots$ to the perturbed first- and second-order densities ρ^a and ρ^{ab} :

$$\begin{aligned} \rho^a(\mathbf{x}) &= \int d\mathbf{y} \frac{\delta \rho(\mathbf{x})}{\delta v_{\text{ext}}(\mathbf{y})} \mu_a E^a(\mathbf{y}) \\ \rho^{ab}(\mathbf{x}) &= \int d\mathbf{y} \int d\mathbf{y}' \frac{\delta^2 \rho(\mathbf{x})}{\delta v_{\text{ext}}(\mathbf{y}) \delta v_{\text{ext}}(\mathbf{y}')} \mu_a E^a(\mathbf{y}) \mu_b E^b(\mathbf{y}'). \end{aligned} \quad (9.27)$$

Combining the notation of the xc kernels with these identities, and substituting everything in Equation (9.24) leads to:

$$\begin{aligned} v_{\text{xc}}(\mathbf{x}) &= v_{\text{xc}}^{(0)}(\mathbf{x}) + \sum_a \int d\mathbf{z} f_{\text{xc}}(\mathbf{x}, \mathbf{z}) \rho^a(\mathbf{z}) \\ &+ \frac{1}{2!} \sum_{a,b} \left[\int d\mathbf{z} \int d\mathbf{z}' g_{\text{xc}}(\mathbf{x}, \mathbf{z}', \mathbf{z}) \rho^a(\mathbf{z}') \rho^b(\mathbf{z}) + \int d\mathbf{z} f_{\text{xc}}(\mathbf{x}, \mathbf{z}) \rho^{ab}(\mathbf{z}) \right] + \dots \end{aligned} \quad (9.28)$$

We want to write this equation in the same shorthand notation as was used for the density matrix in Equations (9.21) and (9.22), using the fact that the n -th order density $\rho^{ab\dots n}$ is known in terms of the associated density matrix:

$$\rho^{ab\dots n}(\mathbf{r}, t) = \sum_{\mu\nu} [D^{ab\dots n}(t)]_{\mu\nu} \chi_\mu(\mathbf{r}) \chi_\nu(\mathbf{r}). \quad (9.29)$$

If we furthermore use that only the differences $t - t'$, $t - t''$ between the time variables t , t' , and t'' , associated with respectively x , z , and z' , are of importance, we arrive after some algebra at the final result for this section:

$$\begin{aligned} [v_{\text{xc}}^a(\omega_a)]_{\kappa\lambda} &= \sum_{\mu\nu} [f_{\text{xc}}(\omega_a)]_{\kappa\lambda\mu\nu} [D^a(\omega_a)]_{\mu\nu} \\ [v_{\text{xc}}^{ab}(\omega_a, \omega_b)]_{\kappa\lambda} &= \sum_{\mu\nu} [f_{\text{xc}}(\omega_a + \omega_b)]_{\kappa\lambda\mu\nu} [D^{ab}(\omega_a, \omega_b)]_{\mu\nu} \\ &+ \sum_{\mu\nu} \sum_{\sigma\tau} [g_{\text{xc}}(\omega_a, \omega_b)]_{\kappa\lambda\mu\nu\sigma\tau} [D^a(\omega_a)]_{\mu\nu} [D^b(\omega_b)]_{\sigma\tau}, \end{aligned} \quad (9.30)$$

where we have adopted the following notation for the matrix elements of the Fourier-transformed xc kernels:

$$\begin{aligned} [f_{\text{xc}}(\omega_a)]_{\kappa\lambda\mu\nu} &= \iint d\mathbf{r} d\mathbf{r}' \chi_\kappa(\mathbf{r}) \chi_\lambda(\mathbf{r}) f_{\text{xc}}(\mathbf{r}, \mathbf{r}', \omega_a) \chi_\mu(\mathbf{r}') \chi_\nu(\mathbf{r}') \\ [g_{\text{xc}}(\omega_a, \omega_b)]_{\kappa\lambda\mu\nu\sigma\tau} &= \iiint d\mathbf{r} d\mathbf{r}' d\mathbf{r}'' \chi_\kappa(\mathbf{r}) \chi_\lambda(\mathbf{r}) g_{\text{xc}}(\mathbf{r}, \mathbf{r}', \mathbf{r}'', \omega_a, \omega_b) \chi_\mu(\mathbf{r}') \chi_\nu(\mathbf{r}') \chi_\sigma(\mathbf{r}'') \chi_\tau(\mathbf{r}'') \end{aligned} \quad (9.31)$$

We emphasize already at this point that these matrix elements are never actually evaluated in practical calculations, as this would be very time-consuming. Equation (9.30) for $v_{xc}^{(2)}$ is a generalization of Equation (79) in Reference [298] for the static case, which reads:

$$v_{xc}^{bc} = v'_{xc}\rho^{bc} + v''_{xc}\rho^b\rho^c, \quad (9.32)$$

and which can be regarded as an application of the ordinary chain rule for differentiation. The frequency-dependent extension of the related third-order expression

$$v_{xc}^{abc} = v'''_{xc}\rho^a\rho^b\rho^c + v''_{xc}\left(\rho^{ab}\rho^c + \rho^{ac}\rho^b + \rho^{bc}\rho^a\right) + v'_{xc}\rho^{abc} \quad (9.33)$$

is required for such properties as THG.

9.6 Expressions for the higher-order Kohn–Sham matrices in DFT

Using the results of the previous section, and the same expansion of the KS matrix as was given for the density matrix in Equations (9.21) and (9.22), we can derive the DFT expression for the higher-order KS matrices. The zeroth-order KS matrix is the one used in ordinary (time-independent) DFT:

$$F_s^{(0)} = h^{(0)} + D^{(0)} \times (2J) + v_{xc}^{(0)}, \quad (9.34)$$

where $h^{(0)}$ contains the external potential terms which are of zero order in the external field: the kinetic energy and nuclear Coulomb field. The Coulomb supermatrix J is independent of the field, resulting in a Coulomb term in the n -th order KS matrix $F_s^{ab\dots n}(\omega_a, \omega_b, \dots, \omega_n)$ of the form $D^{ab\dots n}(\omega_a, \omega_b, \dots, \omega_n) \times (2J)$. Only in the first-order KS matrices, the external perturbation H^a appears:

$$\begin{aligned} F_s^a(\omega_a) &= H^a + D^a(\omega_a) \times (2J) + v_{xc}^a(\omega_a) \\ F_s^a(0) &= H^a + D^a(0) \times (2J) + v_{xc}^a(0). \end{aligned} \quad (9.35)$$

Here, v_{xc}^a is given by Equation (9.30). All higher-order KS matrices contain only a Coulomb and an xc part. The Coulomb part is the same as in TDHF theory. Using the notation established above for the xc part, we can give the general formula for the higher-order KS matrices:

$$F_s^{ab\dots n}(\omega_a, \omega_b, \dots, \omega_n) = D^{ab\dots n}(\omega_a, \omega_b, \dots, \omega_n) \times (2J) + v_{xc}^{ab\dots n}(\omega_a, \omega_b, \dots, \omega_n), \quad (9.36)$$

where the frequencies $\omega_a, \omega_b, \dots, \omega_n$ are equal to zero or $\pm\omega$ in this work. The matrices $v_{xc}^{ab\dots n}(\omega_a, \omega_b, \dots, \omega_n)$ have been given in Equation (9.30) for first and second-order. The higher-order results can straightforwardly be obtained from the results in the previous sections.

9.7 Solving the nonlinear response equations using the $(2n + 1)$ -theorem

Now that we have established the form of the higher-order KS matrices in DFT, we can continue with the solution of the (nonlinear) response equations. First, we will give an outline of how the equations are derived and after that, how they are solved efficiently. One starts by inserting the Taylor expansions for F_s , C , ε , and D in the time-dependent KS equations [Equation (9.8)], the normalization condition [Equation (9.9)], and expression for the density matrix [Equation (9.10)]. Equating expressions on the left- and right-hand sides of these equations with the same time-dependence leads to the higher-order coupled equations. Up to third-order, these have been written out by Karna and Dupuis in Tables 2, 3, and 4 of Reference [104]. For example, the first-order time-dependent KS equations can be written as:

$$F_s^a(\omega)C^{(0)} + F_s^{(0)}C^a(\omega) + \omega S^{(0)}C^a(\omega) = S^{(0)}C^a(\omega)\varepsilon^{(0)} + S^{(0)}C^{(0)}\varepsilon^a(\omega), \quad (9.37)$$

where $\omega = 0$ for the static first-order equations and can be equal to either ω or $-\omega$ in the frequency-dependent case. As the higher-order expressions become rather lengthy and the DFT equations are identical to the TDHF equations, because the explicit form of the Fock or KS operator is not yet required, we will not repeat those expressions, and simply refer to Tables 2, 3, and 4 of Reference [104].

In order to calculate the desired NLO properties, one needs to solve the TDKS equations iteratively up to a certain order n , each time using the solutions to the lower-order equations. As a start, the static KS equations are solved, resulting in the matrices $F_s^{(0)}$, $C^{(0)}$, $\varepsilon^{(0)}$, and $D^{(0)}$, which yields the converged SCF density $\rho^{(0)}$. These matrices are needed for the solution of the first-order KS equations, which yields the first-order density matrix, from which the frequency-dependent polarizability is immediately obtained through Equation (9.19). We have previously described[34] how this first-order density can be obtained in an efficient, iterative N^3 process, by making use of auxiliary basis function techniques, which are also often used for speeding up ordinary (zeroth-order) DFT calculations.

After the first-order equations have been solved, all the ingredients for an iterative solution of the second-order equations are available, which can be solved with the same techniques as the first-order equations. After the second-order equations are solved, the second-order density matrix is available, from which the frequency-dependent hyperpolarizability tensor is obtained through Equation (9.19). This process can be repeated to arbitrary order, giving access to $\gamma_{abcd}(-\omega_\sigma; \omega_b, \omega_c, \omega_d)$ and even higher-order hyperpolarizability tensors. However, this will require many iterative calculations if the full hyperpolarizability tensors are required (all possible combinations for a, b, c, d) for different optical processes (different combinations of frequencies $\omega_b, \omega_c, \omega_d$).

A more efficient approach is obtained from the use of the $(2n + 1)$ -theorem. It can be shown that for the calculation of the frequency-dependent first hyperpolarizability tensors β , only first-order quantities are needed[104]. Similarly, the calculation of γ and δ (the third hyperpolarizability tensor) requires the knowledge of second-order quantities only. For example, only nine first-order response equations need to be solved in order to obtain all components abc of the first hyperpolarizability tensors β governing SHG [$\beta_{abc}(-2\omega; \omega, \omega)$],

EOPE [$\beta_{abc}(-\omega; \omega, 0)$], Optical Rectification (OR) [$\beta_{abc}(0; \omega, -\omega)$] and the static hyperpolarizability [$\beta(0; 0, 0)$]. If the $(2n + 1)$ -theorem would not be used, the self-consistent solution of 27 second-order equations would be required in the most general case. If only the first hyperpolarizability tensor governing static effects is needed, the solution of only three first-order equations suffices.

After the first-order equations have been solved, the first hyperpolarizability tensors are obtained from a series of matrix multiplications, which do not contribute significantly to the required computing time. A practical consideration is that less programming effort is needed for the implementation of the $(2n + 1)$ equations, as only low-order response equations have to be solved. This explains the desirability of obtaining equations for β in terms of first-order quantities only. Karna and Dupuis have presented equations for all β and γ tensors which govern optical effects involving fields of frequency ω and frequency 0, in which the $(2n + 1)$ -theorem has been used. For the important SHG and THG cases, they also give a step-by-step derivation of these results for the TDHF case. The DFT results can be obtained by following those steps. Here we will discuss the SHG case, for which an eight step algorithm is given by Karna and Dupuis (page 494-495 of Ref. [104]). As the first seven steps do not use the explicit form of the Fock or KS matrices, the DFT equations remain identical to the TDHF equations, until the final step. After the first seven steps for the SHG case, we have:

$$\begin{aligned}
& C^{a\dagger}(+2\omega)F^{bc}(\omega, \omega)C^0 + C^{a\dagger}(+2\omega)F^b(\omega)C^c(\omega) + C^{a\dagger}(+2\omega)F^c(\omega)C^b(\omega) \\
& + C^{a\dagger}(+2\omega)F^0C^{bc}(\omega, \omega) + 2\omega C^{a\dagger}(+2\omega)S^0C^{bc}(\omega, \omega) \\
& - C^{0\dagger}F^a(-2\omega)C^{bc}(+\omega, +\omega) - C^{a\dagger}(+2\omega)F^0C^{bc}(+\omega, +\omega) - 2\omega C^{a\dagger}(+2\omega)S^0C^{bc}(+\omega, +\omega) \\
& + C^{0\dagger}F^{bc}(+\omega, +\omega)C^a(-2\omega) + C^{c\dagger}(-\omega)F^b(+\omega)C^a(-2\omega) + C^{b\dagger}(-\omega)F^c(+\omega)C^a(-2\omega) \\
& + C^{bc\dagger}(-\omega, -\omega)F^0C^a(-2\omega) - 2\omega C^{bc\dagger}(-\omega, -\omega)S^0C^a(-2\omega) \\
& - C^{bc\dagger}(-\omega, -\omega)F^a(-2\omega)C^0 - C^{bc\dagger}(-\omega, -\omega)F^0C^a(-2\omega) + 2\omega C^{bc\dagger}(-\omega, -\omega)S^0C^a(-2\omega) \\
& = C^{a\dagger}(+2\omega)S^0C^{bc}(\omega, \omega)\varepsilon^0 + C^{a\dagger}(+2\omega)S^0C^b(\omega)\varepsilon^c(\omega) + C^{a\dagger}(+2\omega)S^0C^c(\omega)\varepsilon^b(\omega) \\
& + C^{a\dagger}(+2\omega)S^0C^0\varepsilon^{bc}(\omega, \omega) - \varepsilon^0C^{a\dagger}(+2\omega)S^0C^{bc}(+\omega, +\omega) - \varepsilon^{a\dagger}(+2\omega)C^{0\dagger}S^0C^{bc}(+\omega, +\omega) \\
& + \varepsilon^0C^{bc\dagger}(-\omega, -\omega)S^0C^a(-2\omega) + \varepsilon^c(+\omega)C^{b\dagger}(-\omega)S^0C^a(-2\omega) + \varepsilon^b(+\omega)C^{c\dagger}(-\omega)S^0C^a(-2\omega) \\
& + \varepsilon^{bc}(+\omega, +\omega)C^{0\dagger}S^0C^a(-2\omega) - C^{bc\dagger}(-\omega, -\omega)S^0C^a(-2\omega)\varepsilon^0 \\
& - C^{bc\dagger}(-\omega, -\omega)S^0C^0\varepsilon^a(-2\omega)
\end{aligned} \tag{9.38}$$

In the final step, the goal is to end up with an equation of the form

$$\beta_{abc}(-2\omega; \omega, \omega) = -\text{Tr} \left[H^a D^{bc}(\omega, \omega) \right] = \text{Tr}[\text{first - order quantities}] \tag{9.39}$$

This is achieved by multiplying Equation (9.38) on both sides with the occupation number matrix n and taking the trace. One furthermore adds the quantity $\text{Tr}[n \{ C^{b\dagger}(-\omega)F^a(-2\omega)C^c(+\omega) + C^{c\dagger}(-\omega)F^{a\dagger}(+2\omega)C^b(+\omega) \}]$ to both sides of the equation[104]. While some second-order terms cancel in a trivial way, others can be removed by using the property of the trace operator that $\text{Tr}[ABC] = \text{Tr}[CAB]$, the fact that n is a diagonal matrix and the properties of the ε Lagrangian matrices[104]. One furthermore rewrites the equation in terms of the second-order density matrix and the dipole moment matrix, in order to obtain a result of the form of Equation (9.39).

All this proceeds in exactly the same way in the DFT and TDHF cases. The remaining term which needs to be removed contains the second-order Fock or KS matrix. This term is of the form:

$$\text{Tr} \left[-F_s^a(-2\omega)D^{bc}(+\omega, +\omega) + D^a(-2\omega)F_s^{bc}(+\omega, +\omega) \right] \quad (9.40)$$

Using the DFT expressions for the first and second-order KS matrices, this can be rewritten to:

$$\begin{aligned} & \text{Tr} \left[-F_s^a(-2\omega)D^{bc}(+\omega, +\omega) + D^a(-2\omega)F_s^{bc}(+\omega, +\omega) \right] \\ &= -\text{Tr} \left[H^a D^{bc}(+\omega, +\omega) + D^a(-2\omega) \times (2J^0) D^{bc}(+\omega, +\omega) + f_{xc}(2\omega) D^a(-2\omega) D^{bc}(+\omega, +\omega) \right. \\ & \quad \left. - D^a(-2\omega) D^{bc}(+\omega, +\omega) \times (2J^0) - D^a(-2\omega) \left(f_{xc}(2\omega) D^{bc}(\omega, \omega) + g_{xc}(\omega, \omega) D^b(\omega) D^c(\omega) \right) \right] \\ &= -\text{Tr} \left[H^a D^{bc}(+\omega, +\omega) - g_{xc}(\omega, \omega) D^a(-2\omega) D^b(\omega) D^c(\omega) \right]. \end{aligned} \quad (9.41)$$

Here, Equation (9.30) has been used for the xc terms. The second term on the right-hand side of Equation (9.41) is an additional term in the DFT expression for $\beta(-2\omega; \omega, \omega)$, not present in the TDHF case, which is due to the nonlinearity of v_{xc} in terms of the density. Repeating this procedure for the other processes yields a general expression for the extra terms:

$$\left[\beta^{\text{DFT}} \right]_{abc}(-\omega_\sigma; \omega_b, \omega_c) = \left[\beta^{\text{HF}} \right]_{abc}(-\omega_\sigma; \omega_b, \omega_c) + \text{Tr} \left[g_{xc}(\omega_b, \omega_c) D^a(-\omega_\sigma) D^b(\omega_b) D^c(\omega_c) \right]. \quad (9.42)$$

These equations are very schematic in the sense that the rest of the $(2n + 1)$ -expression for β is equal in form only for the DFT and HF cases. Explicit expressions are given below, and can also be found in Table VII of Reference [104]. The final term (the extra DFT term) is most efficiently calculated through a numerical integration:

$$\begin{aligned} & \text{Tr} \left[g_{xc}(\omega_b, \omega_c) D^a(-\omega_\sigma) D^b(\omega_b) D^c(\omega_c) \right] = \\ & \int d^3 \mathbf{r} \int d^3 \mathbf{r}' \int d^3 \mathbf{r}'' g_{xc}(\mathbf{r}, \mathbf{r}', \mathbf{r}'', \omega_b, \omega_c) \rho^a(\mathbf{r}, -\omega_\sigma) \rho^b(\mathbf{r}', \omega_b) \rho^c(\mathbf{r}'', \omega_c). \end{aligned} \quad (9.43)$$

This numerical integration looks quite expensive, but, in the usual approximation to g_{xc} (see following section), it becomes trivial as it reduces to a single, instead of triple, integral. For the static case, the extra DFT term was already obtained by Fournier[298], and by Colwell *et al.*[134], while Komornicki and Fitzgerald[299] have also considered the efficient evaluation of similar terms.

9.8 Approximations used in DFT response calculations

Although the density functional formalism for the treatment of frequency-dependent NLO response is exact in principle, practical calculations require approximations to the unknown xc functionals. The functionals which have to be approximated are the usual xc potential $v_{xc}(\mathbf{r})$, which is needed in the zeroth-order KS equations, and its functional derivatives f_{xc} , g_{xc} , and so on. For $v_{xc}(\mathbf{r})$, which is the functional derivative of the xc energy functional E_{xc} with respect to the (time-independent) density, many approximations exist. The most

usual ones are those based upon the Local Density Approximation (LDA), for example in the Vosko–Wilk–Nusair (VWN) parametrization[4], or the potentials based on the Generalized Gradient Approximations (GGAs), such as the exchange functional by Becke[138], and the Perdew[139] or Lee–Yang–Parr[129] correlation functionals.

The xc potential determines the zeroth-order KS orbitals and their one-electron energies. It is consequently clear that the quality of the xc potential is of the utmost importance for the hyperpolarizability results. In fact, the usual potentials mentioned above are not the most suitable ones for response calculations as they decay exponentially, whereas the correct decay should be Coulombic. It has been shown several times[74, 184] that potentials which do possess the correct asymptotic behavior provide significantly more accurate results than the LDA or GGA potentials. The choice of the xc potential hardly influences the time needed in the response calculation, as it is needed in the solution of the usual KS equations only. After that, only the resulting orbitals and one-electron energies are needed.

The xc kernels are more complicated functionals than the xc potential. Whereas the xc potential depends upon \mathbf{r} only, g_{xc} , for example, depends upon the spatial variables \mathbf{r} , \mathbf{r}' , and \mathbf{r}'' and the frequency variables ω_b and ω_c . Very little is known about the xc kernels f_{xc} and g_{xc} . Because of the lack of more refined approximations as well as for efficiency reasons, one has usually employed very simple approximations to these kernels in the practical calculations until now. Although a frequency-dependent model for f_{xc} exists (the Gross-Kohn kernel[160, 206, 31]), such a model is not available for the higher-order kernels. Furthermore, the Gross–Kohn kernel exhibits some undesired properties. As a consequence, in virtually all molecular applications of time-dependent density functional response theory, the so-called adiabatic approximation has been invoked. The term adiabatic is used because the time-dependent xc potential is assumed to depend in the same way on the time-dependent density as the static xc potential depends upon the time-independent density, which is a good approximation for slow (adiabatic) processes. A direct consequence of this approximation is that the frequency-independent versions of the xc kernels are used:

$$\begin{aligned} f_{xc}^{\text{adiabatic}}(\mathbf{r}, \mathbf{r}', \omega) &= f_{xc}(\mathbf{r}, \mathbf{r}', \omega = 0) \\ g_{xc}^{\text{adiabatic}}(\mathbf{r}, \mathbf{r}', \mathbf{r}'', \omega_a, \omega_b) &= g_{xc}(\mathbf{r}, \mathbf{r}', \mathbf{r}'', \omega_a = 0, \omega_b = 0). \end{aligned} \quad (9.44)$$

This approximation is justified for small ω -values, but it appears to work well even outside this domain. At the moment, it remains unclear whether or not the adiabatic approximation is a severe one. If one uses the functional derivative of the LDA potential, in combination with the adiabatic approximation, one obtains the simple ALDA kernels, which are local in space as well:

$$\begin{aligned} f_{xc}^{\text{ALDA}}(\mathbf{r}, \mathbf{r}', \omega) &= f_{xc}^{\text{hom}}(\mathbf{r}, \mathbf{r}', \omega = 0)\delta(\mathbf{r} - \mathbf{r}') \\ g_{xc}^{\text{ALDA}}(\mathbf{r}, \mathbf{r}', \mathbf{r}'', \omega_a, \omega_b) &= g_{xc}^{\text{hom}}(\mathbf{r}, \mathbf{r}', \mathbf{r}'', \omega_a = 0, \omega_b = 0)\delta(\mathbf{r} - \mathbf{r}')\delta(\mathbf{r} - \mathbf{r}''). \end{aligned} \quad (9.45)$$

Here, we have added the specification "hom" to the kernel in order to specify that this approximation is based upon the homogeneous electron gas. The spatial locality of the ALDA kernels ensures the computational efficiency of the DFT response calculations. If a model is used in which the spatial nonlocality of the kernels is taken into account (as for example in the f_{xc} -kernel based upon the time-dependent optimized effective potential (TDOEP) in

the exchange-only approximation[101]), this efficiency is lost to a great extent. This is due to the fact that six-dimensional numerical integrations will have to be performed for f_{xc} and nine-dimensional numerical integrations for g_{xc} . In the ALDA, only three-dimensional numerical integrations are required, due to the delta functions in Equation (9.45).

At present, there are no models for f_{xc} which clearly improve upon the ALDA, although such models will likely appear in the future. For this reason, the ALDA seems the most logical choice for the moment. If more refined approximations for f_{xc} and g_{xc} will appear in the future, a compromise between accuracy and efficiency will be required. Numerical evidence for atoms and small molecules[272] suggests however that the major approximation made in the response calculations is usually due to the xc potential, and not to its functional derivatives. Our preliminary hyperpolarizability results[120] suggest furthermore that g_{xc} has only a small influence on the final β -values (at least in the ALDA). As a nonlocal model for g_{xc} will enormously increase the computational cost of the calculations, this will probably not be worthwhile for a long time. The influence of the chosen model for f_{xc} on β is larger.

9.9 Implementation

In this section we are concerned with the question what the most efficient implementation of the DFT equations for the frequency-dependent hyperpolarizabilities should look like. As we have described our implementation for the solution of the linear response equations previously[34], we will be mainly concerned with the hyperpolarizabilities here, but we will discuss the most important points of the linear response calculations. Using Karna and Dupuis' notation, where G stands for the Fock/KS matrix on eigenfunction basis, we can write for the first-order KS matrix G_s^a :

$$[G_s^a(\omega)]_{pq} = \int d\mathbf{r} \phi_p(\mathbf{r}) [\mu_a E^a(\mathbf{r}, \omega) + v_{\text{Coul}}^a(\mathbf{r}) + v_{xc}^a(\mathbf{r})] \phi_q(\mathbf{r}). \quad (9.46)$$

All matrix elements of this type, whether they are on eigenfunction basis or on AO basis, are determined by numerical integration, because the complicated xc term makes an analytical evaluation impossible.

As the KS matrix G_s depends upon the first-order density matrix, through the potential terms $v_{\text{Coul}}^a(\mathbf{r})$ and $v_{xc}^a(\mathbf{r})$, a self-consistent solution is required, as the first-order density matrix in its turn is determined by the first-order KS matrix. In our implementation, this iterative process can be performed either in the AO basis or in the eigenfunction basis. For very large systems, the AO option has the advantage that integral prescreening and more general linear scaling techniques[114] can be applied. This would result in a drastic reduction of the number of integrals which have to be calculated and in the cost per integral, since the parts of space which do not contribute to a certain integral can be excluded from the numerical integration. As in the solution of the ordinary KS equations, such techniques will in the future result in a solution of the linear response equations which scales linearly with the number of atoms.

However, for medium-sized and highly symmetric systems, the eigenfunction basis is preferred, as only matrix elements between occupied and virtual orbitals are required, and

as symmetry can be used straightforwardly to further reduce the number of numerical integrations. Because one needs substantial basis sets for an accurate hyperpolarizability calculation, the number of occupied orbitals times the number of virtual orbitals may be substantially less than $N * (N + 1)/2$, where N is the number of (primitive) AOs. As the linear scaling techniques have not yet been implemented, the eigenfunction option is the default one in our implementation. The Coulomb potential of the first-order density in Equation (9.46) is obtained from a fitted density $\tilde{\rho}^{(1)}$, reducing the cost of the solution of the KS equations and the linear response equations from N^4 to N^3 [34].

The most demanding hyperpolarizability calculation for β is one where all components of β for all optical effects considered in this work are required. In such a case, the linear response equations need to be solved at frequencies $0, \omega$ and 2ω , with external fields in the x, y , and z directions. The converged first-order KS matrices are passed to the part of the code for calculating the first hyperpolarizabilities. Although only the occupied-virtual block of the first-order KS matrix is needed in a linear response calculation, the occupied-occupied and virtual-virtual blocks are also generated (from the converged first-order density matrix), because they are necessary for the nonlinear response calculations. From the KS matrices, all other first-order information can be regenerated. For example, the first-order transformation matrices $U^a(\omega_a)$, defined by[104]

$$C^{(0)}U^a(\omega_a) = C^a(\omega_a) \quad (9.47)$$

are, with a suitable (nondiagonal!) choice for the Lagrangian multiplier matrices[104], given by:

$$[U^a(\omega_a)]_{pq} = \frac{[G_s^a(\omega_a)]_{pq}}{\varepsilon_q^{(0)} - \varepsilon_p^{(0)} - \omega_a}, \quad (9.48)$$

where $\varepsilon_q^{(0)}$ and $\varepsilon_p^{(0)}$ are the KS one-electron energies and where U is nonzero only for the occupied-virtual blocks. This choice for the ε -matrix represents what Gonze[249] calls the parallel-transport gauge. An alternative choice is to take a diagonal Lagrangian multiplier matrix ε , the diagonal gauge[249]. Certain technical problems which have to be addressed in the diagonal gauge, are absent in the parallel-transport gauge, such as the fact that the occupied-occupied block of the U -matrix is no longer zero. In this block, divergent terms may appear if $\varepsilon_q^{(0)} = \varepsilon_p^{(0)}$ and $\omega = 0$. For this reason, most practical implementations use the parallel-transport gauge[104, 249], in which the first-order Lagrangian matrices ε^a are block-diagonal and given by:

$$[\varepsilon^a(\omega_a)]_{pq} = [G_s^a(\omega_a)]_{pq}, \quad (9.49)$$

where p and q are both occupied or both virtual.

The equations of the previous section can be used to obtain the DFT expressions for the first hyperpolarizability tensors. Using the fact that the diagonal parts of the first-order Fock matrices in Table VII of Reference [104] are equal to the diagonal blocks of the first-order Lagrangian multiplier matrices ε [Equation (9.49)], we obtain the following compact $(2n+1)$ -expressions for the DFT frequency-dependent hyperpolarizabilities $\beta_{abc}(-\omega_\sigma; \omega_b, \omega_c)$:

$$\begin{aligned} \beta_{abc}(-\omega_\sigma; \omega_b, \omega_c) &= \text{Tr} \left\{ nU^a(-\omega_\sigma)[G_s^b(\omega_b), U^c(\omega_c)]_- \right\} \\ &+ \text{all permutations of } (a, -\omega_\sigma), (b, \omega_b), (c, \omega_c) \end{aligned}$$

$$+ \text{Tr} [g_{xc}(\omega_b, \omega_c) D^a(-\omega_\sigma) D^b(\omega_b) D^c(\omega_c)], \quad (9.50)$$

where $[\]_-$ stands for the ordinary commutator and where the final term is the extra term of the DFT equations. In this work, the frequencies ω_b and ω_c are assumed to be equal to zero or ω , but Equation (9.50) is valid for general frequencies.

It should be clear from the above that the work which is needed for the calculation of the first hyperpolarizability tensors β is determined by the time needed for the solution of the linear response equations (9 linear response equations in the worst case). Afterwards, a few matrix multiplications suffice for the determination of all discussed β tensors. One can use the form of these matrices [for example the fact that the matrices are block-off-diagonal (U) or diagonal (n)] to further reduce the work done in these matrix multiplications, but this is not the time-determining factor in the calculation.

The term which is extra in the DFT expression for β (the final term in Equation (9.50)) should be treated carefully. One should not calculate the term in the form in which it is given in Equation (9.50). That would require evaluating all matrix elements $[g_{xc}]_{\kappa\lambda\mu\nu\sigma\tau}$ in Equation (9.31), which would be very expensive. Instead one should numerically evaluate the integral in Equation (9.43)[298], which, with the ALDA kernel, reduces to:

$$\int d^3\mathbf{r} g_{xc}^{\text{ALDA}}(\mathbf{r}) \rho^a(\mathbf{r}, -\omega_\sigma) \rho^b(\mathbf{r}, \omega_b) \rho^c(\mathbf{r}, \omega_c). \quad (9.51)$$

The numerical evaluation of this integral requires a negligible amount of computer time[298], but extreme care is needed in its evaluation. This can be seen from the asymptotic behavior of g_{xc}^{ALDA} . This kernel behaves as $\rho^{-5/3}$, implying that it diverges at infinity. This is counterbalanced by the first-order densities, which go to zero in an exponential fashion. This requires an accurate first-order density in the outer region of the molecule. The fitted first-order density displays certain anomalies in the outer region where the density is low, such as small oscillations around the exact density. For this reason, the exact (not fitted) first-order densities are calculated in the integration points and stored. Similarly, the xc kernels are calculated using the exact zero-order density $\rho^{(0)}$. Regions where the zero-order density is below a certain threshold are not taken into account, in order to prevent the occurrence of numerical problems in the evaluation of the integral. Similar remarks about the evaluation of this term were made by Lee and Colwell[135] for the static case.

9.10 Tests on the implementation and discussion of effects of a finite auxiliary basis set

The equations for the various hyperpolarizability tensors which have been derived in the previous sections hold rigorously if one does not use a density fit, or if the set of auxiliary basis functions (fit functions) is complete. In our implementation we have assumed that these results also hold to a good approximation for finite but large auxiliary basis sets. For example, we make the approximation that Equation (9.41) is valid for fitted densities as well. Similar approximations were made by Fournier[298] when considering static perturbations. Although taking the finiteness of the fit set into account would in principle be possible and

desirable, it would lead to considerable extra programming effort. Fournier, Andzelm and Salahub[300] have considered the analytic calculation of first-order derivatives in the presence of a fit. Second derivatives have been considered by both Dunlap and Andzelm[301] and by Komornicki and Fitzgerald[299], while Fournier[298] has considered both second and third derivatives in the presence of a density fit. All these authors consider time-independent properties only, but their work could still be followed to a large extent in order to obtain expressions where the fit approximation has been explicitly taken into account. In the ADF program the situation will be somewhat different from the case considered in these papers, as the density is fitted directly and not the potential due to this density.

It should be emphasized at this point that our aim here is primarily to document the technical accuracy of our implementation. We have previously shown that our implementation can be applied to molecules of the size of C_{60} [76], for which $\gamma_{zzzz}(0;0,0,0)$, $\gamma_{zzzz}(-\omega;\omega,0,0)$ and $\gamma_{zzzz}(-2\omega;\omega,\omega,0)$ were calculated for a range of frequencies. A calibration study on a wide set of small molecules, in which the appropriateness of several xc potentials is tested, and in which both static and frequency-dependent first and second hyperpolarizabilities are treated, is in progress[120]. A further application of our implementation to large polyene chains will also be presented in the near future[130].

Here, we will show that for (very) large basis and fit sets, the results from analytic calculations of β and finite difference calculations with respect to the polarizability in various small electric fields, are in fact identical. Tests are performed on He and CO in large basis sets (Tables 9.1 and 9.2) and on *para*-nitroaniline in a standard basis (Table 9.3). For Helium we calculate γ_{zzzz} from $\gamma_{zzzz}(-\omega;\omega,0,0) \approx 1000 \times \beta_{zzz}(-\omega;\omega,0) |_{E_1^z=0.001}$, where β_{zzz} is either calculated analytically, or from the FF differentiation of $\alpha_{zz}(-\omega;\omega)$ at $E = E_1^z \pm E_2^z$ and $E = E_1^z \pm 2E_2^z$ [302]:

$$\begin{aligned} \beta_{zzz}^{\text{FF}}(-\omega;\omega,0) |_{E=E_1^z} &= \frac{1}{E_2^z} \left(\frac{2}{3} \left[\alpha_{zz}(-\omega;\omega) |_{E=E_1^z+E_2^z} - \alpha_{zz}(-\omega;\omega) |_{E=E_1^z-E_2^z} \right] \right. \\ &\quad \left. - \frac{1}{12} \left[\alpha_{zz}(-\omega;\omega) |_{E=E_1^z+2E_2^z} - \alpha_{zz}(-\omega;\omega) |_{E=E_1^z-2E_2^z} \right] \right), \quad (9.52) \end{aligned}$$

where β^{FF} stands for the FF approximation to β , and where α is obtained analytically from the solution of the first-order KS equations. Although we are aware that γ_{zzzz} can be obtained more directly and efficiently from α , we use the present approach because it provides a more direct test of our implementation. Our static LDA[4] result of $\gamma_{zzzz} = \gamma = 87.9$ a.u. (which, in view of the huge basis and fit sets we used, should be close to the basis set limit) is too large by roughly a factor of two[251].

This is expected from the well-known deficiencies of the LDA approximation, and better results can be obtained with asymptotically correct xc potentials such as the Van Leeuwen–Baerends (LB94) potential[121]. However, as we have only implemented the ALDA for the xc kernels f_{xc} and g_{xc} , we can only perform "mixed" calculations with the LB94 potential, in which f_{xc} is not the functional derivative of v_{xc} . This implies that we cannot test the LB94 results with FF calculations, and that renders them useless for our present purpose of testing the implementation. In another work[120], the quality of different xc potentials for hyperpolarizability calculations will be established. The results from the finite difference calculations for Helium are compared to the analytical result in Table 9.1, for various field strengths E_2^z .

Both the static hyperpolarizability result and the EOKE result at $\omega = 0.05$ a.u. agree very well with the finite difference results, proving the correctness of the implementation for these effects.

In Table 9.2, we show our analytic and finite difference results [obtained from equations similar to Equation (9.52) but at zero field: $E = 0$] for the hyperpolarizability of CO. Here, we investigate the effects of using a finite auxiliary basis set. The basis set which has been used is quite large and gives results close to the basis set limit, as shown by a comparison of our most accurate results to those obtained in a basis set free manner by Dickson and Becke[203]. With a FF LDA calculation, they obtain -33.7 and -8.6 for β_{zzz} and β_{zxx} respectively, where we find -33.90 and -8.44. In the first three rows of Table 9.2, the analytic and finite difference results for the two independent components β_{zxx} and β_{zzz} of the static hyperpolarizability tensor of CO are compared. In these calculations, the fitted density was used for the evaluation of the (zeroth-order) xc potential in the solution of the KS equations. In the response equations, the xc terms are evaluated from the exact (not the fitted) density. It is clear that the agreement between the analytic and FF values is acceptable, in view of the sensitivity of this property, but not completely satisfactory. The deviations are 0.4% and 0.2%. If the xc potential is evaluated from the exact density (as shown in the fourth and fifth rows) the agreement between the finite difference and analytic results increases considerably. The deviations have reduced to 0.1% and 0.003%. A more important observation is that these results differ significantly from the results with an xc potential obtained from a fitted density. This shows that accuracy is required in all parts of the calculation if reliable hyperpolarizability results are required.

This becomes even clearer from the results in the final two rows, obtained in the same way as those from the first three rows, but with a medium-sized instead of a large fit set. (The large fit set consists of 13s, 11p, 10d, 10f, and 8g functions, giving a total of 254 STO auxiliary basis functions per atom. The medium-sized fit set consists of 8s, 7p, 6d, 7f, and 6g basis functions, which yields a total of 184 functions. This is to be compared with the basis set which consists of 4s, 3p, 1d, and 1f function to which we added diffuse functions: 2s, 2p, 2d, and 2f functions.) The analytic results differ in the order of 10% from the results in the first rows, showing that a large auxiliary basis is needed for a reliable analytic determination of hyperpolarizabilities of small systems. Furthermore, the deviations between the FF and analytic results have increased enormously. The differences are no less than 7.4% and 7.7%. This implies that in the results with a medium-sized fit set, the difference between a FF calculation and an analytic calculation is not negligible anymore. However, even in the FF case, a large fit set is required for high reliability.

Our final example is the *para*-nitroaniline molecule, in which we investigate the accuracy which can be reached for a medium-sized molecule in a standard valence triple zeta basis with two polarization functions, the largest standard basis in ADF. There is a large interest in this molecule[303, 237, 304, 302, 305], which we study in the BLYP[138, 129]-optimized planar $C(2v)$ geometry, due to its large hyperpolarizability β of which the zzz -component is the dominating part. As in Ref. [259], we have tested our implementation for the SHG tensor by checking if the dispersion formula (Refs.[306, 251] and references therein)

$$\beta_{zzz}(-\omega_\sigma; \omega_b, \omega_c) = \beta_{zzz}(0; 0, 0) \times \left(1 + A_{zzz}(\omega_\sigma^2 + \omega_b^2 + \omega_c^2) + \dots \right), \quad (9.53)$$

relating the frequency dependences of the various NLO effects, holds in our case if a normal basis set is used. From a fit to our $\beta_{zzz}(-\omega; \omega, 0)$ results at six frequencies from 0 to 0.005 a.u., we obtain $A_{zzz} = 54.845$ a.u., in excellent agreement with the value $A_{zzz} = 54.842$ a.u. from the analytic $\beta_{zzz}(-2\omega; \omega, \omega)$ results, which provides a strong indication for the correctness of our implementation for the SHG tensor. If we calculate $\beta_{zzz}(-\omega; \omega, 0)$ from a FF calculation on $\alpha_{zz}(-\omega; \omega)$ we obtain $\beta_{zzz}(0; 0, 0) = -1959$ a.u. and $A_{zzz} = 54.7$ a.u. both within 1% of the analytic result, which is very satisfactory as it shows that even standard basis and fit sets can be sufficiently accurate for large molecules. Incidentally, our value for A_{zzz} is close to the value of 50.6 a.u. from a fit[304] to the experimental values for the average β .

We have gathered our LDA and LB94 results for the first and second average hyperpolarizabilities in Table 9.3. Both the $\beta(-2\omega; \omega, \omega)$ and $\gamma(-2\omega; \omega, \omega, 0)$ results are in much improved agreement with the experimental values in comparison to previous *ab initio* studies [303, 237, 304, 302]. The static results as well as the frequency dependence are substantially higher than in those papers. We consider this improved agreement with the experimental values to be fortuitous in this case and relate it to the position of the all-important amino-to-nitro excitation energy, for which our LDA value of 3.41 eV is accidentally close to the experimental value[307] of 3.46 eV, obtained in a solvent. The resulting agreement supports the suggestion that the discrepancy between the experimental and *ab initio* values can be attributed to the solvent effect, for the description of which a simple two-state model [304] may be sufficient. A basis set study of our results falls outside of the scope of the present work, but due to the dominance of the amino-to-nitro excitation, we believe our values for β to be reliable, as the addition of diffuse functions is known to have a limited effect for this system[302]. For the second hyperpolarizability, the neglect of diffuse functions could be more important.

Our test calculations in which the numerical integration accuracy was varied indicate that demanding 5 accurate digits for a set of test integrals is generally sufficient for converged results, while the default value of 4 is sufficient for standard cases. Finally, we note that in other applications to large molecules, like polyene chains, [130] the effects of using a modest basis and fit set are seen to be acceptable. There, the use of the small standard double-zeta STO basis set in ADF with the accompanying standard fit sets gave satisfactory agreement with FF calculations, in comparison to the results for CO and *para*-nitroaniline shown here. We therefore conclude that the use of auxiliary basis functions ("the fit set") and the numerical integrations are additional sources of errors, which can however be kept under control.

9.11 Summary and outlook

In this work, we have derived the equations which are needed for calculating frequency-dependent hyperpolarizabilities using time-dependent DFT. The efficiency and accuracy of our computer implementation have been discussed, as well as the connection to related work. In particular, the differences with the closely-related TDHF approach have been emphasized. In similar manner, the equations can be extended to higher-order hyperpolarizabilities. In previous and future applications, the implementation has been shown to be applicable to

Table 9.1: Test calculation on the γ_{zzzz} second hyperpolarizability component of Helium, calculated from β_{zzz} values at $E_1^z = 0.001$. All quantities in a.u.

Method	E_1^z, E_2^z	$\gamma_{zzzz}(0; 0, 0, 0)^a$	$\gamma_{zzzz}(-\omega; \omega, 0, 0)^{a,b}$
FF from α_{zz}	0.001, 0.00025	87.915	89.359
FF from α_{zz}	0.001, 0.00050	87.9163	89.3605
FF from α_{zz}	0.001, 0.00100	87.9164	89.3595
FF from β_{zzz}	0.001, analytic	87.9163	89.3595

^a γ_{zzzz} obtained from β_{zzz} at $E_1^z = 0.001$ a.u., where β_{zzz} was calculated either analytically or from Equation (9.52).

^btensor related to the Electro-optical Kerr effect (EOKE), at $\omega = 0.05$ a.u.

Table 9.2: Influence of finite auxiliary basis set on static hyperpolarizability of CO

Fit set	Density used for v_{xc}	Method	β_{zzx} (a.u.)	β_{zzz} (a.u.)
large ^a	fitted	analytic	-8.239	-33.522
large	fitted	finite field ^b	-8.274	-33.588
large	fitted	finite field ^c	-8.275	-33.593
large	exact	analytic	-8.433	-33.900
large	exact	finite field ^b	-8.440	-33.901
medium ^d	fitted	analytic	-7.054	-31.023
medium	fitted	finite field ^b	-7.573	-33.421

^aThe large fit set consists of 254 STO fit functions per atom. See text.

^bUsing $E_2 = 0.0005$ a.u. in Equation (9.52)

^cUsing $E_2 = 0.001$ a.u. in Equation (9.52)

^dThe medium-sized fit set consists of 184 STO fit functions per atom. See text.

large systems. An application of the present work to a set of small molecules, in which the reliability of various density functionals will be assessed, is forthcoming.

9.12 Acknowledgements

The authors wish to thank Robert van Leeuwen from the University of Lund for very useful discussions, in particular on the role of the Lagrangian multipliers. The authors gratefully acknowledge financial support from the Netherlands organization for scientific research (NWO) through its foundations SON and NCF.

Table 9.3: Static and frequency-dependent average hyperpolarizabilities of *para*-nitroaniline at $\lambda = 1060$ nm ($\omega = 0.043$ a.u.)

Property	LDA/ALDA ^a	LB94/ALDA ^a	HF ^b	MP2 ^c	Expt.
$\beta_{\text{vec}}(0; 0, 0)^{\text{d}}$	14.89	16.28	4.37	8.55	-
$\beta_{\text{vec}}(-2\omega; \omega, \omega)^{\text{d}}$	33.97	42.31	4.88	12.0	50.7 ^e
$\bar{\gamma}(0; 0, 0, 0)^{\text{f}}$	7.34	2.62	1.48	3.21	-
$\bar{\gamma}(-2\omega; \omega, \omega, 0)^{\text{f}}$	20.18	11.98	2.11	4.6	32 ^c

^a This work, using ALDA for functional derivatives of v_{xc} , and either LDA or LB94 for v_{xc} itself

^b Ref.[303]

^c Results obtained or referenced by Sim *et al.*[302], frequency dispersion was estimated from TDHF calculation.

^d $\beta_{\text{vec}} = \beta_z = (1/3) \sum_a \beta_{zaa} + \beta_{aza} + \beta_{aaz}$, given in units of 10^{-30} esu, as in Refs.[303, 304, 302]

^e In 1,4-dioxane[307]

^f $\bar{\gamma} = (1/15) \sum_{a,b} (2\gamma_{aabb} + \gamma_{abba})$, in 10^{-36} esu, as in Ref.[303]

Summary and outlook

In this thesis, time-dependent density functional theory has been applied to the calculation of optical response properties of molecules, such as polarizabilities and excitation energies. Time-dependent density functional theory is a first-principles theory in which the time-dependent electron density is the central quantity. If this electron density can be accurately determined for a molecule subject to external perturbations such as electric fields, an accurate determination of the molecular response properties becomes straightforward.

In time-dependent density functional theory, the time-dependent electron density is determined, in principle exactly, from a set of equations for noninteracting particles. These particles move in an effective field determined by a time-dependent local potential, the so-called Kohn–Sham potential, which is however unknown for all but the simplest systems.

Once a certain approximation has been chosen for the Kohn–Sham potential, the determination of the electron density of the noninteracting particle system, which would be equal to the exact density if the exact Kohn–Sham potential could be used, proceeds in a self-consistent manner. This is necessary as the Kohn–Sham potential is a functional of the density which has to be determined. Both the density and the Kohn–Sham potential are updated iteratively, until they change only insignificantly, in which case a converged solution for the density has been reached.

The techniques by which the density can be calculated once a specific approximation for the Kohn–Sham potential (or more accurately: its unknown part, the exchange-correlation potential) has been chosen are well-established by now and do not pose problems of significance. The selection of an appropriate approximation for the Kohn–Sham potential, however, is a difficult matter, and the accuracy of the final results crucially depends upon it.

Many people are involved in the pursuit of more accurate density functionals for the exchange-correlation potential and the exchange-correlation energy, from which the energy of a system can be calculated as a functional of the density. If one is interested in (linear) response properties, such as polarizabilities which form an important topic of the present work, the density functionals of key interest are the exchange-correlation potential, which determines the density if no external field is present, and the exchange-correlation kernel, which determines the change in the exchange-correlation potential due to small changes in the density which occur if the system is slightly perturbed. One of the topics which has been treated in this thesis, is the assessment of exchange-correlation potentials and kernels for the use in response calculations. In this respect, it was found that certain approximations which are very accurate, and therefore popular, for the calculation of molecular equilibrium geometries and binding energies, display important deficiencies, which renders them less ap-

appropriate for use in accurate response calculations. The popular local density approximation and generalized gradient approximations for the exchange-correlation potential fall into this category. Although it may seem surprising that approximations which have been shown to give results of very good accuracy for a variety of properties suddenly seem inappropriate for response property calculations, this can be understood from the fact that the description of the outer region of a molecule is of utmost importance for many response properties, while it is relatively unimportant for molecular structures and energies. It is precisely this region of space in which the popular approximations such as the local density approximation are known to be poor.

Fortunately, this deficiency can be removed fairly easily by making a simple correction to the exchange-correlation potential of the local density approximation, which improves its behavior in the outer region of the molecule, leading to good results at a low computational cost. Furthermore, it has been shown in this thesis that one can be optimistic about the improvements which are to be expected from more refined exchange-correlation potentials. This is based upon test calculations on small systems with very accurate exchange-correlation potentials. For atoms and small molecules, such an accurate exchange-correlation potential can be generated if an accurate density is available. A further optimistic conclusion which can be drawn from the present work, is that even a very simple approximation for the complicated exchange-correlation kernel, the so-called adiabatic local density approximation, can lead to accurate results in practical calculations. It seems that the limiting factor of the accuracy of time-dependent density functional response property calculations is at present in the accuracy of the exchange-correlation potential, instead of in the exchange-correlation kernel. This is fortunate, as the exchange-correlation kernel may be very difficult to model accurately.

Apart from these investigations which concern improvements in the accuracy of density functional response calculations, we have also been involved in the development and improvement of the techniques which can be used to calculate response properties within density functional theory. We have described in detail how the occurring linear response equations can be solved efficiently by making use of iterative solution techniques, in which repeated matrix-vector multiplications are the time-determining step. The efficient computer implementation of this matrix-vector product has been considered in detail. Also nonlinear response properties have been considered, such as Raman intensities and hyperpolarizabilities. In the case of hyperpolarizabilities, the expensive solution of second-order equations has been circumvented by making use of the $(2n + 1)$ -theorem of perturbation theory. In this manner, hyperpolarizabilities can be determined from the solutions of linear response equations only.

With the computer implementation, of which the characteristics and possibilities have been described in this thesis, molecular properties are now accessible in a trivial manner which were previously out of reach in density functional theory. In addition to the implementations for polarizabilities and excitation energies, the first density functional calculations of molecular Van der Waals dispersion coefficients, frequency-dependent hyperpolarizabilities, and frequency-dependent Raman intensities were obtained.

There are several interesting possibilities to go beyond this work. One could calculate magnetic properties, such as magnetizabilities, and mixed electric and magnetic properties, in

the framework of time-dependent current-density functional theory, with virtually the same techniques as applied in this work. The analytic evaluation of mixed electric and nuclear displacement derivatives would enable an efficient determination of Raman and hyper-Raman scattering properties, as well as the determination of vibrational contributions to the (hyper)polarizabilities. If the second-order response equations are solved iteratively, one can analytically obtain the second and third frequency-dependent hyperpolarizability tensors, which govern effects such as third and fourth harmonic generation. A model for a molecule in a solvent could be implemented to assess the possibly significant influence of the surrounding on the desired response properties. An implementation of linear scaling techniques will allow for an even more efficient implementation which could presumably be applied to large molecules with up to one thousand atoms. A fully parallel implementation, in which the memory usage is also parallelized, will enable an even more efficient use of massively parallel computer architectures, thus further enlarging the scope of possible applications. In order to improve the accuracy which can be obtained, new exchange-correlation functionals should be devised and tested. In particular, they should combine the correct asymptotic behavior for the exchange-correlation potential with good approximations for the exchange-correlation energy and kernels. This will lead the way to future, accurate response calculations on large molecules which will be directly comparable to experimental numbers, and can be used for the prediction and verification of those numbers.

Samenvatting en vooruitblik

In dit proefschrift is tijdsafhankelijke dichtheidsfunctionaaltheorie toegepast op het berekenen van optische responseeigenschappen van moleculen, zoals polariseerbaarheden en excitatie-energieën. Tijdsafhankelijke dichtheidsfunctionaaltheorie is een theorie die uitgaat van de grondbeginselen en waarbij de tijdsafhankelijke elektronendichtheid de centrale grootheid is. Als deze elektronendichtheid nauwkeurig kan worden bepaald voor een molecule onder invloed van externe storingen, zoals elektrische velden, is de nauwkeurige bepaling van de moleculaire responseeigenschappen een eenvoudige zaak.

In tijdsafhankelijke dichtheidsfunctionaaltheorie wordt de tijdsafhankelijke elektronendichtheid, in principe exact, bepaald door een stelsel vergelijkingen voor niet-wisselwerkende deeltjes. Deze deeltjes bewegen in een effectief veld dat bepaald wordt door een tijdsafhankelijke lokale potentiaal, de zogenaamde Kohn–Sham potentiaal, die echter, op enkele zeer eenvoudige systemen na, onbekend is.

Nadat een bepaalde benadering is gekozen voor de Kohn–Sham potentiaal, verloopt de bepaling van de tijdsafhankelijke elektronendichtheid van het niet-wisselwerkende systeem (die gelijk zou zijn aan de exacte dichtheid van het wisselwerkende systeem indien de exacte Kohn–Sham potentiaal gebruikt zou kunnen worden) op een zelfconsistente manier. Dit is noodzakelijk omdat de Kohn–Sham potentiaal een functionaal is van de dichtheid die bepaald moet worden. Zowel de dichtheid als de Kohn–Sham potentiaal worden iteratief aangepast, totdat ze nog maar verwaarloosbaar veranderen. In dit geval is een geconvergeerde oplossing voor de dichtheid bereikt.

De technieken waarmee de dichtheid berekend kan worden als een benadering voor de Kohn–Sham potentiaal is gekozen (of preciezer gesproken: het onbekende gedeelte daarvan, de exchange-correlatie potentiaal) zijn goed bekend en leveren geen problemen op. De keuze van een geschikte Kohn–Sham potentiaal daarentegen is een ingewikkelde zaak, waarvan de nauwkeurigheid van de uiteindelijke resultaten sterk afhangt.

Velen houden zich bezig met het zoeken naar nauwkeurigere benaderingen voor de exchange-correlatie potentiaal en de exchange-correlatie energie, waaruit de energie van een systeem uitgerekend kan worden als functionaal van de dichtheid.

Indien men geïnteresseerd is in lineaire responseeigenschappen, zoals polariseerbaarheden, die een belangrijk onderdeel van dit werk vormen, zijn de belangrijkste dichtheidsfunctionalen de exchange-correlatie potentiaal, die de dichtheid bepaalt voor het geval dat er geen externe storing aanwezig is, en de exchange-correlatie kern, die de verandering bepaalt in de exchange-correlatie potentiaal als gevolg van kleine dichtheidsveranderingen veroorzaakt door de externe storingen. Een van de onderwerpen die behandeld is in dit proefschrift, is het testen van exchange-correlatie potentialen en kernen voor gebruik in responsbereke-

ningen. Wat dit betreft is gevonden dat bepaalde benaderingen die zeer nauwkeurig zijn, en derhalve populair, voor het berekenen van moleculaire evenwichtsgeometrieën en bindingsenergieën, belangrijke gebreken vertonen, die ze minder geschikt maken voor het gebruik in nauwkeurige responsberekeningen. De populaire lokale dichtheidsbenadering en gegeneraliseerde gradiëntbenaderingen vallen in deze categorie. Hoewel het verrassend kan lijken dat benaderingen waarvan aangetoond is dat ze zeer nauwkeurige resultaten geven voor allerlei eigenschappen opeens ongeschikt lijken te zijn voor berekeningen aan responseigenschappen, kan dit begrepen worden uit het feit dat de beschrijving van het buitengebied van een molecule van groot belang is voor veel responseigenschappen, terwijl het relatief onbelangrijk is voor moleculaire structuren en energieën. Precies van dit gedeelte van de ruimte is bekend dat het slecht beschreven wordt door de populaire benaderingen, zoals de lokale dichtheidsbenadering.

Gelukkig kan dit gebrek relatief eenvoudig verholpen worden door een simpele correctie aan de exchange-correlatie potentiaal van de lokale dichtheidsbenadering toe te voegen, die het gedrag in het buitengebied van het molecule verbetert, hetgeen leidt tot goede resultaten tegen lage kosten in termen van computertijd.

Verder is aangetoond dat men optimistisch kan zijn over de verbeteringen die te verwachten zijn van nog betere benaderingen voor de exchange-correlatie potentiaal. Dit is gebaseerd op testberekeningen op kleine systemen met zeer nauwkeurige exchange-correlatie potentialen. Voor atomen en kleine moleculen kan een dergelijke nauwkeurige exchange-correlatie potentiaal gegenereerd worden indien een nauwkeurige dichtheid beschikbaar is. Een volgende optimistische conclusie die getrokken kan worden uit dit werk, is dat zelfs een zeer eenvoudige benadering op de ingewikkelde exchange-correlatie kern, de zogenaamde adiabatische lokale dichtheidsbenadering, kan leiden tot nauwkeurige resultaten in praktische berekeningen. Het lijkt er op dat de beperkende factor voor de nauwkeurigheid van responseigenschap berekeningen in het kader van tijdsafhankelijke dichtheidsfunctionaaltheorie op dit moment in de nauwkeurigheid van de exchange-correlatie potentiaal gelegen is, in plaats van in de exchange-correlatie kern. Dit is gunstig, aangezien de exchange-correlatie kern wel eens zeer ingewikkeld te modelleren zou kunnen zijn.

Behalve dit gedeelte van het onderzoek dat gerelateerd is aan verbeteringen in de nauwkeurigheid van responsberekeningen in dichtheidsfunctionaaltheorie, zijn er ook methoden ontwikkeld en verbeterd om responseigenschappen te berekenen binnen dichtheidsfunctionaaltheorie. In detail is beschreven hoe de lineaire responsvergelijkingen efficiënt kunnen worden opgelost door gebruik te maken van iteratieve methoden, waarbij herhaalde matrix-vector vermenigvuldigingen de tijdbepalende stap vormen. De efficiënte computerimplementatie van deze matrix-vector vermenigvuldiging is in detail bestudeerd. Ook niet-lineaire responseigenschappen zijn aan de orde gekomen, zoals Ramanintensiteiten en hyperpolariseerbaarheden. In het geval van de hyperpolariseerbaarheden is het dure oplossen van de tweede orde responsvergelijkingen vermeden door gebruik te maken van het $(2n + 1)$ - theorema van storingstheorie. Op deze wijze kunnen hyperpolariseerbaarheden bepaald worden uit enkel de oplossingen van de eerste orde vergelijkingen.

Met de computerimplementatie, waarvan de eigenschappen en mogelijkheden in dit proefschrift zijn beschreven, zijn moleculaire eigenschappen nu op eenvoudige wijze toegankelijk die voorheen niet verkrijgbaar waren in dichtheidsfunctionaaltheorie. Naast de implemen-

taties voor polariseerbaarheden en excitatie-energieën zijn de eerste dichtheidsfunctionaal berekeningen voor moleculaire Van der Waals dispersiecoëfficiënten, frequentie-afhankelijke hyperpolariseerbaarheden, en frequentie-afhankelijke Ramanintensiteiten verkregen.

Er bestaan verscheidene interessante manieren om voort te bouwen op dit werk. Men zou magnetische eigenschappen, zoals magnetiseerbaarheden, en gemengd magnetische-elektrische eigenschappen kunnen uitrekenen, in het kader van tijdsafhankelijke stroomdichtheidstheorie, met gebruikmaking van vrijwel dezelfde technieken als in dit proefschrift staan beschreven. De analytische berekening van energie-afgeleiden ten gevolge van gemengde elektrische verstoringen en kernverplaatsingen zou een efficiënte bepaling van Raman en hyper-Raman verstrooiingseigenschappen mogelijk maken, alsmede de analytische bepaling van vibrationele bijdragen tot de (hyper)polariseerbaarheden. Indien de tweede orde responsvergelijkingen iteratief worden opgelost, kunnen tweede en derde frequentie-afhankelijke hyperpolariseerbaarheidstensors analytisch berekend worden, die effecten zoals derde en vierde harmonische generatie bepalen. Een model voor een molecule in een vloeistof zou geïmplementeerd kunnen worden om de mogelijk belangrijke invloed van de omgeving op de gewenste responseigenschappen te bepalen. Een implementatie van lineaire schalingstechnieken zal een nog efficiëntere implementatie mogelijk maken, die vermoedelijk toegepast zou kunnen worden op grote moleculen met tot duizend atomen. Een volledig parallelle implementatie, waarbij het geheugengebruik ook geparallelliseerd is, zal het mogelijk maken nog efficiënter gebruik te maken van massief parallelle computerarchitecturen, waarmee het bereik van de mogelijke toepassingen nog vergroot zou worden. Om de nauwkeurigheid van de berekeningen te verbeteren zouden nieuwe exchange-correlatie functionalen ontworpen en getest moeten worden. Deze zouden het correcte asymptotische gedrag voor de exchange-correlatie potentiaal met goede benaderingen voor de exchange-correlatie energie en kern moeten combineren. Dit alles zal in de toekomst leiden tot nauwkeurige responsberekeningen aan grote moleculen, die direct vergelijkbaar zijn met experimentele resultaten, en die gebruikt kunnen worden voor de voorspelling en controle van die resultaten.

Dankwoord

Op deze plaats wil ik enige mensen bedanken die op directe of indirecte wijze hebben bijgedragen aan het tot stand komen van dit proefschrift.

In de eerste plaats wil ik mijn promotoren, Jaap Sniijders en Evert-Jan Baerends hartelijk bedanken. Jullie voortdurende bereidheid om te discussiëren over grote en kleine problemen die tijdens het onderzoek naar boven kwamen, heeft de afgelopen vier jaar voor een zeer prettige werksfeer gezorgd. Van jullie uitgebreide en brede kennis heb ik veel geleerd over zowel responseeigenschappen als dichtheidsfunctionaaltheorie, en ik hoop dat ook in de toekomst te kunnen blijven doen.

It is a great pleasure to thank Professor Gross for taking place in the reading committee and for taking the time to study the manuscript. Ook de Nederlandse leden van de leescommissie, Dr. P.E.S. Wormer, Dr. L. Visscher, en Dr. P.L. de Boeij, wil ik hartelijk danken voor het bestuderen van het manuscript en voor de gedane suggesties.

Vincent Osinga, Freddie Kootstra, en Jeroen Groeneveld, die zich als hoofdvakstudenten met responseeigenschappen hebben bezig gehouden, wil ik bedanken voor de aangename en vruchtbare samenwerking. De resultaten van jullie werk zijn reeds gedeeltelijk in dit proefschrift en in publicaties tot uitdrukking gekomen, en kunnen in de toekomst nog door vele anderen gebruikt gaan worden.

Robert van Leeuwen, jou wil ik bedanken voor de vele stimulerende discussies over allerlei aspecten van tijdsafhankelijke dichtheidsfunctionaaltheorie. Ook is in dit proefschrift dankbaar gebruik gemaakt van de door jou samen met Evert-Jan ontwikkelde LB94 potentiaal, wat de resultaten zeer ten goede is gekomen.

Pieter Schipper, jou bedank ik voor de prettige samenwerking die het mogelijk maakte "exacte" exchange-correlatie potentialen te combineren met het berekenen van responseeigenschappen, waardoor we dieper inzicht hebben gekregen in het belang van verscheidene benaderingen.

Oleg Gritsenko, I would like to thank you also for the fruitful cooperation on the exchange-correlation potentials. I have especially enjoyed your attempts to find logical explanations for results which came as a complete surprise to me, thus giving me a lot of food for thought, even if the explanations were sometimes "time-dependent".

I would like to thank Professor Bernard Kirtman en Dr. Benoît Champagne for all the open and inspiring discussions concerning our cooperation on the optical properties of conjugated molecular chains.

Martin Petersilka, I thank you for many useful discussions on several aspects of time-dependent density functional theory, which have helped me very much in my research.

Pier Philipsen, ik wil jou bedanken voor het aangename kamergenootschap gedurende

174 DANKWOORD

vier jaar, met allerlei zinnige en minder zinnige discussies over fysica en andere zaken. Pieter Vernooijs, Olivier Visser, en Bert te Velde wil ik bedanken voor de vele malen dat zij mij geholpen hebben in mijn pogingen ADF te doorgronden, hetgeen mijn programmeertaak zeer heeft vereenvoudigd. Ook Gijsbert Wiesenekker en Walter Ravenek bedank ik voor de keren dat ze mij geholpen hebben met allerlei programmeer- en andere computerproblemen.

Deze en overige (ex-)leden van de vakgroep, onder wie Ad van Eulem, Andreas Ehlers, Antoinette Sisto, Bernd Ensing, Célia Fonseca-Guerra, Erik van Lenthe, Evert-Jan Meijer, Jonathan Go, Luuk Visscher, Matthias Bickelhaupt, Remco Bouten, en Roar Olsen wil ik bedanken voor de goede sfeer die steeds geheerst heeft, vooral bij de dagelijkse "werkbesprekingen" tijdens de koffie.

I would like to thank the foreign guests in our group, Angela Rosa, Paolo Belanzoni, and others for making the Theoretical Chemistry group a more interesting place.

Mijn ouders, mijn broer Maxim, en Mirna wil ik tenslotte hartelijk bedanken voor hun interesse in mijn werk en voor de steun die ze mij steeds hebben gegeven.

List of publications

S. J. A. van Gisbergen, J. G. Snijders and E. J. Baerends,
to be submitted to *Comp. Phys. Commun.*, Chapter 2
Implementation of time-dependent density functional response equations

S. J. A. van Gisbergen, J. G. Snijders and E. J. Baerends,
J. Chem. Phys. **103**, 9347-9354 (1995), Chapter 3
A density functional theory study of frequency-dependent polarizabilities and Van der Waals dispersion coefficients for polyatomic molecules

S. J. A. van Gisbergen, V. P. Osinga, O. V. Gritsenko, R. van Leeuwen, J. G. Snijders
and E. J. Baerends,
J. Chem. Phys. **105**, 3142-3151 (1996), Chapter 4
*Improved density functional theory results for frequency-dependent polarizabilities, by the use
of an exchange-correlation potential with correct asymptotic behavior*

S. J. A. van Gisbergen, J. G. Snijders and E. J. Baerends,
Chem. Phys. Lett. **259**, 599-604 (1996), Chapter 5
Application of time-dependent density functional response theory to Raman scattering

V. P. Osinga, S. J. A. van Gisbergen, J. G. Snijders and E. J. Baerends,
J. Chem. Phys. **106**, 5091-5101 (1997), Chapter 6
*Density functional results for isotropic and anisotropic multipole polarizabilities and C_6 , C_7
and C_8 Van der Waals dispersion coefficients*

S. J. A. van Gisbergen, J. G. Snijders and E. J. Baerends,
Phys. Rev. Lett. **78**, 3097-3100 (1997), Chapter 7
Time-dependent density functional results for the dynamic hyperpolarizability of C_{60}

S. J. A. van Gisbergen, F. Kootstra, P. R. T. Schipper, O. V. Gritsenko, J. G. Snijders
and E. J. Baerends,
Phys. Rev. A **57**, 2556-2571 (1998), Chapter 8
*Density functional theory response property calculations with accurate exchange-correlation
potentials*

170
S. J. A. van Gisbergen, J. G. Snijders and E. J. Baerends,
submitted for publication, Chapter 9

Calculating frequency-dependent hyperpolarizabilities using time-dependent density functional theory

B. Champagne, E. A. Perpète, S. J. A. van Gisbergen, E. J. Baerends, J. G. Snijders,
C. Soubra-Ghaoui, K. Robins, and B. Kirtman,
submitted for publication, not included in present work

Assessment of conventional density functional schemes for computing the polarizabilities and hyperpolarizabilities of conjugated oligomers: An ab initio investigation of polyacetylene chains

S. J. A. van Gisbergen, J. G. Snijders, and E. J. Baerends,
submitted for publication, not included in present work

Accurate density functional calculations on frequency-dependent hyperpolarizabilities of small molecules

Bibliography

- [1] P. Hohenberg and W. Kohn, Phys. Rev. 136 (1964) B864.
- [2] E. Bright Wilson, unpublished (1965).
- [3] W. Kohn and L. J. Sham, Phys. Rev. 140 (1965) A1133.
- [4] S. H. Vosko, L. Wilk, and M. Nusair, Can. J. Phys. 58 (1980) 1200.
- [5] D.M. Ceperley and B.J. Alder, Phys. Rev. Lett. 45 (1980) 566.
- [6] R. M. Dreizler and E. K. U. Gross, Density Functional Theory: An Approach to the Quantum Many-Body Problem. Springer-Verlag, Berlin, Berlin, (1990).
- [7] R.G. Parr and W. Yang, Density-Functional Theory of Atoms and Molecules. Oxford University Press, (1990).
- [8] V. Peuckert, J. Phys. C11 (1978) 4945.
- [9] A. Zangwill and P. Soven, Phys. Rev. A21 (1980) 1561.
- [10] B.M. Deb and S.K. Ghosh, J. Chem. Phys. 77 (1982) 342.
- [11] S.K. Ghosh and B.M. Deb, Chem. Phys. 71 (1982) 295.
- [12] S.K. Ghosh and B.M. Deb, Theoret. Chim. Acta 62 (1983) 209.
- [13] S.K. Ghosh and B.M. Deb, J. Mol. Struct. 103 (1983) 163.
- [14] L.J. Bartolotti, Phys. Rev. A24 (1981) 1661.
- [15] L.J. Bartolotti, Phys. Rev. A26 (1982) 2243.
- [16] L.J. Bartolotti, J. Chem. Phys. 80 (1984) 5687.
- [17] L.J. Bartolotti, Phys. Rev. A36 (1987) 4492.
- [18] Z. H. Levine and P. Soven, Phys. Rev. B24 (1981) 4121.
- [19] Z. H. Levine and P. Soven, Phys. Rev. A29 (1984) 625.
- [20] Z. H. Levine, Phys. Rev. B42 (1990) 3567.

- [21] Z. H. Levine and D. C. Allan, Phys. Rev. Lett. 63 (1989) 1719.
- [22] Z. H. Levine and D. C. Allan, Phys. Rev. Lett. 66 (1991) 41.
- [23] M.J. Stott and E. Zaremba, Phys. Rev. A21 (1980) 12.
- [24] H. Zhong, Z. H. Levine, and J. W. Wilkins, Phys. Rev. A43 (1991) 4629.
- [25] H. Zhong, Z. H. Levine, D. C. Allan, and J. W. Wilkins, Phys. Rev. Lett. 69 (1992) 379.
- [26] A. Zangwill and P. Soven, Phys. Rev. Lett. 45 (1980) 204.
- [27] A. Zangwill and P. Soven, Phys. Rev. B24 (1981) 4121.
- [28] P. Gies and R.R. Gerhardts, Phys. Rev. B31 (1985) 6843.
- [29] P. Gies and R.R. Gerhardts, Phys. Rev. B36 (1987) 4422.
- [30] G. D. Mahan and K. R. Subbaswamy, Local Density Theory of Polarizability. Plenum, New York, (1990).
- [31] E. K. U. Gross and W. Kohn, Adv. Quantum Chem. 21 (1990) 255.
- [32] E. K. U. Gross, C. A. Ullrich, and U. J. Gossmann. Density Functional Theory of Time-Dependent Systems, volume 337 of *NATO ASI Ser. B*, 149. Plenum, New York, (1995).
- [33] E. K. U. Gross, J. F. Dobson, and M. Petersilka, in *Density Functional Theory*, edited by R.F. Nalewajski, Springer Series "Topics in Current Chemistry" (Springer, Heidelberg, 1996).
- [34] S. J. A. van Gisbergen, J. G. Snijders, and E. J. Baerends, J. Chem. Phys. 103 (1995) 9347 [Chapter 3 of present work].
- [35] Ch. Jamorski, M. E. Casida, and D. R. Salahub, J. Chem. Phys. 104 (1996) 5134.
- [36] E. K. U. Gross and S. Kurth, NATO ASI series, Series B, Physics 318 (1994) 367.
- [37] M. E. Casida, in "Recent Advances in Density-Functional Methods", edited by D.P. Chong (World Scientific, Singapore, 1995) 155.
- [38] E. Runge and E. K. U. Gross, Phys. Rev. Lett. 52 (1984) 997.
- [39] G. Vignale and M. Rasolt, Phys. Rev. Lett. 59 (1987) 2360.
- [40] G. Vignale and M. Rasolt, Phys. Rev. B37 (1988) 10685.
- [41] G. Vignale, M. Rasolt, and D.J.W. Geldart, Adv. Quantum Chem. 21 (1990) 235.
- [42] S. M. Colwell and N. C. Handy, Chem. Phys. Lett. 217 (1994) 271.

- [43] A. M. Lee, S. M. Colwell, and N. C. Handy, *Chem. Phys. Lett.* 229 (1994) 225.
- [44] K. Capelle and E.K.U. Gross, *Phys. Rev. Lett.* 78 (1997) 1872.
- [45] P. Craig and T. Thirunamachandran, *Molecular Quantum Electrodynamics*. Academic Press, New York, (1984).
- [46] J.M. Pacheco and J.L. Martins, *J. Chem. Phys.* 106 (1997) 6039.
- [47] M. Stener and P. Decleva, *J. Phys. B* 30 (1997) 4481.
- [48] H.B.G. Casimir and D. Polder, *Phys. Rev.* 73 (1948) 360.
- [49] A. van der Avoird, P.E.S. Wormer, F. Mulder, and R.M. Berns, *Topics in Current Chemistry* 93 (1980) 1.
- [50] P.E.S. Wormer. PhD thesis, Katholieke Universiteit, Nijmegen, The Netherlands, (1975).
- [51] W. Kohn, Y. Meir, and D. E. Makarov, *Phys. Rev. Lett.* 80 (1998) 4153.
- [52] E. Bright Wilson (jr.), J. C. Decius, and P. C. Cross, *Molecular vibrations: the theory of infrared and Raman vibrational spectra*. McGraw-Hill, New York, (1955).
- [53] D.A. Long, *Raman Spectroscopy*. McGraw-Hill, New York, (1977).
- [54] P.G. Szalay and G. Fogarasi, *Chem. Phys. Lett.* 270 (1997) 406.
- [55] E.J. Heller, R.L. Sundberg, and D. Tannor, *J. Phys. Chem.* 86 (1982) 1822.
- [56] A. Sassara, G. Zerza, M. Chergui, F. Negri, and G. Orlandi, *J. Chem. Phys.* 107 (1997) 8731.
- [57] D. M. Bishop, *Rev. Mod. Phys.* 62 (1990) 343.
- [58] D. M. Bishop, B. Kirtman, H.A. Kurtz, and J.E. Rice, *J. Chem. Phys.* 98 (1993) 8024.
- [59] D. M. Bishop and E. K. Dalskov, *J. Chem. Phys.* 104 (1996) 1004.
- [60] J. M. Luis, M. Duran, and J. L. Andrés, *J. Chem. Phys.* 107 (1997) 1501.
- [61] D. M. Bishop and S. P. A. Sauer, *J. Chem. Phys.* 107 (1997) 8502.
- [62] R. D. Amos, *Chem. Phys. Lett.* 124 (1986) 376.
- [63] T. Ziegler, A. Rauk, and E. J. Baerends, *Theoret. Chim. Acta* 43 (1977) 261.
- [64] U. von Barth, *Phys. Rev. A* 20 (1979) 1693.
- [65] C. Daul, *Int. J. Quantum Chem.* 52 (1994) 867.
- [66] R. M. Dickson and T. Ziegler, *Int. J. Quantum Chem.* 58 (1996) 681.

- [67] A. Zangwill, *J. Chem. Phys.* 78 (1983) 5926.
- [68] G. D. Mahan, *Phys. Rev. A* 22 (1980) 1780.
- [69] G. D. Mahan, *J. Chem. Phys.* 76 (1982) 493.
- [70] K. R. Subbaswamy and G. D. Mahan, *J. Chem. Phys.* 84 (1986) 3317.
- [71] G. Senatore and K. R. Subbaswamy, *Phys. Rev. A* 34 (1986) 3619.
- [72] G. Senatore and K. R. Subbaswamy, *Phys. Rev. A* 35 (1987) 2440.
- [73] L. J. Bartolotti, L. Ortiz, and Q. Xie, *Int. J. Quantum Chem.* 49 (1994) 449.
- [74] S. J. A. van Gisbergen, V. P. Osinga, O. V. Gritsenko, R. van Leeuwen, J. G. Snijders, and E. J. Baerends, *J. Chem. Phys.* 105 (1996) 3142 [Chapter 4 of present work].
- [75] S. J. A. van Gisbergen, J. G. Snijders, and E. J. Baerends, *Chem. Phys. Lett.* 259 (1996) 599 [Chapter 5 of present work].
- [76] S. J. A. van Gisbergen, J. G. Snijders, and E. J. Baerends, *Phys. Rev. Lett.* 78 (1997) 3097 [Chapter 7 of present work].
- [77] V. P. Osinga, S. J. A. van Gisbergen, J. G. Snijders, and E. J. Baerends, *J. Chem. Phys.* 106 (1997) 5091 [Chapter 6 of present work].
- [78] S. J. A. van Gisbergen, F. Kootstra, P. R. T. Schipper, O. V. Gritsenko, J. G. Snijders, and E. J. Baerends, *Phys. Rev. A* 57 (1998) 2556 [Chapter 8 of present work].
- [79] S. J. A. van Gisbergen, J. G. Snijders, and E. J. Baerends, unpublished [Chapter 9 of present work].
- [80] M. E. Casida, C. Jamorski, F. Bohr, J. Guan, and D. R. Salahub, in "Theoretical and Computational Modeling of NLO and Electronic Materials", edited by S.P. Karna and A.T. Yeates (ACS, Washington, D.C.) (1996) 145.
- [81] M. E. Casida, in "Recent developments and applications of modern density functional theory", edited by J.M. Seminario (Elsevier, Amsterdam, 1996) (1996).
- [82] M. E. Casida, C. Jamorski, K. C. Casida, and D. R. Salahub, *J. Chem. Phys.* 108 (1998) 4439.
- [83] S. M. Colwell, N. C. Handy, and A. M. Lee, *Phys. Rev. A* 53 (1996) 1316.
- [84] A. G. Ioannou, S. M. Colwell, and R. D. Amos, *Chem. Phys. Lett.* 278 (1997) 278.
- [85] A. G. Ioannou and R. D. Amos, *Chem. Phys. Lett.* 279 (1997) 17.
- [86] R. Bauernschmitt and R. Ahlrichs, *Chem. Phys. Lett.* 256 (1996) 454.

- [87] R. Bauernschmitt, M. Häser, O. Treutler, and R. Ahlrichs, *Chem. Phys. Lett.* 264 (1997) 573.
- [88] RESPONSE, extension of the ADF program for linear and nonlinear response calculations, by S.J.A. van Gisbergen, J.G. Snijders and E.J. Baerends, with contributions by J.A. Groeneveld, F. Kootstra, and V.P. Osinga.
- [89] E. J. Baerends, D. E. Ellis, and P. Ros, *Chem. Phys.* 2 (1973) 41.
- [90] G. te Velde and E. J. Baerends, *J. Comput. Phys.* 99 (1992) 84.
- [91] C. Fonseca Guerra, O. Visser, J. G. Snijders, G. te Velde, and E. J. Baerends, published in *Methods and Techniques in Computational Chemistry* edited by E. Clementi and G. Corongiu (STEF, Cagliari(Italy), 1995) 305.
- [92] H. Hellmann, *Einführung in die Quantenchemie*. Franz Deuticke, Leipzig, (1937).
- [93] R.P. Feynman, *Phys. Rev.* 56 (1939) 340.
- [94] A. Willetts, J. E. Rice, D. M. Burland, and D. P. Shelton, *J. Chem. Phys.* 97 (1992) 7590.
- [95] P. Pulay, *Chem. Phys. Lett.* 73 (1980) 393.
- [96] P. Pulay, *J. Comput. Chem.* 3 (1982) 556.
- [97] C-A. Ullrich. Time-dependent density-functional approach to atoms in strong laser pulses. PhD thesis, Universität Würzburg, (1995).
- [98] C. A. Ullrich, U. J. Gossmann, and E. K. U. Gross, *Phys. Rev. Lett.* 74 (1995) 872.
- [99] Xiao-Min Tong and Shih-I Chu, *Phys. Rev.* A57 (1998) 452.
- [100] J. G. Snijders, internal report, Vrije Universiteit, Amsterdam.
- [101] M. Petersilka, U. J. Gossmann, and E. K. U. Gross, *Phys. Rev. Lett.* 76 (1996) 1212.
- [102] R. McWeeny, *Methods of Molecular Quantum Mechanics*. Academic Press, New York, (1990).
- [103] P. Jørgensen and J. Simons, *Second Quantization-Based Methods in Quantum Chemistry*. Academic Press, New York, (1981).
- [104] S. P. Karna and M. Dupuis, *J. Comput. Chem.* 12 (1991) 487.
- [105] M. Petersilka and E. K. U. Gross, *Int. J. Quantum Chem. Symp.* 30 (1996) 181.
- [106] K. L. Liu and S. H. Vosko, *Can. J. Phys.* 67 (1989) 1015.
- [107] K.L. Liu, *Can. J. Phys.* 69 (1991) 573.

- 102
- BIBLIOGRAPHY
- [108] J. Olsen, H.J.Aa. Jensen, and P. Jørgensen, *J. Comput. Phys.* 74 (1988) 265.
 - [109] E.R. Davidson, *J. Comput. Phys.* 17 (1975) 87.
 - [110] B. Liu, *Proceedings, Numerical Algorithms in Chemistry: Algebraic Methods, Workshop of the National Resource for Computation in Chemistry, Berkeley (1978)* 49.
 - [111] E.R. Davidson, *Computers in Physics* 7 (1993)
 - [112] A. Stathopoulos and C.F. Fischer, *Comp. Phys. Comm.* 79 (1994) 268.
 - [113] A. Savin, C. J. Umrigar, and X. Gonze, *Chem. Phys. Lett.* 288 (1998) 391.
 - [114] C. Fonseca Guerra, J. G. Snijders, G. te Velde, and E. J. Baerends, unpublished.
 - [115] P. M. Boerrigter, G. te Velde, and E. J. Baerends, *Int. J. Quantum Chem.* 33 (1988) 87.
 - [116] G. te Velde. PhD thesis, Vrije Universiteit, Amsterdam, The Netherlands, (1990).
 - [117] J.F. Cornwell, *Group Theory in Physics*. Academic Press, New York, (1984).
 - [118] J.A. Groeneveld, internal report, Vrije Universiteit, Amsterdam (1998).
 - [119] V. Sunderam, *Concurrency: Practice Experience* 2(4) (1990).
 - [120] S. J. A. van Gisbergen, J. G. Snijders, and E. J. Baerends, unpublished.
 - [121] R. van Leeuwen and E. J. Baerends, *Phys. Rev.* A49 (1994) 2421.
 - [122] J. B. Krieger, Y. Li, and G. J. Iafrate, *Phys. Rev.* A46 (1992) 5453.
 - [123] Y. Li, J. B. Krieger, and G. J. Iafrate, *Phys. Rev.* A47 (1993) 165.
 - [124] D. J. Tozer and N. C. Handy, *J. Chem. Phys.* 108 (1998) 2545.
 - [125] M. Filatov and W. Thiel, *Phys. Rev.* A57 (1998) 189.
 - [126] M. Petersilka. Diplomarbeit, Universität Würzburg, (1993).
 - [127] M. Petersilka, U. J. Gossmann, and E. K. U. Gross, in: "Electronic Density Functional Theory: Recent Progress and New Directions", edited by J.F. Dobson, G. Vignale and M.P. Das, (Plenum, New York, 1998) 177-197.
 - [128] A. D. Becke, *J. Chem. Phys.* 98 (1988) 5648.
 - [129] C. Lee, W. Yang, and R.G. Parr, *Phys. Rev.* B37 (1988) 785.
 - [130] B. Champagne, E. A. Perpète, S. J. A. van Gisbergen, E. J. Baerends, J. G. Snijders, C. Soubra-Ghaoui, K. Robins, and B. Kirtman, submitted.

- [131] S. J. A. van Gisbergen, J. A. Groeneveld, J. G. Snijders, and E. J. Baerends, unpublished.
- [132] N. A. Beach and H.B. Gray, *J. Am. Chem. Soc.* 90 (1968) 5731.
- [133] C. Pollak, A. Rosa, and E.J. Baerends, *J. Am. Chem. Soc.* 119 (1997) 7324.
- [134] S. M. Colwell, C. W. Murray, N. C. Handy, and R. D. Amos, *Chem. Phys. Lett.* 210 (1993) 261.
- [135] A. M. Lee and S. M. Colwell, *J. Chem. Phys.* 101 (1994) 9704.
- [136] L. Geng and J. C. Wright, *Chem. Phys. Lett.* 249 (1996) 105.
- [137] P. Norman, Y. Luo, D. Jonsson, and H. Ågren, *J. Chem. Phys.* 106 (1997) 8788.
- [138] A. D. Becke, *Phys. Rev.* A38 (1988) 3098.
- [139] J.P. Perdew, *Phys. Rev.* B33 (1986) 8822.
- [140] H. B. Gray and N. A. Beach, *J. Am. Chem. Soc.* 85 (1963) 2922.
- [141] K. Pierloot, E. Tsokos, and L. G. Vanquickenborne, *J. Phys. Chem.* 100 (1996) 16545.
- [142] A. A. Quong and M. R. Pederson, *Phys. Rev.* B46 (1992) 12906.
- [143] G. B. Talapatra, N. Manickam, M. Samoc, M. E. Orczyk, S. P. Karna, and P. N. Prasad, *J. Phys. Chem.* 96 (1992) 5206.
- [144] J. Li, J. Feng, and C. Sun, *Chem. Phys. Lett.* 203 (1993) 560.
- [145] T. Hara, Y. Nomura, S. Narita, and T. Shibuya, *Chem. Phys. Lett.* 240 (1995) 610.
- [146] M. Fanti, G. Orlandi, and F. Zerbetto, *J. Am. Chem. Soc.* 117 (1995) 6101.
- [147] J. S. Meth, H. Vanherzeele, and Y. Wang, *Chem. Phys. Lett.* 197 (1992) 26.
- [148] Y. Wang and L.-T. Cheng, *J. Phys. Chem.* 96 (1992) 1530.
- [149] N. Tang, J. P. Partanen, R. W. Hellwarth, and R. J. Knize, *Phys. Rev.* B48 (1993) 8404.
- [150] H. Hettema, P. E. S. Wormer, and A. J. Thakkar, *Mol. Phys.* 80 (1993) 533.
- [151] D. M. Bishop and J. Pipin, *Int. J. Quantum Chem.* 45 (1993) 349.
- [152] S. A. C. McDowell, R. D. Amos, and N. C. Handy, *Chem. Phys. Lett.* 235 (1995) 1.
- [153] D.A. Dixon and N. Matsuzawa, *J. Phys. Chem.* 98 (1994) 3967.
- [154] N. Matsuzawa and D.A. Dixon, *J. Phys. Chem.* 98 (1994) 2545.

- 104
- BIBLIOGRAPHY
- [155] J. Guan, P. Duffy, J. T. Carter, D. P. Chong, K. C. Casida, M. E. Casida, and M. Wrinn, *J. Chem. Phys.* 98 (1993) 4753.
- [156] W. Rijks and P.E.S. Wormer, *J. Chem. Phys.* 88 (1988) 5704.
- [157] J. M. Pérez-Jordá and A. D. Becke, *Chem. Phys. Lett.* 233 (1995) 134.
- [158] S. Kristyán and P. Pulay, *Chem. Phys. Lett.* 229 (1994) 175.
- [159] H. Hettema. PhD thesis, Katholieke Universiteit Nijmegen, (1993).
- [160] E. K. U. Gross and W. Kohn, *Phys. Rev. Lett.* 55 (1985) 2850.
- [161] F. Visser, P.E.S. Wormer, and P. Stam, *J. Chem. Phys.* 79 (1983) 4973.
- [162] U. Hohm, *Chem. Phys.* 179 (1994) 533.
- [163] A. Kumar and W.J. Meath, *Chem. Phys.* 189 (1994) 467.
- [164] E. J. Baerends and P. Ros, *Int. J. Quantum Chem. Symp.* 12 (1978) 169.
- [165] J. G. Snijders, E. J. Baerends, and P. Vernooijs, *At. Nucl. Data Tables* 26 (1982) 483.
- [166] G.D. Zeiss, W.R. Scott, N. Suzuki, D.P. Chong, and S.R. Langhoff, *Mol. Phys.* 37 (1979) 1543.
- [167] L. Sutton, editor, *Tables of Interatomic Distances and Configuration in Molecules and Ions*. The Chemical Society, London, (1965).
- [168] P. J. Leonard, *At. Nucl. Data Tables* 14 (1974) 22.
- [169] J.P. Perdew and A. Zunger, *Phys. Rev.* B23 (1981) 5048.
- [170] O. Gunnarsson and B. I. Lundqvist, *Phys. Rev.* B13 (1976) 4274.
- [171] N.J. Bridge and A.D. Buckingham, *Proc. Roy. Soc. A* 295 (1966) 334.
- [172] G.R. Alms, A.K. Burnham, and W.H. Flygare, *J. Chem. Phys.* 63 (1975) 3321.
- [173] W.J. Meath and A. Kumar, *Int. J. Quantum Chem. Symp.* 24 (1990) 501.
- [174] A. J. Thakkar, H. Hettema, and P. E. S. Wormer, *J. Chem. Phys.* 97 (1992) 3252.
- [175] P.E.S. Wormer and H. Hettema, *J. Chem. Phys.* 97 (1992) 5592.
- [176] W. Rijks and P.E.S. Wormer, *J. Chem. Phys.* 90 (1989) 6507.
- [177] A. Kumar and W.J. Meath, *Mol. Phys.* 54 (1985) 823.
- [178] G.D. Zeiss and W.J. Meath, *Mol. Phys.* 33 (1977) 1155.
- [179] B.L. Jhanwar and W.J. Meath, *Chem. Phys.* 67 (1982) 185.

- [180] B.L. Jhanwar and W.J. Meath, *Mol. Phys.* 41 (1980) 1061.
- [181] P.W. Langhoff, R.G. Gordon, and M. Karplus, *J. Chem. Phys.* 55 (1971) 2126.
- [182] U. Hohm, private communication.
- [183] N. Matsuzawa and D.A. Dixon, *Synth. Met.* 71 (1995) 1667.
- [184] M. Stener, P. Decleva, and A. Lisini, *J. Phys.* B28 (1995) 4973.
- [185] L. Hedin and S. Lundqvist, *Phys. Rev.* 139 (1965) A796.
- [186] L. Hedin and S. Lundqvist, *Solid State Phys.* 23 (1969) 1.
- [187] V. G. Malkin, O. L. Malkina, M. E. Casida, and D. R. Salahub, *J. Am. Chem. Soc.* 116 (1994) 5898.
- [188] O. V. Gritsenko, R. van Leeuwen, and E. J. Baerends, *Phys. Rev.* A52 (1995) 1870.
- [189] Q. Zhao, R.C. Morrison, and R.G. Parr, *Phys. Rev.* A50 (1994) 2138.
- [190] R.C. Morrison and Q. Zhao, *Phys. Rev.* A51 (1995) 1980.
- [191] Y. Wang and R.G. Parr, *Phys. Rev.* A47 (1993) R1591.
- [192] V. E. Ingamells and N. C. Handy, *Chem. Phys. Lett.* 248 (1996) 373.
- [193] E. Engel, J. A. Chevary, L. D. Macdonald, and S. H. Vosko, *Z. Phys.* D23 (1992) 7.
- [194] H. Przybylski and G. Borstel, *Solid State Commun.* 49 (1984) 317.
- [195] H. Przybylski and G. Borstel, *Solid State Commun.* 52 (1984) 713.
- [196] O. V. Gritsenko, R. van Leeuwen, E. van Lenthe, and E. J. Baerends, *Phys. Rev.* A51 (1995) 1944.
- [197] Oleg V. Gritsenko, Robert van Leeuwen, and Evert Jan Baerends, *Int. J. Quantum Chem.* 61 (1997) 231.
- [198] R. Neumann, R. H. Nobes, and N. C. Handy, *Mol. Phys.* 87 (1996) 1.
- [199] P. R. Taylor, T. J. Lee, J. E. Rice, and J. Almlöf, *Chem. Phys. Lett.* 163 (1989) 359.
- [200] I. Cernusak, G.H.F. Diercksen, and A.J. Sadley, *Chem. Phys. Lett.* 128 (1986) 18.
- [201] G. Maroulis and A. J. Thakkar, *J. Chem. Phys.* 89 (1988) 7320.
- [202] R.C. Weast, editor, *Handbook of Chemistry and Physics*, 69th edition. Chemical Rubber, Boca Raton, FL , U.S.A., (1988-1989).
- [203] R. M. Dickson and A. D. Becke, *J. Phys. Chem.* 100 (1996) 16105.

- [204] M.A. Spackman, *J. Chem. Phys.* 94 (1991) 1288.
- [205] E. K. U. Gross and W. Kohn, *Phys. Rev. Lett.* 57 (1986) 923.
- [206] N. Iwamoto and E. K. U. Gross, *Phys. Rev.* B35 (1987) 3003.
- [207] G. Vignale, *Phys. Rev. Lett.* 74 (1995) 3233.
- [208] M. Petersilka, private communication.
- [209] G. Schreckenbach and T. Ziegler, *J. Phys. Chem.* 99 (1995) 606.
- [210] A. M. Lee, N. C. Handy, and S. M. Colwell, *J. Chem. Phys.* 103 (1995) 10095.
- [211] M. Castro, M. E. Casida, and D. R. Salahub, private communication.
- [212] G. Placzek and E. Teller, *Z. Phys.* 81 (1933) 209.
- [213] G. Placzek, in: *Handbuch der Radiologie*, vol. 6, edited by E. Marx (1934) 205.
- [214] T. Stroyer-Hansen and E.N. Svendsen, *Int. J. Quantum Chem. Symp.* 18 (1984) 519.
- [215] V. Bakken and H. Heiberg, private communication (1995).
- [216] A.T. Wong, G.B. Bacskay, and N.S. Hush, *Mol. Phys.* 74 (1991) 1037.
- [217] J. Oddershede and E.N. Svendsen, *Chem. Phys.* 64 (1982) 359.
- [218] B.G. Johnson and J. Florián, *Chem. Phys. Lett.* 247 (1995) 120.
- [219] A. Stirling, *J. Chem. Phys.* 104 (1996) 1254.
- [220] D. Porezag and M.R. Pederson, *Phys. Rev.* B54 (1996) 7830.
- [221] E. J. Baerends and P. Ros, *Chem. Phys.* 2 (1973) 52.
- [222] H.W. Schrötter and H.W. Klöckner, in: *Raman spectroscopy of gases and liquids*, edited by A. Weber, (Springer, Berlin, 1979) (1979) 123.
- [223] B. Fontal and T.G. Spiro, *Spectrochim. Acta* 33A (1977) 507.
- [224] T. Yoshino and H.J. Bernstein, *J. Mol. Spectry.* 2 (1958) 213.
- [225] W.F. Murphy, W. Holzer, and H.J. Bernstein, *Appl. Spectry.* 23 (1969) 211.
- [226] W. Holzer, W.F. Murphy, and H.J. Bernstein, *J. Chem. Phys.* 52 (1970) 399.
- [227] J. Florián and B.G. Johnson, private communication.
- [228] Y. LeDuff and W. Holzer, *J. Chem. Phys.* 60 (1974) 2175.
- [229] Y. Andersson. *van der Waals Density Functionals*. PhD thesis, Chalmers University of Technology and Göteborg University, Göteborg, Sweden, (1996).

- [230] B.I. Lundqvist, Y. Andersson, H. Shao, S. Chan, and D.C. Langreth, *Int. J. Quantum Chem.* 56 (1995) 247.
- [231] Y. Andersson, D.C. Langreth, and B.I. Lundqvist, *Phys. Rev. Lett.* 76 (1996) 102.
- [232] E. Hult, Y. Andersson, B.I. Lundqvist, and D.C. Langreth, *Phys. Rev. Lett.* 77 (1996) 2029.
- [233] J.F. Dobson and B.P. Dinte, *Phys. Rev. Lett.* 76 (1996) 1780.
- [234] A.J. Stone, *The Theory of Intermolecular Forces*. Clarendon Press, (1996).
- [235] V.P. Osinga, unpublished (1996).
- [236] P.E.S. Wormer, private communication.
- [237] H. Ågren, O. Vahtras, H. Koch, P. Jørgensen, and T. Helgaker, *J. Chem. Phys.* 98 (1993) 6417.
- [238] P. Norman, D. Jonsson, H. Ågren, P. Dahle, K. Ruud, T. Helgaker, and H. Koch, *Chem. Phys. Lett.* 253 (1996) 1.
- [239] G. Maroulis and A. J. Thakkar, *J. Chem. Phys.* 92 (1990) 812.
- [240] G. Maroulis, *Theoret. Chim. Acta* 84 (1992) 245.
- [241] G. Maroulis, *J. Phys. Chem.* 100 (1996) 13466.
- [242] G. Maroulis, *Chem. Phys. Lett.* 199 (1992) 244.
- [243] I.G. John, G.B. Bacskay, and N.S. Hush, *Chem. Phys.* 51 (1980) 49.
- [244] C. Hättig and B. A. Hess, *J. Chem. Phys.* 105 (1996) 9948.
- [245] H. Sekino and J. Bartlett, *J. Chem. Phys.* 85 (1986) 976.
- [246] J. E. Rice, R. D. Amos, S. M. Colwell, N. C. Handy, and J. Sanz, *J. Chem. Phys.* 93 (1990) 8828.
- [247] J. Frenkel, In: *Wave Mechanics, Advanced General Theory*, p.436, (Oxford. Univ. Press, London and New York, 1934).
- [248] A. Dal Corso, F. Mauri, and A. Rubio, *Phys. Rev. B* 53 (1996) 15638.
- [249] X. Gonze, *Phys. Rev. A* 52 (1995) 1096.
- [250] D. P. Shelton, *J. Chem. Phys.* 84 (1986??) 404.
- [251] D. M. Bishop, *Adv. Quantum Chem.* 25 (1994) 3.
- [252] C. S. Yannoni, P. P. Bernier, D. S. Bethune, G. Meijer, and J. R. Salem, *J. Am. Chem. Soc.* 113 (1991) 3190.

- [253] H. Weiss, R. Ahlrichs, and M. Häser, *J. Chem. Phys.* 99 (1993) 1262.
- [254] E. Westin, A. Rosén, G. te Velde, and E. J. Baerends, *J. Phys. B* 29 (1996) 5087.
- [255] S. Leach, M. Vervloet, A. Després, E. Bréheret, J. P. Hare, T. J. Dennis, H. W. Kroto, R. Taylor, and D. R. M. Walton, *Chem. Phys.* 160 (1992) 451.
- [256] G. E. Whyman and M. M. Mestechkin, *Opt. Commun.* 109 (1994) 410.
- [257] Jianliang Li, Shufeng Wang, Hong Yang, Qihuang Gong, Xin An, Huiying Chen, and Di Qiang, *Chem. Phys. Lett.* 288 (1998) 175.
- [258] H. Sekino and J. Bartlett, *Chem. Phys. Lett.* 234 (1995) 87.
- [259] C. Hättig, O. Christiansen, H. Koch, and P. Jørgensen, *Chem. Phys. Lett.* 269 (1997) 428.
- [260] J. Olsen and P. Jørgensen, *Time-dependent response theory*, notes used during 2nd European Summer School in Quantum Chemistry, 1995.
- [261] J. E. Rice and N. C. Handy, *J. Chem. Phys.* 94 (1991) 4959.
- [262] F. Aiga and R. Itoh, *Chem. Phys. Lett.* 251 (1996) 372.
- [263] C. Hättig and B. A. Hess, *Chem. Phys. Lett.* 233 (1995) 359.
- [264] U. Hohm, D. Goebel, and S. Grimme, *Chem. Phys. Lett.* 272 (1997) 1059.
- [265] F. Kootstra, internal report, Vrije Universiteit, Amsterdam, 1997.
- [266] P. R. T. Schipper, O. V. Gritsenko, and E. J. Baerends, *Theoret. Chim. Acta* 98 (1997) 16.
- [267] R. O. Esquivel and A. V. Bunge, *Int. J. Quantum Chem.* 32 (1987) 295.
- [268] A. V. Bunge and R. O. Esquivel, *Phys. Rev. A* 34 (1986) 853.
- [269] C. J. Umrigar and X. Gonze, *Phys. Rev. A* 50 (1994) 3827.
- [270] C. J. Umrigar and X. Gonze, in: *High Performance computing and its Application to the Physical Sciences*, proceedings of the Mardi Gras '93 conference, edited by D.A. Browne et al., (World Scientific, Singapore, 1993); unpublished.
- [271] C. Filippi, C. J. Umrigar, and X. Gonze, *J. Chem. Phys.* 107 (1997) 9994.
- [272] S. J. A. van Gisbergen, J. G. Snijders, and E. J. Baerends, unpublished.
- [273] <http://tc.chem.vu.nl/~vgisberg/basissets.html>.
- [274] V. R. Saunders and J. H. van Lenthe, *Mol. Phys.* 48 (1983) 923.

- [275] A. Savin, H. Stoll, and H. Preuss, *Theoret. Chim. Acta* 70 (1986) 407.
- [276] D. E. Woon and T. H. Dunning Jr., *J. Chem. Phys.* 100 (1994) 2975.
- [277] D. Tunega, J. Noga, and W. Klopper, *Chem. Phys. Lett.* 269 (1997) 435.
- [278] A. J. Thakkar, *Phys. Rev. A* 40 (1989) 1130.
- [279] G. Maroulis and A. J. Thakkar, *J. Phys. B* 21 (1988) 3819.
- [280] G. W. F. Drake, in *Atomic, Molecular, and Optical Physics Handbook*, edited by G.W.F. Drake (AIP Press, Woodbury, NY, 1996) 154.
- [281] A. Kono and S. Hattori, *Phys. Rev. A* 29 (1984) 2981.
- [282] A. Görling and M. Levy, *Phys. Rev. B* 47 (1993) 13105.
- [283] A. Görling and M. Levy, *Int. J. Quantum Chem. Symp.* 29 (1995) 93.
- [284] S. Bashkin and J. A. Stoner jr., *Atomic energy levels and grotrian diagrams 1*. North-Holland, Amsterdam, (1975).
- [285] J. B. Krieger, Jiqiang Chen, Yan Li, and G. J. Iafrate, *Int. J. Quantum Chem. Symp.* 29 (1995) 79.
- [286] T. Grabo and E. K. U. Gross, *Chem. Phys. Lett.* 240 (1995) 141.
- [287] T. Grabo and E. K. U. Gross, *Int. J. Quantum Chem.* 64 (1997) 95.
- [288] Xiao-Min Tong and Shih-I Chu, *Phys. Rev. A* 55 (1997) 3406.
- [289] L. A. Eriksson, O. L. Malkina, V. G. Malkin, and D. R. Salahub, *J. Chem. Phys.* 100 (1994) 5066.
- [290] P. Belanzoni, E. J. Baerends, S. van Asselt, and P. B. Langewen, *J. Phys. Chem.* 99 (1995) 13094.
- [291] J. D. Swann and D. Westmoreland, *Inorg. Chem.* 36 (1997) 5348.
- [292] G. Schreckenbach and T. Ziegler, *J. Phys. Chem. A* 101 (1997) 3388.
- [293] P.W. Langhoff, S.T. Epstein, and M. Karplus, *Rev. Mod. Phys.* 44 (1972) 602.
- [294] P.-O. Löwdin and P.K. Mukherjee, *Chem. Phys. Lett.* 14 (1972) 1.
- [295] R. van Leeuwen, private communication.
- [296] S.P. Karna, *J. Chem. Phys.* 104 (1996) 6590.
- [297] R. Van Leeuwen. Kohn-Sham potentials in density functional theory. PhD thesis, Vrije Universiteit, Amsterdam, The Netherlands, (1994).

- [298] R. Fournier, *J. Chem. Phys.* 92 (1990) 5422.
- [299] A. Komornicki and G. Fitzgerald, *J. Chem. Phys.* 98 (1993) 1398.
- [300] R. Fournier, J. Andzelm, and D.R. Salahub, *J. Chem. Phys.* 90 (1989) 6371.
- [301] B.I. Dunlap and J. Andzelm, *Phys. Rev.* A45 (1992) 81.
- [302] F. Sim, S. Chin, M. Dupuis, and J.E. Rice, *J. Phys. Chem.* 97 (1993) 1158.
- [303] S.P. Karna and P.N. Prasad, *J. Chem. Phys.* 94 (1991) 1171.
- [304] Y. Luo, H. Ågren, O. Vahtras, and P. Jørgensen, *Chem. Phys. Lett.* 207 (1993) 190.
- [305] Z. Shuai, S. Ramashesha, and J.L. Brédas, *Chem. Phys. Lett.* 250 (1996) 14.
- [306] D. M. Bishop, *J. Chem. Phys.* 95 (1991) 5489.
- [307] C. C. Teng and A. F. Garito, *Phys. Rev.* B28 (1983) 6766.